

✓

**THE OXIDATIVE DEHYDROGENATION OF *n*-HEXANE
AND *n*-OCTANE OVER VANADIUM MAGNESIUM OXIDE
CATALYSTS**

By

Jonathan Chetty

Submitted in fulfilment of the academic requirements for the degree of
Doctor of Philosophy in the School of Chemistry,
University of KwaZulu-Natal,
Durban,
South Africa

DEDICATION

To the loving memory of my brother Ashley Chetty (1977-2001)

"And God shall wipe away all tears from their eyes; and there shall be no more death, neither sorrow, nor crying, neither shall there be any more pain: for the former things are passed away."

Revelation 21:4

ABSTRACT

Vanadium magnesium oxide (VMgO) catalysts with different vanadium loadings were synthesized and tested for catalytic activity using pure *n*-hexane and *n*-octane as feeds. High surface area catalysts were obtained by the wet impregnation of magnesium oxide with an aqueous ammonium metavanadate solution. The optimum loading of vanadium was shown to be 19 % (calculated as weight % of V₂O₅). Catalysts were characterized by x-ray diffraction (XRD), inductively coupled plasma – atomic emission spectroscopy (ICP-AES), Brunauer-Emmet-Teller (BET) surface area, differential scanning calorimetry – thermogravimetric analysis (DSC-TGA), Fourier transform infrared spectroscopy (FTIR), laser Raman spectroscopy (LRS), x-ray induced photoelectron spectroscopy (XPS), energy dispersive x-ray spectroscopy (EDS) and scanning electron microscopy (SEM). Magnesium oxide (MgO) and magnesium orthovanadate (Mg₃(VO₄)₂) were the only phases observed in each catalyst.

VMgO catalysts were tested under both oxygen-rich and oxygen-lean conditions. *n*-Hexane as feed yielded benzene, 1-hexene, 2-hexene, propane, propene, carbon oxides and water as products. *n*-Octane as feed yielded styrene, ethylbenzene, xylene, benzene, octenes, carbon oxides and water. 19VMgO was promoted with different loadings of molybdenum oxide (MoO₃), cesium oxide (Cs₂O), antimony oxide (Sb₂O₅), niobium oxide (Nb₂O₅), bismuth oxide (Bi₂O₃) and tellurium oxide (TeO₂). The promoted catalysts were tested in specially designed and constructed parallel fixed bed continuous flow reactors.

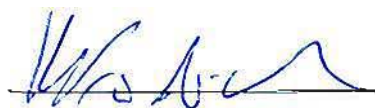
T-080191

PREFACE

The experimental work described in this thesis was carried out in the School of Chemistry, University of KwaZulu-Natal, Howard College, Durban, from April 2001 to March 2004, under the supervision of Dr. Holger B. Friedrich.

These studies represent original work by the author and have not otherwise been submitted in any form or degree or diploma to any tertiary institution. Where use has been made of the work of others it is duly acknowledged in the text.

Jonathan Chetty
M. Sc (UND)



Holger B. Friedrich
(Supervisor)

ACKNOWLEDGEMENTS

First and foremost I thank God for His blessings and guidance. I would like to thank SASOL for sponsoring this project from both a financial and an academic perspective as well as THRIP for their financial support. I thank my supervisor, Dr. Holger Friedrich for his guidance, valuable advice and constant encouragement. I would also like to thank Dr. Thys Botha, Dr. Matthys Janse van Vuuren and Dr. Reinier Nel, from SASOL R&D, for academic and technical advice.

My thanks go to Mr. Jodie Couling for his assistance in the building and setting up of the reactor, Mr. Gregory Moodley for making sure that chemicals and materials are always available as well as his friendly advice, Mrs. Thiloshnee Naidoo for her assistance in providing the necessary apparatus, Mr. Rickey Parasram for his assistance in electrical matters and the ever patient Mrs. Jay Govender for her efficient handling of all financial and administrative matters. To members of the Geology department at the University of Natal-Durban for XRD analysis, the late Dr. Fiona Graham for EDS, elemental maps and SEM analysis I extend my heartfelt gratitude. I would also like to thank Mr Mfanawenkosi for his assistance with the operation of my reactors.

To my colleagues and friends at the University of Natal, thank you for all your help and support. I would like to thank my brother for providing me with accommodation and transport during the duration of my study, my mother and aunty for their loving support and Monica for her patience and benevolence.

CONFERENCE CONTRIBUTIONS

Part of the work reflected in the following thesis has been presented at the following conferences as oral and poster presentations:

CATSA Conference 2001, Pilanesberg, poster presentation, *Partial oxidation of n-hexane over zeolites and mixed oxide catalysts*

CATSA Conference 2002, Cape Town, oral presentation, *Oxidative dehydrogenation of n-hexane over vanadium magnesium oxide catalysts*

CATSA Conference 2003, Durban, oral presentation, *Oxidative dehydrogenation of n-hexane and n-octane over vanadium magnesium oxide catalysts*

ABBREVIATIONS

| | | |
|-----------------|---|---|
| AA | = | atomic absorption spectroscopy |
| AES | = | Auger electron spectroscopy |
| AV | = | average oxidation state |
| BET | = | Brunauer-Emmet-Teller (surface area characterisation technique) |
| C | = | conversion |
| CO _x | = | carbon oxides |
| CSTR | = | continuous stirred tank reactor |
| DSC-TGA | = | differential scanning calorimetry – thermogravimetric analysis |
| EB | = | ethylbenzene |
| EDS | = | energy dispersive x-ray spectroscopy |
| ESR | = | electron spin resonance spectroscopy |
| EXAFS | = | extended X-ray absorption fine structure spectroscopy |
| FBR | = | fluidized bed reactor |
| FID | = | flame ionisation detector |
| FTIR | = | Fourier transform-infrared |
| GC | = | gas chromatography |
| GC-MS | = | gas chromatography - mass spectrometry |
| GDP | = | gross domestic product |
| GHSV | = | gas hourly space velocity |
| HPLC | = | high pressure liquid chromatography |
| ICP-AES | = | inductively coupled plasma – atomic emission spectroscopy |
| LEL | = | lower explosive limit |
| LHSV | = | liquid hourly space velocity |
| LRS | = | laser Raman spectroscopy |
| MSDS | = | material safety data sheet |
| ODH | = | oxidative dehydrogenation |
| PFR | = | plug flow reactor |
| PRV | = | pressure relief valve |
| PVC | = | polyvinyl chloride |

| | | |
|--------|---|--------------------------------------|
| S | = | selectivity |
| SEM | = | scanning electron microscopy |
| soln. | = | solution |
| STY | = | styrene |
| TCD | = | thermal conductivity detector |
| TDS | = | total dehydrogenation selectivity |
| TDY | = | total dehydrogenation yield |
| UEL | = | upper explosive limit |
| UV-vis | = | ultra violet visible spectroscopy |
| VMgO | = | vanadium magnesium oxide |
| wt | = | weight |
| XANES | = | x-ray absorption near edge structure |
| XPS | = | x-ray photoelectron spectroscopy |
| XRD | = | x-ray diffraction |
| XRF | = | x-ray fluorescence |
| Y | = | yield |

DEFINITIONS AND CALCULATIONS

1. Gas hourly space velocity (GHSV) = $\frac{\text{gaseous feed flowrate (ml/hr)}}{\text{volume of catalyst bed (ml)}}$

2. Hexane Conversion: $C = \frac{N_{hexin} - N_{hexout}}{N_{hexin}} \times 100\%$

(where C = conversion, N = concentration of hexane in moles and the subscripts 'in' and 'out' referring to the respective concentrations of the feed and outlet, $hexin$ = hexane feed in and $hexout$ = hexane in product stream)

3. Selectivity to P : $S_P = \frac{N_P}{N_{hexin} - N_{hexout}} \times 100\%$

(where P = product, and S = selectivity, N_P = moles carbon of product, $N_{hexin} - N_{hexout}$ = hexane conversion)

4. Yield to P : $Y_p = \frac{X}{100} S_p$

(where C = conversion and S_p = Selectivity to P)

5. Equilibrium constant: $K = k_f / k_r$

(where k_f and k_r are the rate constants for the forward and reverse reaction respectively)

6. Gibbs free energy: $\Delta G = -RT \ln K$

(where R = gas constant, T = temperature and K = equilibrium constant)

7. Specific activity (T) = conversion (T) / surface area

LIST OF FIGURES

| | |
|---|----|
| Figure 1.1: A Catalytic cycle | 2 |
| Figure 1.2: A Maxwell-Boltzmann distribution plot adjacent to a reaction profile graph for ammonia synthesis | 3 |
| Figure 2.1: Equilibrium constants for <i>n</i> -paraffin dehydrogenation at 500 °C | 24 |
| Figure 2.2: Temperatures for 10 and 40% conversion of C ₂ -C ₁₅ <i>n</i> -paraffins at 1 atm | 24 |
| Figure 3.1: Parameters affecting the properties of precipitated catalysts | 38 |
| Figure 3.2: Components for the surface analysis of a catalyst | 42 |
| Figure 3.3: Diffraction of x-rays | 45 |
| Figure 3.4: Illustration of x-ray production by irradiation with x-rays | 46 |
| Figure 3.5: Components of a FTIR spectrometer | 48 |
| Figure 3.6: A Michelson interferometer | 48 |
| Figure 3.7: An energy diagram illustrating Rayleigh and Raman scattering of incident photons | 49 |
| Figure 4.1: Influences on the design of catalytic reactors | 55 |
| Figure 4.2: Classification of laboratory reactors | 56 |
| Figure 4.3: An adiabatic fixed bed reactor and a multitubular fixed bed reactor | 57 |
| Figure 4.4: Sasol's commercial fixed bed Fischer-Tropsch reactor | 59 |
| Figure 4.5: Schematic of a Sasol Advanced Synthol (SAS) reactor | 61 |
| Figure 4.6: Schematic representation of a continuous stirred tank reactor | 62 |
| Figure 4.7: Schematic representation of a batch reactor containing heating and cooling coils | 63 |
| Figure 4.8: Different shapes and sizes of monolith material | 65 |
| Figure 5.1: The local environment of vanadium | 71 |
| Figure 5.2: Structure of the orthovanadate phase | 72 |
| Figure 5.3: Structure of the pyrovanadate phase | 72 |
| Figure 5.4: Structure of the metavanadate phase | 73 |
| Figure 5.5: Highest yields to propylene reported for the oxidative dehydrogenation of propane | 77 |

| | |
|---|-----|
| Figure 6.1: Flow chart for the synthesis of VMgO catalysts | 81 |
| Figure 6.2: Schematic showing the four parallel reactors setup for <i>n</i> -hexane ODH | 87 |
| Figure 6.3: Schematic showing the reactor setup used for <i>n</i> -octane ODH | 88 |
| Figure 6.4: Block diagram of the analytical system used | 89 |
| Figure 6.5: 6 port valve in standby mode | 89 |
| Figure 6.6: 6 port valve in sampling mode | 89 |
| Figure 6.7: 10 port valve in standby and sampling mode | 90 |
| Figure 6.8: Schematic of a packed reactor | 91 |
| Figure 6.9: The Bubbler system used to produce the <i>n</i> -hexane in air feed above the LEL | 92 |
| Figure 7.1: Overlaid XRD patterns | 97 |
| Figure 7.2: Graph showing the effect of vanadium loading on the surface area of VMgO catalysts | 100 |
| Figure 7.3: Graph showing the effect of mol % Mg ₃ (VO ₄) ₂ on the BET surface areas | 100 |
| Figure 7.4: Raman spectra for 19VMgO | 102 |
| Figure 7.5: FTIR spectrum of 19VMgO | 105 |
| Figure 7.6: XPS spectrum of 19VMgO showing V _{2p} ^{3/2} peak deconvolution | 107 |
| Figure 7.7: SEM image of V ₂ O ₅ | 108 |
| Figure 7.8: SEM image of MgO | 108 |
| Figure 7.9: SEM image of unused 19VMgO | 108 |
| Figure 7.10: SEM image of aged 19VMgO | 108 |
| Figure 7.11: SEM image of aged 19VMgO | 109 |
| Figure 7.12: SEM image of unused 19VMgO | 109 |
| Figure 7.13: Effect of temperature on the non-catalytic conversion of <i>n</i> -hexane in carborundum filled reactors. | 114 |
| Figure 7.14: Effect of temperature on the non-catalytic conversion of <i>n</i> -octane in carborundum filled reactors. | 114 |
| Figure 8.1: Effect of temperature on conversion and selectivity in <i>n</i> -hexane ODH over MgO and V ₂ O ₅ | 118 |
| Figure 8.2: Effect of temperature on <i>n</i> -hexane conversion | 120 |
| Figure 8.3: Temperature required for a 20 % <i>n</i> -hexane conversion | 121 |
| Figure 8.4: Effect of temperature on <i>n</i> -hexane conversion, selectivity to benzene, selectivity to CO _x and yield of benzene for 19VMgO | 122 |

| | |
|---|-----|
| Figure 8.5: Selectivity to benzene on VMgO catalysts at 30 % conversion | 122 |
| Figure 8.6: Effect of temperature on conversion in <i>n</i> -hexane ODH | 125 |
| Figure 8.7: Effect of temperature on selectivity in <i>n</i> -hexane ODH over 16VMgO | 126 |
| Figure 8.8: Effect of temperature on selectivity in <i>n</i> -hexane ODH over 19VMgO | 126 |
| Figure 8.9: Effect of temperature on selectivity in <i>n</i> -hexane ODH over 24VMgO | 127 |
| Figure 8.10: Effect of temperature on the total dehydrogenation selectivity (TDS) in <i>n</i> -hexane ODH over 16VMgO, 19VMgO and 24VMgO | 127 |
| Figure 8.11: Highest selectivity to benzene and highest selectivity to dehydrogenation products obtained with 16VMgO, 19VMgO and 24VMgO | 128 |
| Figure 8.12: Highest yield obtained for benzene and highest yield obtained for dehydrogenation with 16VMgO, 19VMgO and 24VMgO | 128 |
| Figure 8.13: Effect of GHSV on <i>n</i> -hexane conversion, benzene selectivity, TDS and propane and propene selectivity obtained with 19VMgO | 129 |
| Figure 8.14: Effect of GHSV on the yield and selectivity towards benzene | 130 |
| Figure 8.15: Effect of variation in the <i>n</i> -hexane to air ratio on conversion, selectivity and yield | 131 |
| Figure 8.16: Effect of temperature on conversion in <i>n</i> -hexane ODH over 19VMgO and molybdenum promoted 19VMgO | 134 |
| Figure 8.17: Effect of temperature on the selectivity to benzene over 19VMgO and molybdenum promoted 19VMgO catalysts | 135 |
| Figure 8.18: Conversion of <i>n</i> -hexane, selectivity to benzene, total ODH selectivity, yield of benzene and the total ODH yield obtained with 19VMgO and molybdenum promoted 19VMgO catalysts at 525 °C | 135 |
| Figure 8.19: Effect of temperature on conversion in <i>n</i> -hexane ODH over 19VMgO and cesium promoted 19VMgO | 137 |
| Figure 8.20: Effect of temperature on the selectivity to cracked products over 19VMgO and cesium promoted 19VMgO catalysts | 139 |
| Figure 8.21: Selectivity to hexenes, selectivity to benzene, total ODH selectivity (TDS), yield of benzene and the total ODH yield obtained with 19VMgO and cesium promoted 19VMgO catalysts at 525 °C | 140 |
| Figure 8.22: Effect of temperature on conversion in <i>n</i> -hexane ODH over 19VMgO and antimony promoted 19VMgO | 141 |

| | |
|--|-----|
| Figure 8.23: Selectivity to hexenes, selectivity to benzene, TDS, yield of benzene and the TDY obtained with 19VMgO and antimony promoted 19VMgO catalysts at 525 °C | 143 |
| Figure 8.24: Effect of temperature on conversion in <i>n</i> -hexane ODH over 19VMgO and niobium promoted VMgO | 144 |
| Figure 8.25: Conversion of <i>n</i> -hexane, selectivity to benzene, total ODH selectivity, yield of benzene and the total ODH yield obtained with 19VMgO and niobium promoted VMgO catalysts at 525 °C | 145 |
| Figure 8.26: Effect of temperature on conversion in <i>n</i> -hexane ODH over 19VMgO and bismuth promoted VMgO | 146 |
| Figure 8.27: Conversion of <i>n</i> -hexane, selectivity to benzene, total ODH selectivity (TDS), yield of benzene and the total ODH yield obtained with 19VMgO and bismuth promoted VMgO catalysts at 525 °C | 147 |
| Figure 8.28: Effect of temperature on conversion in <i>n</i> -hexane ODH over 19VMgO and tellurium promoted VMgO | 148 |
| Figure 8.29: Selectivity to hexenes, selectivity to benzene, TDS, yield of benzene and TDY's obtained with 19VMgO and tellurium promoted VMgO catalysts at 525 °C | 148 |
| Figure 9.1: Effect of temperature on selectivity and conversion in <i>n</i> -octane ODH over 19VMgO | 155 |
| Figure 9.2: Variation of selectivity to ODH products with <i>n</i> -octane conversion | 156 |
| Figure 9.3: Effect of GHSV on <i>n</i> -octane conversion and styrene selectivity and yield | 156 |
| Figure 9.4: Effect of <i>n</i> -octane to air feed ratio on conversion, selectivity and yield of styrene | 157 |
| Figure 9.5: Selectivity to products observed during <i>n</i> -octane ODH of 19VMgO and promoted 19VMgO | 158 |
| Figure 9.6: Comparison of <i>n</i> -octane conversion, styrene selectivity and styrene yield obtained with 19VMgO and molybdenum, cesium and antimony promoted 19VMgO | 159 |
| Figure 10.1: Effect of temperature on the conversion of benzene over 19VMgO | 161 |
| Figure 10.2: Alkyl radical formation | 162 |
| Figure 10.3: Proposed reaction network in oxidative dehydrogenation of <i>n</i> -hexane | 162 |
| Figure 10.4: Mechanism of 1-hexene and 2-hexene formation | 163 |
| Figure 10.5: Proposed mechanisms for the cyclisation of <i>n</i> -hexane | 164 |

LIST OF SCHEMES

| | |
|---|----|
| Scheme 1: Products from synthesis gas over different catalysts | 11 |
| Scheme 2.1: Oxygen atoms / ions responsible for oxidation | 27 |
| Scheme 2.2: The mechanism proposed by Mars and van Krevelen | 28 |
| Scheme 2.3: Schematic representation of spill-over oxygen burning out deposited coke | 29 |
| Scheme 2.4: Electronegativity and hydrogen abstraction ability of metal oxides | 31 |

LIST OF TABLES

| | |
|--|----|
| Table 1.1: Examples of homogeneous catalysis | 5 |
| Table 1.2: Phase combinations for heterogeneous catalysis | 6 |
| Table 1.3: A comparison of homogeneous and heterogeneous catalysis | 6 |
| Table 1.4: Comparison of physisorption and chemisorption | 8 |
| Table 1.5: Examples of promoters in the chemical industry | 14 |
| Table 2.1: Monomers derived from homogeneous catalytic aerial oxidation processes | 17 |
| Table 2.2: Monomers derived from heterogeneous catalytic aerial oxidation processes | 18 |
| Table 2.3: Processes under study or development for the oxidative transformation of paraffins | 19 |
| Table 2.4: Commonly used oxidants | 21 |
| Table 2.5: Performance of UOP's Pacol™ and Oleflex™ dehydrogenation processes | 23 |
| Table 2.6: Important considerations in paraffin oxidation | 33 |
| Table 2.7: Important catalyst features in paraffin oxidation | 34 |
| Table 3.1: Types of impregnation | 39 |
| Table 3.2: Common catalyst shapes | 41 |
| Table 3.3: Criteria for choosing the shape and size of catalyst particles | 41 |
| Table 3.4: Methods for catalyst characterization using photons as the exciting source | 43 |
| Table 3.5: Methods for catalyst characterization using electrons as the exciting source | 43 |
| Table 3.6: Methods for catalyst characterization using ions as the exciting source | 44 |
| Table 4.1: Information obtained from different reactors | 56 |

| | |
|---|-----|
| Table 5.1: Catalytic properties of vanadium based catalysts | 74 |
| Table 5.2: Summary of the catalytic performance of VMgO | 76 |
| Table 6.1: Chemicals used for synthesis, calibration and as feedstock | 79 |
| Table 6.2: Gases used in calibration, operation of GC and as feedstock | 79 |
| Table 6.3: Calcination conditions used for synthesis of unpromoted VMgO | 80 |
| Table 6.4: Calcination conditions used for synthesis of promoted VMgO | 82 |
| Table 6.5: Labeling of unpromoted catalysts and their corresponding chemical composition | 82 |
| Table 6.6: Labeling of promoted catalysts and their corresponding theoretical chemical composition | 83 |
| Table 7.1: X-ray diffraction lines of synthesized 19VMgO compared to those previously reported | 96 |
| Table 7.2: Chemical characteristics of synthesized VMgO catalysts | 98 |
| Table 7.3: The average vanadium oxidation state of freshly synthesized VMgO catalysts | 99 |
| Table 7.4: BET surface areas, pore volumes and pore diameters for synthesized VMgO catalysts | 99 |
| Table 7.5: Effect of calcination times on the BET surface area at 550 °C | 101 |
| Table 7.6: Comparison of Raman frequencies of the $Mg_3(VO_4)_2$ phase of 19VMgO | 103 |
| Table 7.7: Raman Frequencies for 14VMgO, 16VMgO, 19VMgO, 24VMgO, 35VMgO, 49VMgO, 60VMgO, V_2O_5 and MgO. | 104 |
| Table 7.8: Binding energy and surface atomic ratio's for 19VMgO | 106 |
| Table 7.9: Physico-chemical characteristics of unpromoted and promoted VMgO catalyst | 111 |
| Table 7.10: Physico-chemical characteristics of unpromoted and promoted VMgO catalysts | 112 |
| Table 8.1: <i>n</i> -Hexane ODH over 14VMgO | 119 |
| Table 8.2: <i>n</i> -Hexane ODH over 16VMgO | 119 |
| Table 8.3: <i>n</i> -Hexane ODH over 19VMgO | 119 |
| Table 8.4: <i>n</i> -Hexane ODH over 24VMgO | 119 |
| Table 8.5: <i>n</i> -Hexane ODH over 35VMgO | 119 |
| Table 8.6: <i>n</i> -Hexane ODH over 49VMgO | 119 |
| Table 8.7: <i>n</i> -Hexane ODH over 60VMgO | 119 |
| Table 8.8: Specific activity for MgO, V_2O_5 and VMgO catalysts at 350 °C | 121 |

| | |
|--|-----|
| Table 8.9: The effect of temperature on conversion, selectivity and yield in <i>n</i> -hexane ODH over 16VMgO | 124 |
| Table 8.10: The effect of temperature on conversion, selectivity and yield in <i>n</i> -hexane ODH over 19VMgO | 124 |
| Table 8.11: The effect of temperature on conversion, selectivity and yield in <i>n</i> -hexane ODH over 24VMgO | 124 |
| Table 8.12: The effect of temperature on conversion, selectivity and yield in <i>n</i> -hexane ODH over 0.5MoVMgO | 133 |
| Table 8.13: The effect of temperature on conversion, selectivity and yield in <i>n</i> -hexane ODH over 1.0MoVMgO | 133 |
| Table 8.14: The effect of temperature on conversion, selectivity and yield in <i>n</i> -hexane ODH over 2.5MoVMgO | 133 |
| Table 8.15: The effect of temperature on conversion, selectivity and yield in <i>n</i> -hexane ODH over 5MoVMgO | 133 |
| Table 8.16: The effect of temperature on conversion, selectivity and yield in <i>n</i> -hexane ODH over 0.5CsVMgO | 138 |
| Table 8.17: The effect of temperature on conversion, selectivity and yield in <i>n</i> -hexane ODH over 1.0CsVMgO | 138 |
| Table 8.18: The effect of temperature on conversion, selectivity and yield in <i>n</i> -hexane ODH over 2.5CsVMgO | 138 |
| Table 8.19: The effect of temperature on conversion, selectivity and yield in <i>n</i> -hexane ODH over 5CsVMgO | 138 |
| Table 8.20: The effect of temperature on conversion, selectivity and yield in <i>n</i> -hexane ODH over 0.5SbVMgO | 142 |
| Table 8.21: The effect of temperature on conversion, selectivity and yield in <i>n</i> -hexane ODH over 1.0SbVMgO | 142 |
| Table 8.22: The effect of temperature on conversion, selectivity and yield in <i>n</i> -hexane ODH over 2.5SbVMgO | 142 |
| Table 8.23: The effect of temperature on conversion, selectivity and yield in <i>n</i> -hexane ODH over 5SbVMgO | 142 |
| Table 10.1: Major and minor products observed by feeding intermediates over 19VMgO | 165 |

CONTENTS

| | |
|------------------------------|--------|
| Title | (i) |
| Abstract | (ii) |
| Preface | (iii) |
| Acknowledgements | (iv) |
| Conference contributions | (v) |
| Abbreviations | (vi) |
| Definitions and calculations | (viii) |
| List of figures | (ix) |
| List of schemes | (xiii) |
| List of tables | (xiii) |
| Contents | (xvi) |

Chapter 1: Introduction to Catalysis

| | | |
|-----|--|----|
| 1.1 | Definition | 1 |
| 1.2 | Importance | 4 |
| 1.3 | Classification of catalysis | 5 |
| | 1.3.1 Enzyme catalysis | 5 |
| | 1.3.2 Homogeneous catalysis | 5 |
| | 1.3.3 Heterogeneous catalysis | 6 |
| 1.4 | Principles and key concepts | 7 |
| | 1.4.1 Steps in heterogeneous catalysis | 7 |
| | 1.4.2 Mass-transport phenomena in a catalyst | 10 |
| | 1.4.3 Selectivity, activity and stability | 10 |
| | 1.4.3.1 Selectivity | 11 |
| | 1.4.3.2 Activity | 12 |
| | 1.4.3.3 Stability | 13 |
| | 1.4.4 Promoters | 14 |
| 1.5 | References | 15 |

Chapter 2: Selective Hydrocarbon Oxidation

| | | |
|-----|---|----|
| 2.1 | Introduction | 17 |
| 2.2 | The use of paraffins as feedstocks | 20 |
| 2.3 | Choice of oxidant | 21 |
| | 2.3.1 Air versus oxygen processes | 22 |
| 2.4 | Limits of flammability (Explosive limits) | 22 |
| 2.5 | Oxidative dehydrogenation of paraffins | 23 |
| | 2.5.1 Oxidative dehydrogenation versus dehydrogenation | 23 |
| | 2.5.2 Catalytic systems used for oxidative dehydrogenation | 26 |
| 2.6 | Theory of selective oxidation catalysis | 27 |
| | 2.6.1 Oxygen activation in oxidation catalysis | 27 |
| | 2.6.2 Mars and van Krevelen mechanism | 28 |
| | 2.6.3 Phase co-operation in selective oxidation catalysts | 29 |
| | 2.6.4 Paraffin activation and the role of acid-base properties in catalytic oxidation | 30 |
| | 2.6.5 The dynamic state of oxide surfaces | 31 |
| | 2.6.6 Paraffin / air composition | 32 |
| | 2.6.7 The role of the paraffin in oxidation | 32 |
| | 2.6.8 Summary: Crucial considerations in paraffin oxidation | 33 |
| 2.7 | References | 35 |

Chapter 3: Catalyst Preparation and Characterization

| | | |
|-----|---|----|
| 3.1 | Introduction to catalyst preparation | 37 |
| | 3.1.1 Precipitation | 37 |
| | 3.1.2 Impregnation | 38 |
| 3.2 | Washing, filtering and drying | 40 |
| 3.3 | Calcining | 40 |
| 3.4 | Catalyst forming | 41 |
| 3.5 | Introduction to catalyst characterization | 42 |
| | 3.5.1 X-ray diffraction (XRD) | 44 |
| | 3.5.2 X-ray fluorescence (XRF) | 46 |

| | | |
|-------|--|----|
| 3.5.3 | X-ray induced photoelectron spectroscopy (XPS) and Auger electron spectroscopy (AES) | 46 |
| 3.5.4 | Fourier transform infrared spectroscopy (FTIR) and laser Raman spectroscopy (LRS) | 47 |
| 3.5.5 | Scanning electron microscopy (SEM) and energy dispersive x-ray spectroscopy (EDS) | 50 |
| 3.5.6 | Differential scanning calorimetry (DSC) and thermogravimetric analysis (TGA) | 51 |
| 3.5.7 | Brunauer-Emmett-Teller (BET) surface area | 51 |
| 3.5.8 | Inductively coupled plasma – atomic emission spectroscopy (ICP-AES) | 52 |
| 3.6 | References | 53 |

Chapter 4: Reactors in Catalysis

| | | |
|-------|---|----|
| 4.1 | Introduction | 55 |
| 4.1.1 | Plug flow fixed bed reactors | 57 |
| 4.1.2 | Fluidized bed reactors | 60 |
| 4.1.3 | Continuous stirred tank reactors (CSTR) | 62 |
| 4.1.4 | Batch reactors | 63 |
| 4.1.5 | Transient reactors | 64 |
| 4.1.6 | Monolith reactors | 65 |
| 4.1.7 | Membrane reactors | 66 |
| 4.2 | References | 67 |

Chapter 5: The Vanadium Magnesium Oxide (VMgO) Catalytic System

| | | |
|-----|--|----|
| 5.1 | Vanadium in selective oxidation | 68 |
| 5.2 | Supported vanadia | 68 |
| 5.3 | Preparation of magnesium vanadates | 69 |
| 5.4 | Magnesium vanadates | 71 |
| 5.5 | Nature and influences of the active site | 74 |
| 5.6 | Stability of products | 75 |
| 5.7 | The performance of the VMgO catalytic system | 76 |
| 5.8 | References | 78 |

Chapter 6: Experimental

| | | |
|--------|--|----|
| 6.1 | Materials used | 79 |
| 6.2 | Catalyst preparation | 80 |
| 6.2.1 | Synthesis of magnesium oxide (MgO) and vanadium pentoxide (V ₂ O ₅) | 80 |
| 6.2.2 | Synthesis of vanadium magnesium oxide (VMgO) | 80 |
| 6.3 | Labeling the catalysts | 82 |
| 6.4 | Catalyst characterization | 84 |
| 6.4.1 | X-ray diffraction (XRD) | 84 |
| 6.4.2 | X-ray fluorescence (XRF) | 84 |
| 6.4.3 | X-ray photoelectron spectroscopy (XPS) | 84 |
| 6.4.4 | Fourier transform infrared spectroscopy (FTIR) | 85 |
| 6.4.5 | Laser Raman spectroscopy (LRS) | 85 |
| 6.4.6 | Scanning electron microscopy (SEM) and energy dispersive x-ray spectroscopy (EDS) | 85 |
| 6.4.7 | Differential scanning calorimetry - thermogravimetric analysis (DSC-TGA) | 85 |
| 6.4.8 | Brunauer-Emmett-Teller (BET) surface area | 85 |
| 6.4.9 | Inductively coupled plasma – atomic emission spectroscopy (ICP- AES) | 85 |
| 6.4.10 | Gas chromatography – mass spectrometry (GC-MS) | 86 |
| 6.4.11 | Average vanadium oxidation state | 86 |
| 6.5 | Reactor configuration | 87 |
| 6.5.1 | Reactor setup for <i>n</i> -hexane oxidative dehydrogenation | 87 |
| 6.5.2 | Reactor setup for <i>n</i> -octane oxidative dehydrogenation | 88 |
| 6.6 | The analytical system | 89 |
| 6.6.1 | The gas sampling valve box | 89 |
| 6.6.2 | Gas chromatography | 90 |
| 6.6.3 | Product analysis | 91 |
| 6.7 | Catalyst Testing | 91 |
| 6.7.1 | Reactor used for <i>n</i> -hexane oxidative dehydrogenation | 91 |
| 6.7.2 | Reactor used for <i>n</i> -octane oxidative dehydrogenation | 92 |
| 6.7.3 | Catalyst testing and flammability limits | 92 |
| 6.7.4 | Feed used for <i>n</i> -hexane oxidative dehydrogenation | 92 |
| 6.7.5 | Feed used for <i>n</i> -octane oxidative dehydrogenation | 93 |

| | | |
|-----|------------|----|
| 6.8 | References | 94 |
|-----|------------|----|

Chapter 7: Results and Discussion

| | | |
|-------|--|-----|
| 7.1 | Introduction, aim and overview | 95 |
| 7.2 | Catalyst characterization: VMgO | 96 |
| 7.2.1 | X-ray diffraction (XRD) | 96 |
| 7.2.2 | Chemical composition | 98 |
| 7.2.3 | Average vanadium oxidation state | 98 |
| 7.2.4 | Brunauer-Emmet-Teller (BET) surface area | 99 |
| 7.2.5 | Differential scanning calorimetry – thermogravimetric analysis (DSC-TGA) | 101 |
| 7.2.6 | Laser Raman spectroscopy (LRS) | 102 |
| 7.2.7 | Fourier transform infrared spectroscopy (FTIR) | 105 |
| 7.2.8 | X-ray induced photoelectron spectroscopy (XPS) | 106 |
| 7.2.9 | Scanning electron microscopy (SEM) | 108 |
| 7.3 | Catalyst characterization: Promoted VMgO | 110 |
| 7.4 | Non-catalytic reactor studies | 113 |
| 7.4.1 | Introduction | 113 |
| 7.4.2 | Homogeneous reactions | 113 |
| 7.4.3 | Conclusion | 115 |
| 7.5 | References | 116 |

Chapter 8: Oxidative Dehydrogenation of *n*-Hexane

| | | |
|-------|--|-----|
| 8.1 | Catalyst testing below the lower explosive limit | 118 |
| 8.2 | Catalyst testing above the upper explosive limit | 123 |
| 8.3 | Variation in gas hourly space velocity (GHSV) | 129 |
| 8.4 | <i>n</i> -Hexane ODH in the flammable region | 130 |
| 8.5 | Promoted VMgO | 132 |
| 8.5.1 | Molybdenum oxide (MoO ₃) | 132 |
| 8.5.2 | Cesium oxide (Cs ₂ O) | 137 |
| 8.5.3 | Antimony oxide (Sb ₂ O ₅) | 141 |
| 8.5.4 | Niobium oxide (Nb ₂ O ₅) | 144 |

| | | |
|-------|---|-----|
| 8.5.5 | Bismuth oxide (Bi_2O_3) | 146 |
| 8.5.6 | Tellurium oxide (TeO_2) | 147 |
| 8.6 | Conclusion | 150 |
| 8.7 | References | 152 |

Chapter 9: Oxidative Dehydrogenation of *n*-Octane

| | | |
|-----|---|-----|
| 9.1 | Introduction | 154 |
| 9.2 | Catalyst testing | 154 |
| 9.3 | Variation in gas hourly space velocity (GHSV) | 156 |
| 9.4 | Variation in the <i>n</i> -octane to air feed ratio | 157 |
| 9.5 | Promoted 19VMgO | 158 |
| 9.6 | Conclusion | 159 |
| 9.7 | References | 160 |

Chapter 10: Mechanistic Studies

| | | |
|------|--|-----|
| 10.1 | Introduction | 161 |
| 10.2 | Stability of benzene over 19VMgO | 161 |
| 10.3 | Reaction network and mechanism | 162 |
| | 10.3.1 Homogeneous gas phase reactions | 162 |
| | 10.3.2 Heterogeneous reactions | 162 |
| | 10.3.2.1 Mechanism of 1-hexene and 2-hexene formation | 163 |
| | 10.3.2.2 Oxidative dehydrocyclisation of <i>n</i> -hexane to benzene | 164 |
| 10.4 | Conclusion | 166 |
| 10.5 | References | 167 |

Chapter 11: Summary and Conclusion

Appendix 1: Experimental

Appendix 2: MSDS

Appendix 3: Unpromoted VMgO

Appendix 4: Promoted VMgO

CHAPTER 1: Introduction to Catalysis

1.1 Definition

“I shall therefore call it the *catalytic power* of substances, and the decomposition by means of this power *catalysis*, just as we use the word analysis to denote separation of the component parts of bodies by means of ordinary chemical forces. Catalytic power actually means that substances are able to awake affinities which are asleep at this temperature by their mere presence and not by their own affinity.”

J. J. Berzelius, 1836.

It is generally accepted that J. J. Berzelius first recognized the phenomenon of catalysis in 1836. Berzelius proposed the introduction of the term ‘catalysis’ which he claimed to arise from a ‘catalytic force’. Almost sixty years later Ostwald recognized that catalysis could be explained in terms of the laws of physical chemistry. He identified catalysis as an ubiquitous phenomenon and emphasized that a catalyst cannot change the equilibrium position in a reversible reaction. In a catalytic reversible reaction, an increase in the rate constant in the forward direction, k_f , is accompanied by an increase in the rate constant of the reverse reaction, k_r .

| | |
|-----------------|-------------------------|
| $K = k_f / k_r$ | unchanged by a catalyst |
|-----------------|-------------------------|

A catalyst can be therefore defined as a substance that changes the kinetics but not the thermodynamics of a chemical reaction. A catalyst cannot initiate chemical reactions that are not thermodynamically favourable ($\Delta G < 0$).

| | |
|--------------------------|-------------------------|
| $\Delta G_o = -RT \ln K$ | unchanged by a catalyst |
|--------------------------|-------------------------|

A more insightful definition of a catalyst is: a catalyst is a substance that transforms reactants into products, through an uninterrupted and repeated cycle of elementary steps in which the catalyst participates while being regenerated in its original form at the end of each cycle during the life of the catalyst [1,2]. Catalysis is therefore a cyclic process whereby reactants bind to one form of the catalyst and products are released from another form (Figure 1.1). In this way the initial state of a catalyst is regenerated after one complete cycle [3].

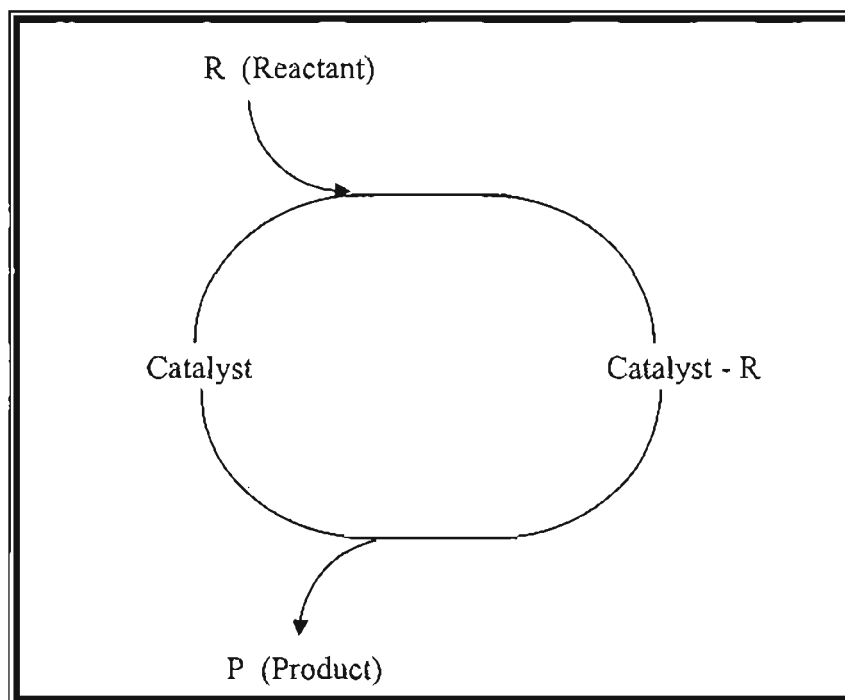


Figure 1.1: A Catalytic cycle [3]

The energy that must be provided to the reactants, in a chemical reaction, to reach an intermediate or activated state from which the products of the reaction can form is called the activation energy, E° . A catalyst lowers both the activation energy for the forward and the reverse reaction. Consider the decomposition reaction for ammonia:



In the absence of a catalyst the reaction has activation energy of 335 kJmol^{-1} . In the presence of an osmium catalyst the activation energy is lowered to 197 kJmol^{-1} . The activation energy is even lower with a tungsten catalyst, 163 kJmol^{-1} [4]. Different catalysts can affect the activation energy in different ways and to different extents. A catalyst can alter the activation energy by forming bonds with the reactants, thereby reducing the energy requirements to complete the reaction. It can stabilize reactive transition states. A catalyst can also enable reactants to come together in the most suitable orientation resulting in a reduction of entropy of the adsorbed or transition state [4]. A catalyst mediated proximity effect on the reactants can thus ensure a decrease in entropy. The entropy for the overall reaction is unaltered in the presence or absence of a catalyst.

The speed of reactant molecules in a particular mixture will vary from very slow particles (low energy) to very fast particles (high energy). Most of the particles, however, will be moving at a speed that is close to the average. The distribution of the speeds (energies) of a mixture of moving particles at a particular temperature is described by the Maxwell-Boltzmann distribution [5,6].

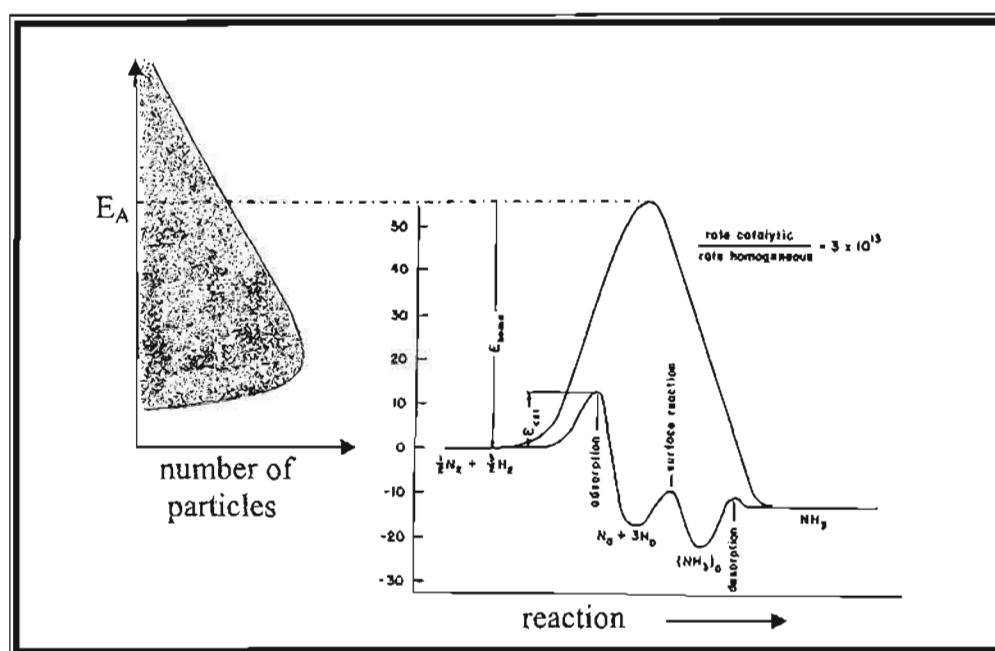
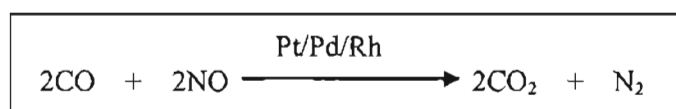


Figure 1.2: A Maxwell-Boltzmann distribution plot adjacent to a reaction profile graph, for ammonia synthesis [7]

Molecules that have relatively lower energies collide and rebound without reacting. Molecules with higher energies may collide and these collisions may result in the formation of products. If we look at a typical Maxwell-Boltzmann distribution plot next to the potential energy profile graph for ammonia synthesis (Figure 1.2), it can be seen that only a small amount of particles have sufficient kinetic energy (greater than E_A) to react. If the E_A is decreased (by a catalyst) more molecules will be able to overcome the E_A . The rate of conversion will increase i.e. more collisions will lead to a conversion of reactant to product.

1.2 Importance

Catalysis is crucial to life and to our modern lifestyles. Innumerable biological reactions are catalysed by different enzymes with different functionalities thus ensuring the sustainability of life. Industrial catalysis controls and directs our economy thus influencing our lifestyle. Catalysis has become central to global problems relating to energy, resources and our environment [8]. The biggest catalyst user is the United States of America [9]. Ninety percent of all chemical processes are catalytic [10]. The chemical industry contributes a significant factor of the gross domestic product (GDP) and it has a positive trade balance of approximately twenty billion dollars in the USA [10]. Catalyst markets are divided into three types: petroleum refining catalysts, chemical processing catalysts and emission control catalysts. It is estimated that 35 percent of the global GDP is dependent on catalysis [11,12]. Catalysis has become vital for environmental conservation. Catalysts are used in catalytic converters to change environmentally unfriendly carbon monoxide and nitrogen oxides, emitted from car exhausts, into harmless molecules [13,14]:



Catalysis is becoming increasingly important in the conservation of energy and hence our natural resources. The development of more efficient catalysts will enable industrial processes to operate at lower temperatures thus allowing energy to be saved. Catalysis affects our lifestyles in terms of plastics used, transportation, detergents, food supply and the synthesis of pharmaceuticals. Catalysts are employed in the synthesis of plastics, either in monomer synthesis or in the polymerization process itself [15]. Plastics have a wide array of uses. They can even be used as a substitute for metal. Most modern cars use plastic in their construction ensuring a reduction in weight as well as cost. The manufacture of tyres for motor vehicles is also dependent on catalysis. In addition to this, the efficient conversion of crude oil into high-octane fuels is only possible through catalysis [15]. Catalytically synthesized chemicals make up a variety of surfactants and detergents that are utilized daily. About one hundred and forty million tons of catalytically produced ammonia is used to make agricultural fertilizer annually [16]. Without this synthetic fertilizer the world demand for food would be greater than the supply. It is clear that catalysis is the key to sustainability. Vital chemical products, which might have been prohibitively expensive or unobtainable, are now very accessible.

1.3 Classification of catalysis

Catalysts can be divided into two main types: heterogeneous and homogeneous. In heterogeneous reactions, the catalyst is in a different phase from the reactants. In homogeneous reactions, catalysts are in the same phase as the reactants. A third division of catalysts exists and is called enzyme catalysis.

1.3.1 Enzyme catalysis

Enzymes are protein molecules of colloidal size. They are considered to be in between molecular homogeneous and macroscopic heterogeneous catalysts [3,7]. Enzymes are organic molecules and usually have a metal center. They can catalyze reactions with extremely high selectivities and under very mild conditions. The enzyme *catalase* can decompose H_2O_2 at a rate of 6×10^{26} molecules per second per gram of catalyst [3,7]. For this particular reaction, the enzyme catalyst is about 10^9 times faster than any known inorganic catalyst.

1.3.2 Homogeneous catalysis

Homogeneous catalysis is usually associated with high selectivity. Examples of homogeneous catalysts are transition metal ions, transition metal complexes, inorganic acids and inorganic bases. The main disadvantage of homogeneous catalysis is the difficulty of separating the product from the catalyst. Separation can sometimes be achieved through distillation. Complications arise when the catalyst is unstable at distillation temperatures. **Table 1.1** shows examples of different types of homogeneous catalysis.

| Catalyst | Reactant | Example |
|----------|----------|---|
| Liquid | Liquid | Hydrolysis of esters by acids |
| Vapor | Vapor | Oxidation of SO_2 by NO_2 |
| Solid | Solid | Decomposition of potassium chlorate by MnO_2 |

Table 1.1: Examples of homogeneous catalysis [7]

The market share of homogeneous catalysis is estimated to be about ten to fifteen percent [7]. The Monsanto acetic acid process is possibly one of the most successful examples of a homogeneously catalyzed industrial process [17,18]. This process involves the rhodium and iodide catalyzed carbonylation of methanol to acetic acid. It is estimated that sixty percent of the world production of acetic acid i.e. five million tons per annum, is synthesized in this way [17].

1.3.3 Heterogeneous catalysis

Heterogeneous catalysis is more suitable for large-scale industrial applications than homogeneous catalysis. Transition metals, transition metal oxides, zeolites, silica and alumina are examples of known heterogeneous catalysts. Heterogeneous catalysis can be complex and often is not fully understood. Phase combinations for heterogeneous catalysis are shown below in Table 1.2.

| Catalyst | Reactant | Example |
|----------|--------------|--|
| Liquid | Gas | Polymerization of alkenes catalyzed by H_3PO_4 |
| Solid | Liquid | Decomposition of H_2O_2 catalyzed by gold |
| Solid | Gas | Ammonia synthesis catalyzed by iron |
| Solid | Liquid + gas | Hydrogenation of nitrobenzene catalyzed by palladium |

Table 1.2: Phase combinations for heterogeneous catalysis [19]

Both homogeneous and heterogeneous catalysis have their own unique characteristics and properties. They are not to be regarded as competitors. Table 1.3 below provides a comparison of both types of catalysis:

| | Homogeneous | Heterogeneous |
|-------------------------|---|--|
| Active centers | All metal atoms | Only surface atoms |
| Selectivity | High | Lower |
| Reaction conditions | Mild (50-200 °C) | More severe (often >250 °C) |
| Diffusional problems | Practically absent | Present (mass transfer controlled reactions) |
| Applicability | Limited | Wide |
| Activity loss | Irreversible reaction with products (cluster formation) | Sintering of metal crystallites, poisoning |
| Structure/stoichiometry | Defined | Undefined |
| Thermal stability | Low | High |
| Catalyst separation | Often laborious | Fixed bed: unnecessary |
| Catalyst recycling | Possible | Unnecessary or easy |
| Cost of catalyst lost | High | Low |

Table 1.3: A comparison of homogeneous and heterogeneous catalysis [3]

1.4 Principles and key concepts

1.4.1 Steps in heterogeneous catalysis

Heterogeneous catalyzed reactions are composed of purely chemical and purely physical reaction steps [20]. The following reaction steps are expected for a catalytic gas reaction on a porous catalyst [20, 21]:

1. Transport of reactants to the catalyst:
 - Diffusion of reactants to the external surface of the catalyst (external diffusion)
 - Diffusion of reactants into the pores (internal pore diffusion)
2. Adsorption of the reactants on the catalyst surface
3. Chemical reaction on the catalyst surface
4. Desorption of the products from the catalyst surface
5. Transport of products away from the catalyst:
 - Diffusion of the products out of the pores
 - Diffusion of products away from the catalyst and into the gas-phase

Steps two to four are chemical in nature. Steps one and five are physical processes. Changing the linear velocity of the gas reactants as well as the diameter, density and viscosity of the catalyst particles can alter the rate of external diffusion [21]. Decreasing the radius of catalyst particles or increasing the pore radius can increase internal pore diffusion [21]. Once inside the pores, reactants must be adsorbed onto the catalyst surface. Adsorption refers to the preferential accumulation of molecules (called the adsorbate) at a surface and is different from absorption. Absorption refers to the uptake of one substance by another. Absorption is a bulk phenomenon. Adsorption is a surface phenomenon. Adsorption can be divided into two categories i.e. physical adsorption (physisorption) and chemical adsorption (chemisorption).

Physisorption is associated with relatively weak forces of physical attraction similar to van der Waals forces. Enthalpy changes are usually small, less than 20 kJmol^{-1} [22]. There is no significant redistribution of electron density in the molecule or at the substrate surface [23].

Chemisorption involves the formation of a chemical bond between the adsorbate and a surface. This involves a substantial rearrangement of electron density. Enthalpy change upon chemisorption is in the range of chemical reactions and can be as low as 50 kJmol^{-1} . In 1970 IUPAC listed seven features for recognizing chemisorption at a gas-solid interface [24, 25]:

- The phenomenon is characterized by chemical specificity
- Changes in the electronic state may be detectable by suitable physical methods
- The chemical nature of the adsorbate may be altered by a surface reaction in such a way that chemisorption may not be reversible
- The energy involved in chemisorption is of the same order of magnitude as the energy change in a chemical reaction between a solid and a gas
- The elementary step in chemisorption often involves activation energy
- If the E_A for adsorption is large, true equilibrium may not be achieved
- Adsorbed molecules occupy certain adsorption sites on the surface and only one layer of chemisorbed molecules is formed

A comparison of physisorption and chemisorption is given in Table 1.4 below [20]:

| | Physisorption | Chemisorption |
|--------------------|---|--|
| Cause | Van der Waals forces, no electron transfer | Covalent / electrostatic forces, electron transfer |
| Adsorbents | All solids | Some solids |
| Adsorbates | All gasses below the critical point, intact molecules | Some chemically reactive gasses, dissociation into atoms, ions, radicals |
| Temperature range | Low temperatures | Generally high temperatures |
| Heat of adsorption | Low, always exothermic | Higher, usually exothermic |
| Rate | Very fast | Strongly temperature dependent |
| Activation energy | Low | Generally high |
| Surface coverage | Multi-layers | Mono-layer |
| Reversibility | Highly reversible | Often reversible |
| Applications | Determination of surface area and pore size | Determination of surface concentrations, kinetics, rates of adsorption and desorption, and active centers. |

Table 1.4: Comparison of physisorption and chemisorption [20]

Chemisorption of whole molecules may result in the formation of molecular fragments on a surface and this is the basis for catalytic activity on a surface [26]. Thus, catalysis is always preceded by chemisorption. The specific sites on a catalyst, which describe the locus of catalytic conversion, are called active sites. Taylor first put forward the idea of active sites in 1925 [27]. He observed that only a small amount of carbon monoxide was adsorbed on quartz and this led him to conclude that only a small fraction of the surface was active. Chemisorption takes place preferentially at active sites i.e. on a catalyst surface where atoms are situated at peaks, fissures and other topographical discontinuities [28].

Two mechanisms can arise in a bimolecular surface catalyzed reaction. According to the Langmuir-Hinshelwood mechanism both reacting species are adsorbed onto the catalyst surface in a heterogeneous bimolecular reaction. Examples of this type of mechanism are the oxidation of carbon monoxide on platinum catalysts and the hydrogenation of ethylene on a copper catalyst [20]. The other possibility is given by the Eley-Rideal mechanism, which states that heterogeneous reactions take place between adsorbed molecules on the catalyst surface and molecules in the gas-phase. An example of the Eley-Rideal mechanism is the oxidation of ethylene to ethylene oxide. Here adsorbed molecular oxygen reacts with ethylene from the gas-phase [20]. The Langmuir-Hinshelwood mechanism is more frequently encountered [29].

After adsorption of reactants occurs, a chemical reaction occurs. The final step (step five) in a heterogeneous catalytic reaction involves the desorption of product molecules from the surface of the catalyst. Product molecules diffuse out of the pores and away from the catalyst into the gas-phase. Catalysis requires a balance between adsorption and desorption. A good catalyst must have the ability to adsorb reactants strongly enough to hold and activate them, but not so strongly that the products cannot desorb.

1.4.2 Mass-transport phenomena in a catalyst

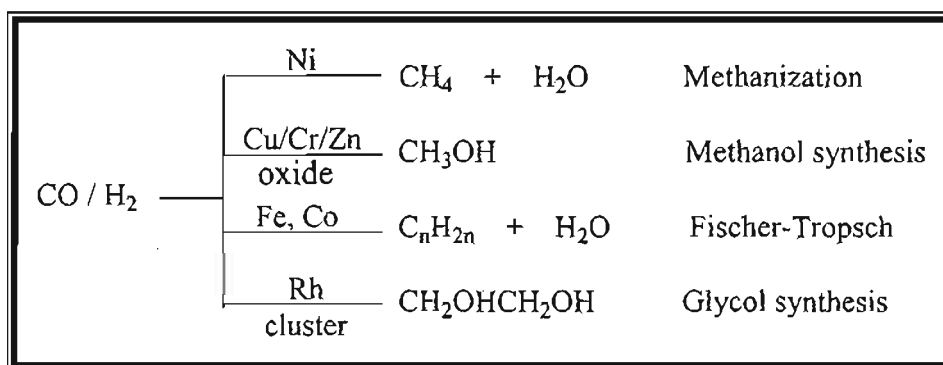
Any one of the five steps discussed in Section 1.4.1 could be the rate-limiting step in a catalytic reaction. The diffusion process whereby reactants are brought to the active sites on the surface of the catalyst (step one) or whereby product molecules move away from the active sites of a catalyst (step five) is known as mass transport or mass transfer. When the rate of any reaction is strongly influenced by the transport of molecules to or away from the catalyst, the reaction is said to be mass-transport limited (diffusion limited). Mass-transport becomes rate limiting when the chemical reactions (steps two to four) are faster than the supply of reactants to the surface and/or the removal of products from the catalyst. Sometimes mass-transport limited reactions are preferred since this can improve the selectivity towards a specific product. Generally this is not the case, as mass-transport influenced reactions imply that the catalyst is not being utilized to its limit. If a catalytic reaction is not mass-transport influenced, then the activity of the catalyst is known as its intrinsic activity.

1.4.3 Selectivity, activity and stability

Three important properties of any catalyst are the activity, selectivity and the stability of the catalyst. Ideally a catalyst should be optimized on the basis of each of these three variables. In reality, this is usually not possible and certain trade-offs have to be made. Often these variables have an inversely proportional relationship. Typically activity increases with temperature, at the same time the stability of the catalyst decreases with temperature. Selectivity can go up or down depending on the product and reaction. Therefore choices have to be made and these choices depend on the demands of any particular process or reaction for which that catalyst will be utilized.

1.4.3.1 Selectivity

Most industrial catalytic processes place most emphasis on selectivity. Selectivity is defined as the ratio of the moles of a particular (usually the desired) product formed to the moles of all products formed or to the moles of reactant converted. It is a measure of the extent to which a catalyst accelerates the reaction to form one or more specified products relative to others. Selectivity varies with temperature, pressure, conversion of reactants, feed composition and with different catalysts. Completely different products can be obtained depending on the catalyst used (Scheme 1) [3]:



Scheme 1: Products from synthesis gas over different catalysts

When comparing selectivities of different catalysts, temperature and conversion or space velocity must be kept constant [3]. Conversion is defined as the fraction of the feed or some component of the feed that is converted to products. Thus percent conversion is:

$$\frac{\text{Moles of feed that react} \times 100}{\text{Moles of feed introduced}}$$

The volume of gas (or liquid) passing through a specified volume of catalyst per unit time is known as the space velocity:

$$\frac{\text{Flow rate (ml / hr)}}{\text{Volume of catalyst (ml)}}$$

The ratio of the number of moles of a specific product formed to the total number of moles of reactant into a reactor is called the yield of that product. Whilst selectivity calculations only considers the amount of reactant consumed; yield is calculated on the basis of the total reactant into the reactor. It is the product of selectivity and conversion:

$$\text{Yield} = \text{Selectivity} \times \text{Conversion}$$

It follows that at total conversion, the selectivity of a product will be equal to its yield.

1.4.3.2 Activity

The activity of a catalyst is the rate at which it causes a reaction to proceed towards equilibrium. The following activity measurements can be used for activity comparison [3]:

- Conversion under constant reaction conditions
- Space velocity at constant conversions
- Space-time yield
- Temperature required for a specific conversion

The quantity space-time yield is the amount of product made in a reactor per unit time and per unit of reactor volume. The performance of reactors of different size and construction can be compared in this way. When measuring the temperature required for a specific conversion, the best catalyst is the one that gives the desired conversion at a lower temperature. This method can sometimes result in misinterpretations as the kinetics of a reaction sometimes change at higher temperatures [3,28]. It is frequently used to carry out deactivation measurements on catalysts in pilot plants [3].

1.4.3.3 Stability

The activity or the lifetime of a catalyst is dependent on its mechanical, physical and chemical stability under operating conditions. Any process that decreases the activity of a catalytic surface is called deactivation. Mechanical deactivation results from physical breakage or attrition of catalyst particles. Physical deactivation can occur through sintering or agglomeration of metal crystallites in supported metal catalysts. Sintering causes loss of surface area due to growth of particles and this process is irreversible. Physical loss of catalytically active ingredients also results in loss of activity. Here, metals in the catalyst vaporize slowly as a result of high temperatures and oxidizing atmospheres. An example of this is the Ostwald process (oxidation of ammonia) [31].

Chemical deactivation occurs through poisoning or fouling. A catalyst poison is an impurity present in the feed stream that gradually reduces catalytic activity. Poisons are usually strongly chemisorbed on active sites and this results in the restricted access of reactant molecules to the surface. Poisons may also exhibit an electronic effect in which bond strength of an adsorbed reactant or product molecule is altered [32]. Sulphur is a well-known poison. Fouling is the loss of catalytic activity due to the formation of coke on the surface of the catalyst. Coke refers to fine carbonaceous deposits produced by organic reactions. The mechanisms of coke formation are complex and not well understood. Burning off the coke in air can sometimes regenerate a coked catalyst. This regeneration process can be built into a process and the heat produced by regenerating spent catalysts can be utilized for an endothermic reaction within that process.

General regeneration methods include: oxidation, reduction, exposure to high temperatures to decompose or desorb poisons and chemical treatment such as treatment of the catalyst with dilute acid. If the deactivated catalyst cannot be regenerated, it has to be disposed in an environmentally friendly manner. Sometimes it can be economical to recover components from the catalyst. This is especially the case if the catalyst contains precious metals [31].

1.4.4 Promoters

A promoter is any substance that is added to a catalyst to enhance its activity, selectivity or stability. They are usually added in relatively small amounts. They can be incorporated into the catalyst at any step in its synthesis and in some cases promoters are added during the course of the reaction [33]. There are four types of promoters [34]:

1. **Structural promoters:** These promoters are directly involved in the solid-state reaction of the active metal surface. Structural promoters can result in favouring of a specific reaction pathway by influencing the catalyst surface.
2. **Electronic promoters:** Alters the chemical binding strength of reactants, intermediates and products.
3. **Textural promoters:** Prevents the coalescence of catalytically active particles thereby impeding loss of active surface. They act by a physical effect. Textural promoters are smaller in particle size, than the active species and they are very well dispersed.
4. **Catalyst-poison-resistant promoters:** These promoters protect the active sites against poisoning by impurities, either from an impure feed or from a poison formed in a side reaction.

Very few promoters are discovered by systematic research. Most promoters are discovered serendipitously [34]. Examples of promoters used commercially are given in **Table 1.5** below:

| Catalyst (use) | Promoters | Function |
|---|--------------------------------|--|
| Al ₂ O ₃ (support and catalyst.) | SiO ₂ | Increases thermal stability |
| | MgO | Slows sintering of active components |
| | HCl | Increases acidity |
| Fe ₃ O ₄ (NH ₃ synthesis) | K ₂ O | Electron donor, favours N ₂ dissociation |
| | Al ₂ O ₃ | Structural promoter |
| Ag (epoxide synthesis) | Alkali metals | Increases selectivity, hinders crystal growth, stabilizes certain oxidation states |
| Ni / ceramic support (steam reforming) | K | Improved coke removal |

Table 1.5: Examples of promoters in the chemical industry [34]

1.5 References

1. Boudart, M., *Perspectives in Catalysis*, Blackwell, Oxford, 1992, p. 183.
2. Ertl, G., Knozinger, H. and Weitkamp, J., *Handbook of Heterogeneous Catalysis*, Wiley-VCH, Federal Republic of Germany, Vol. 1, 1997, p. 1.
3. Hagen, J., *Industrial Catalysis – A Practical Approach*, Wiley-VCH, Federal Republic of Germany, 1999, pp. 1-11.
4. http://www.uyseg.org/catalysis/pages/catalyst_frames.htm (Accessed: before June 2005)
5. Levine, I. N., *Physical Chemistry*, McGraw-Hill Inc., New York, 1988, pp. 447-450.
6. Atkins, P. W., *Physical Chemistry*, Oxford University Press, Oxford, 1982, pp. 12-15.
7. Richardson, J. T., *Principles of Catalyst Development*, Plenum Press, New York, 1989, pp. 2-8.
8. Srivastava, R. D., *Heterogeneous Catalytic Science*, CRC Press, Florida, 1988, p. 1.
9. Fink, U., Hajduk, F. and Yoneyama, M., *Catalysts*, SRI Consulting Report, 2004, p. 155.
10. <http://www.science.doe.gov/bes/CRA15.pdf> (Accessed: before June 2005)
11. <http://www.iac.org.uk> (Accessed: before June 2005)
12. <http://www.acs.org> (Accessed: before June 2005)
13. <http://www.mysite.freemove.com/chemsheets2/AS303.doc> (Accessed: before June 2005)
14. <http://www.uvm.edu/~swgordon/131-01/131web/amandaclark/equations.html> (Accessed: before June 2005)
15. Leach, B. E., *Applied Industrial Catalysis*, Academic Press, Inc., New York, 1983, Vol. 1, pp. 20-29.
16. Thomas, J. M. and Thomas W. J., *Principles and Practice of Heterogeneous Catalysis*, VCH Publishers Inc., New York, 1997, p. 1.
17. Maitlis, P. M., Haynes, A., Sunley, G. J. and Howard, J., *J. Chem. Soc., Dalton Trans.*, 1996, 2187.
18. Forster, D., *Adv. Organomet. Chem.*, **17**, 1979, 255.
19. Bond, G. C., *Heterogeneous Catalysis: Principles and Applications*, Oxford University Press, Oxford, 1987, p. 8.
20. Hagen, J., *Industrial Catalysis – A Practical Approach*, Wiley-VCH, Federal Republic of Germany, 1999, pp. 83-98.
21. Richardson, J. T., *Principles of Catalyst Development*, Plenum Press, New York, 1989, pp. 11-15.
22. Laidler, K. J. and Meiser, J. H., *Physical Chemistry*, Houghton Mifflin Company, New York, 1999, p. 846.

23. http://www.chem.qmw.ac.uk/surfaces/scc/scat2_2.htm (Accessed: 01/10/2006)
24. Robertson, A. J. B., *Catalysis in Chemistry*, Methuen Educational Ltd., London, 1972, p. 24.
25. http://www.iupac.org/reports/2001/colloid_2001/manual_of_s_and_t/node16.htm (Accessed: 01/10/2006)
26. Atkins, P. W., *Physical Chemistry*, Oxford University Press, Oxford, 1982, p. 26.
27. Taylor, H. S., *Proc. Roy. Soc.* A108, 1925, p. 105.
28. Thomas, J. M. and Thomas W. J., *Principles and Practice of Heterogeneous Catalysis*, VCH Publishers Inc., New York, 1997, pp. 29-31.
29. Thomas, J. M. and Thomas W. J., *Principles and Practice of Heterogeneous Catalysis*, VCH Publishers Inc., New York, 1997, p. 65.
30. Bond, G. C., *Heterogeneous Catalysis: Principles and Applications*, Oxford University Press, Oxford, 1987, p. 59.
31. Ertl, G., Knozinger, H. and Weitkamp, J., *Handbook of Heterogeneous Catalysis*, Wiley-VCH, Federal Republic of Germany, Vol. 1, 1997, p. 9.
32. Anderson, J. R. and Boudart, M., *Catalysis – Science and Technology*, Springer – Verlag, Berlin, Vol. 6, 1984, pp 2-4.
33. Wijngaarden, R. J., Kronberg, A. and Westerterp, K. R., *Industrial Catalysis*, Wiley – VCH, New York, 1998, p 29.
34. Hagen, J., *Industrial Catalysis – A Practical Approach*, Wiley-VCH, Federal Republic of Germany, 1999, pp. 174-175.

CHAPTER 2: Selective Hydrocarbon Oxidation

2.1 Introduction

Selective hydrocarbon oxidation or partial oxidation involves the breaking of a limited number of carbon-carbon or carbon-hydrogen bonds with oxygen. In this way, relatively cheap feedstocks can be upgraded into more valuable chemical products. Selective oxidation implies that a desired product or products are favoured over undesired ones. Undesired products include the thermodynamically favoured total oxidation products, carbon monoxide and carbon dioxide. Interest in selective oxidation of organic compounds, in particular hydrocarbons, has steadily grown in recent years. These reactions are the basis for several industrial processes [1]. More than sixty percent of the chemicals and intermediates synthesized via catalytic processes are products of oxidation [2]. Between two hundred and two hundred and fifty million US dollars are spent on oxidation catalysts annually [3]. More than half of these catalysts are used in Europe. Western Europe produces approximately fifty million tons of organic chemicals and at least ninety percent of these chemicals are produced by selective oxidation [2,4]. Globally, it has been estimated that up to forty billion US dollars worth of organic chemical products are produced annually by selective oxidation [2,4].

Several monomers, which are essential precursors or additives in the polymer and plastic industries, are derived from selective catalytic hydrocarbon oxidation processes. Tables 2.1 and 2.2 list some of the monomers that are derived from homogeneous and heterogeneous catalytic aerial oxidation processes respectively [5].

| Reactants | Product | Conversion (%) | Selectivity (%) | Principal Use |
|----------------------|-------------------|----------------|-----------------|--------------------------|
| Cumene | Phenol / acetone | 35-40 | 90 | Solvents, paints, resins |
| <i>p</i> -Xylene | Terephthalic acid | 90 | 85-95 | Polyester fibres |
| Ethene / acetic acid | Vinyl acetate | 20-35 | 98-99 | Solvents, plastics |
| Cyclohexane | Cyclohexanone | 5-15 | 85-90 | Adipic acid synthesis |

Table 2.1: Monomers derived from homogeneous catalytic aerial oxidation processes [5]

| Reactants | Product | Conversion (%) | Selectivity (%) | Principal Use |
|---------------------|--------------------|----------------|-----------------|--|
| Methanol | Formaldehyde | 99 | 94 | Thermoplastic resins |
| <i>n</i> -Butane | Maleic anhydride | 70-80 | 65-70 | Unsaturated polyester resins |
| Benzene | Maleic anhydride | 98 | 75 | |
| <i>o</i> -xylene | Phthalic anhydride | 98 | 75 | Plasticisers |
| Naphthalene | Phthalic anhydride | 100 | 79 | |
| Propene/ ammonia | Acrylonitrile | 97-99 | 73-82 | Acrylic fibres |
| Propene | Acrolein | >90 | 80-85 | Animal foods, allyl alcohol |
| Acrolein | Acrylic acid | >95 | 90-95 | Polyacrylate, methacrylate esters |
| Isobutene | Methacrolein | >97 | 85-90 | Methacrylic acid synthesis |
| Methacrolein | Methacrylic acid | 70-75 | 80-90 | Methacrylate esters |
| Ethene | Ethene oxide | 90 | 80 | Anti-freeze solvents, polyester fibres |
| Ethene / HCl | 1,2-Dichloroethane | >95 | >95 | Solvents for paints, resins |

Table 2.2: Monomers derived from heterogeneous catalytic aerial oxidation processes [5]

In industry, heterogeneous oxidation catalysis is desirable because of the ease of separation of reactants and products from the catalyst. Several heterogeneous paraffin oxidation processes, which are currently under research and development, are shown in Table 2.3 [6,7]. Many catalysts, which show good catalytic performance in terms of both activity and selectivity towards desired products, still remain to be developed to the level where such processes can become industrially viable.

| Raw material | Product | Stage of development |
|-------------------|--|---|
| Methane | Methanol Syngas Ethylene | Pilot plant Industrial Pilot plant |
| Ethane | Vinyl chloride Acetaldehyde Acetic acid Ethylene | Pilot plant Research Research Research |
| Propane | Acrolein, acrylic acid Propyl alcohol Acrylonitrile Propylene | Research Research Demonstration plant Research |
| <i>n</i> -Butane | Acetic acid | Industrial |
| Isobutane | Methacrylic acid Isobutene | Pilot plant Research |
| <i>n</i> -Pentane | Phthalic anhydride | Research |
| Cyclohexane | Cyclohexanone | Research |

Table 2.3: Processes under study or development for the oxidative transformation of paraffins [6,7].

There are three key types of reactions for selective paraffin catalytic oxidation:

1. The oxidative removal of hydrogen (oxidative dehydrogenation reactions).
2. The introduction of oxygen as a functional group (oxygen insertion reactions).
3. The formation of nitriles through oxidative coupling with ammonia (ammoxidation).

The catalytic synthesis of maleic anhydride from butane is a well-known and well-studied oxygen insertion reaction. It is the only industrial application of selective paraffin oxidation by a heterogeneous gas-solid catalytic process [8]. This reaction involves a fourteen electron oxidation, abstraction of eight hydrogen atoms and the insertion of three oxygen atoms. The direct conversion of propane to acrylonitrile with ammonia and oxygen is an example of an ammoxidation reaction. The development of this reaction is at the pilot-plant stage and its potential for commercialization is very promising [1,9]. In oxidative dehydrogenation reactions, paraffins are converted to olefins usually with air or oxygen. The production of water as a byproduct provides the thermodynamic driving force for the process and allows the dehydrogenation reaction to be carried out at a lower temperature than in the absence of oxygen. Paraffin oxidative dehydrogenation catalysis will form the principal focus of this chapter and is indeed, the basis of this thesis.

2.2 The use of paraffins as feedstocks

Olefins and aromatics are currently the most important feedstocks in the petrochemical industry [5]. These feedstocks are mainly derived from steam cracking of naphtha and fluidized catalytic cracking in oil refining. In South Africa, Sasol's Fischer-Tropsch processes produce substantial amounts of olefins and aromatics [10]. Nevertheless, the demands for these feedstocks are increasing and it is this increasing demand, which warrants research into alternate sources of feedstocks. The vast amounts of easily available and cheap paraffins make them prime substitutes for olefinic and aromatic feedstocks. But paraffins have the potential to be more than mere substitutes for olefinic and aromatic feedstocks. The utilization of paraffins as feedstocks can facilitate lower environmental impact processes and lower cost processes. Paraffins are much easier to store and use as feeds than olefins and many toxic aromatics.

Sixty percent of the cost of producing an oxidation product is attributed to the raw materials used [3]. Therefore paraffin oxidation processes would be extremely cost effective. In addition to this, using paraffins as feedstocks can lead to process simplification. There is potential to replace multi-step processes resulting in reduced or even single step processes. This would have significant benefits such as lower capital investments as well as lower operating expenses. The potential of paraffins in catalytic oxidation has been realized by the selective oxidation of *n*-butane to maleic anhydride. The use of butene as a feed for this process was abandoned because of the many byproducts and the lower selectivity to maleic anhydride than that obtained with butane [3]. In contrast *n*-butane oxidation is a clean oxidation, producing only traces of acetic acid and carbon oxides [11].

Paraffins are easily obtained from natural gas and petroleum. Considerable amounts of *n*-paraffins are also produced by Fischer-Tropsch processes [10]. The strategic use of paraffins to produce and replace olefins and aromatics will confer greater stability and economic profitability on a global chemical industry.

2.3 Choice of oxidant

Table 2.4 below characterizes commonly used oxidizing agents [2]:

| Donor oxidant | % Active Oxygen | By-product | Comment |
|---|-----------------|-----------------------------------|--|
| O ₂ | 100 | None | Nonradical chain aerobic oxygenation can be achieved |
| H ₂ O ₂ | 47 | H ₂ O | Environmentally attractive, can be relatively expensive |
| O ₃ | 33 | O ₂ | Attractive if generated <i>in situ</i> |
| NaClO | 21.6 | NaCl | Inorganic salt byproducts are usually avoided, toxic byproducts |
| <i>t</i> -BuOOH | 17.8 | <i>t</i> -BuOH | Commercially important in catalyzed oxygenations |
| C ₅ H ₁₁ NO ₂ (NMO) | 13.7 | C ₅ H ₁₁ NO | Not commercially suitable |
| KHSO ₅ | 10.5 | KHSO ₄ | Generates a marginally toxic salt |
| C ₆ H ₅ IO | 7.3 | C ₆ H ₅ I | Metal catalyzed oxidations are selective but cost is prohibitive |

Table 2.4: Commonly used oxidants [2]

In addition to these oxidants, SO₂, CO₂ [13,14], and N₂O have been proposed as gas-phase oxidizing agents for paraffin activation [15-20]. A good oxidant must be capable of activating paraffins under relatively mild conditions thereby limiting undesired consecutive reactions, which become prominent with more severe conditions. A very active but selective oxidizing species is required. Molecular oxygen still remains the most desired gas-phase oxidant due to its low price and the absence of environmental problems [2,21]. An increasingly important oxidant, which has much potential, is N₂O. It has been successfully used to provide a controlled source of highly reactive oxygen. Selective dehydrogenation of ethane was accomplished over a silica-supported molybdenum catalyst at 400 °C [15,16]. N₂O has also been used to selectively oxidize methane to methanol and formaldehyde over supported molybdenum and vanadium catalysts [18-20]. N₂O is a co-product in the industrial synthesis of adipic acid. For every mole of adipic acid produced, one mole of N₂O is co-produced. Since N₂O is known to be a potent greenhouse gas, the use of adventitious N₂O as an oxidant would be beneficial from an environmental perspective [22].

2.3.1 Air versus oxygen processes

It has been suggested that in the near future, most industrial processes will be changed from air-based to oxygen-based [23]. Oxygen-based processes can have improved performance, better process economics and reduced environmental impact. Process streams containing lower volumes of inert gas (nitrogen) require smaller equipment for product recovery and purification. According to Centi *et al.* [23] a lower content of nitrogen, a ballast with very poor thermal conduction properties, can allow for better control of the temperature profile in the presence of strongly exothermic reactions.

The main problem of an oxygen-based process is safety. The formation of flammable or explosive mixtures is more likely to occur than in the corresponding air-based process. Careful reactor design and the inclusion of safety valves and membranes to minimize the consequences of an explosion are critical requirements for all oxygen-based processes.

2.4 Limits of flammability (Explosive limits)

Knowledge of the limits of flammability or explosive limits for paraffin / oxidant mixtures is imperative for safe operation in paraffin oxidation catalysis. The flammability range describes the concentration range of organic combustible substances in air or any other oxidizing agent in which fire or even explosions may occur. This range is dependent on both temperature and pressure. Oxidation of paraffins in air is usually carried out above or below the explosive limits. Below the lower explosive limit (LEL) oxygen is in excess (oxidizing atmosphere). Above the upper explosive limit (UEL) there is limited amount of oxygen available (reducing atmosphere). Any paraffin / air feed with a concentration between the LEL and UEL may lead to an explosion. Operation of oxidation processes within the explosive limits is becoming possible through careful reactor design and proper safety precautions [23].

2.5 Oxidative dehydrogenation of paraffins

The oxidative dehydrogenation of paraffins to olefins and aromatics has much potential to change the way in which many important organic chemicals are manufactured. The increasing demand for olefins has stimulated considerable research into this new technology. The increased use of olefins in the polymer industry and a relative decrease in their production, arising from changes in operating conditions in steam and catalytic cracking units, accounts for their global shortage [24]. Catalytic paraffin dehydrogenation for the production of olefins has been in commercial use since the late 1930's. Catalytic dehydrogenation is considered to be a relatively mature and well-established technology, whilst oxidative dehydrogenation is regarded as being in its infancy [14].

2.5.1 Oxidative dehydrogenation versus dehydrogenation

Catalytic dehydrogenation of paraffins operates commercially through processes such as UOP's (Universal Oil Products) Oleflex™ and Pacol™, Lummus Catofin™, Snamprogetti-Yarsintez fluidized bed dehydrogenation, Phillips STAR™ and Linde™-BASF. These processes use platinum-based or chromium-based catalysts. The performance of two UOP processes are shown in Table 2.5 below [14,25]:

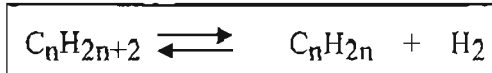
| Process | Description | Feed | Conversion (%) | Olefin Selectivity (%) |
|----------|--|--|----------------|------------------------|
| Oleflex™ | Catalytic dehydrogenation technology for production of light olefins from paraffins | Propane | 40 | 90 |
| | | <i>n</i> -Butane | 50 | 85 |
| | | <i>iso</i> -butane | 50 | 92 |
| Pacol™ | Dehydrogenates <i>n</i> -paraffins in a vapor phase reaction to corresponding mono-olefins | <i>n</i> -Heptane | 20 | 90 |
| | | <i>n</i> -C ₁₀ -C ₁₃ | 13 | 90 |
| | | <i>n</i> -C ₁₁ -C ₁₄ | 13 | 90 |

Table 2.5: Performance of UOP's Pacol™ and Oleflex™ dehydrogenation processes [14]

In 2002 there were ten Oleflex™ process units in operation and an additional unit was under construction [14]. Approximately one million metric tons per annum of propylene and over two million metric tons of isobutylene were produced by these units [14]. Linear mono-olefins produced by the Pacol™ process are largely used to manufacture linear alkylbenzenes, which are used as detergents.

Catalytic dehydrogenation processes have several limitations [24]:

- Reactions are thermodynamically restricted
- Thermal cracking is a significant side reaction
- Difficulty in separation of paraffins, olefins and by-products
- Strongly endothermic reaction is energy intensive
- Short catalyst lifespan necessitates frequent regeneration
- Harsh reaction conditions may render catalyst irreversibly deactivated.



The thermodynamics of the above reaction are such that the paraffin is favoured by the equilibrium at relatively low temperatures and at atmospheric pressure [21,26]. The equilibrium constants for *n*-paraffin dehydrogenation at 500 °C are shown in Figure 2.1 below. The temperatures required to achieve ten and forty percent conversion of *n*-paraffins at one atmospheric pressure are shown in Figure 2.2 [14].

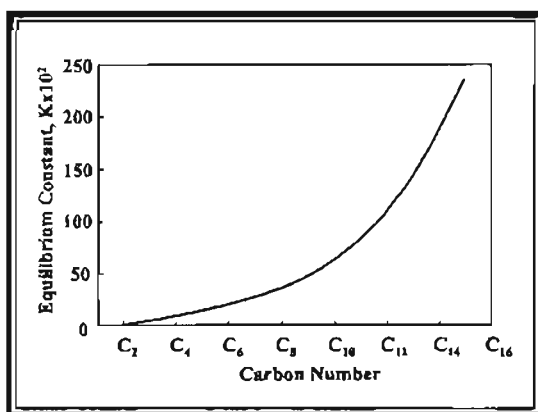


Figure 2.1: Equilibrium constants for *n*-paraffin dehydrogenation at 500 °C [14].

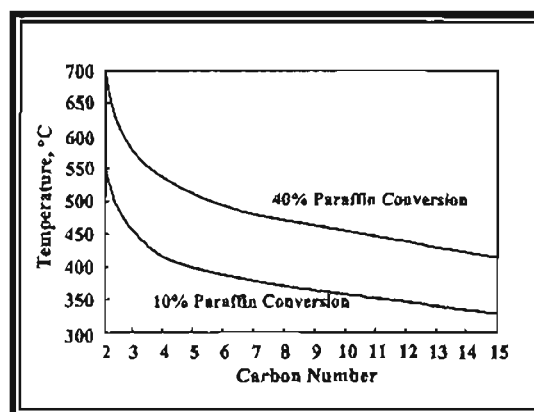


Figure 2.2: Temperatures for 10 and 40% conversion of C₂-C₁₅ *n*-paraffins at 1 atm [14]

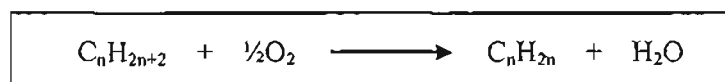
Paraffin dehydrogenation reactions are strongly endothermic. From Figures 2.1. and 2.2, it can be seen that reaction conditions become more severe with decreasing carbon chain lengths. Ethane dehydrogenation is the least thermodynamically favoured reaction.

The use of high temperatures to increase the equilibrium conversion in catalytic dehydrogenation results in an increase of side reactions such as paraffin cracking. Coke formation and catalyst deactivation is also accelerated. Coke formation can be a very serious problem, requiring frequent catalyst regeneration. Regeneration may even be required after only minutes of operation [14,28]. Catalysts are regenerated by burning the coke off with oxygen and the heat produced by this reaction can be incorporated into the dehydrogenation process. Nevertheless, additional energy is also required. Although deactivation by coking may be reversible, some catalysts may become irreversibly deactivated by the severe reaction conditions of dehydrogenation processes.

There are four lines of research to overcome these limitations [24]:

1. Development of catalysts with better selectivity and greater resistance to deactivation
2. Oxygen-assisted dehydrogenation i.e. coupling of dehydrogenation (endothermic) with hydrogen oxidation (exothermic)
3. Use of catalytic membranes to remove hydrogen and hence shift the equilibrium towards product formation
4. Oxidative dehydrogenation.

In oxygen assisted dehydrogenation, deactivation through coking is still a problem. It is also difficult to find a hydrogen oxidation catalyst over which all products and reactants are stable. The use of catalytic membranes in dehydrogenation is unfavourable due to the costs of these membranes. Oxidative dehydrogenation is regarded as the leading pathway to overcome the limitations of catalytic dehydrogenation [14]. In this reaction, oxygen reacts directly with the paraffin molecule on the surface of a catalyst.



The products of oxidative dehydrogenation reactions are olefins and water. The formation of water makes this reaction very thermodynamically favourable. In principle, almost complete conversion can occur even at low temperatures and high pressures, and this can have considerable advantages from an economic and process engineering point of view [21].

Oxidative dehydrogenation reactions are exothermic and they can be carried out at lower temperatures than dehydrogenation reactions. Thus the formation of coke and cracked products is relatively insignificant [21,26]. Frequent catalyst regeneration is not required in oxidative dehydrogenation. Oxygen may also help to remove any coke or its precursors which may form during the reaction [28].

The main limitation of oxidative dehydrogenation of paraffins is selectivity. Carbon dioxide and carbon monoxide are the most thermodynamically stable products. Suitable catalysts must therefore be found which are capable of minimizing total oxidation products. A secondary limitation of oxidative dehydrogenation involves reactor operation. These reactions are highly exothermic and special care is required during operation to prevent the possibility of reaction runaway. Another secondary limitation concerns the feed composition. Certain feed compositions may be explosive. Safe feed compositions may not yield optimal productivity. Specially developed reactor configurations such as the fluidized-bed reactor may allow for operation within the explosion limits. Here the continuous movement of catalyst mass efficiently inhibits radical chain propagation [24]. Even so, safety is still an issue here, especially in the case of a malfunction.

Notwithstanding safety issues, selectivity problems and the economics of losing hydrogen as a by-product, oxidative dehydrogenation is regarded as more promising than dehydrogenation [21]. It is expected that capital and operation efficiencies would be gained by eliminating the need for a furnace and for decoking shutdowns, lowering operating temperatures, lessening material demands and conducting less maintenance operations [29]. Its outlook for development on an industrial scale is thus viewed as having much potential [24].

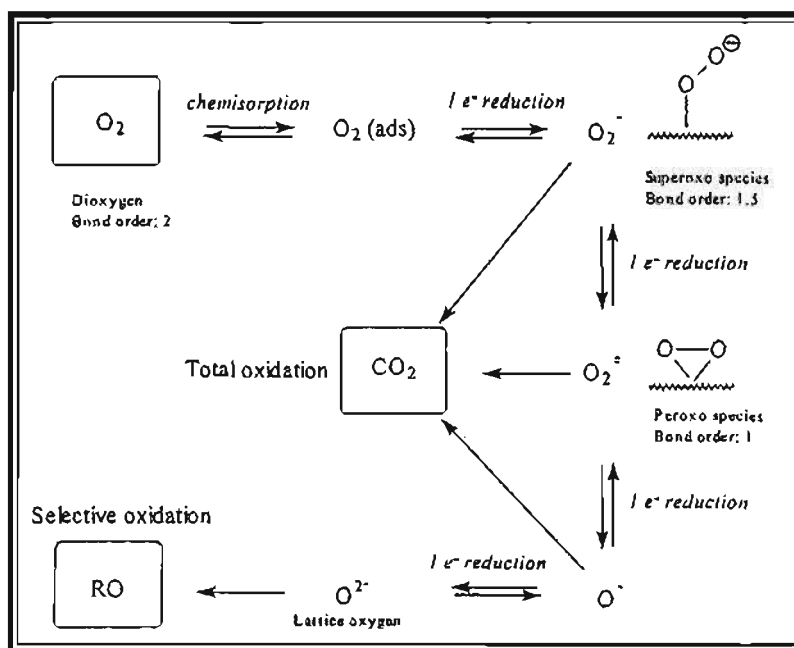
2.5.2 Catalytic systems used for oxidative dehydrogenation

Catalysts containing either vanadium or nickel oxides or both have been reported to give the highest yields to oxidatively dehydrogenated products [21]. Unsupported vanadium pentoxide, vanadia supported on silica, alumina or titania and nickel molybdates have been extensively researched on lower paraffins [21,26].

2.6 Theory of oxidation catalysis

2.6.1 Oxygen activation in oxidation catalysis

Gas-phase oxygen is activated by interacting with the surface of an oxide catalyst. Adsorbed oxygen can exist in different forms on the oxide surface i.e. molecular, atomic, neutral or charged. Once adsorbed onto the surface, oxygen can accept electrons one by one going in succession all the way to the fully reduced form, i.e. O^{2-} (Scheme 2.1) [30]:



Scheme 2.1: Oxygen atoms / ions responsible for oxidation [31]

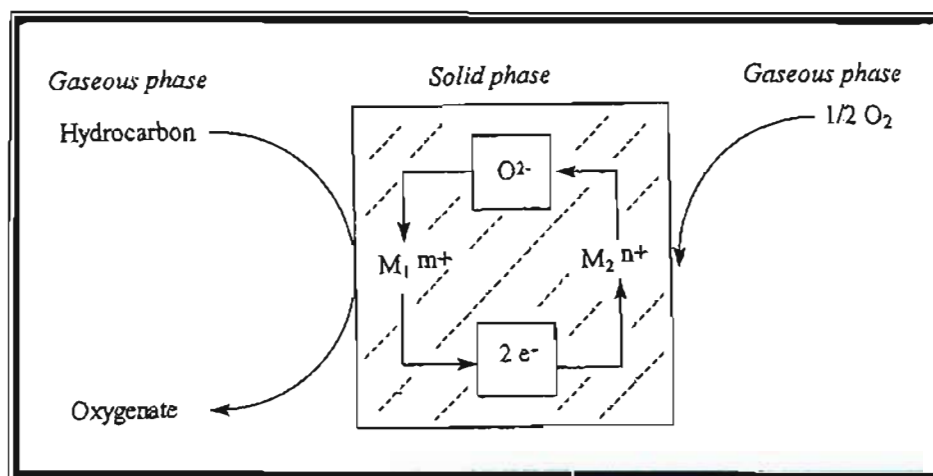
The state of oxygen on the catalyst surface is of great importance in oxidation catalysis [32]. Adsorbed oxygen can be classified into two types, electrophilic or nucleophilic, which differ in reactivity. Electrophilic oxygen species such as O^{\cdot} (oxide), $O_2^{\cdot -}$ (superoxide) and O_2^{2-} (peroxide) are thought to be responsible for total oxidation. These species are electron deficient and attack the electron-rich regions of olefins (π bonds) resulting in carbon oxide formation [21,30]. Nucleophilic oxygen (O^{2-}) or lattice oxygen is believed to be involved in partial oxidation [21,30-32]. Partial oxidation catalysts can serve as a source of active oxygen, for a limited time, in the absence of oxygen in the gas-phase [32]. They are high electron density species and therefore prefer to react with electron-poor molecular sites [21]. It is therefore believed that selectivity can be controlled by the ratio of the rate of primary oxygen activation to the rate of its subsequent incorporation into the lattice of the catalyst [30]. No conclusive proof regarding the active oxygen species is possible due to the rapid interconversion of oxygen species.

The main parameter determining oxygen reactivity on the catalyst is the energy of oxygen binding with the catalyst [32]. Oxygen binding energy can be correlated with the rate of catalytic oxidation. Total oxidation is favoured by weak oxygen binding to the catalyst. Therefore selective oxidation catalysts should have a limited amount or no weakly bound oxygen on the surface.

The optimal density of active oxygen is also an important concept [33]. The active site must not contain too many or too few oxygen ions that can participate in the reaction. Too many would lead to excessive oxidation, whilst too few would lead to an inactive catalyst.

2.6.2 Mars and van Krevelen mechanism

In many cases, the catalytic properties in oxidation reactions involve a redox mechanism between the reactant and the active sites on the surface. This mechanism is known as the Mars and van Krevelen mechanism (Scheme 2.2) [34]:



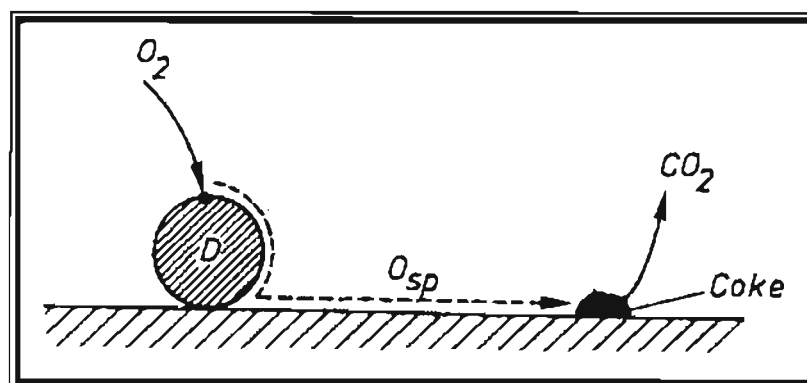
Scheme 2.2: The mechanism proposed by Mars and van Krevelen [34]

This mechanism requires that a catalyst contain a viable redox couple (M_1 and M_2) at the operating temperature. This is possible with transition metal ions present in the catalyst. In addition to this, the catalyst must exhibit high electrical conductivity to favour electron transfer. Furthermore, there must be high lattice oxygen anion mobility within the catalyst to ensure the reoxidation of the catalyst. According to this mechanism, the substrate is oxidized by a solid catalyst and not directly by molecular oxygen from the gas-phase. The role of molecular oxygen is to regenerate or maintain the oxidized state of the catalyst. The oxygen

species used to activate or oxidize a substrate, such as a paraffin, originates from the lattice of the catalyst and has an oxidation state of -2 . In oxidative dehydrogenation reactions, it is the lattice oxygen which is used to form water molecules. This Mars and van Krevelen mechanism involves the presence of two distinct active sites: an active cationic site that oxidizes the substrate and another site active for oxygen reduction [34].

2.6.3 Phase co-operation in selective oxidation catalysts

Oxidation catalysts usually contain two or more oxide phases. Experimental results indicate that there is a definite co-operation or synergy between two distinctly separate phases in working oxidation catalysts [35]. It has been proposed that the synergy is usually due to a remote control effect [35]. According to this mechanism, one phase (the donor) dissociates oxygen to form a surface mobile species which spills over to the other phase (the acceptor). The acceptor is the potentially active phase. This phase needs to be constantly replenished by spill-over oxygen to exhibit maximum activity and selectivity. Furthermore, the spill-over oxygen maintains the acceptor phase in a high oxidation state, preventing the destruction of the active sites and inhibiting the formation of carbonaceous deposits. The latter effect is one of the most important effects of spill-over in catalysis (Scheme 2.3) [25]. It has been shown that spill-over oxygen can remove coke more efficiently than molecular oxygen [35].



Scheme 2.3: Schematic representation of spill-over oxygen burning out deposited coke [35]

The role of spill-over oxygen as a direct reactant is considered to be minor [36]. The interpretation of the co-operation between phases has enabled definite roles to be attributed to the oxide phases present in a catalyst [35].

2.6.4 Paraffin activation and the role of acid-base properties in catalytic oxidation

The acid-base characteristics of an oxide catalyst can influence the behaviour of the catalyst in two important ways:

- i) It influences the activation of the hydrocarbon
- ii) It influences the rate of adsorption and desorption of reactants and products

The effect of acid-base catalyst properties on the activation of paraffins is reaction specific [37]. The ODH of propane is considered as it is one of the most studied reactions in paraffin oxidation.

The selective activation and functionalization of propane is difficult due to its low reactivity. The bonds present in propane are resistant to chemical attack. Propane is characterized by the absence of empty orbitals and low polarity carbon–hydrogen bonds [21]. Functionalized products will possess bonds which will be more reactive i.e. π bonds and polarized bonds. Products of oxidation reactions are usually two to three orders of magnitude higher in reactivity than the starting paraffin [3]. For high selectivities, catalysts with special properties are therefore required. It is important that these catalysts activate paraffins at low temperatures due to the high reactivity of products, such as olefins, at elevated temperatures.

The oxidation of a propane molecule must begin with the activation of a carbon–hydrogen bond. The breaking of the first carbon-hydrogen bond, leading to a propyl species, is considered to be the rate-determining step [21,32,37]. Different authors disagree on how the propyl species is formed. Some believe that breaking of the carbon–hydrogen bond is homolytic resulting in the formation of a propyl radical [21,37,38]. This radical species can be converted into propene either by desorbing into the gas phase and reacting with oxygen or propane or the propyl species can convert *via* a surface reaction. Low temperatures and reducible catalysts will promote the surface reaction route. It is believed that the hydroxyl species created in the first hydrogen abstraction step is responsible for the second hydrogen abstraction leading to the formation of water [37].

Other authors believe that the activation of propane involves the heterolytic splitting of the carbon–hydrogen bond resulting in the formation of a carbocation by hydride abstraction or a carbanion by proton abstraction [21,38,39]. The formation of carbocations by hydride abstraction is believed to occur on strong acid catalysts. Matsuura *et al.* [40] have reported that Nb_2O_5 , which has strong acidic sites, is responsible for hydride abstraction from

isobutane forming the $(\text{CH}_3)_3\text{C}^+$ ion. Busca *et al.* [39] claim that strong Lewis acid sites provided by V^{4+} ions are capable of abstracting a hydride ion from *n*-butane forming a V-H bond. The formation of carbanions by proton abstraction is believed to occur on strong basic catalysts. Pantazidis *et al.* [41] suggest that basic sites on the surface of a zinc vanadium catalyst improve catalytic activity by promoting proton abstraction from propane molecules.

Although the mechanisms of paraffin activation are still being disputed, it must be understood that any proposed mechanism may be valid for specific reactions. Usually, heterolytic breaking of the carbon-hydrogen bond is preferable, since the radical sites needed for homolytic activation may cause also the appearance of radical oxygen species, which lead mainly to total oxidation [32,38].

The strength of Lewis acid and base sites on a catalyst will also determine the strength of the interaction of the products with the surface and in this way affects selectivity [42]. An oxidation product possessing strong acidic properties would be strongly adsorbed by a basic catalyst and this interaction would increase the probability of the product being completely oxidized to carbon oxides. Thus use of an acidic catalyst would favour desorption of an acidic product, thereby resulting in enhanced selectivity. Similarly, catalysts with basic surfaces will favour the desorption of basic products e.g. olefins and thereby reduce the conversion of such products *via* consecutive pathways. However, acid–base sites are responsible for paraffin activation. Therefore a balance between acid and base sites present on the surface of a catalyst is required for optimal productivity of that catalyst.

2.6.5 The dynamic state of oxide surfaces

It is mostly accepted that the surface of a catalyst is in dynamic interaction with the gas-phase in heterogeneous oxidation catalysis [1,7,43,44]. It has been proposed that a heterogeneous catalytic system be considered a three-phase system, involving the gas-phase reactants, the solid catalyst and the surface region built of adsorbed molecules interacting with the surface layer of the solid [1]. A catalytic oxide system may respond to a paraffin / air mixture resulting in [1,43]:

- Partial reduction of the catalyst surface and the bulk of the catalyst
- Linear and point defects may be formed
- Segregation of elements and phases may occur

These differences between a fresh catalyst and a working catalyst strongly reflect the importance of *in situ* studies in catalysis.

2.6.6 Paraffin / air composition

Operation under fuel-rich conditions occurs when molecular oxygen is the limiting reactant. When molecular oxygen is in excess, operation conditions are referred to as fuel-lean. Under fuel-rich conditions the active component in a catalyst has a lower oxidation state than under fuel-lean conditions [7]. This corresponds to a change in the activity and selectivity of the catalyst. Usually more oxidized surfaces result in more active but less selective catalysts and more reduced surfaces show the opposite performance [7].

It was observed during *n*-pentane oxidation over a vanadium phosphorus oxide catalyst, that when the catalyst surface was saturated with the paraffin, by-products were formed which were not observed at all for low *n*-pentane concentrations in the feed [45,46]. The formation of the final stable products was hindered due to the deficiency in oxygen insertion sites. Under the fuel-lean conditions tested, the reaction became unselective. Thus, the paraffin / air ratio is critical for attaining high selectivities and therefore its optimization is an important parameter in catalytic testing.

2.6.7 The role of the paraffin in oxidation

Propane and butane are more reactive than ethane because secondary carbon-hydrogen bonds are more reactive than primary ones. The ODH of paraffins with 3 or more carbon results in the formation of allylic carbon-hydrogen bonds which are susceptible to further oxidation. Under the stringent conditions usually required for paraffin oxidation, oxygen could easily be inserted into the paraffin molecule leading to the formation of alcohols, aldehydes, ketones, carboxylic acids, ethers and carbon oxides. Further ODH of the paraffin may also occur. The stability of the partially oxidized products depends largely on the reaction conditions and on their residence time on the catalyst surface. As discussed previously (Chapter 2.6.4), the residence time of olefinic intermediates on the catalyst surface is influenced by the alkalinity of the catalyst. Since the basicity of olefins increases with the length of the carbon chain, it can be expected that the longer the olefin, the less time it will spend on the surface of a more basic catalyst [27].

In the case of catalysts with isolated active sites, the size of the paraffin may influence both the reactivity and the selectivity of those catalysts [47]. This influence would be dependent on the distance between active sites. It can be envisaged that a longer chain paraffin molecule such as hexane would be able to simultaneously interact with two active sites and produce a deeper oxidation than a shorter chain paraffin such as propane if the active sites were isolated and at an appropriate distance apart.

2.6.8 Summary: Crucial considerations in paraffin oxidation

Tables 2.6 and 2.7 summarize the principals which are fundamental to our understanding of selective heterogeneous paraffin oxidation [7,48]. Control in selective oxidation can only be possible if these key aspects become well established.

| Principal understanding | Considerations |
|---|---|
| Oxygen activation of the paraffin | <ul style="list-style-type: none"> - The role of oxygen species - The importance of the mode of paraffin oxidation |
| Reactivity of reactants and products | <ul style="list-style-type: none"> - The mechanism of activation of the carbon – hydrogen bond (heterolytic or homolytic) - The role of stability of the products |
| The mechanism of transformation of the reactant | <ul style="list-style-type: none"> - The importance of nondesorption of reaction intermediates - The importance of the ratio between olefin dehydrogenation and oxygen insertion in affecting selectivity - The role of the nature of the reaction intermediate in determining the direction of transformation - The contributions from homogeneous reactions, particularly at high temperatures (greater than 400 °C) - The effect of coadsorbates in facilitating the dissociative adsorption of paraffins |

Table 2.6: Important considerations in paraffin oxidation [7,48]

| Principal understanding | Considerations |
|--|--|
| The surface of the catalyst and the nature of the active sites | <ul style="list-style-type: none"> - The density of the active sites - The role of surface acidity - The need for multifunctionality on the surface, particularly for complex oxidation |
| The structure of the catalyst | <ul style="list-style-type: none"> - redox properties of metals in transition metal oxide catalysts. These properties include: metal reducibility, active site reoxidizability and the metal – oxygen bond strength - The reactivity of specific crystal planes, resulting in different oxidation reactions and consequently forming a reaction network - The role of structural defects in favouring the mobility of ionic species in the bulk - The importance of co-operative effects of different oxide phases - The importance of the interaction between the support and the active phase in modifying the catalytic properties of the active phase |

Table 2.7: Important catalyst features in paraffin oxidation [7,48]

2.7 References:

1. Grzybowska-Swierkosz, B., *Top. Catal.*, **11/12**, 2000, 23.
2. Centi, G., Cavani, F. and Trifiro, F., *Selective Oxidation by Heterogeneous Catalysis*, Kluwer Academic / Plenum Publishers, New York, 2001, pp. 1 – 4.
3. Centi, G., *Catal. Lett.*, **22**, 1993, 53.
4. Oyama, S. T., Desikan, A. N. and Hightower, J. W., *Catalytic Selective Oxidation*, ACS Symposium Series 523, *J. Am. Chem. Soc.*, Washington DC, 1993, p. 1.
5. Cavani, F. and Trifiro, F., *Appl. Catal. A.*, **88**, 1992, 115.
6. Cavani, F. and Trifiro, F., *Catal. Today*, **36**, 1997, 431.
7. Cavani, F. and Trifiro, F., *Catal. Today*, **51**, 1999, 561.
8. Birkeland, K. E., Babitz, S. M., Bethke, G. K. and Kung, H. H., *J. Phys. Chem. B.*, **101**, 1997, 6895.
9. Centi, G., Cavani, F. and Trifiro, F., *Selective Oxidation by Heterogeneous Catalysis*, Kluwer Academic / Plenum Publishers, New York, 2001, p. 172.
10. Dry, M. E., *Applied Industrial Catalysis* (Leach, B. E., ed.), Academic Press Inc., London, Vol. 2, 1983, pp. 186-187.
11. Sookraj, S. H. and Engelbrecht, D., *Catal. Today*, **49**, 1999, 161.
12. Mamedov, A. K., Shiryayev, P. A., Shashkin, D. P. and Krylov, O. V., *New Developments in Selective Oxidation*, Studies in Surface Science and Catalysis, Elsevier Science, Amsterdam, **55**, 1990, p. 477.
13. Sugino, M., Shimada, H., Turuda, T., Miura, H., Ikenaga, N. and Suzuki, *Appl. Catal. A*, **121**, 1995, 125.
14. Bhasin, M. M., McCain, J. H., Vora, B. V., Imai, T. and Pujado, P. R., *Appl. Catal. A*, **221**, 2001, 397.
15. Mendelovici, L. and Lunsford, J. H., *J. Catal.*, **94**, 1985, 37.
16. Ward, B. M., Lin, M. J. and Lunsford, J. H., *J. Catal.*, **50**, 1977, 306.
17. Liu, R. S., Iwamoto, M. and Lunsford, J. H., *J. Chem. Soc. Chem. Commun.*, 1982, 78.
18. Lin, H. F., Liu, R. S., Liew, K. Y., Johnson, R. E. and Lunsford, J. H., *J. Am. Chem. Soc.*, **106**, 1984, 4117.
19. Khan, M. M. and Somorjai, G. A., *J. Catal.*, **91**, 1985, 263.
20. Zhen, K. J., Khan, M. M., Mak, C. H., Lewis, K. B. and Somorjai, G. A., *J. Catal.*, **94**, 1985, 501.
21. Madeira, L. M. and Portela, M. F., *Catal. Rev.*, **44**, 2002, 247.

22. <http://www.soilcc.ca/pdfs/facsheet%204%20-%20N20.pdf> (Accessed before June 2005)
23. Centi, G., Cavani, F. and Trifiro, F., *Selective Oxidation by Heterogeneous Catalysis*, Kluwer Academic / Plenum Publishers, New York, 2001, pp. 67-69.
24. Centi, G., Cavani, F. and Trifiro, F., *Selective Oxidation by Heterogeneous Catalysis*, Kluwer Academic / Plenum Publishers, New York, 2001, pp. 204-209.
25. Grasselli, R. K., *Catal. Today.*, **48**, 1999, 141.
26. Mamedov, E. A. and Corberan, V. C., *Appl. Catal. A*, **127**, 1995, 1.
27. Blasco, T. and Lopez Nieto, J. M., *Appl. Catal. A*, **157**, 1997, 117.
28. Chaar, M. A., Patel, D. and Kung, H. H., *J. Catal.*, **109**, 1988, 463.
29. <http://www.oit.doe.gov/chemicals/factsheets/catoxdehy.pdf> (Accessed before June 2005)
30. Panov, I. G., Uriarte, A. K., Rodkin, M. A., Sobolev, V. I., *Catal. Today*, **41**, 1988, 365.
31. Janse van Vuuren, M. J., Sasol Report, 2000.
32. Sokolovskii, V. D., *Catal. Rev. Sci. Eng.*, **32**, 1990, 1.
33. Grasselli, R. K. and Burrington, T. D., *Adv. Catal.*, **30**, 1980, 133.
34. Mars, P. and van Krevelen, D. W., *Chem. Eng. Sci. Special Suppl.*, **3**, 1954, 41.
35. Weng, L. T. and Delmon, B., *Appl. Catal. A*, **81**, 1992, 141.
36. Weng, L. T., Ruiz, P., Delmon, B. and Duprez, D., *J. Mol. Catal.*, **52**, 1989, 349.
37. Centi, G., Cavani, F. and Trifiro, F., *Selective Oxidation by Heterogeneous Catalysis*, Kluwer Academic / Plenum Publishers, New York, 2001, pp. 425-4399.
38. Mamedov, E. A. and Corberan, V. C., *Appl. Catal. A*, **127**, 1995, 1.
39. Busca, G., Centi, G. and Trifiro, F., *Appl. Catal. A*, **25**, 1986, 265.
40. Matsuura, I., Oda, H. and Oshida, K., *Catal. Today.*, **16**, 1993, 547.
41. Pantazidis, A., Aurox, A., Herrmann, J. M. and Mirodatos, C., *Catal. Today.*, **32**, 1996, 81.
42. Ai, M. and Ikawa, T., *J. Catal.*, **40**, 1975, 203.
43. Haber, J., *New Developments in Selective Oxidation*, Studies in Surface Science and Catalysis, Elsevier Science, Amsterdam, **72**, 1992, p. 279.
44. Mamedov, E. A., *Appl. Catal. A*, **116**, 1994, 49.
45. Albonetti, S., Cavani, F., Trifiro, F., Venturoli, P., Calestani, G., Lopez Granados, M. and Fierro, J. L. G., *J. Catal.*, **160**, 1996, 52.
46. Cavani, F., Colombo, A., Giuntoli, F., Gobbi, E., Trifiro, F. and Vazquez, P., *Catal. Today*, **32**, 1996, 125.
47. Michalakos, P. M., Kung, M. C., Jahan, I. and Kung, H. H., *J. Catal.*, **140**, 1996, 226.
48. Centi, G., Cavani, F. and Trifiro, F., *Selective Oxidation by Heterogeneous Catalysis*, Kluwer Academic / Plenum Publishers, New York, 2001, pp. 29-30.

CHAPTER 3: Catalyst Preparation and Characterization

3.1 Introduction to catalyst preparation

A heterogeneous catalyst is usually a composite material, characterized by [1]:

- The relative amounts of different components i.e. the active species, promoters and supports
- Size and shape
- Pore volume and distribution
- Surface area

An optimum catalyst is the one that provides the required combination of properties such as activity, selectivity, lifetime, toxicity and ease of regeneration at an acceptable cost [1]. Various methods of catalyst preparation exist and one catalyst can usually be prepared by several routes. The preparation of a heterogeneous catalyst consists of a number of physical and chemical steps. The conditions used in each step have a vital influence on the catalyst properties [2]. Parameters such as concentrations, stirring conditions (shape and volume of vessel may also be important), temperature and temperature changes as well as the sequence and duration of all operations can be crucial for a successful synthesis [3]. The following processing steps are usually involved in the synthesis of many catalysts:

- Precipitation or impregnation
- Filtration
- Washing
- Drying
- Calcining
- Forming
- Activation

3.1.1 Precipitation

Precipitation is one of the most widely used preparation methods and is used to prepare either single component catalysts and supports or mixed catalysts [1,4]. Precipitated catalysts are usually prepared by mixing two or more solutions, causing the precipitation of an amorphous or crystalline precipitate. Precipitation occurs in three phases: supersaturation, nucleation and growth. A supersaturated solution is unstable and any disturbance results in precipitation [5]. Supersaturation can be achieved by lowering the temperature, increasing the pH or by increasing the concentration in the solution by evaporation of the solvent. Particles in a

supersaturated solution develop through nucleation and growth. Parameters that influence the properties of the final precipitate are shown in Figure 3.1. The parameters for industrially precipitated catalysts are mostly empirically optimized and these parameters are highly confidential [4].

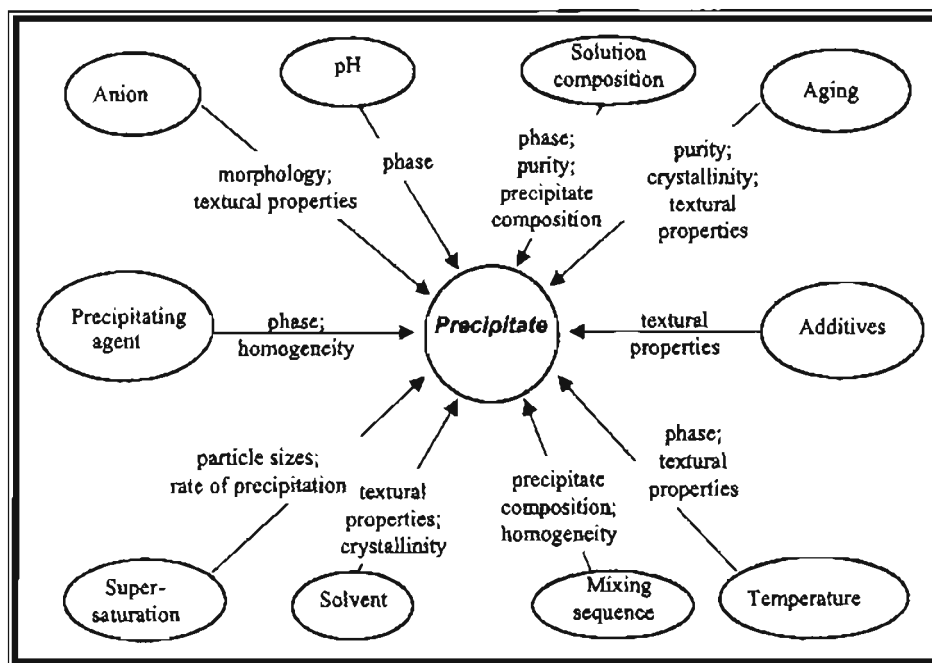


Figure 3.1: Parameters affecting the properties of precipitated catalysts [4]

The general advantages of precipitation are [6]:

- It provides for a more uniform mixing on a molecular scale of the various catalytic components
- The distribution of the active species in the final catalyst is uniform
- It is usually easier to achieve high concentrations of the catalytic active phase
- Better control over the pore size distribution is possible

3.1.2 Impregnation

Impregnation involves the addition of a solid component to a solution of another component. The dissolved component is deposited onto the surface of the solid component. The solid component is usually a support. Active components with thermally unstable anions such as carbonates, nitrates, acetates or hydroxides are usually used. Parameters such as: the concentration of the dissolved active components, the stirring rate, temperature, pH, the nature of the solvent and impregnation time are strictly controlled. Different impregnation techniques are described in Table 3.1.

During impregnation different processes can occur at different rates [3]. These include:

- Selective adsorption by coulombic forces, van der Waals forces or hydrogen bonding
- Ion exchange between the charged surface and the electrolyte
- Polymerization or depolymerization of the species attached to the surface
- Partial dissolution of the surface of the solid.

| Method | Description |
|---|---|
| Impregnation by soaking or with an excess of solution | Slow, requires several days. Extensive restructuring of the surface may occur. Impregnation is not quantitative. Excess liquid removed by evaporation or by filtering. Distribution of species is well controlled and high dispersion may be obtained. |
| Dry impregnation | Best suited for impregnation of species that interact weakly with the surface of the support. The required amounts of components are introduced in a volume, corresponding to the pore volume of the support. |
| Incipient wetness impregnation | Liquid is slowly added to a porous solid support. This liquid is first adsorbed in the pores and the powder flows as if it is dry. When the pores have been filled the outside suddenly becomes wet. Addition of liquid such that the pores of liquid are filled and the outside of powder grains is dry is called incipient wetness. |
| Impregnation by percolation | The dissolved phase is adsorbed or ion exchanged by percolation through a bed containing the solid support. A faster approach to equilibrium may be achieved. The progress of the impregnation may be followed by analyzing the effluent. |
| Co-impregnation | Multi-components may be introduced in a single step. Uniform distribution is difficult to achieve, as more strongly adsorbed components will be deposited preferentially on the surface. |
| Successive impregnation | After the impregnation of a component the catalyst is dried. Subsequent impregnations with the same component or a different one may then be carried out. |

Table 3.1: Types of impregnation [3]

Impregnation may have certain advantages over precipitation. In precipitated catalysts, usually part of the active component is enclosed by the other components present. This is of particular importance when expensive components such as the platinum group metals are used as the active components. Filtering and washing of the catalyst is also usually eliminated in impregnation. However, whilst catalysts with small metal loadings are easily prepared by impregnation, it may not be possible to prepare catalysts with higher metal loadings in this way.

3.2 Washing, filtering and drying

Soluble impurities, mobile anions, mobile cations and byproducts can be removed from a catalyst by washing it thoroughly. These steps are usually time consuming. The solvent used for washing may be decanted, centrifuged or filtered off depending on the nature of the particles. The catalyst is then dried with care. Drying a catalyst results in the removal of solvent from the pores of a solid. Conditions such as temperature, heating rate and duration can change the physical properties of the resulting catalyst. These parameters must be measured and kept constant. The porosity of precipitated catalysts are dependent on the drying procedure. Drying of impregnated catalysts can change the distribution of the active component [5].

3.3 Calcining

Calcination is a further treatment of the catalyst with heat after drying. It can be carried out in an oxidizing or inert atmosphere, usually at temperatures slightly above the operating temperature of a catalyst. Calcination results in the stabilization of physical, chemical and catalytic properties of a catalyst [6]. Several processes may occur during calcination [5,6]:

- Loss of chemically bound water, CO₂, binders, unstable anions and cations such as hydroxides, carbonates, nitrates and organic salts. These are usually converted to oxides.
- Decomposition products can form new compounds by solid-state reactions
- Changes in pore structure and mechanical strength of precipitated catalysts can occur
- Amorphous regions of a catalyst can become crystalline
- Surface conditioning may occur

Calcination may occur before or after catalyst forming.

3.4 Catalyst forming

Catalysts, which are manufactured as a powder, are formed into particles whose shape and size is determined by its end use. Catalyst forming determines important characteristics of a catalyst such as its mechanical properties, resistance to thermal shock and the ease of gas flow through the reactor [3]. The size and shape of catalyst particle can therefore promote catalytic activity, strengthen particle resistance to crushing and abrasion, minimize pressure drop over a catalyst bed and reduce fabrication costs [7]. Common catalyst shapes and sizes are shown below in Table 3.2 [2,5,8]:

| Shape | Size | Example | Description |
|------------|---|--------------------------------------|---|
| Spheres | 1-10 mm (<i>d</i>) | Impregnated precious metal catalysts | Low manufacturing costs, can result in high pressure drop |
| Granules | 1-20 mm (<i>d</i>) | Ammonia synthesis catalysts | Low surface area catalysts, not commonly used |
| Pellets | 3-15mm (<i>d,h</i>) | Hydrogenation catalysts | Highly regular shape, good strength, expensive to produce |
| Extrudates | 1-50 mm (<i>d</i>) 3-300 mm (<i>l</i>) | Hydrodesulphurisation catalysts | Made by squeezing catalyst through holes, poor strength |
| Powders | 20-300 μm | Used in slurry reactors | Produced by spray-drying |

Table 3.2: Common catalyst shapes [2,5,8]

The choice of the shape and size of catalysts is dependent on the type of reactor and on the hydrodynamics and heat and mass transfer limitations within that reactor (Table 3.3) [1,7].

| Reactor | Problem | Best shape |
|---------------|------------------------------------|--|
| Fluidized bed | Poor recovery by cyclones | Larger spheres |
| | Poor bed fluidization | Smaller spheres |
| Slurry | Difficult filtration | Smaller spheres |
| | Poor suspension | Larger particles |
| Fixed bed | Pressure drop | Large size and not regular shape |
| | Poisons in the feed | Extrudates (large external surface area) |
| | Large internal diffusion phenomena | Extrudates |
| | Cost | Extrudates |

Table 3.3: Criteria for choosing the shape and size of catalyst particles [7]

3.5 Introduction to catalyst characterization

The performance of solid catalysts in heterogeneous oxidation depends on the structure, phase composition, surface chemical composition and the morphology of its catalytic particles. Catalyst characterization enables the catalytic scientist to correlate chemical and structural properties of catalysts to their performance. Although a vast array of techniques exists, only few are capable of characterizing a catalyst under its true operating conditions. Traditional methods for catalyst characterization include: the determination of surface area, pore volume, pore-size distribution, aperture dimension and the degree of dispersion of a supported catalyst [9]. This information was obtained by using the principles of physical and chemical adsorption. Electrical conductivity measurements were also traditionally used for characterization.

Instruments for analysis of a surface require three components: an exciting source, an outgoing signal and a detector for measurements of the outgoing signal (Figure 3.2).

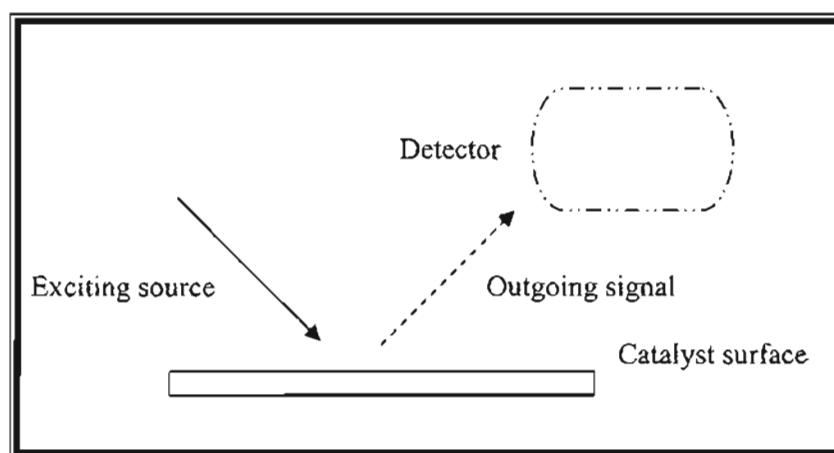


Figure 3.2: Components for the surface analysis of a catalyst

Excitation sources include: photons, electrons, ions or neutral particles. When these hit the catalyst, surface atoms or molecules will be excited. To return to their ground state (most stable state), these atoms or molecules will release energy. This can be in the form of photons, electrons, ions or neutral particles. These are captured by a detector and processed. Characterization methods can be classified according to their ability to absorb, emit or scatter photons, electrons, neutrons or ions (Tables 3.4-3.6).

| Outgoing beam | | |
|---|--|---|
| Photons | Electron | Ions |
| Nuclear magnetic resonance (NMR) | UV-induced photoelectron spectroscopy (UPS) | Laser microprobe mass spectrometry (LMMS) |
| Electron-spin resonance (ESR) | X-ray induced photo-electron spectroscopy (XPS) | Photoelectron emission microscopy (PEEM) |
| Fourier transform infra-red (FTIR) | X-ray induced photo-electron diffraction (XPD) | |
| Raman spectroscopy | Conversion-electron Moessbauer spectroscopy (CEMS) | |
| Moessbauer spectroscopy | | |
| X-ray absorption (near edge) spectroscopy (XANES) | | |
| Extended x-ray absorption fine structure (EXAFS) | | |
| X-ray fluorescence (XRF) | | |
| X-ray diffraction (XRD) | | |
| Optical microscopy | | |

Table 3.4: Methods for catalyst characterization using photons as the exciting source [9]

| Outgoing beam | |
|-----------------------------------|--|
| Photons | Electrons |
| X-ray emission spectroscopy (XRE) | Low-energy electron diffraction (LEED) |
| Cathodoluminescence (CL) | Auger-electron spectroscopy (AES) |
| | Scanning-Auger-microscopy (SAM) |
| | High-resolution electron-energy-loss spectroscopy (HREELS) |
| | Electron-energy-loss spectroscopy (EELS) |
| | Scanning electron microscopy (SEM) |
| | Transmission electron microscopy (TEM) |
| | Electron diffraction (ED) |
| | High resolution electron microscopy (HREM) |
| | Scanning tunneling microscopy (STM) |

Table 3.5: Methods for catalyst characterization using electrons as the exciting source [9]

| Outgoing beam | |
|--|--|
| Photons | Ions |
| Proton-induced x-ray emission (PIXE) | Ion-scattering spectroscopy (ISS) |
| Positron annihilation spectroscopy (PAS) | Secondary-ion mass spectroscopy (SIMS) |
| | Ion-microprobe microanalysis (IMM) |
| | Rutherford back-scattering (RBS) |

Table 3.6: Methods for catalyst characterization using ions as the exciting source [9]

In addition to these methods, thermal and calorimetric analyses are frequently used for catalyst characterization. Characterization techniques used in this thesis are further described below.

3.5.1 X-ray diffraction (XRD)

XRD is one of the most important techniques for catalyst characterization [10]. The diffraction pattern is the fingerprint of any crystalline phase and powder diffraction is used to identify mixture of phases in a catalyst [11]. Phase identification is achieved through comparison with a pure reference phase or with a database. The amount of phases present in a catalyst can be quantified with calibration procedures. X-rays, which are electromagnetic radiation with wavelengths of the order 10^{-10} m, can be produced by either x-ray tubes or synchrotron radiation. X-ray tubes are commonly used in laboratory instruments. In these tubes, x-rays are produced by bombarding a metal with high-energy electrons. Synchrotron radiation is emitted by electrons or positrons which travel at the speed of light. This radiation source is much more intense than the radiation produced by x-ray tubes. They can be thousands to millions of times more intense. Synchrotron radiation has played a major role in the advancement of our understanding of catalysis [12]. It enables dynamic experiments to be carried out in real time [13].

X-ray diffraction in a crystal is shown in **Figure 3.3**. Bragg's law is an important law used for interpreting x-ray diffraction data. According to this law the conditions for a reflected or diffracted beam are given by:

$$n \lambda = 2d \sin \theta$$

This equation relates the wavelength of the x-rays (λ) and the order of the diffraction peak (n) to the lattice spacing (d) and the angle between the atomic plane and both the incident and reflected x-ray beam (θ).

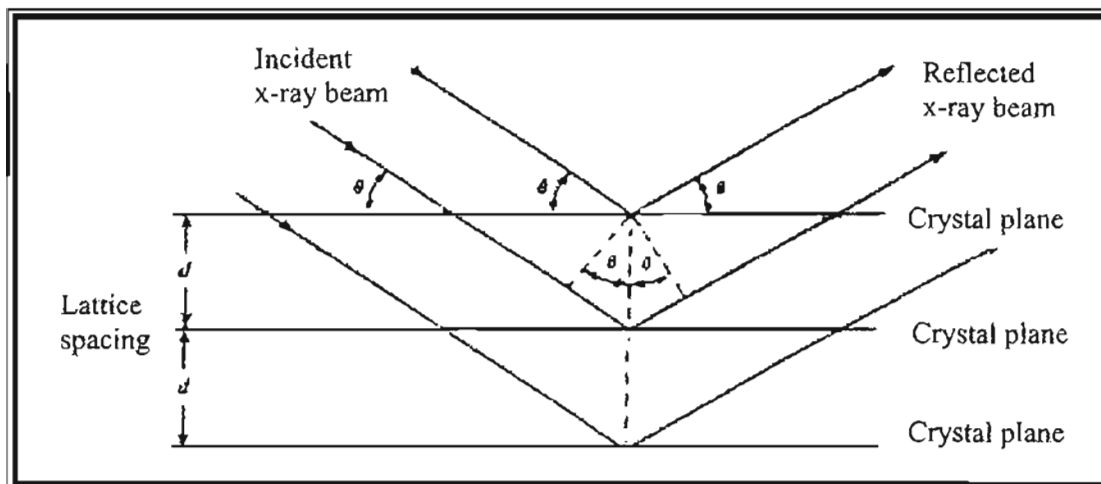


Figure 3.3: Diffraction of x-rays [14]

An x-ray diffractogram obtained can provide important information such as [9]:

1. The crystallinity of the catalyst or a component of it
2. An estimate of the size of microcrystallites present
3. Insight into the atomic constituents of the unit cell (from d -spacings and unit cell dimensions)
4. In-situ experiments can show the effect of a reactant on the structure of a catalyst.

The limitations of XRD include:

1. The minimal limit of detection is approximately five percent for compounds and approximately one percent for elements (depending on atomic weight) [15]
2. Diffraction lines broaden as crystallite size decreases and discrimination is difficult with crystallites less than 5 nanometers [16]
3. Diffraction patterns from different components may overlap and/or interfere with each other.

Modern computer software programs are used to minimize these limitations [16].

3.5.2 X-ray fluorescence (XRF)

When a catalyst is irradiated with an intense x-ray beam, electrons are liberated from the inner core levels (Figure 3.4). The first electron to be ejected leaves a hole in a low energy orbital. An electron from a higher energy orbital then falls into this low energy orbital. The energy released during this process can result in the generation of radiation. This radiation is called x-ray fluorescence. Fluorescent emissions are characteristic of a particular element and nearly independent of its chemical state. XRF is a non-destructive technique.

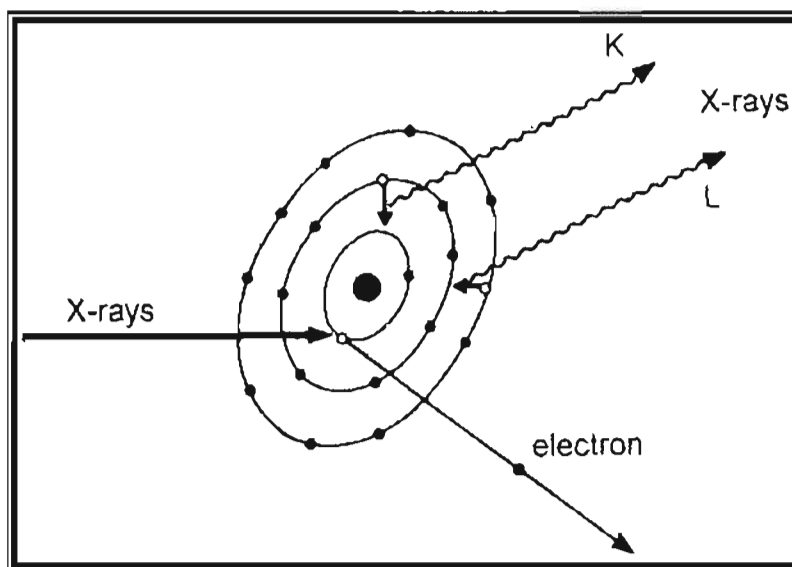


Figure 3.4: Illustration of x-ray production by irradiation with x-rays [9].

X-ray fluorescence can be detected by an energy dispersive or wavelength dispersive detector. Elements in the sample are identified by the wavelengths of the emitted x-rays. The concentrations of the elements are determined by the intensity of those x-rays. XRF is a bulk analysis technique. The suitability of XRF for rapid and accurate multiple-element analysis makes it a valuable technique.

3.5.3 X-ray induced photoelectron spectroscopy (XPS) and Auger electron spectroscopy (AES)

The chemical nature and composition of the surface of a catalyst can be rapidly analyzed by XPS and AES. Approximately two to ten atom layers of the surface can be analyzed with good sensitivity [10]. XPS is used in catalysis for [10]:

- Providing general qualitative analysis
- Investigating concentration-depth profiles of a catalyst. This is obtained by the progressive erosion of the surface with an ion beam followed by XPS
- Providing estimates of dispersion, clustering and other morphological variations
- Investigating metal-metal and metal-support interactions
- Determining chemical states of all components in the catalyst.

In x-ray induced photoelectron spectroscopy, a catalyst is irradiated with monochromatic x-rays under an ultra high-vacuum. This causes the removal of a core electron. An escaping core electron possesses kinetic energy. This kinetic energy is dependent on the exciting x-ray energy and the electron binding energy of that atom i.e. how tightly the electron was held in the atom. By measuring the kinetic energy of ejected electrons with a electrostatic energy spectrometer, the binding energy of the elements in a catalyst can be determined. This is then used to determine oxidation states and bonding information. The use of a high vacuum environment in XPS, rather than real catalytic working conditions, is a limitation of this technique [17].

Auger electron spectroscopy is complimentary with XPS and both spectroscopic methods can usually be performed on the same instrument. AES is a surface-sensitive analytical technique, which enables the surface elemental composition to be determined. The elemental composition is determined by measuring the energies of Auger electrons. The Auger electron energies are characteristic of the elements from which the electrons originate. The Auger effect is the emission of a second electron after a core electron has been removed. An excitation beam removes the first electron from the core level of an atom, thereby producing a vacancy. An electron from a higher energy level fills this vacancy with a corresponding release of energy. This energy causes a secondary or Auger electron to be emitted. Auger electrons have very low energy and are only emitted from the surface of a catalyst.

3.5.4 Fourier transform infrared spectroscopy (FTIR) and laser Raman spectroscopy (LRS)

Molecular vibrational spectroscopy can be used to detect changes in a molecular environment and structure. In addition to providing structural information about a catalyst, information on surface functional groups and adsorbates can be obtained. In situations where x-ray diffraction techniques are not applicable, vibrational spectroscopy can provide information on phase transitions and changes in compositions of bulk catalysts, on their crystallinity and on

the nature of surface functional groups [18]. FTIR and Raman spectroscopy are two important vibrational spectroscopic techniques.

FTIR is routinely used in catalyst characterization. The components of a FTIR are shown in Figure 3.5 below:

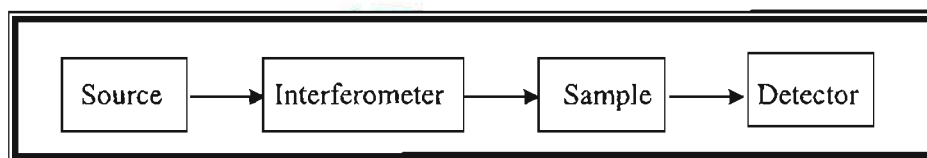


Figure 3.5: Components of a FTIR spectrometer

FTIR is a method of obtaining infrared spectra by first collecting an interferogram of a catalyst using an interferometer (Figure 3.6). A Fourier transform is then performed on the interferogram to obtain a spectrum.

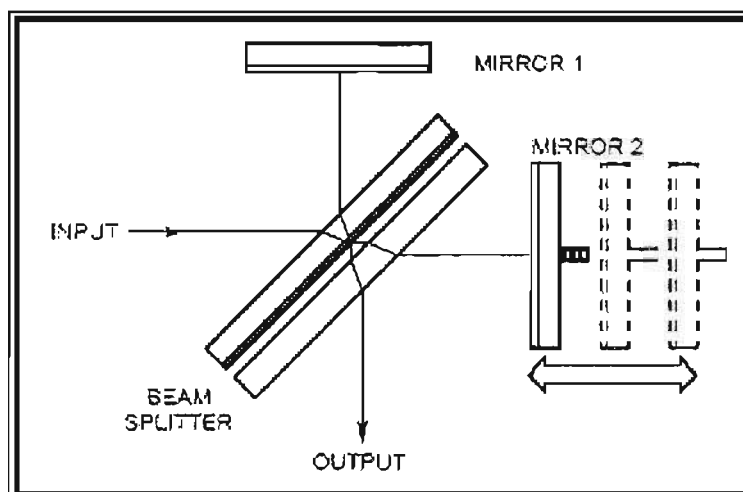


Figure 3.6: A Michelson interferometer [19]

The Michelson interferometer consists of a beam splitter, a fixed mirror and a mirror that can move with great precision. The interferometer splits the beam from the sample into two and introduces a variable path difference, into one of the beams. When the two component beams recombine there is therefore a phase difference between them. The beams may interfere with each other, constructively or destructively, depending on the difference in path lengths [20]. An interferogram is a recording of the intensity that results from the constructive and destructive interference for all the wavelengths of light output from the interferometer as a function of path length difference [21]. The interferogram is then converted into a wavelength spectrum by means of a Fourier transform.

Laser Raman spectroscopy is complimentary to infrared spectroscopy. Symmetric vibrations are Raman active but infrared inactive, whilst the opposite is true for asymmetric vibrations. Raman spectroscopy has the following unique features [18]:

- *In situ* spectra of a catalyst can be obtained at high temperatures and pressures as the interference of gas-phase spectra is very weak
- Simple glass or quartz cells are often used
- Solid state spectra between fifty and twelve hundred cm^{-1} can usually be recorded under *in situ* conditions
- Raman scattering probabilities of solid supports are frequently low. Thus Raman spectra of surface species can be recorded.

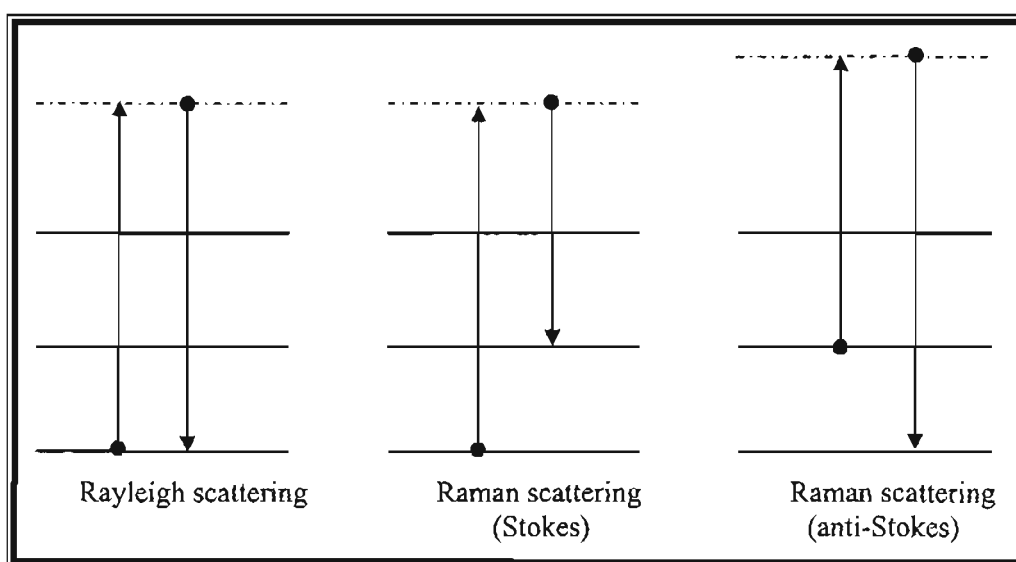


Figure 3.7: An energy diagram illustrating Rayleigh and Raman scattering of incident photons [22]

A molecule in the ground vibrational state absorbs energy from an incident photon and moves to an unstable higher energy state. Elastic Rayleigh scattering occurs when the excited molecule returns to the ground state by emitting a photon with the same energy as the incident photon. Raman scattering occurs when the energies of the incident photon and the emitted photon are different (Figure 3.7). The Raman effect occurs in approximately one in ten million incident photons [20]. Therefore, sensitive photo-multiplier detectors are required. The major problems encountered in LRS are [18]:

- Sample may be sensitive to heating effects of the laser beam
- Low sensitivity
- Background fluorescence may mask weak Raman signals.

3.5.5 Scanning electron microscopy (SEM) and energy dispersive x-ray spectroscopy (EDS)

SEM is a technique used to study the surface topography of a catalyst. A finely focused electron beam is scanned across a catalyst resulting in the generation of a variety of signals i.e. secondary electrons, Auger electrons, backscattered electrons, x-rays and photons with different energies. The backscattered electrons and the secondary electrons are important in SEM and these electrons are used to form an image on a cathode-ray tube. A backscattered electron is produced when an electron from an electron beam is deflected on a catalyst. The amount of backscattered electrons produced is dependent on atomic number. Backscatter images yield compositional information. Elements with higher atomic numbers appear as brighter areas. Backscattered electrons have higher energy than secondary electrons. The latter are produced when an electron is ejected from the near surface of a catalyst. The amount of secondary electrons emitted is dependent on the angle between the catalyst surface and both the electron beam as well as the detector. Hence, topographical differences will result in different amounts of secondary electrons sent to the cathode ray tube and therefore images with different intensities would be produced. Magnifications of twenty to fifty thousand are possible with a resolution of approximately five nanometers [23]. The size, shape and distribution of crystallites can be obtained if they are larger than five nanometers. Catalysts capable of conducting an electric charge require almost no sample preparation [24]. Nonconductive samples are coated with gold or carbon to reduce or to eliminate electric charge build-up.

In energy dispersive x-ray spectroscopy (EDS), x-rays generated by an electron beam are analyzed qualitatively and quantitatively by a solid-state energy dispersive detector. The energy of x-rays emitted from a catalyst is dependent on the elements presents in a catalyst. For quantitative work, standards are used for calibration. EDS is usually used in conjunction with SEM. It is a bulk study of a catalyst and not a surface technique. A commonly used detector in EDS is the lithium drifted silicon detector, which must be operated at liquid nitrogen temperatures. This detector is usually protected by a beryllium window [25]. This prohibits the detection of elements below the atomic number of eleven as their x-rays are absorbed by the beryllium window [25].

3.5.6 Differential scanning calorimetry (DSC) and thermogravimetric analysis (TGA)

Thermal analysis comprises of a group of techniques in which a physical property of a substance is measured as a function of temperature. In thermogravimetry, measurements of changes in the mass of a catalyst with temperature are recorded. A precision electronic balance with a temperature programmable furnace and a suitable recording system is required. TGA's of catalysts are useful for studying the rate of coking, dehydration, sorption of poisons and catalyst regeneration [15]. TGA can be useful for the characterization of oxidation catalysts, where weight gain or weight loss may reveal the state of oxidation [15].

In DSC, the energy required to maintain a catalyst and an inert reference at the same temperature throughout a controlled temperature program is measured. The energy difference is recorded against temperature. Using DSC, various types of chemical transformations that are accompanied by significant energy changes can be observed [15]. DSC is also used to study catalyst regeneration.

DSC and TGA are usually combined and used to investigate the genesis of solid catalytic material. This is particularly useful for studying catalysts produced by solid-state reactions.

3.5.7 Brunauer-Emmett-Teller (BET) surface area

Gas adsorption methods are used to determine the total surface area and pore size distribution of catalysts. The Brunauer-Emmett-Teller (BET) adsorption method is the most widely used standard procedure [10]. In the BET method physical adsorption is used to determine the total surface area. The BET method is an oversimplified model expressed by the following equation [26]:

$$\frac{P}{V(P_0 - P)} = \frac{1}{V_m C} + \frac{(C-1)P}{V_m C P_0}$$

Where:

V = volume of gas adsorbed at pressure P

V_m = volume of gas adsorbed in the monolayer

C = a constant related exponentially to the heats of adsorption and liquefaction of the gas

P₀ = saturation pressure of adsorbate gas at the experimental temperature

It is based on the following assumptions:

- For the first layer, the rate of evaporation is considered to be equal to the rate of condensation
- The heat of adsorption is taken to be independent of coverage
- Except for the first layer, the rate of adsorption is taken to be proportional to the fraction of the lowest layer still vacant
- The heat of adsorption for all layers except the first layer is assumed to be equal to the heat of liquefaction of the adsorption gas.

In spite of its theoretical limitations, the BET method is widely used because it can be reproduced with considerable accuracy. Nitrogen is usually used as a suitable adsorbate [27].

3.6.8 Inductively coupled plasma – atomic emission spectroscopy (ICP-AES)

ICP-AES is used for determining the elemental composition of a catalyst. A plasma i.e. a gas in which a significant fraction of the atomic species are in the form of ions, is formed by argon gas flowing through a high radio-frequency field. Argon ions formed in the plasma are capable of absorbing power from the radio-frequency generator and thereby maintaining a high temperature and propagating the ionization process [28]. In ICP-AES, the catalyst is first dissolved in an aqueous medium. Concentrated acid is usually used to dissolve the catalysts. Thermal treatment or microwave digestion may be required for solids, which are difficult to digest. The digested catalyst is then diluted so as to bring their concentrations into an appropriate range. The digested catalyst can then be nebulized by a flow of argon gas and then carried into the plasma. Temperatures in the plasma range from six thousand to eight thousand Kelvin [28]. The injected sample is ionized in the plasma. When excited atoms and ions relax, energy is given off in the form of light. The wave length of emitted light is peculiar to an element. A solid-state detector is used to identify the wavelength and its intensity. The intensity of the signal is then compared to previous measured intensities of known concentration of the element.

The main advantage of ICP is its ability to simultaneously analyze several elements. This multi-element analysis can be achieved rapidly and with excellent sensitivity.

3.6 References

1. Campanati, M., Fornasari, G. and Vaccari, A., *Catal. Today*, **77**, 2003, 299.
2. Hagen, J., *Industrial Catalysis – A Practical Approach*, Wiley-VCH, Federal Republic of Germany, 1999, p. 207.
3. Haber, J., Block, J. H. and Delmon, B., *Handbook of Heterogeneous Catalysis*, (Ertl, G., Knozinger, H. and Weitkamp, eds.), Wiley-VCH, Federal Republic of Germany, Vol. 3, 1997, pp. 1530-1533.
4. Schuth, F. and Unger, K., *Handbook of Heterogeneous Catalysis*, (Ertl, G., Knozinger, H. and Weitkamp, eds.), Wiley-VCH, Federal Republic of Germany, Vol. 1, 1997, pp. 72-79.
5. Richardson, J. T., *Principles of Catalyst Development*, Plenum Press, New York, 1989, pp. 95-134.
6. Wijngaarden, R. J., Kronberg, A. and Westerterp, K. R., *Industrial Catalysis*, Wiley-VCH, New York, 1998, p 30-33.
7. Perego, C. and Villa, P. L., *Catal. Today*, **34**, 1997, 281.
8. Pearce, R. and Patterson, W. R., *Catalysis and Chemical Processes*, Blackie and Son Ltd, London, 1981, pp. 20-23.
9. Thomas, J. M. and Thomas W. J., *Principles and Practice of Heterogeneous Catalysis*, VCH Publishers Inc., New York, 1997, pp. 146-152.
10. Haber, J., Block, J. H. and Delmon, B., *Handbook of Heterogeneous Catalysis*, (Ertl, G., Knozinger, H. and Weitkamp, J., eds.), Wiley-VCH, Federal Republic of Germany, Vol. 3, 1997, pp. 1520-1545.
11. Bergeret, G., *Handbook of Heterogeneous Catalysis*, (Ertl, G., Knozinger, H. and Weitkamp, J., eds.), Wiley-VCH, Federal Republic of Germany, Vol. 2, 1997, pp. 464.
12. <http://www.mrl.ucsb.edu/mrl/centralfacilities/xray/xray-basics/Xray-basics.html>
(Accessed 01/10/2005)
13. Clausen, B. S., Steffensen, G., Fabius, B., Villadsen, J., Fiedenhaus, L. R. and Topsoe, H., *J. Catal.*, **132**, 1991, 524.
14. <http://ceiba.cc.ntu.edu.tw/catalysis/course/Chap5.pdf> (Accessed: before June 2005)
15. Satterfield, C. N., *Heterogeneous Catalysis in Industrial Practice*, Mcgraw-Hill, Inc., New York, 1991, pp 170-172.
16. Richardson, J. T., *Principles of Catalyst Development*, Plenum Press, New York, 1989, p. 138.
17. Venezia, A. M., *Catal. Today*, **77**, 2003, 359.

18. Mestl, G. and Knozinger, H., Handbook of Heterogeneous Catalysis, (Ertl, G., Knozinger, H. and Weitkamp, J., eds.), Wiley-VCH, Federal Republic of Germany, Vol. 2, 1997, pp. 539-542.
19. <http://www.oriel.com/down/pdf/05004.pdf> (Accessed: before June 2005)
20. Atkins, P. W., Physical Chemistry, Oxford University press, Oxford, 1997, pp.456-457.
21. Srivastava, R. D., Heterogeneous Catalytic Science, CRC Press, Florida, 1988, p. 17.
22. Anderson, J. R. and Pratt, K. C., Introduction to Characterization and Testing of Catalysts, Academic Press Inc., London, 1985, p. 412.
23. Richardson, J. T., Principles of Catalyst Development, Plenum Press, New York, 1989, p. 158.
24. <http://www.geocities.com/CapeCanaveral/Lab/1987/zfundam6.html> (Accessed: before June 2005)
25. <http://www.uksaf.org/technique/edx.html> (Accessed: before June 2005)
26. Sing, K. S. W. and Rouquerol, J., Handbook of Heterogeneous Catalysis, (Ertl, G., Knozinger, H. and Weitkamp, J., eds.), Wiley-VCH, Federal Republic of Germany, Vol. 2, 1997, p 429.
27. Hagen. J., Industrial Catalysis – A Practical Approach, Wiley-VCH, Federal Republic of Germany, 1999, pp. 194-197.
28. Skoog, D. A. and West, D. M., Principles of Instrumental Analysis, Saunders College, Philadelphia, 1980, pp. 340-341.

CHAPTER 4: Reactors in Catalysis

4.1 Introduction

Reactor choice and configuration, coupled with catalyst design is necessary for optimization of the yield, selectivity and conversions of heterogeneous catalytic reactions. The choice and configuration of a reactor is influenced by several factors (Figure 4.1) [1]. Both theoretical as well as empirical considerations are the basis for industrial reactor design.

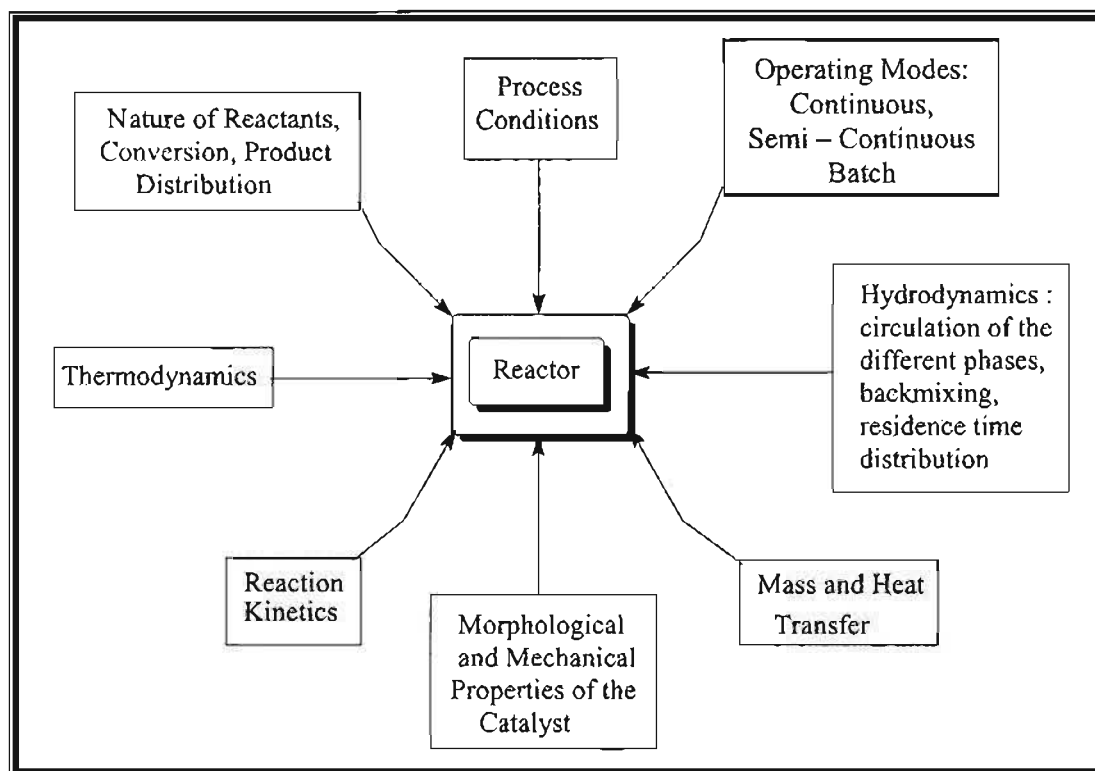


Figure 4.1: Influences on the design of catalytic reactors [1]

Catalytic reactors can be broadly classified according to their phase conditions. A two-phase reactor is defined as any vessel or region in space where the two phases come into contact and this results in a change in the chemical composition of one phase. Similarly, a three-phase reactor requires three phases to be present. Laboratory reactors are used to provide information on the activity, selectivity and life of a catalyst. They can be divided into steady-state (continuous) and non-steady-state reactors (Figure 4.2) [2]. Steady-state reactors can be further divided into plug flow and mixed flow reactors. A plug flow reactor with low feed conversions, and thus requiring recycling, is said to operate in the differential mode and for high conversions over the catalyst bed, the operation is in the integral mode (no recycling). If the composition of a reactor (no inlet and outlet feed) changes as a function of time, that reactor is called a batch reactor.

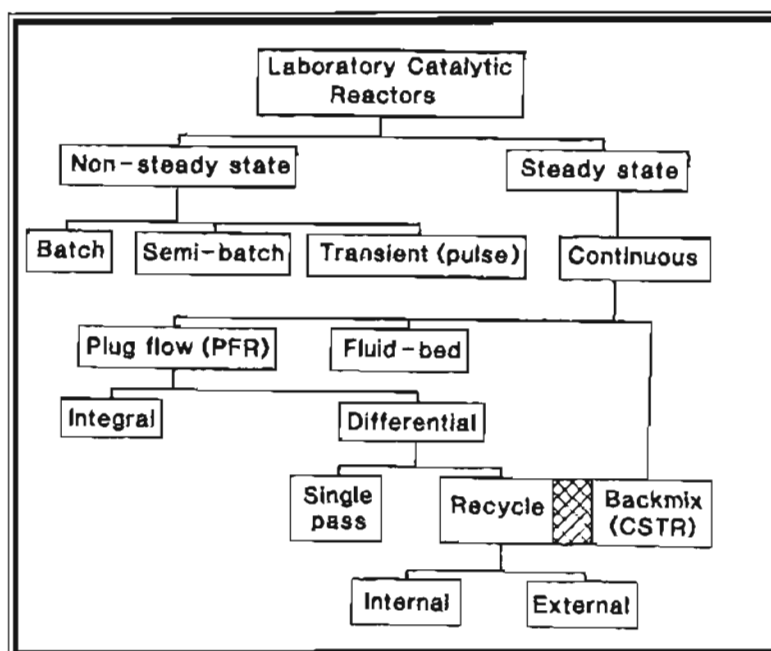


Figure 4.2: Classification of laboratory reactors [2]

Steady state reactors (continuous flow), especially packed bed reactors, are most frequently encountered in catalyst testing. These reactors are easily operated and their costs are relatively low. Transient operation can be used to establish reaction networks and detailed kinetic information, under conditions that are quite different from continuous operation. For example, isotopically labelled species under steady-state conditions such as positron emission profiling is used in pulse reactors [3]. Different reactors such as the plug flow fixed bed (PFR), continuous stirred tank (CSTR), fluidized bed (FBR), batch and discontinuous flow reactor are chosen based on the types of information required (Table 4.1):

| | PFR | CSTR | FBR | Batch | Discontinuous |
|---|-----|------|-----|-------|---------------|
| Comparison of catalysts | ✓ | ✓ | ✓ | ✓ | ✓ (Limited) |
| Study slow changes in activity | ✓ | ✓ | | | |
| Study rapid changes in activity | | | | | ✓ |
| Study heat and mass transfer | ✓ | ✓ | | ✓ | |
| Derive kinetic equations | ✓ | ✓ | | ✓ | |
| Kinetic data for modelling of industrial reactors | ✓ | ✓ | | ✓ | |

Table 4.1: Information obtained from different reactors [4]

4.1.1 Plug flow fixed bed reactors

These reactors are made up of glass or a stainless steel tube. Solid catalysts (neat or diluted) are held between plugs of quartz or glass wool through which reactants pass through. Thermo-couples are placed either in the catalyst bed or attached to the wall of the reactor. Feed of a known composition passes through the catalyst bed at a constant flow rate. In an ideal fixed bed reactor there is no back mixing and the contact time in the reactor is the same for all components in the feed. Reactant and product partial pressures are only a function of the reactor length coordinate. Therefore the length of the reactor as well as the diameter is important in determining plug flow performance. In the laboratory, the easiest and the most common way of carrying out a heterogeneously catalyzed gas-phase reaction is by passing the gas mixture over a fixed catalyst. In industry, fixed bed reactors are also the standard type of reactors for heterogeneously catalyzed gas-phase reactions.

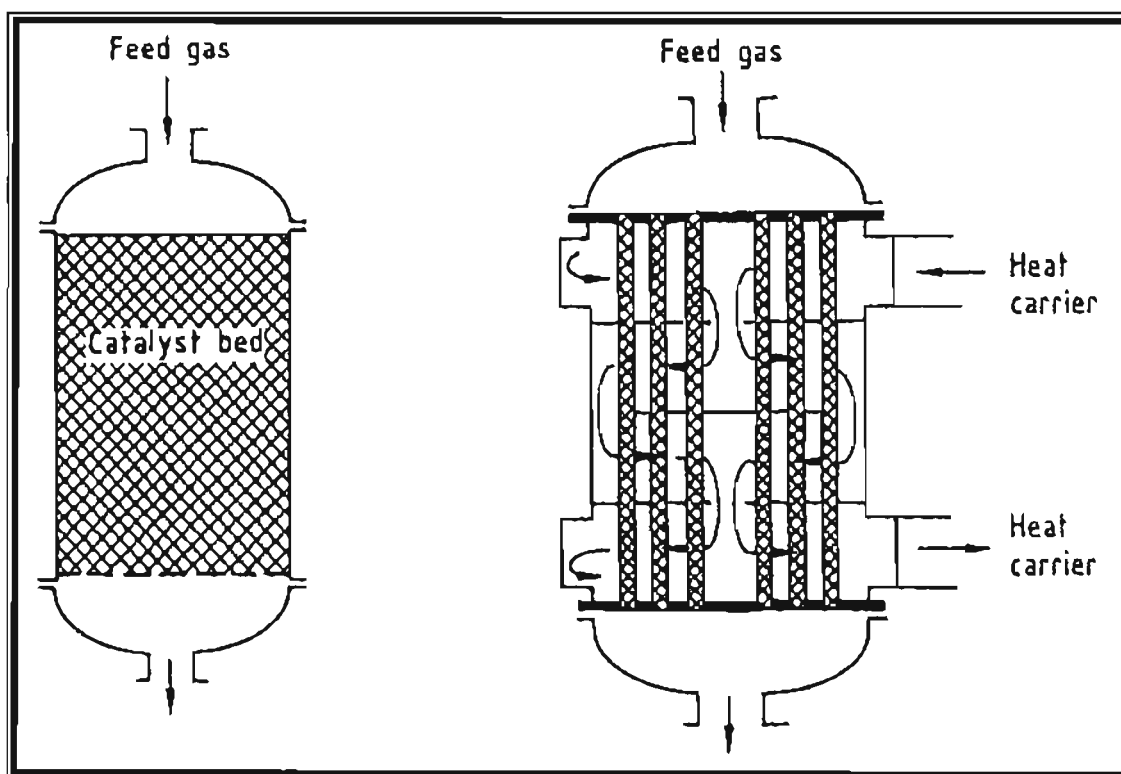


Figure 4.3: An adiabatic fixed bed reactor and a multitubular fixed bed reactor [5]

Fixed beds can be operated adiabatically or isothermally. Adiabatic reactors are usually applied for reactions with low heats of reactions or where there is only one major reaction pathway. The simplest adiabatic fixed bed consists of a cylindrical jacket in which the catalyst is loosely packed on a support and reactant flow is from the top to the bottom in an axial direction [4]. The top to bottom flow suppresses catalyst abrasion.

Multistage reactors consisting of sequential adiabatic stages may be separated by interstage heat exchangers. Isothermal fixed bed reactors are cooled or heated through the reactor walls. Isothermal fixed beds are of particular importance to oxidation reactions, which are highly exothermic. In a multitubular fixed bed reactor, the catalyst is arranged in the tubes, and a heat carrier circulates externally around the tubes.

Fixed bed reactors may be operated at very low conversions as a differential reactor or at high conversions as an integral reactor. In a differential flow reactor, the residence time is short so that the conversion remains small. This is usually achieved by using short catalytic beds or with the use of high feed flow rates. In this mode of operation, the whole catalyst is considered to be exposed to the same concentration of reactants. Variations in the volumetric flow rate are neglected and the observed or apparent conversion rate is determined directly from measuring concentrations at the inlet and outlet of the reactor [6].

The advantages of using a fixed bed in the differential mode are [4]:

- Parameters such as temperature, pressure and concentration can be separately studied
- Provides good kinetic data, true plug flow is easier to achieve
- Mass and heat transfer influences reduced

The disadvantages of using a fixed bed in the differential mode are [4]:

- Large errors in analysis can occur (small conversions)
- Technique is time consuming in kinetic measurements
- High gas velocities may be required to keep conversion low

The integral reactor has several advantages, which make it a commonly used system. Large conversions facilitate analysis and provide accurate kinetic data. Integral reactors are easier and cheaper to build compared to reactors that require recycling. The main disadvantage of an integral reactor is the difficulty in maintaining an isothermal operation. Additionally, high conversions lead to concentration gradients, as there may be significant mass transfer resistance or axial dispersion [2].

An example of a commercial fixed bed reactor is shown in **Figure 4.4** below:

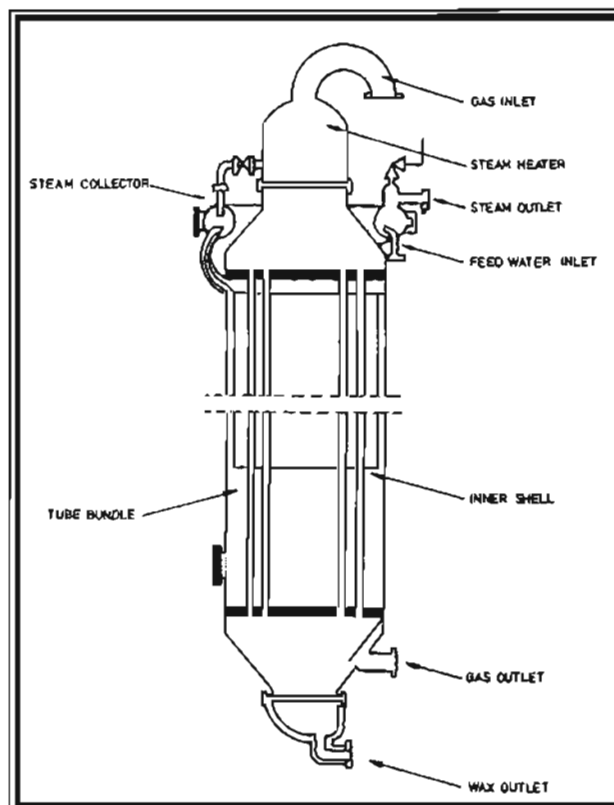


Figure 4.4: Sasol's commercial fixed bed Fischer-Tropsch reactor [7]

The above reactor is used by Sasol to produce liquid hydrocarbons and waxes. It was first used in 1955. This fixed bed reactor performs well with no major problems [7]. Each fixed bed reactor consists of two thousand and fifty tubes of fifty millimeters in internal diameter (only four shown in **Figure 4.4**). The length of the tubes is twelve meters. About twenty litres of pellet shaped catalysts are packed into these tubes. The tubes are surrounded by water. The desired reactor temperature is maintained by controlling the steam pressure above the water. This reactor operates between 200 and 250 °C. The normal operating pressure is about 27 atm. Fischer-Tropsch reactions are highly exothermic and efficient heat removal is required. High linear velocities of feed are used to ensure a high rate of heat exchange between the catalyst particles and the tube walls.

4.1.2 Fluidized bed reactors

In this reactor, gasses or liquids are forcefully fed from the bottom upwards through the catalyst bed. The initially stationary catalyst bed is brought to a fluidized-state when the volume flow rate of the gas or liquid exceeds a certain limiting value, the minimum fluidization volume flow rate. Catalyst particles are suspended in the fluid stream. Fluidized bed reactors are characterized by excellent gas-solid contact in the bed (catalyst is in contact with reactants and products at all times), good mass transfer and high bed-wall heat transfer coefficients. Some applications for these reactors include: rapid catalyst deactivation systems, slow catalyst deactivation systems and catalytic systems operating within the flammability limits. Catalytic cracking is carried out in fluidized bed reactors because the solid acid catalysts are rapidly deactivated by coke deposition. The catalyst is continuously discharged from the reactor and regenerated in an air fluidized generator bed where the coke is burned off. The regenerated catalyst can then be returned to the reactor. Relatively large amounts of catalyst are required for fluidized bed reactors and this diminishes its suitability for catalytic studies.

The major advantages of a fluidized bed reactor include [8]:

- Easy handling and transport of catalysts due to the liquid-like behavior of the fluidized bed
- Uniform temperature distribution due to intensive catalysts mixing, no hot spots are formed even with strongly exothermic reactions
- Better utilization of the surface of non-porous catalysts due to smaller sizes of particles used
- High heat transfer coefficients between bed and immersed heating or cooling surfaces
- High gas throughput and high product concentration
- May be cheaper to construct than a multi-tube reactor of the same capacity.

The major disadvantages of a fluidized bed reactor include [8]:

- Expensive catalyst separation or gas purification equipment required because of catalyst entrainment by fluidizing gas
- High catalyst mixing rate can result in backmixing of gas and lower conversions. To provide a comparable conversion to that of a fixed bed reactor, a fluidized bed must be much larger
- Bubble formation may lead to a broad residence-time distribution
- Attrition of catalysts result from high flow velocities. Catalysts must be resistant to abrasion but not excessively hard so as to erode equipment
- Agglomeration may lead to defluidization
- Scaling up from a laboratory to an industrial scale and reactor modeling can be complex.

An example of a commercial fluidized bed is shown below [7]:

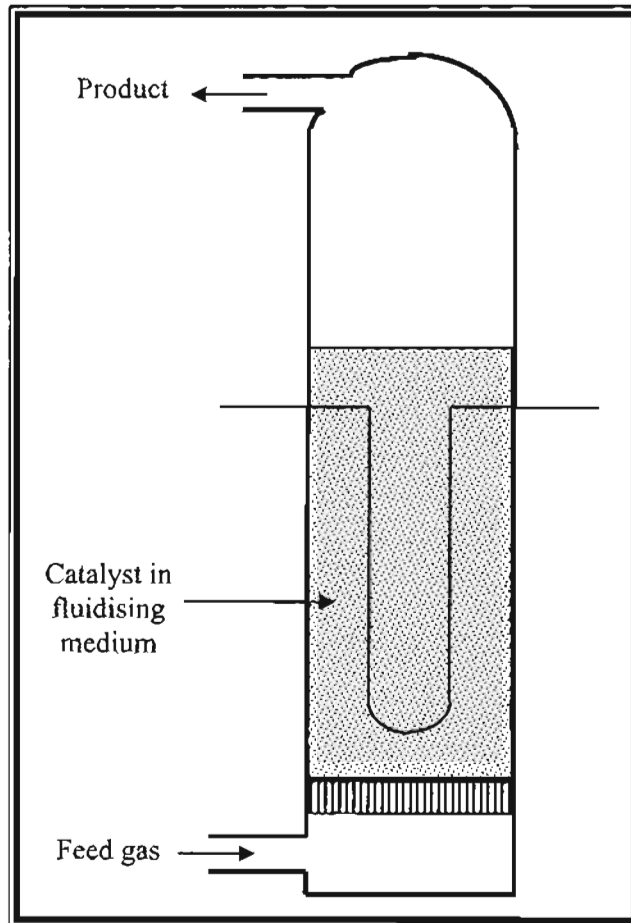


Figure 4.5: Schematic of a Sasol Advanced Synthol (SAS) reactor [7]

The above reactor is used mainly to make petrol, diesel and olefins. Gas is fed from the bottom. This pushes the catalyst particles upwards while gravity causes the particles to drop. This results in a fluidized bed. The reactor is operated at 350 °C and the operating pressure is between 20 to 40 bar.

4.1.3 Continuous stirred tank reactors (CSTR)

The CSTR and the plug flow reactor are the two extremes of continuous reactor types. Whilst the plug flow reactor does not have mixing, the CSTR has extremely good mixing (Figure 4.6).

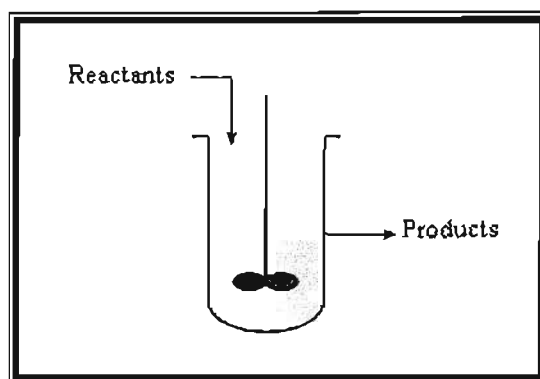


Figure 4.6: Schematic representation of a continuous stirred tank reactor (CSTR)

The CSTR reactor is used frequently for the study of liquid phase reactions at a constant temperature. It has been adapted for the study of heterogeneous gas-solid reactions [9]. The Carberry reactor is a well-known example of a gas-phase CSTR [2,4]. Other types of CSTR reactors include: Berty reactor, stirred tank reactor and the jet-loop reactor. In the Carberry reactor, a fixed amount of catalyst is contained in a wire mesh basket, which rotates at high speed in the vicinity of the reactant gas. Since the reactant gas is well mixed and in intimate contact with the catalyst particles, the concentration and temperature of the contents of the reactor will be essentially constant [9]. Uncertainty of the catalyst temperature is a major disadvantage of this reactor [4]. The temperature is usually inferred from the heat of the reaction, the rate of heat and mass transfer or the reaction rate. These reactors are therefore not recommended for oxidation reactions or highly endothermic reactions. In addition, gas-phase reactions are usually fast and in CSTR systems, the intrinsic rates may be obscured by heat and mass transfers [2].

4.1.4 Batch reactors

These reactors can be used for liquid reactants with solid / liquid catalysts or for gas reactions with solid catalysts. In the latter case, a closed system with circulation of the gas is frequently used (Figure 4.7). The partial pressures or concentrations of reactants and products, in the system, vary throughout the reaction. The progress of the reaction can be monitored by partial pressure changes or by sampling.

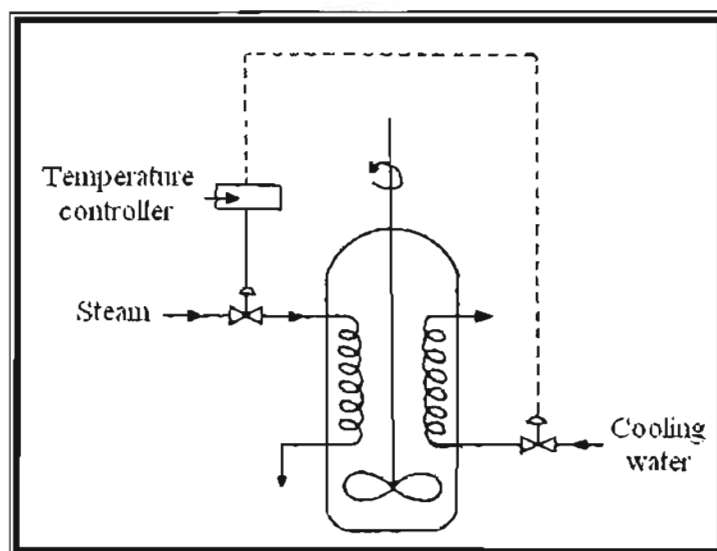


Figure 4.7: Schematic representation of a batch reactor containing heating and cooling coils [9]

The advantages of a batch reactor are [4]:

- It is simple and allows rapid measurements
- Multiple experiments can be accomplished in a short time
- It is convenient when using pure, expensive, corrosive or high boiling temperature chemicals
- It can be used more effectively with poison sensitive catalysts, as there are no accumulation effects
- By varying the stirring conditions, it may be possible to investigate the influence of heat and mass processes

The disadvantages of a batch reactor are [4]:

- The large thermal capacity of the reactor may limit the heating up and cooling down rates
- It may be difficult to determine the start of the reaction
- Sampling may require separation of products from catalyst
- It may be difficult to control the temperature and pressure independently

4.1.5 Transient reactors

The pulse reactor is an example of a transient reactor. The pulse reactor can be made up of a tube through which a carrier gas flows at a constant rate. A single pulse of reactant is injected into this carrier gas before the reactor tube. Reactants and products in the exit pulse are separated and analyzed. Extremely small amounts of catalyst are used in these reactors. Pulse reactors are suitable for mechanistic investigation with isotopic tracers. The advantages of this reactor are:

- relatively simple system
- small amounts of reactant and catalyst are required
- tests can be conducted quickly.

The disadvantages of pulse reactors include:

- The measurements of precise kinetic data is not always convenient
- Kinetic treatment requires complex mathematical analysis
- Selectivities observed may be misleading, as steady conditions have not been established
- Material balances are difficult to establish.

Another important reactor is the TAP (temporal analysis of products) reactor. It is a powerful reactor used for gaining insight into the mechanisms of complex catalytic reactions [13]. No carrier gas is used in this reactor. Gas transport results from a pressure gradient.

4.1.6 Monolith reactors

Monoliths are single solid blocks manufactured from ceramic or metal. They contain multiple arrays of well-defined finned or unfinned channels (Figure 4.8). The walls between the channels are usually thin and impregnated by high surface area washcoat layers into which catalytic material is impregnated [14]. The channels in the monoliths can be honeycomb, square or circular shaped. They are widely used as catalytic converters. Short contact time monoliths have been recently used for selective oxidations [14]. High temperatures (1000 °C) and millisecond contact times were used. Paraffin-rich feeds were converted to olefins using a limited amount of oxygen.

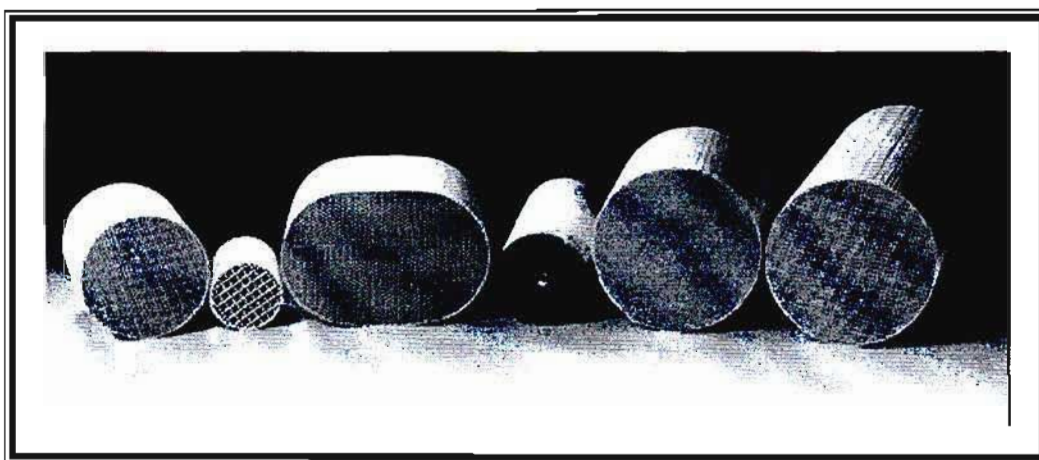


Figure 4.8: Different shapes and sizes of monolith material [15]

4.1.7 Membrane reactors

Catalytic membrane reactors are reactors that couple, in the same unit, a conversion effect (catalyst) and a separation effect (membrane). These reactors are suitable for equilibrium restricted reactions such as paraffin dehydrogenation reactions. The selective removal of hydrogen from the reaction shifts the equilibrium towards olefin formation. These reactors may also result in improved selectivity of catalytic reactions. Membranes can control the addition of reactants by selective permeation thereby reducing secondary reactions. Most catalytic membranes are made up of inorganic material. They can be either dense or porous and made from metals or metal oxides. The catalytic membrane reactor (CMR), the catalytic nonpermselective membrane reactor (CNMR), the packed bed membrane reactor (PBMR) and the packed bed catalytic membrane reactor (PBCMR) are four common catalytic membrane reactor types. The CMR consists of a support layer and a permselective layer (membrane) with a catalytic function. The CNMR consists of a support layer and a nonpermselective catalytic layer. The PBMR consists of an inactive permselective layer with the catalyst located in the feed stream. In the PBCMR, the catalyst is located external to the supported permselective membrane.

4.2 References

1. Hagen, J., *Industrial Catalysis – A Practical Approach*, Wiley-VCH, Federal Republic of Germany, 1999, p. 327.
2. Anderson, J. R. and Pratt, K. C., *Introduction to Characterization and Testing of Catalysts*, Academic Press Inc., London, 1985, pp. 292-321.
3. Kapteijn, F. and Moulijn, J. A., *Handbook of Heterogeneous Catalysis*, (Ertl, G., Knozinger, H. and Weitkamp, eds.), Wiley-VCH, Federal Republic of Germany, Vol. 3, 1997, pp.1359-1376.
4. Haber, J., Block, J. H. and Delmon, B., *Handbook of Heterogeneous Catalysis*, (Ertl, G., Knozinger, H. and Weitkamp, eds.), Wiley-VCH, Federal Republic of Germany, Vol. 3, 1997, pp. 1546-1549.
5. Eigenberger, G. I., *Handbook of Heterogeneous Catalysis*, (Ertl, G., Knozinger, H. and Weitkamp, eds.), Wiley-VCH, Federal Republic of Germany, Vol. 3, 1997, pp. 1399-1408.
6. Wijngaarden, R. J., Kronberg, A. and Westerterp, K. R., *Industrial Catalysis*, Wiley-VCH, New York, 1998, p 91.
7. Dry, M. E., *Applied Industrial Catalysis*, Academic Press Inc., (Leach, B. E., ed.), London, 1983, pp. 171-174.
8. Werther, J. and Schoenfelder, H., *Handbook of Heterogeneous Catalysis*, (Ertl, G., Knozinger, H. and Weitkamp, eds.), Wiley-VCH, Federal Republic of Germany, Vol. 3, 1997, pp. 1426-1427.
9. Thomas, J. M. and Thomas W. J., *Principles and Practice of Heterogeneous Catalysis*, VCH Publishers Inc., New York, 1997, pp. 477-502.
10. Beenackers, A. A. C. M., *Handbook of Heterogeneous Catalysis*, (Ertl, G., Knozinger, H. and Weitkamp, eds.), Wiley-VCH, Federal Republic of Germany, Vol. 3, 1997, pp. 1444-1460.
11. <http://www.cffls.uky.edu/C1/2002%20meeting/ROukaci%20Current%20FT%200vreview.pdf> (Accessed: before June 2005)
12. <http://www.p.lodz.pl/chemical/kongres/sekcja/1/ku/8a.doc> (Accessed: before June 2005)
13. http://w3.rz-berlin.mpg.de/~jentoft/lehre/breitkopf_tapssitka_141103.pdf
14. Dudukovic, M. P., Larachi, F. and Mills, P. L., *Catal. Rev.*, **44**, 2002, 123.
15. <http://www.dct.tudelft.nl/monoliet/Intro/introduction.html> (Accessed: 01/10/2006)

CHAPTER 5: The Vanadium Magnesium Oxide (VMgO) Catalytic System

5.1 Vanadium in selective oxidation catalysts

The only selective gas-phase paraffin oxidation practiced commercially is the *n*-butane to maleic anhydride process. The vanadium phosphorus oxide (VPO) catalytic system is used. Vanadium, together with nickel and molybdenum are essential components in most known selective oxidation catalysts. The preferred element is vanadium [1]. It is generally accepted that the first step in the selective oxidation of paraffins involves the activation of the paraffin *via* hydrogen abstraction. The vanadium oxide catalytic system shows superior activity in this activation step. This high activity permits the oxidation reaction to be carried out at lower temperatures than other metal oxide systems. The use of milder conditions imparts improved selectivity towards non-combustion products with vanadium oxide catalytic systems. Unsupported vanadium oxide, on its own, is unsuitable for selective oxidation of paraffins. It favours the formation of total oxidation products. To form a selective paraffin oxidation catalyst, vanadia are appropriately dispersed on a suitable support.

5.2 Supported vanadia

The advantage of supporting metal oxides includes: high mechanical strength, greater thermal stability and larger surface areas [2]. It is well known that spreading vanadia on a support results in the formation of centers with peculiar physico-chemical features and reactivity [1,2]. The nature and the catalytic behaviour of supported vanadia are dependent on the nature of the support. Supports, which have been tested, are [1-6]:

- Metal oxides – SiO_2 , TiO_2 , Al_2O_3 , MgO
- Mixed metal oxides – $\text{TiO}_2/\text{SiO}_2$, $\text{TiO}_2/\text{Al}_2\text{O}_3$, $\text{SiO}_2/\text{Al}_2\text{O}_3$, calcined hydrotalcites
- Zeolites – aluminophosphates such as $\text{AlPO}_4\text{-5}$
- Monolithic ceramic supports and inert ceramic membranes

Acidic supports favour the agglomeration of acidic vanadium oxide species on the surface. With basic supports, the interaction between vanadium oxide species and the support is stronger and the vanadium oxide species are well dispersed on the support. The vanadium magnesium mixed metal oxide (VMgO) is the most selective oxidative dehydrogenation catalytic system reported for short chain paraffins [1-3,6]. Supporting vanadia on magnesium oxide leads to the formation of magnesium vanadate.

5.3 Preparation of magnesium vanadates

Magnesium vanadates are prepared by solid-state reactions. Vanadium pentoxide is an acidic oxide that readily reacts with basic magnesium oxide. The easiest preparative method involves the physical mixing of vanadium pentoxide and magnesium oxide in the appropriate stoichiometry. This mixture is calcined at an appropriate temperature and for a specific time. Differential thermal analysis (DTA) studies are useful in the selection of such parameters, although other factors are also significant, such as the purity of the starting material. Depending on the conditions used, pure or mixed phases can be obtained. This method is unsuitable for obtaining high surface area vanadates [7]. Vanadates with high surface areas can be obtained by impregnation techniques.

The preparation technique has been shown to influence the catalytic properties of magnesium vanadates. It was found that different vanadium species, surface areas and vanadium/magnesium ratios could be obtained in the synthesis. The source of vanadium is either ammonium metavanadate or vanadium oxalate. These can be impregnated onto magnesium hydroxide [9], magnesium oxide [8,10] or magnesium oxalate [8]. Magnesium oxide can be obtained from its corresponding carbonate (1), hydroxide (2) or oxalate (3) as follows [8]:

(1) Magnesium carbonate is precipitated at pH 6.5, by adding ammonium carbonate to a magnesium nitrate solution. The resultant precipitate is filtered, washed and dried at 80 °C for 16 hours. The magnesium carbonate produced is then calcined at 700 °C for 3 hours to yield MgO-1.

(2) Magnesium hydroxide is precipitated at pH 10, by adding ammonium hydroxide to a magnesium sulphate solution. The resultant precipitate is filtered, washed and dried at 80 °C for 16 hours. The magnesium hydroxide produced is then calcined at 600 °C for 6 hours to yield MgO-2.

(3) Magnesium oxalate is precipitated at pH 5-6, by adding oxalic acid to a magnesium acetate solution. The resultant precipitate is filtered, washed and dried at 80 °C for 16 hours. The magnesium oxalate produced is then calcined at 700 °C for 3 hours to yield MgO-3.

MgO-3 gave vanadates with the highest surface area whilst the lowest surface areas were obtained with MgO-1 [8]. Differences in surface area were close to 100 m²/g. Differences in pore sizes were also observed.

Impurities in the starting oxides were also shown to affect the preparation of vanadate phases and their catalytic activity. Residual amounts of potassium, in particular, were shown to reduce the selectivity to dehydrogenated products in the oxidative dehydrogenation of butane. Potassium was found to facilitate the formation of the pyrovanadate phase and to increase its thermal stability [11].

Another way of preparing magnesium vanadates is by the citrate method [12]. This method has the following advantages:

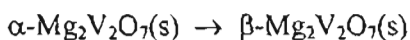
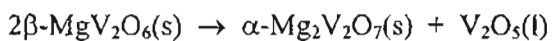
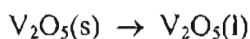
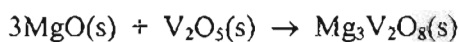
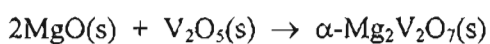
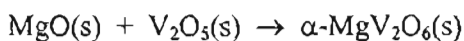
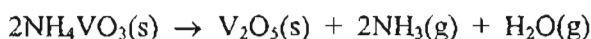
- Oxide compounds can be obtained from very homogeneous citrate precursors
- Lower calcination temperatures could be used
- Higher surface area of the vanadate phases can be realized
- Contamination from other residual elements can be minimized

The main steps of the citrate method are [12]:

- Preparation of a transparent solution of magnesium nitrate and ammonium metavanadate in such a concentration that the atomic ratio of Mg/V in solution is equal to that in the resulting catalyst
- Addition of small amounts of nitric acid in order to avoid precipitation
- Addition of citric acid in such a manner that the molar number of equivalent anions is equal to that of the cations (Mg^{2+} and V^{5+})
- Evaporation of the obtained solution at 40 °C under reduced pressure, until the solution becomes viscous, and then at 90 °C until a solid is obtained
- Decomposition of the solid at 380 °C for 18 hours, followed by calcination at 550 °C for 6 hours

5.4 Magnesium vanadates

Three distinct stable phases of magnesium vanadates are known. These are magnesium orthovanadate ($\text{Mg}_3\text{V}_2\text{O}_8$), magnesium pyrovanadate ($\text{Mg}_2\text{V}_2\text{O}_7$) and magnesium metavanadate (MgV_2O_6) [13]. Polymorphic forms for the pyrovanadate and metavanadate can also be formed. The appropriate stoichiometry, the calcination temperature and heating rate, the calcination time and the purity of the starting oxides determine which phases are present. The possible phase transitions, which can occur when solid ammonium vanadate reacts with magnesium hydroxide below 900 °C are [9]:



The arrangements of oxygen atoms around the vanadium atom in vanadates are shown below:

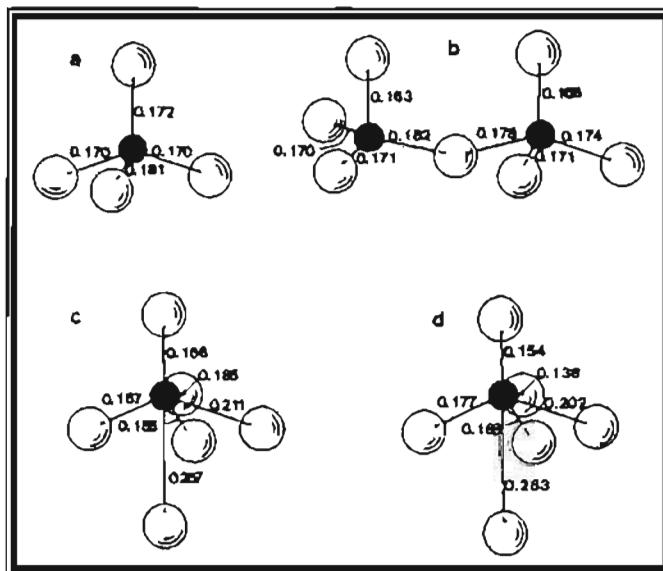


Figure 5.1: The local environment of vanadium in a) $\text{Mg}_3\text{V}_2\text{O}_8$, b) $\beta\text{-Mg}_2\text{V}_2\text{O}_7$, c) MgV_2O_6 and d) V_2O_5 (distances are given in nanometers) [9]. The black balls represent vanadium and the white balls represent oxygen.

The structure of $\text{Mg}_3\text{V}_2\text{O}_8$ is characterized by chains of edge-sharing MgO_6 units linked by isolated VO_4 tetrahedra. All oxygen atoms are bridged between a vanadium and a magnesium atom. The oxygen packing around the vanadium atom is highly constricted (Figure 5.1) [9]. Magnesium orthovanadate consists of near cubic close packing of oxygen atom layers with the magnesium atoms in octahedral sites and the vanadium atoms in tetrahedral sites (Figure 5.2) [14]. The vanadium-oxygen bonds possess a covalent character.

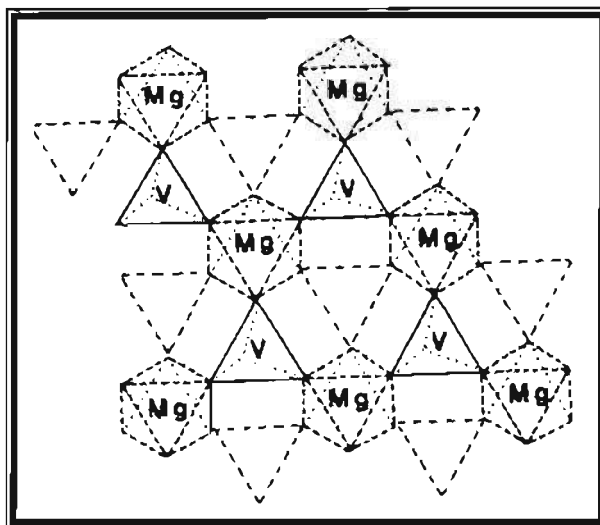


Figure 5.2: Structure of the orthovanadate phase [14]

$\alpha\text{-Mg}_2\text{V}_2\text{O}_7$ is made up of corner-sharing VO_4 tetrahedra that form V_2O_7 units. The structure consists of rows of these V_2O_7 groups with long vanadium-oxygen bridges within these groups (Figure 5.3) [15]. Each of the terminal oxygen atoms of the V_2O_7 groups is shared with two magnesium atoms, except the oxygen with the shortest bond (0.163 nm), which is connected to only one magnesium atom. The vanadium-oxygen bonds are less covalent than those in the orthovanadate structure [9].

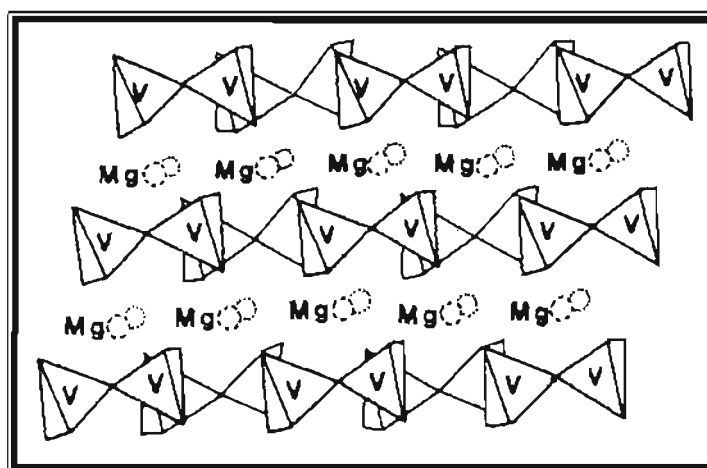


Figure 5.3: Structure of the pyrovanadate phase [15]

MgV_2O_6 consists of VO_5 octahedra joined by edges and connected together through MgO_6 octahedra (Figure 5.4) [16]. The VO_6 octahedra are highly distorted and are similar to those in V_2O_5 . The vanadium-oxygen bonds possess an ionic character.

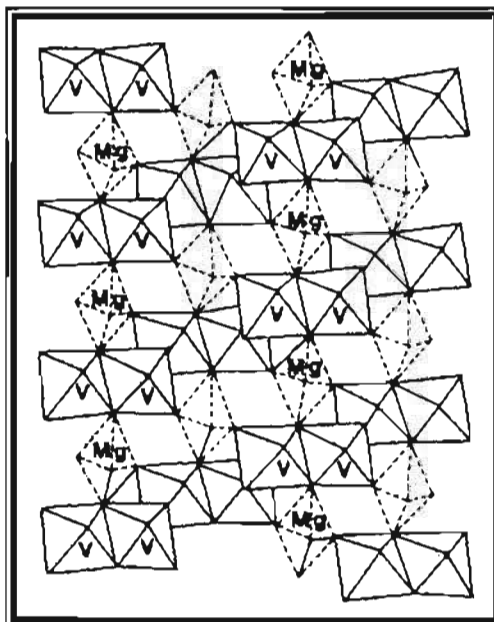
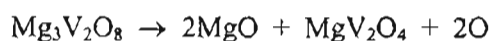


Figure 5.4: Structure of the metavanadate phase [16]

Recent evidence suggests that under reaction conditions, the surface of the VMgO catalyst can undergo structural changes [17]. Both structural ordering and disordering have been observed. Under mildly reducing conditions, it was shown that magnesium orthovanadate transforms to a cubic spinel structure i.e. $\text{Mg}_2\text{V}_2\text{O}_7$. The following reaction has been proposed [17]:



Conclusive proof remains to be established. It is clear though, that an unused catalyst is different from an *in situ* characterized catalyst.

5.5 Nature and influences of the active site

The catalytic properties of the vanadate phases, vanadium pentoxide and the VPO catalyst are shown in Table 5.1 [2]. The two main active phases of VMgO for the oxidative dehydrogenation of paraffins are magnesium pyrovanadate (α -Mg₂V₂O₇) and magnesium orthovanadate (Mg₃V₂O₈). The more active and selective phase is controversial. Both phases have been reported by recognized research groups to be superior [9,10,18,19]. Although the subject remains contentious, it has emerged that the presence of one phase alone inadequately explains catalytic performance. Recently the orthovanadate phase, either with a co-existing pyrovanadate phase or with an excess of the magnesium oxide phase, was considered to give optimum catalytic performance [6,20]. Pure magnesium oxide has low activity and is relatively unselective. The enhanced catalytic performance is presumed to come from a synergistic effect between the vanadate phase and excess magnesium oxide. This is consistent with the observation that pure vanadates have exhibited lower activity and selectivity [19].

| Catalyst | Vanadium species | H-abstraction selectivity | Oxygen insertion power |
|---|---|---------------------------|------------------------|
| Mg ₃ V ₂ O ₈ | Isolated VO ₄ | ↑ | Undetected ↓ |
| MgV ₂ O ₆ | Isolated VO ₆ | | |
| Mg ₂ V ₂ O ₇ | VO ₃ – O – VO ₃ | | |
| V ₂ O ₅ | VO ₂ – O – VO ₂ | | |
| VPO | (VO) ₂ P ₂ O ₇ | | |

Table 5.1: Catalytic properties of vanadium based catalysts [2]

The specific activity of vanadium has been shown to be dependent on the vanadium content of a VMgO catalyst for propane oxidative dehydrogenation [1]. This indicates that the vanadium ions act as active sites for propane oxidation. Vanadium in its highest oxidation state (+5) is considered to be the key component in gas-phase activation of paraffins [21,22]. The selectivity of the orthovanadate phase is attributed to isolated VO₄ units, separated from each other by MgO₆ units. All lattice oxygen atoms are bridged between V⁵⁺ and Mg²⁺. V⁵⁺–O–V⁵⁺ groups are absent. These groups are associated with total oxidation [23]. The V⁵⁺ ions are easily reduced, thereby allowing lattice oxygen to be removed with ease. These groups are present in the metavanadate and pyrovanadate phases.

Furthermore, it has been conclusively shown that the ease of removal of the lattice oxygen bridging a vanadium atom and a metal ion is an important factor in determining selectivity [23,24]. If the metal cation is more difficult to reduce, then the selectivity will be greater. Aside from magnesium, the rest of the alkaline earth metals do not form selective catalysts. This is because they form stable carbonates under reaction conditions. These alkali earth vanadates slowly decompose into vanadium pentoxide and the corresponding carbonates. Barium vanadate was shown to be quite selective but its performance diminished with increasing carbonate formation [23].

The reducibility of the metal cation has been correlated to its aqueous reduction potential. The Mg^{2+} ion, with a reduction potential of -2.40 V, is one of the most difficult cations to reduce [24]. This is consistent with its high selectivity for dehydrogenated products. The strength of a metal-oxygen bond can also be determined by measuring the heat involved in reoxidation of the reduced oxide or by measuring the temperature of onset of reduction in temperature programmed reduction (TPR) studies [6,25]. Selectivity towards dehydrogenated products can be understood in terms of two competing reactions. One in which bridged lattice ions activate a paraffin to form a surface hydroxyl group and an adsorbed alkyl species, which can then lose a hydrogen atom, forming a dehydrogenated product and the other reaction involves the lattice oxygen forming oxygen containing species. The oxygen-containing species then rapidly form combustion products.

Additionally, greater selectivity is associated with VMgO due to the absence of $V=O$ functional groups in magnesium orthovanadate. This functional group is present in vanadium pentoxide and is also found in VPO catalysts. It has strong oxygen insertion character and its absence results in oxygenated products not being formed in orthovanadate catalysts [10].

5.6 Stability of products

One reason why the only commercialized process for the selective oxidation of paraffins is successful is due to the stability of the product (maleic anhydride). The stability of most products can be improved by decreasing their interaction (residence time) with the catalytic surface. For dehydrogenated products, this is related to the basity of the catalytic surface. The basity of the VMgO surface is due to magnesium oxide. A basic surface favours the desorption of basic products such as olefins (considered basic because of electron dense π bonds) [5]. Rapid desorption of products results in enhanced selectivity as consecutive reactions are suppressed.

5.7 The performance of the VMgO catalytic system

The VMgO catalytic system has been shown to be active for the oxidative dehydrogenation of short chain paraffins and ethyl benzene:

| Feed | Temperature (°C) | Conversion (%) | Selectivity mono-olefins (%) | TDS (%) | Reference |
|------------------|------------------|------------------|------------------------------|---------|-----------|
| Propane | 540 | 12 | 62 | 62 | 18 |
| | | 20 | 54 | 54 | |
| | | 29 | 43 | 43 | |
| | | 40 | 34 | 34 | |
| Propane | 550 | 32 | 38 | 38 | 9 |
| | | 45 | 28 | 28 | |
| | | 63 | 38 | 38 | |
| Propane | 510 | 2.7 | 86 | 86 | 26 |
| <i>n</i> -Butane | 475 | 4 | 53 | 68 | 27 |
| | | 9.5 | 42 | 60 | |
| | 480 | 11 | 28 | 54 | |
| | | 31 | 29 | 53 | |
| | 500-540 | 40 | 20 | 53 | |
| | | 18 | 36 | 53 | |
| 23 | 32 | 53 | | | |
| <i>n</i> -Butane | 520 | 11.3 | 39 | 56.4 | 28 |
| | | 8.1 ^a | 47.4 | 58.2 | |
| Cyclohexane | 484 | 9 | 52 | 88 | 29 |
| | | 11 | 47 | 85 | |
| | | 16 | 37 | 78 | |
| | | 21 | 28 | 80 | |
| Ethylbenzene | 277 | 97 | 76 | 76 | 30 |

^aSteam was added to the feed

Table 5.2: Summary of the catalytic performance of VMgO. TDS = total dehydrogenation selectivity, which includes dienes (butane feed), benzene (cyclohexane feed) and styrene (ethylbenzene feed) produced in addition to any mono-olefins formed.

The performance of the VMgO system achieved in the oxidative dehydrogenation of propane to propylene is compared to that of other catalytic systems in Figure 5.5 [1]:

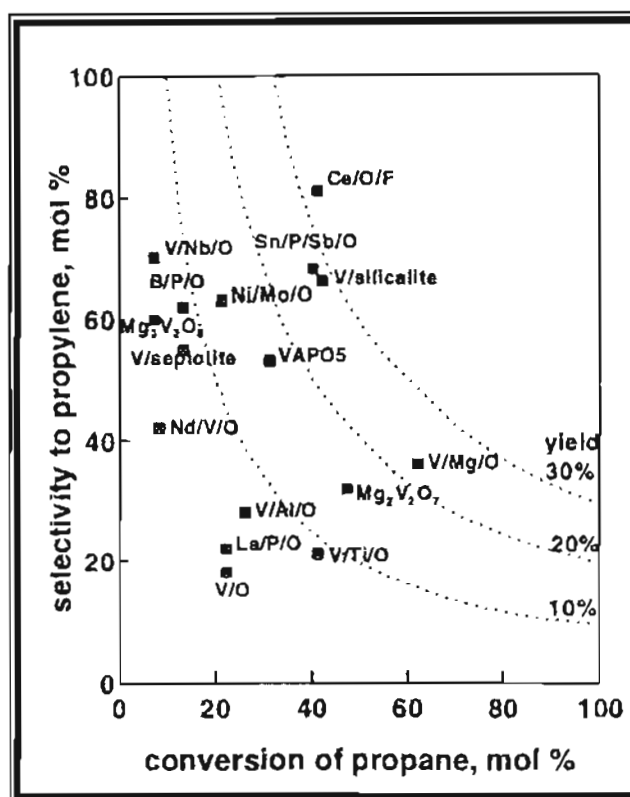


Figure 5.5: Highest yields to propylene reported for the oxidative dehydrogenation of propane [1]

In Figure 5.5, it can be seen that vanadium oxide is a component in most of the catalytic systems studied. The highest yield to propylene obtained with a vanadium magnesium oxide catalyst is 24 % [1,9].

5.8 References

1. Albonetti, S., Cavani, F. and Trifiro, F., *Catal. Rev. Sci. Eng.*, **38**, 1996, 413.
2. Blasco, T. and Lopez Nieto, J. M., *Appl. Catal. A*, **157**, 1997, 117.
3. Mamedov, E. A. and Corberan, V. C., *Appl. Catal. A*, **127**, 1995, 1.
4. Wainright, M. S. and Foster, N. F., *Catal. Rev. Sci. Eng.*, **19**, 1979, 211.
5. Dadyburjor, D. B., Jewur, S. S. and Ruckenstein, E., *Catal. Rev. Sci. Eng.*, **19**, 1979, 293.
6. Madeira, L. M. and Portela, M. F., *Catal. Rev. Sci. Eng.*, **44**, 2002, 247.
7. Kung, H.H. and Kung, M. C., *Appl. Catal. A*, **157**, 1997, 105.
8. Corma, A., Lopez Nieto, J. M and Paredes, N., *J. Catal.*, **144**, 1993, 425.
9. Siew Hew Sam, D., Soenen, V. and Volta, J. C., *J. Catal.*, **123**, 1990, 417.
10. Chaar, M. A., Patel, D., Kung, M. C. and Kung, H. H., *J. Catal.*, **105**, 1987, 483.
11. Kung, H.H. and Kung, M. C., *J. Catal.*, **134**, 1992, 668.
12. Gao, X., Ruiz, P., Xin, Q., Guo, X. and Delmon, B., *Catal. Lett.*, **23**, 1994, 321.
13. Clark, G. M. and Morley, R., *J. Solid State Chem.*, **16**, 1976, 429.
14. Krishnamachari, N. and Calvo, C., *Can. J. Chem.*, **49**, 1971, 1630.
15. Gopal, R. and Calvo, C., *Acta. Crystallogr.*, **30**, 1974, 2491.
16. Ng, H. N. and Calvo, C., *Can. J. Chem.*, **50**, 1972, 3619.
17. Burrows, A., Kiely, C. J., Perregaard, J., Hojlund-Nielsen, P. E., Vorbeck, G., Calvino, J. J. and Lopez-cartes, C., *Catal. Lett.*, **57** 1999, 121.
18. Chaar, M. A., Patel, D., Kung, M. C. and Kung, H. H., *J. Catal.*, **109**, 1988, 463.
19. Eon, J. G., Olier, R. and Volta, J. C., *J. Catal.*, **145**, 1994, 318.
20. Gao, X., Ruiz, P., Xin, Q., Guo, X. and Delmon, B., *J. Catal.*, **148**, 1994, 56.
21. Busca, G., Cavani, F., Centi, G. and Trifiro, F., *J. Catal.*, **99**, 1986, 400.
22. Harrouch Batis, N., Batis, H., Ghorbel, A., Vadrine, J. C. and Volta, J. C., *J. Catal.*, **128**, 1991, 248.
23. Patel, D., Andersen, P. J. and Kung, H. H., *J. Catal.*, **125**, 1990, 132.
24. Owen, O. S. and Kung, H. H., *J. Mol. Catal.*, **79**, 1993, 265.
25. Owen, O. S., Kung, M. C. and Kung, H. H., *Catal. Lett.* **12**, 1992, 45.
26. Creaser, D., Andersson, B., Hudgins, R. R. and Silveston, P. L., *J. Catal.*, **182**, 1999, 264.
27. Hung, H. H., *Adv. Catal.*, **40**, 1, 1994
28. Lemonidou, A. A., Tjatjopoulos, G. J. and Vasalos, I. A., *Catal. Today*, **45**, 65, 1998.
29. Kung, M. C. and Kung, H. H., *J. Catal.*, **128**, 1991, 287.
30. <http://www.ec-combicat.org/downloads/abstracts/Geisler.pdf> (Accessed before June 2005)

CHAPTER 6: Experimental

6.1 Materials used

The materials used are shown in Tables 6.1 and 6.2 below:

| Reagent | Molar mass (g/mol) | Supplier | Purity |
|--|--------------------|--------------------|----------|
| H ₂ C ₂ O ₄ ·2H ₂ O | 90.04 | Aldrich | 99 % |
| Mg(CH ₃ CO ₂) ₂ ·4H ₂ O | 214.46 | Aldrich | 99 % |
| NH ₄ VO ₃ | 116.98 | Aldrich | 99+ % |
| NH ₄ OH (aq) | 35.05 | Rochelle Chemicals | 99.9+ % |
| Sb ₂ O ₃ | 291.50 | Aldrich | 99.999 % |
| Nb ₂ O ₅ | 265.81 | Alfa Aesar | 99.5 % |
| (NH ₄) ₆ Mo ₇ O ₂₄ ·4H ₂ O | 1235.86 | Aldrich | 99.98 % |
| Bi(NO ₃) ₃ ·5H ₂ O | 485.07 | Aldrich | 99.99+ % |
| TeO ₂ | 159.60 | Aldrich | 99.995 % |
| CsNO ₃ | 194.91 | Aldrich | 99 % |
| <i>n</i> -Octane | 114.23 | Acros Organics | 97 % |
| <i>n</i> -Hexane | 86.18 | Acros Organics | 99+ % |
| Styrene | 104.15 | Aldrich | 99+ % |
| 2-Hexene, 3-hexene | 84.16 | Aldrich | 97 % |
| Ethylbenzene | 106.17 | Aldrich | 99% |
| <i>o</i> -Xylene | 106.17 | Aldrich | 98% |

Table 6.1: Chemicals used for synthesis, calibration and as feedstock

| Gas | Usage | Supplier | Purity |
|---|-------------|----------|------------------|
| Nitrogen | GC, diluent | Afrox | Instrument grade |
| Helium | GC, diluent | Afrox | 99.995 % |
| Hydrogen | GC | Afrox | Instrument grade |
| CO, CO ₂ , Benzene, Propane, propene, <i>n</i> -hexane in nitrogen | Calibration | Afrox | - |
| Air | GC, oxidant | Afrox | Instrument grade |
| 0.6 % hexane in air | Feed gas | Afrox | - |

Table 6.2: Gases used in calibration, operation of GC and as feedstock

6.2 Catalyst preparation

6.2.1 Synthesis of magnesium oxide (MgO) and vanadium pentoxide (V₂O₅)

Magnesium oxalate was precipitated at pH 5-6, by adding oxalic acid [H₂C₂O₄.2H₂O] to an aqueous magnesium acetate [Mg(CH₃CO₂)₂.4H₂O] (30 g / 100 ml) solution. The resultant magnesium oxalate precipitate was filtered, washed with doubly distilled water and dried at 70 °C overnight. The magnesium oxalate was then calcined in air (static) at 700 °C for 4 hours, yielding MgO. MgO was then boiled in 500 ml of distilled water overnight in a 1L flask equipped with a reflux condenser. After cooling, the slurry was filtered, and the filter cake dried in an oven at 120 °C. The dried powder was heated to 500 °C over 12 hours and then maintained at 500 °C overnight [1]. Vanadium oxide (V₂O₅) was prepared by calcining ammonium metavanadate (NH₄VO₃) in air (static) at 550 °C for 5 hours.

6.2.2 Synthesis of vanadium magnesium oxide (VMgO)

Vanadium magnesium oxide (VMgO) catalysts were prepared from freshly synthesized MgO and commercially purchased ammonium metavanadate. These catalysts were prepared by wet impregnation of the high surface area magnesium oxide with an aqueous ammonium metavanadate solution, using a similar procedure to one previously reported [2]. An appropriate amount of magnesium oxide, which was previously heated at 350 °C for 3 hours, was added to a well-stirred aqueous solution containing 1 wt % ammonium hydroxide and 1 wt % ammonium metavanadate at 70 °C (Figure 6.1). The resulting suspension was evaporated with stirring until a paste was obtained. This paste was dried at 120 °C for 8 hours. The resultant dried white powder was then calcined in air at 550 °C for 3 hours, using a flow rate of approximately 20 ml/min at atmospheric pressure. The calcined catalysts were pale yellow in colour. Calcination conditions are shown in Table 6.3 below:

| Temperature (start) | Temperature (end) | Heating rate | Time (hours) |
|---------------------|-------------------|--------------|--------------|
| 24 °C | 550 °C | 1.9 °C / min | 4.35 |
| 550 °C | 550 °C | - | 3 |
| 550 °C | 24 °C | - | Overnight |

Table 6.3: Calcination conditions used for synthesis of unpromoted VMgO

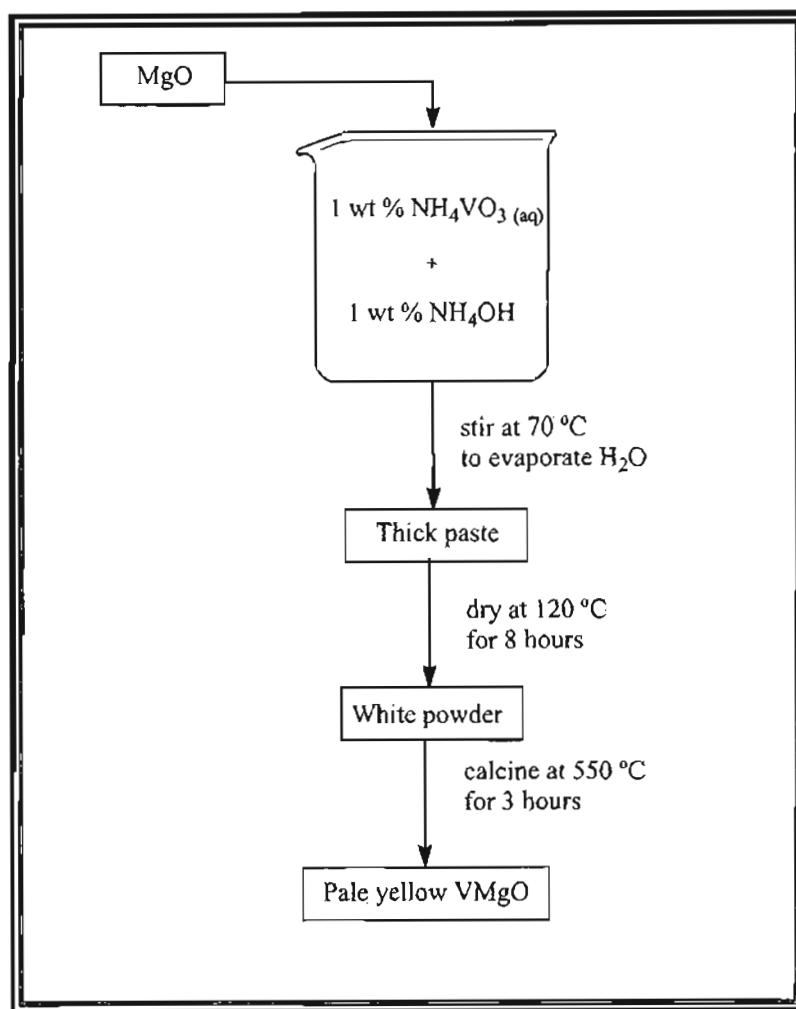


Figure 6.1: Flow chart for the synthesis of VMgO catalysts

The calcined catalyst was either ground and used as a powder or pelletized, crushed and sieved to 300 μm to 600 μm particle size. VMgO catalysts with vanadium loadings between 14 and 60 wt % (calculated as wt % V_2O_5) were synthesized i.e. 14VMgO, 16VMgO, 19VMgO, 24VMgO, 35VMgO, 49VMgO and 60VMgO.

The 19VMgO catalyst was promoted with antimony, tellurium, molybdenum, bismuth, cesium and niobium. MoVMgO, BiVMgO and CsVMgO were prepared by impregnating the 19VMgO catalyst with an aqueous solution of ammonium heptamolybdate $(\text{NH}_4)_6\text{Mo}_7\text{O}_{24}\cdot 4\text{H}_2\text{O}$, bismuth nitrate $(\text{Bi}(\text{NO}_3)_3\cdot 5\text{H}_2\text{O})$, or cesium nitrate (CsNO_3) respectively. An appropriate amount of the 19VMgO catalyst was added to a stirred aqueous solution containing 1 wt % of the promoter at 70 °C. The resulting suspension was evaporated with stirring until a paste was obtained. This paste was dried at 120 °C for 8 hours and then calcined in air at 550 °C for 3 hours. Calcination conditions are shown in Table 6.4.

The mixed metal oxides SbVMgO, TeVMgO and NbVMgO were prepared by physically mixing an appropriate amount of 19VMgO with antimony oxide (Sb_2O_3), tellurium oxide (TeO_2) and niobium oxide (Nb_2O_5) respectively. The physical mixtures were then calcined at 550 °C (Table 6.4). After every ½ hour catalysts were removed, thoroughly mixed and ground and then returned to the furnace at 550 °C.

| Temperature (start) | Temperature (end) | Heating rate | Time (hour) |
|---------------------|-------------------|---------------|-------------|
| 24 °C | 550 °C | 8.75 °C / min | 1 |
| 550 °C | 550 °C | - | 2 |
| 550 °C | 24 °C | - | Overnight |

Table 6.4: Calcination conditions used for synthesis of promoted VMgO

6.3 Labeling the catalysts

Vanadium magnesium oxide catalysts are referred to as VMgO. A number preceding VMgO indicates the weight percent (wt %) vanadium, calculated as V_2O_5 . A promoted catalyst is denoted as XVMgO, where X refers to the chemical promoter. The number preceding XVMgO indicates the weight percent of X, calculated as the weight percent of the oxide of X. The labels and composition of all catalysts synthesized and tested are shown in Tables 6.5 and 6.6:

| Label | Theoretical mass V_2O_5 | Theoretical mass MgO |
|--------|---|----------------------|
| 14VMgO | 14 wt % | 86 wt % |
| 16VMgO | 16 wt % | 84 wt % |
| 19VMgO | 19 wt % | 81 wt % |
| 24VMgO | 24 wt % | 76 wt % |
| 35VMgO | 35 wt % | 65 wt % |
| 49VMgO | 49 wt % | 51 wt % |
| 60VMgO | 60 wt % | 40 wt % |

Table 6.5: Labeling of unpromoted catalysts and their corresponding chemical composition

| Label | Theoretical mass of promoter | Theoretical mass of 19VMgO |
|-----------|---|----------------------------|
| 0.5MoVMgO | 0.5 wt % MoO ₃ | 99.5 wt % |
| 1MoVMgO | 1.0 wt % MoO ₃ | 99.0 wt % |
| 2.5MoVMgO | 2.5 wt % MoO ₃ | 97.5 wt % |
| 5MoVMgO | 5.0 wt % MoO ₃ | 95.0 wt % |
| 0.5SbVMgO | 0.5 wt % Sb ₂ O ₃ | 99.5 wt % |
| 1SbVMgO | 1.0 wt % Sb ₂ O ₃ | 99.0 wt % |
| 2.5SbVMgO | 2.5 wt % Sb ₂ O ₃ | 97.5 wt % |
| 5SbVMgO | 5.0 wt % Sb ₂ O ₃ | 95.0 wt % |
| 0.5TeVMgO | 0.5 wt % TeO ₂ | 99.5 wt % |
| 1TeVMgO | 1.0 wt % TeO ₂ | 99.0 wt % |
| 2.5TeVMgO | 2.5 wt % TeO ₂ | 97.5 wt % |
| 5TeVMgO | 5.0 wt % TeO ₂ | 95.0 wt % |
| 0.5NbVMgO | 0.5 wt % Nb ₂ O ₅ | 99.5 wt % |
| 1NbVMgO | 1.0 wt % Nb ₂ O ₅ | 99.0 wt % |
| 2.5NbVMgO | 2.5 wt % Nb ₂ O ₅ | 97.5 wt % |
| 5NbVMgO | 5.0 wt % Nb ₂ O ₅ | 95.0 wt % |
| 0.5BiVMgO | 0.5 wt % Bi ₂ O ₃ | 99.5 wt % |
| 1BiVMgO | 1.0 wt % Bi ₂ O ₃ | 99.0 wt % |
| 2.5BiVMgO | 2.5 wt % Bi ₂ O ₃ | 97.5 wt % |
| 5BiVMgO | 5.0 wt % Bi ₂ O ₃ | 95.0 wt % |
| 0.5CsVMgO | 0.5 wt % Cs ₂ O | 99.5 wt % |
| 1CsVMgO | 1.0 wt % Cs ₂ O | 99.0 wt % |
| 2.5CsVMgO | 2.5 wt % Cs ₂ O | 97.5 wt % |
| 5CsVMgO | 5.0 wt % Cs ₂ O | 95.0 wt % |

Table 6.6: Labeling of promoted catalysts and their corresponding theoretical chemical composition

6.4 Catalyst characterization

The following techniques were used in the characterization of freshly synthesized and/or aged catalysts: x-ray diffraction (XRD), x-ray fluorescence (XRF), x-ray photoelectron spectroscopy (XPS), Fourier transform infrared spectroscopy (FTIR), laser Raman spectroscopy (LRS), scanning electron spectroscopy (SEM), energy dispersive x-ray spectroscopy (EDS), differential scanning calorimetry - thermogravimetric analysis (DSC-TGA), Brunauer-Emmett-Teller surface area (BET) and inductively coupled plasma – atomic emission spectroscopy (ICP-AES). A theoretical introduction to these techniques was given in Chapter 3.6.

6.4.1 X-ray diffraction (XRD)

X-ray diffractograms were recorded on a Philips 1370/1 instrument operating at 40 kV and 25 mA. Co K α radiation on a long line focus (no filter) was used. The generator tension and current were 40 kW and 30 mA respectively and the irradiated length was 12 mm. Samples were scanned in the $2^\circ < 2\theta < 90^\circ$ range.

6.4.2 X-ray fluorescence (XRF)

A Philips PW2400 wavelength dispersive X-ray fluorescence spectrometer was used for analysis. The PW2400 uses a rhodium anode end window tube with a power of 3000 W and a maximum voltage of 60 kV and a current of 125 mA. Samples were analyzed as compressed powders. The goniometer had an angular accuracy of $0.0025^\circ 2\theta$, a slewing speed of $40^\circ 2\theta$ per second and a scanning speed of $1^\circ 2\theta$ per second.

6.4.3 X-ray photoelectron spectroscopy (XPS)

XPS spectra were recorded on a PHI Quantum 2000 scanning x-ray photoelectron spectrometer. The Quantum 2000 XPS is equipped with a quartz crystal monochromator and a scanning electron source that excites the aluminum anode to produce a focused x-ray beam. The power of the beam was 19.3 W and an energy analyzer angle of 48° was used. Wide scans were obtained with a pass energy of 117.4 eV and an energy resolution of 1 eV. The minimum analysis time was 30 minutes over an irradiation area of 100 μm . The analysis area was 500 x 500 μm . The vacuum in the analysis chamber was less than 5×10^{-8} Torr.

6.4.4 Fourier transform infrared spectroscopy (FTIR)

FTIR spectra were recorded on a Nicolett 400D infrared spectrometer. Samples were diluted with dry KBr powder. The mixture was thoroughly ground and then compressed into a pellet. A background was collected before every analysis.

6.4.5 Laser Raman spectroscopy (LRS)

Raman spectra were acquired in the 180 degree configuration on a System 1000 Renishaw Raman spectrometer. The spectrometer was equipped with a microscope and a CCD detector. An Ar⁺ laser with an incident radiation of 514 nm was used. Samples were analyzed as powders under ambient conditions. Spectra were collected after 8 minutes of acquisition time.

6.4.6 Scanning electron microscopy (SEM) and energy dispersive x-ray spectroscopy (EDS)

Samples were analyzed on a LEO 1450 scanning electron microscope fitted with a Link ISIS energy dispersive x-ray analytical system. Samples were mounted on a graphite stub with double-sided graphitic tape. Samples were sputtered with gold for thirty seconds using a Polaron E5100 SEM coating unit to prevent charging of the incident electron beam.

6.4.7 Differential scanning calorimetry – thermogravimetric analysis (DSC-TGA)

Catalyst samples were analyzed on a SDT 2960 simultaneous DSC-TGA instrument manufactured by TA Instruments. The sample was heated under nitrogen up to 200 °C to remove physically adsorbed species and water molecules. Oxygen was then continuously passed over the sample whilst the sample was heated up to 700 °C.

6.4.8 Brunauer-Emmett-Teller (BET) surface area

BET surface area measurements and pore analysis were performed on a Micromeritics Tristar instrument. Samples were de-gassed at 200 °C with nitrogen. Measurements were performed with nitrogen adsorbate at -195 °C.

6.4.9 Inductively coupled plasma – atomic emission spectroscopy (ICP-AES)

ICP-AES was analyzed on a Jobin-Yvon (JY24) instrument. Standards were prepared containing the required elements over an appropriate concentration range. Samples were digested with minimal amounts of aqua regia (7HCl:3HNO₃). Microwave digestion was utilized for difficult samples.

6.4.10 Gas chromatography – mass spectrometry (GC-MS)

GC-MS studies were done on an Agilent HP-6890 GC fitted with a PONA column. An Agilent 5973 Network mass selective detector (MSD) was used. The following parameters were used:

Oven

Initial temperature: 55°C

Initial time: 2.00 min

Equilibration time: 0.50 min

Ramps:

| # | Rate (°C/min) | Final temperature (°C) | Final time (min) |
|---|---------------|------------------------|------------------|
| 1 | 10.00 | 200 | 5.00 |

Total Run time: 21.50 min

Inlet

Mode – Split

Initial temperature: 250°C

Gauge pressure – 0.547 Bar

Split ratio – 100:1

Split flow – 49.9 mL/min

Total flow – 53.8 mL/min

Gas saver – On

Saver flow – 20.0 mL/min

Saver time – 3.00 min

Gas type – Helium

Column

Capillary column

Model Number – HP 19091S – 001

HP-PONA Methyl Siloxane

Maximum temperature: 325°C

Nominal length – 50.0 m

Nominal diameter – 200.00 µm

Nominal film thickness – 0.50 µm

Mode – constant flow of 0.5 mL/min

Nominal initial pressure – 1.445 Bar

Average velocity – 16 cm/sec

6.4.11 Average vanadium oxidation state

The AV was determined by a redox titration procedure [3]. Approximately 0.1g of catalyst was dissolved in 17 mL of 12 M *ortho*-phosphoric acid (98+ %) and boiled until a clear solution was obtained. This solution was then added to a solution containing H₂SO₄ (10 mL) in water (250 mL). All vanadium ions were oxidized to V⁵⁺ by titration with 0.05 N KMnO₄. The pentavalent vanadium ions were then reduced to V⁴⁺ using a 0.05 N Fe(NH₄)₂(SO₄)₂ solution containing 1% diphenylamine in concentrated H₂SO₄ as an indicator. The average vanadium oxidation state was then calculated as follows:

$$AV = 5 - [\text{Volume KMnO}_4 \text{ solution}] / [\text{Volume Fe (NH}_4)_2(\text{SO}_4)_2 \text{ solution}]$$

6.5 Reactor configuration

6.5.1 Reactor setup for *n*-hexane oxidative dehydrogenation

Four parallel fixed-bed continuous flow micro-reactors were initially designed and constructed for this study (Figure 6.2). The selection was based on factors such as costs and simplicity in setting up. Additionally, this setup would lend itself to facile modification if this was warranted by the progression of the investigation (indeed, this was the case). Oxidation reactions are strongly exothermic and this necessitates the use of a reactor capable of removing this energy. To a large extent this problem could be circumvented by manipulating process conditions such as diluting the feed or catalyst bed. Furthermore, changes to the configuration of the reactor itself could be made if the need arose.

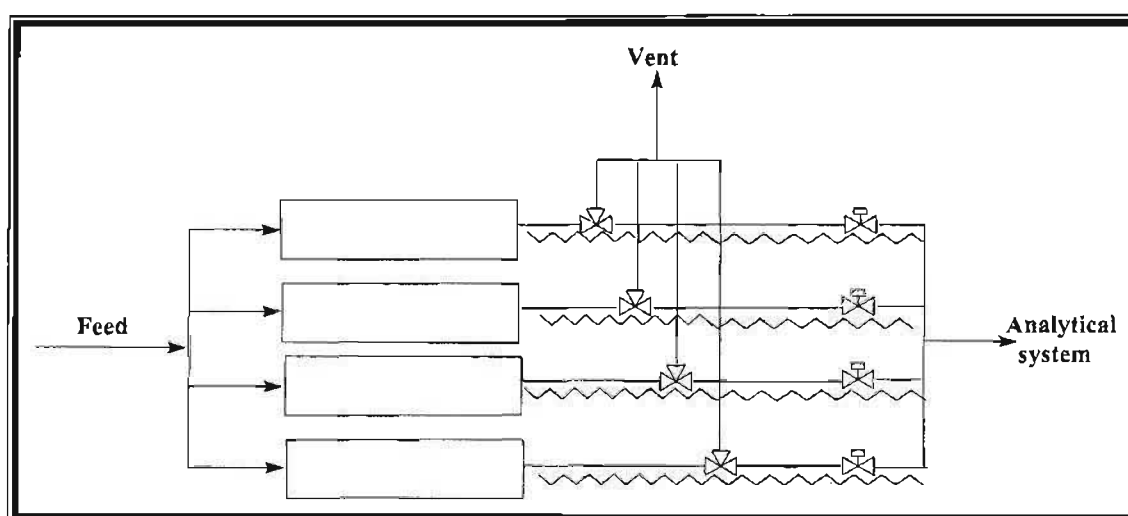


Figure 6.2: Schematic showing the four parallel reactors setup for *n*-hexane ODH

The pressure of the feed was set slightly above atmospheric pressure with a panel-mounted pressure regulator and the pressure was monitored with panel-mounted pressure gauges. The flow rate of the feed to each reactor was individually regulated with a panel-mounted rotameter, which was calibrated for flow rates from 50 to 200 ml/min (Appendix 1). Feed lines were made up of ¼ inch copper tubing. The feed lines were connected to the reactors with stainless steel Swagelok fittings. The reactors were housed in copper blocks, which were surrounded by a heating element. CB-100 temperature controllers containing solid-state relays controlled these elements. The controllers used type K thermocouples and these thermocouples were placed on the outside walls of the reactors. The tips of the thermocouples were attached to the portion of the reactors, which were in intimate contact with the catalysts.

After the reactors, 1/8 inch stainless tubing (316 grade) was used. The exit lines of each reactor were connected to a high temperature three-way valve. Reactor effluent was either vented or sent for online gas chromatographic (GC) analysis via this valve. Effluent lines from the reactors were connected to a 6 port aluminum gas manifold (5 inputs and 1 output). Needle valves and one-way valves restricted the mixing of effluent streams. The 5th port on the manifold was used as a nitrogen purge. The output port of the aluminum manifold was fed into a gas sampling valve box. All lines from the reactors were heat traced. The heating tape around the lines was set at 160 °C.

6.5.2 Reactor setup for *n*-octane oxidative dehydrogenation

One of the reactors setup for *n*-hexane ODH was modified for *n*-octane ODH. A knock-out pot was added to condense unreacted *n*-octane and heavy reaction products (Figure 6.3). Only Stainless steel lines were used and these were heat traced. Whilst the parallel reactors used for *n*-hexane ODH were horizontal, this reactor was vertical with a top to bottom feed.

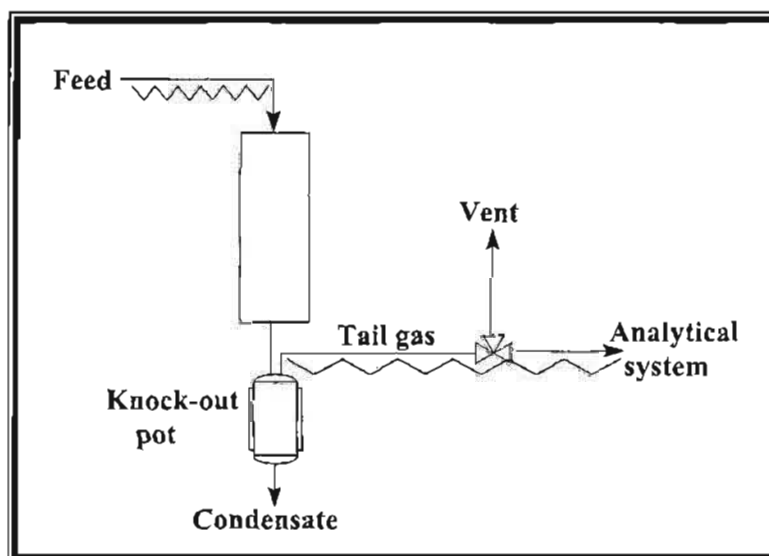


Figure 6.3: Schematic showing the reactor setup used for *n*-octane ODH

6.6 The analytical system

The analytical system used comprised of a heated gas sampling valve box and two gas chromatographs with a flame ionization and a thermal conductivity detector for online analysis (Figure 6.4).

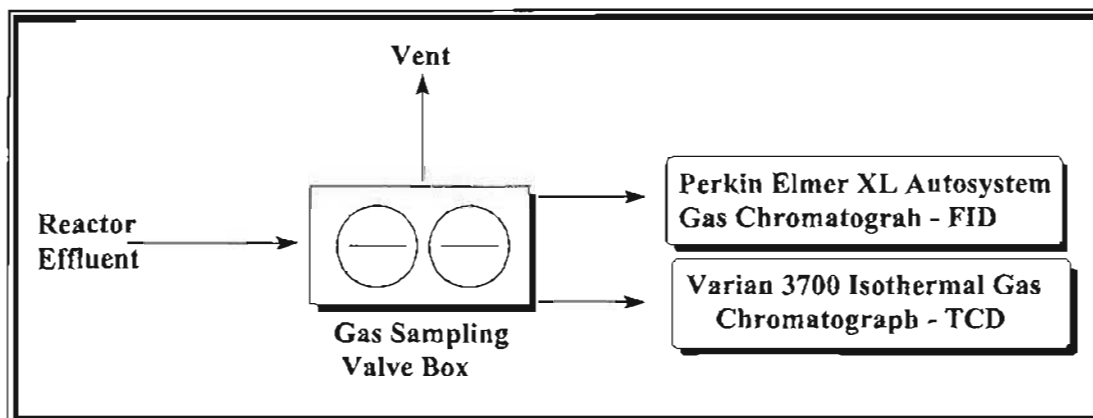


Figure 6.4: Block diagram of the analytical system used

6.6.1 The gas sampling valve box

The gas sampling valve box was heated to 160 °C to prevent condensation of reactor effluent. It contained two Valco rotary valves i.e. a 10 port valve and a 6 port valve. Both valves contained a 500 μL sample loop. The 10 port valve sampled 500 μL of effluent to the Varian 3700 GC. The 6 port valve sampled 500 μL of effluent to the Perkin Elmer GC. The Perkin Elmer GC electronically and pneumatically controlled both valves. The Operation of the 6 port valve is shown in Figures 6.5 and 6.6. In the sampling mode, sample flows through the 500 μL sample loop while the carrier flows directly through to the FID detector. In standby mode, the sample contained in the sample loop and valve flow passage is injected onto the detector.

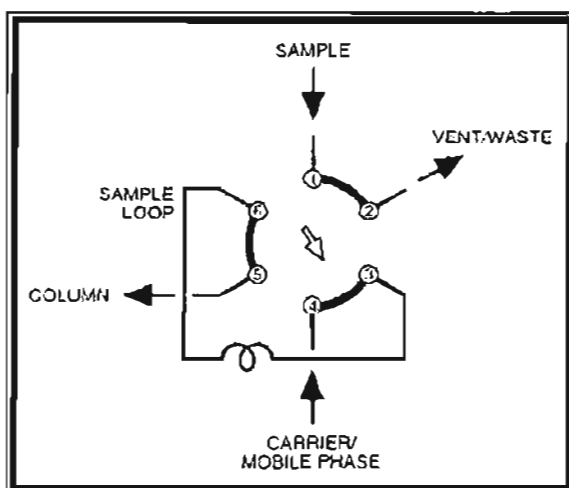


Figure 6.5: 6 port valve in standby mode

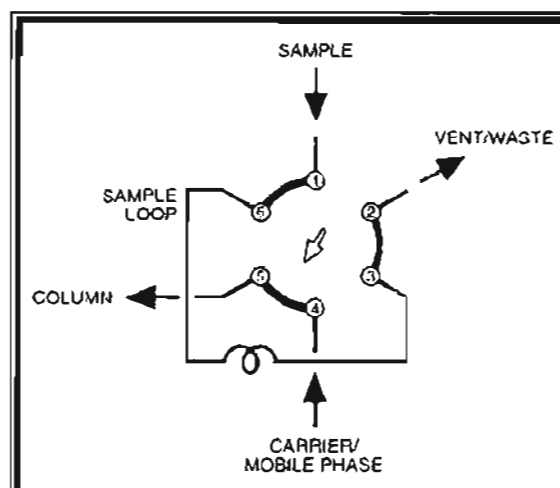


Figure 6.6: 6 port valve in sampling mode

The operation of the 10 port valve is shown in Figure 6.7 below. This setup allowed only gasses (Carbon oxides and air) to pass through to the Carboxen™ 1000 column. Other components were trapped in the pre-column and subsequently back flushed to waste. After the sample loop was loaded in standby mode, the valve was switched to sampling mode to inject the sample onto the pre-column. As soon as carbon oxides and air entered the Carboxen™ 1000 column, the valve was switched back to standby mode. The WHPSP pre-column was then back flushed to the vent during the analysis.

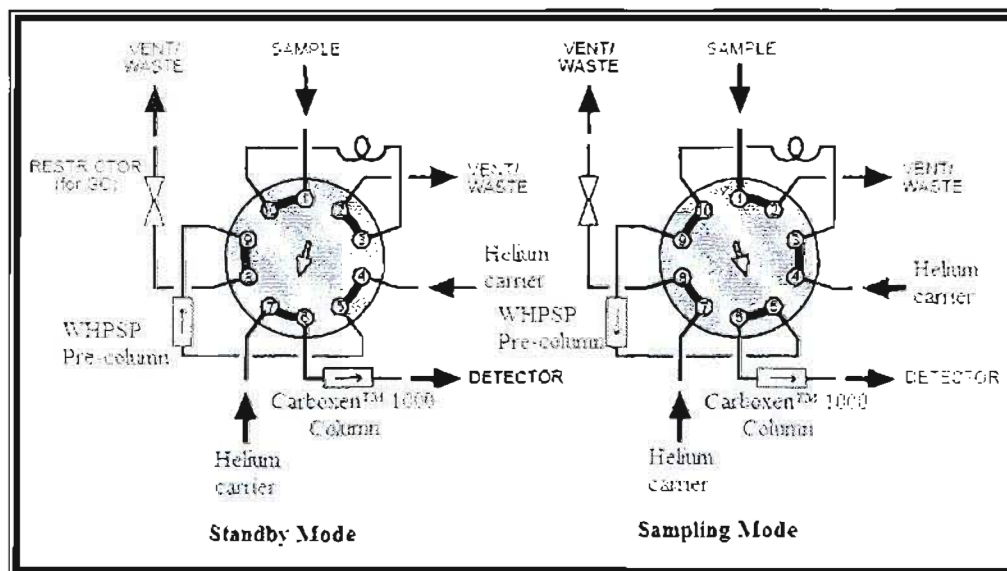


Figure 6.7: 10 port valve in standby and sampling mode

6.6.2 Gas chromatography

The Perkin Elmer XL Autosystem GC contained a flame ionization (FID) detector. Nitrogen was used as the carrier gas. A CP-Sil 24CB column was installed in this GC. All organic products were analyzed by this GC. The analysis time for *n*-hexane ODH was about 10 minutes and about 15 minutes for *n*-octane ODH.

The Varian 3700 GC contained a thermal conductivity detector (TCD). Helium was used as the carrier gas. This GC contained a WHPSP pre-column and a Carboxen™ 1000 column. Only carrier gas, methane, air and carbon oxides passed through the pre-column. Carbon monoxide and carbon dioxide was separated isothermally on the Carboxen™ 1000 column. The specification of both columns and the GC methodology used is given in Appendix 1. Both GC's were calibrated regularly with calibration standards. Columns were frequently baked out to ensure a smooth baseline and consistent results.

6.6.3 Product analysis

Both the feed and the reactor effluent in *n*-hexane ODH were analyzed by online gas chromatography. In *n*-octane ODH, the feed and the tail gas were analyzed online. The liquid condensates from the knock-out pot were analyzed off line. This condensate usually contained an aqueous layer and an organic layer. These layers were separated, weighed and analyzed in the Perkin Elmer GC by manual injection of 0.5 μl of sample.

6.7 Catalyst testing

6.7.1 Reactor used for *n*-hexane oxidative dehydrogenation

Catalysts were tested in horizontal stainless steel reactors. The length of these reactors was 300 mm and the internal diameter was 10 mm (Appendix 1). The catalyst charge was 0.4 g (1.6 ml). The catalyst was loaded neat. Catalysts were packed towards the exit side of the heating element i.e. 200 mm from where the feed entered the reactors (Figure 6.8). Glass wool was used to isolate the catalyst. Carborundum (24 GRIT) was used to fill the void space in the reactor. A thermocouple was attached to the reactor as shown below:

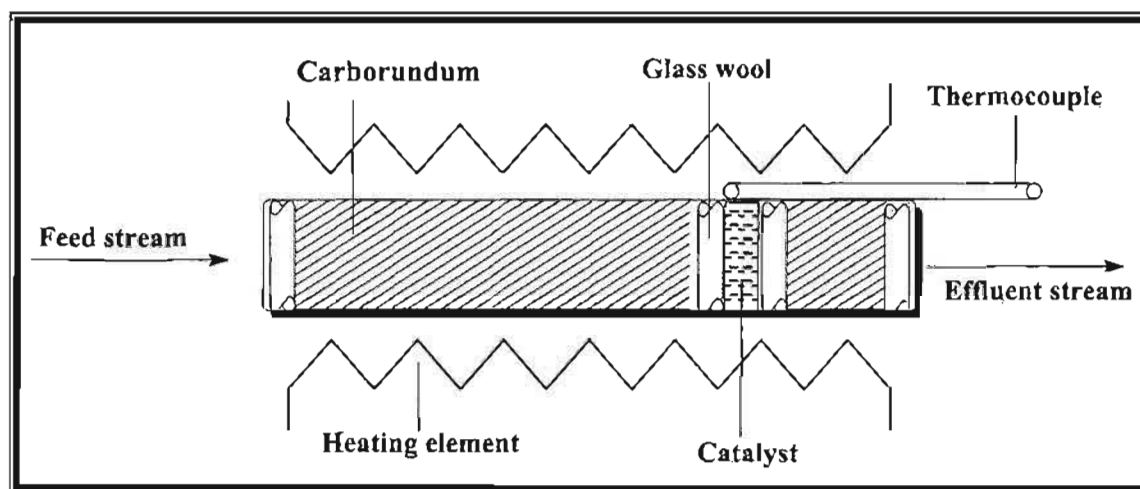


Figure 6.8: Schematic of a packed reactor

Catalysts were tested in the 250-550 $^{\circ}\text{C}$ temperature range. Varying gas hourly space velocities (GHSV) were used. The air (oxidant) to *n*-hexane (fuel) ratio was also varied. The reactor was sampled after a steady state was achieved. Usually this was between 4 to 6 hours after any parameter was changed. Catalysts were evaluated for product selectivity, feed conversion and overall yields. Typical carbon balances were between 96 and 100 percent but usually better than 98 percent.

6.7.2 Reactor used for *n*-octane oxidative dehydrogenation

The dimensions of the reactor used for *n*-octane ODH were exactly the same as those used for *n*-hexane ODH. The orientation of the reactors differed. Whilst those used for *n*-hexane ODH were horizontally orientated, those used for *n*-octane ODH were vertically positioned. Furthermore, sliding thermocouples were intimately positioned in the catalyst bed for *n*-octane ODH. In *n*-hexane ODH, thermocouples were fixed and attached to the outside wall of the reactor in contact with the catalyst bed. The reactor used for *n*-octane ODH is shown in Appendix 1.

6.7.3 Catalyst testing and flammability limits

Oxidation of *n*-hexane and *n*-octane was studied below the LEL, above the UEL and between the LEL and UEL. Below the LEL, there is an excess of oxygen in the system (oxidizing atmosphere). Above the UEL, the amount of oxygen available is limited (reducing atmosphere). It is possible that a fire or an explosion could occur during operation between the LEL and UEL (Chapter 2.4). The LEL and UEL are dependent on temperature and pressure (usually limits are known only for standard conditions). The use of high quality reactors, relatively small amounts of feed and the use of an inert gas were employed as safety precautions.

6.7.4 Feed used for *n*-hexane oxidative dehydrogenation

The feed delivery to the reactor was dependent on whether the reaction was carried out below the LEL, in the explosive limit or above the UEL. Below the LEL, a premixed gas cylinder containing 0.6 percent *n*-hexane in air was used as the feed. Feed above the LEL was obtained by bubbling air through liquid *n*-hexane (Figure 6.9).

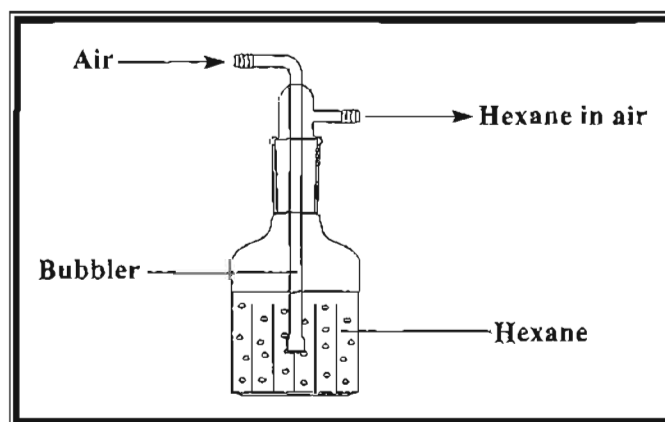


Figure 6.9: The Bubbler system used to produce the *n*-hexane in air feed above the LEL

Air enters the bubbler and a mixture of *n*-hexane in air exits the bubbler. The temperature of hexane was controlled by immersing the apparatus shown above in a chiller. The chiller was filled with isopropanol. The vapour pressure of *n*-hexane in air is dependent on the temperature of *n*-hexane. This relationship is described by the Antoine equation. The Antoine equation is a semi-empirical equation, which expresses vapour pressure as a function of temperature. It is a simple 3-parameter fit to experimental vapour pressures measured over a restricted temperature range:

$$\text{Log } P = A - (B/(T+C)) \dots \dots \dots \text{Antoine Equation}$$

Where:

P = Vapour pressure (Bar)

T = Temperature (Kelvin)

A,B,C = Antoine coefficients

The Antoine equation was used as a guide to select the temperature of the chiller and hence the composition of the feed. The exact composition of the feed was determined by gas chromatography. Antoine coefficients for *n*-hexane are given in Appendix 2.

6.7.5 Feed used for *n*-octane oxidative dehydrogenation

A Series II model high-pressure liquid chromatography (HPLC) pump fitted with a 10 ml self-flush head from Anatech Instruments was used to supply octane to the reactor. This pump is capable of feeding *n*-octane in increments of 0.01 ml/min. *n*-Octane was pumped into a ¼ inch stainless steel line. This line was heated to 160 °C resulting in the vaporization of *n*-octane. The *n*-octane feed was mixed with an air feed and this mixture was fed into the reactor. Both the HPLC pump and the air rotameter was calibrated and subsequently set according to the desired feed composition.

6.8 References:

1. Klabunde, K. J., Stark, J., Koper, O, Mohs, C, Park, D. G., Decker, S, Jiang, Y, Lagadic, I. and Zhang, D., *J. Phys. Chem.*, **100**, 1996 12142.
2. Chaar, M. A., Patel, D., Kung, M. C. and Kung, H. H., *J. Catal.*, **105**, 1987, 483.
3. Nakamura, K., Kawai, K. and Fujiwara, Y., *J. Catal.*, **34**, 1974, 345.

CHAPTER 7: Results and Discussion

7.1 Introduction, aim and overview

Olefins are commonly derived from the steam cracking of naphtha and fluidized catalytic crackers in oil refineries. They are commonly used as feedstock in the synthesis of chemicals in the chemical industry. Paraffins can be obtained from natural gas, LPG and Fischer-Tropsch processes. Activation of paraffins is considered to be more difficult than the corresponding olefin and consequently there has been limited success in utilizing the more economic paraffin feedstock [1].

Most of the available literature on paraffin oxidation is based on short chain paraffins [2-12]. The aim of this study was to investigate the oxidative dehydrogenation of longer chain paraffins i.e. *n*-hexane and *n*-octane, using a heterogeneous catalytic system. The catalytic transformation of longer chain paraffins into more desired products represents a proactive step to counter their predicted surplus arising from anticipated Fischer-Tropsch expansion (coal to liquids and gas to liquids) and changing environmental laws. The vanadium magnesium oxide (VMgO) catalytic system was selected, based on its intrinsic properties (Chapter 5) as well as its relatively good success with butane oxidative dehydrogenation [6,7,13,14]. Several VMgO catalysts with varied amounts of vanadium were synthesized (Chapter 6), characterized (Chapter 7) and their catalytic activity was investigated for *n*-hexane ODH (Chapter 8).

The optimized vanadium loaded catalyst was then promoted with small amounts of antimony, tellurium, molybdenum, bismuth, cesium and niobium oxide in an attempt to improve its selectivity and yield towards ODH products. Promoted catalysts were tested on *n*-hexane (Chapter 8) and *n*-octane (Chapter 9). Process conditions such as space velocities and fuel to oxidant ratios were also optimised. Air was used as the oxidant.

Lastly, to gain an insight into the reaction mechanism, plausible reaction intermediates were fed into the reactors (Chapter 10). These results were evaluated and a potential reaction pathway towards desired products was hypothesized.

The results of catalyst characterization and an evaluation of catalytic performance are now further discussed.

7.2 Catalyst characterization: VMgO

7.2.1 X-ray diffraction (XRD)

The overlaid XRD patterns of VMgO catalysts synthesized with varied vanadium loadings are shown in **Figure 7.1**. The x-ray diffraction patterns of all the catalysts are reflective of low crystallinity and/or small average crystallite size. This is consistent with the high surface areas of these catalysts. Broad peaks for MgO are observed in all the catalysts ($2\theta = 50.3, 73.9$). No diffraction lines for V_2O_5 are observed. As the vanadium loading (hence the mol % of magnesium orthovanadate) increases in the catalysts, diffraction lines for a poorly crystalline magnesium orthovanadate phase can be observed. The diffraction line at $2\theta = 41.2$, in particular, becomes more intense (**Figure 7.1**). This line is strongly associated with the orthovanadate phase [14]. The orthovanadate phase is not detected in the x-ray diffractograms of those catalysts with low vanadium contents. This is due to the amount of orthovanadate phase, present in these catalysts, being below the detection limit of the x-ray diffraction technique and/or the small crystallite size of this phase. Nevertheless, the orthovanadate phase is observed with other techniques (Raman and infrared). Diffraction lines corresponding to other vanadate phases (MgV_2O_6 and $Mg_2V_2O_7$) were not detected in any of the catalysts. The XRD patterns of all the VMgO catalysts were similar to those previously reported [14-19]. X-ray diffraction lines for the 19VMgO catalyst are given in **Table 7.1** below. Full x-ray diffractograms of all catalysts are given in **Appendix 3**.

| 19VMgO $2\theta^a$ | <i>d</i> Spacing (Å) (relative intensity) ^a | <i>d</i> Spacing (Å) (relative intensity) ^b | Assignment |
|--------------------|--|--|--------------|
| 41.06 | 2.55 (8) ^c | | $Mg_3V_2O_8$ |
| 43.19 | 2.43 (6) | 2.42 (6) | MgO |
| 44.96 | 2.34 (5) ^c | | $Mg_3V_2O_8$ |
| 50.29 | 2.10 (100) | 2.10 (100) | MgO |
| 52.41 | 2.02 (23) ^c | | $Mg_3V_2O_8$ |
| 73.76 | 1.49 (54) | 1.49 (53) | MgO |
| 77.28 | 1.43 (4) | 1.269 (5) | MgO |
| | | 1.218 (12), 1.053 (5), 0.966 (3), 0.943 (12) | MgO |

^aSynthesized 19VMgO catalyst, ^b19VMgO according to [14], ^cAssigned to $Mg_3(VO_4)_2$ according to 54VMgO[14]

Table 7.1: X-ray diffraction lines of synthesized 19VMgO compared to those previously reported [14]

7.2.2 Chemical composition

The chemical compositions, determined by inductively coupled plasma–atomic emission spectroscopy (ICP-AES), of MgO, V₂O₅ and synthesised VMgO catalysts are shown in **Table 7.2** below. Samples were prepared for ICP by completely digesting them in aqua regia. ICP is a bulk characterization technique. The experimentally determined compositions were found to be close to the theoretical values. This is consistent with the synthetic technique used (one pot synthesis). Catalysts were also analysed by energy dispersive x-ray spectroscopy (EDS), which is a localized technique. The atomic ratios of magnesium to vanadium determined by ICP compared well to those determined obtained by EDS.

| Catalyst | V ₂ O ₅ (wt %) (ICP) | MgO (wt %) (ICP) | wt % Mg ₃ (VO ₄) ₂ (theoretical) ^a | (Mg/V) _{ICP} (atomic) | (Mg/V) _{EDS} (atomic) |
|-------------------------------|---|---------------------|--|-----------------------------------|-----------------------------------|
| MgO | 0 | 100 | - | - | - |
| 14VMgO | 13.9 | 86.1 | 23.1 | 13.9 | 13.2 |
| 16VMgO | 16.0 | 84.0 | 26.6 | 11.8 | 11.5 |
| 19VMgO | 18.9 | 81.1 | 31.5 | 9.7 | 9.4 |
| 24VMgO | 24.2 | 75.8 | 40.3 | 7.1 | 7.0 |
| 35VMgO | 35.0 | 65.0 | 58.3 | 4.2 | 4.0 |
| 49VMgO | 48.7 | 51.2 | 81.1 | 2.4 | 2.1 |
| 60VMgO | 58.6 | 40.8 | 97.6 | 1.6 | 1.5 |
| V ₂ O ₅ | 100 | 0 | - | - | - |

^a Calculated on the basis that all V₂O₅ reacts with MgO according to $V_2O_5 + 3MgO \rightarrow Mg_3(VO_4)_2$

Table 7.2: Chemical characteristics of synthesized VMgO catalysts

7.2.3 Average vanadium oxidation state

Average vanadium oxidation states were determined by a redox titration procedure [20]. The experimentally determined average vanadium oxidation states of freshly calcined VMgO catalysts were consistent with the expected oxidation state of 5 (**Table 7.3.**). The 19VMgO catalyst had a slightly lower average vanadium oxidation state after being used online for 168 hours.

| Catalyst | Average vanadium oxidation state |
|----------|---|
| 14VMgO | 4.8 (\pm 0.3) |
| 16VMgO | 4.8 (\pm 0.3) |
| 19VMgO | 4.8 (\pm 0.3), 4.5 ^a (\pm 0.3) |
| 24VMgO | 4.7 (\pm 0.3) |
| 35VMgO | 4.8 (\pm 0.3) |
| 49VMgO | 4.8 (\pm 0.3) |
| 60VMgO | 4.9 (\pm 0.3) |

^a value for aged catalyst

Table 7.3: The average vanadium oxidation state of freshly synthesized VMgO catalysts

7.2.4 Brunauer-Emmet-Teller (BET) surface area

The BET surface areas, pore volume and average pore diameters, measured for calcined VMgO catalysts are shown in Table 7.4 below:

| Catalyst | 5 Point BET (m ² /g) | Single BET (m ² /g) | Pore volume (cm ³ /g) | Average pore diameter (Å) |
|-------------------------------|------------------------------------|-----------------------------------|-------------------------------------|------------------------------|
| MgO | 137 | 132 | 0.21 | 62 |
| 14VMgO | 189 | 183 | 0.60 | 111 |
| 16VMgO | 190 | 189 | 0.68 | 142 |
| 19VMgO | 189 | 185 | 0.58 | 123 |
| 24VMgO | 133 | 132 | 0.57 | 146 |
| 35VMgO | 55 | 53 | 0.19 | 139 |
| 49VMgO | 23 | 23 | 0.11 | 191 |
| 60VMgO | 9 | 9 | 0.08 | 342 |
| V ₂ O ₅ | 4 | 4 | 0.02 | 207 |

Table 7.4: BET surface areas, pore volumes and pore diameters for synthesized VMgO catalysts

The 16VMgO catalyst had the highest surface area. Vanadium loadings of up to 24 wt % resulted in catalysts with relatively high surface areas, even higher than that of the MgO precursor. The formation of material with a higher surface area than its precursors is indicative of the formation of a new phase. This is consistent with V₂O₅ not being merely supported on MgO and further supports the XRD data (Chapter 7.2.1). Pore volumes were observed to decrease with an increase in the vanadium loading except for 16VMgO which

between the average pore diameter and vanadium loading could be made. In **Figure 7.2** it can be seen that as the vanadium loading increases beyond 20 wt %, the BET surface area rapidly decreases.

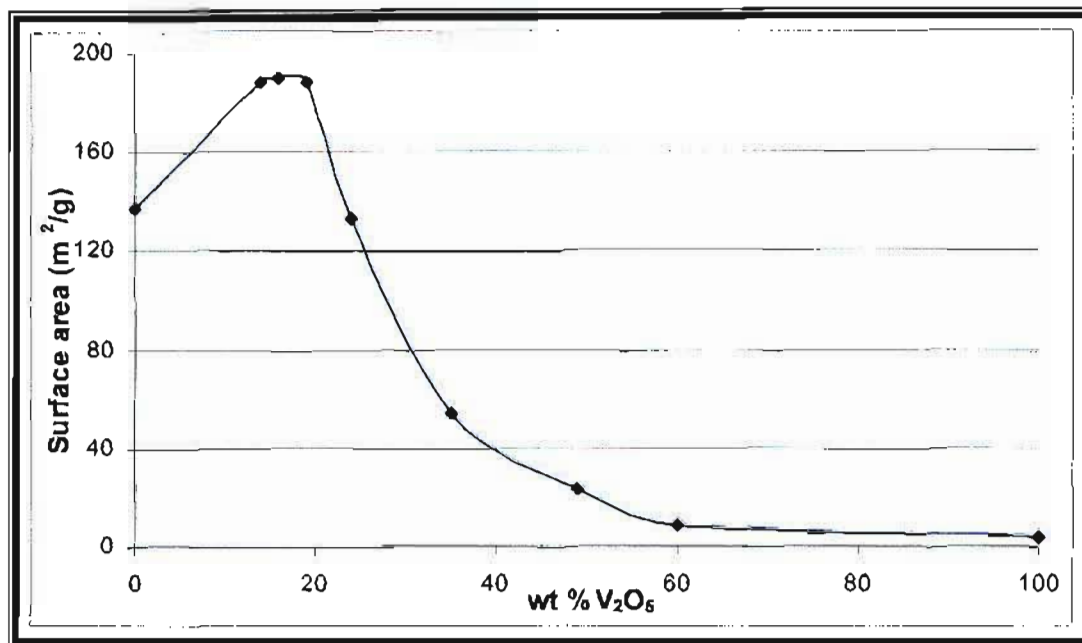


Figure 7.2: Graph showing the effect of vanadium loading on the surface area of VMgO catalysts (0 wt % V_2O_5 = MgO)

The BET data suggests that there exists an optimum mole % of magnesium orthovanadate in VMgO catalysts, which would yield a catalyst with the highest surface area (**Figure 7.3**).

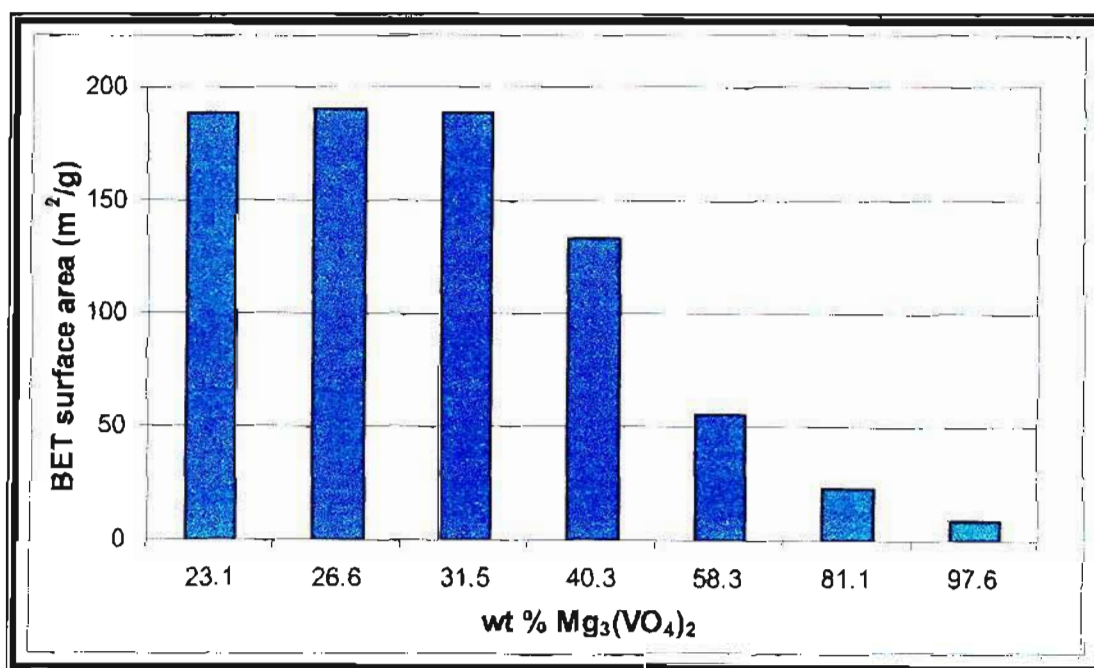


Figure 7.3: Graph showing the effect of wt % $Mg_3(VO_4)_2$ on the BET surface areas

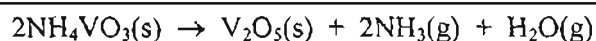
The effects of calcination times on the BET surface area were investigated for the 19VMgO catalyst (Table 7.5). It was observed that at 550 °C, longer calcination times result in catalysts with lower surface areas. On the other hand, calcination times, which are too short, results in the presence of mixed phases.

| Calcination time | BET surface area |
|------------------|------------------|
| < 2hrs | Mixed phases |
| 3hrs | 189 |
| 4hrs | 184 |
| 5hrs | 178 |

Table 7.5: Effect of calcination times on the BET surface area at 550 °C

7.2.5 Differential scanning calorimetry – thermogravimetric analysis (DSC-TGA)

DSC-TGA analysis was carried out on uncalcined 24VMgO (Appendix 3). Heating the catalyst to 200 °C under nitrogen resulted in a 10 % weight loss. This corresponds to the removal of water and surface carbonates and to the decomposition of NH_4VO_3 [18,19]. The endothermic peak at 148 °C is attributed to the decomposition of NH_4VO_3 and the weak intensity endothermic peak at 200 °C is due to the elimination of crystallization water [18,19]:



The very strong intensity endothermic peak at 390 °C is attributed to the decomposition of $\text{Mg}(\text{OH})_2$ to form MgO [18,19,21]:



Thermal peaks corresponding to the formation of Magnesium vanadates were not observed. These thermal peaks are usually observed as low intensity exothermic peaks around 400 °C to 600 °C depending on the preparation procedure and the vanadium loading in the catalyst [18,21,22]. The presence of the strong intensity endothermic peak at 390 °C could have occluded the appearance of any low intensity exothermic peaks in this temperature region. No thermal peak corresponding to the melting of V_2O_5 was observed. This peak normally occurs at 660 °C for pure V_2O_5 [23]. This also suggested that V_2O_5 had completely reacted with MgO and V_2O_5 crystallites were not dispersed on the surface of MgO.



7.2.6 Laser Raman spectroscopy (LRS)

The Raman spectrum of the freshly synthesized 19VMgO catalyst, recorded in the 150 to 1200 cm^{-1} region is shown in **Figure 7.4** below. The spectrum is completely different from that of V_2O_5 or MgO (**Appendix 3**) and is in full agreement with the formation of a new orthovanadate phase. At least nine bands can be clearly observed in the Raman spectrum in the 150 to 1200 cm^{-1} region.

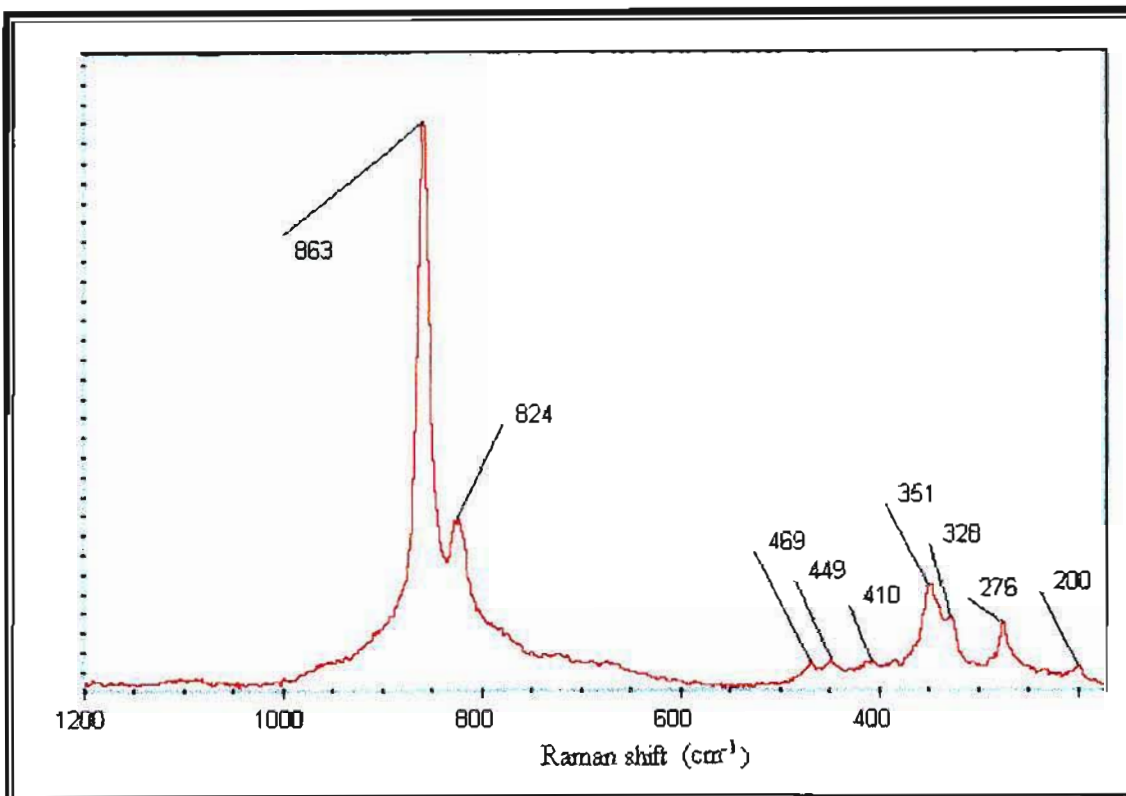


Figure 7.4: Raman spectra for 19VMgO

A comparison of the observed Raman frequencies of the 19VMgO catalyst and the Raman frequencies reported for magnesium orthovanadate are given in **Table 7.6**. The very strong (vs) band at 863 cm^{-1} and the strong (s) band at 824 cm^{-1} are attributed to distorted VO_4 tetrahedra that are highly dispersed on the surface of MgO [23,24]. These bands indicate the presence of the orthovanadate phase. The medium (m) intensity band at 351 cm^{-1} is also characteristic of the orthovanadate phase [15,21,23,25]. Bands relating to the metavanadate and pyrovanadate phases are absent from the Raman spectrum of 19VMgO.

| 19VMgO (cm ⁻¹) | Reference (cm ⁻¹) [25] ^a | Reference (cm ⁻¹) [23] ^a | Reference (cm ⁻¹) [26] ^b | Assignment [23] |
|--|--|--|--|--|
| 863 vs | 861 vs | 868 vs | 848 | $\nu_{as}(\text{VO}_4)$ and $\nu_{as}(\text{VO}_6)$ |
| 824 s | 826 s | 833 s | | |
| | | 828 m | | |
| Stretching observed but bands difficult to discriminate | 723 w | | | $\nu_s(\text{VOV})$ |
| | 671 vw | 541 m | | |
| | | 524 m | | |
| | | 484 m | 488 | |
| 469 w | 470 w | 462 m | | $\delta_s(\text{VO}_4)$ and $\delta_s(\text{VO}_6)$ |
| 449 w | 448 w | 448m | 450 | |
| 410 w | 409 w | 420 m | 400 | |
| | 387 w | 387 w | 380 | |
| 351 m | 350 m | 344 s | | $\delta_{ss}(\text{VO}_4)$ and $\delta_{ss}(\text{VO}_6)$ |
| | 340 m | | | |
| 328 m | 329 m | | | |
| | 289 w | 296 w | | |
| 276 m | 275m | 279 m | | |
| | 269 w | | | |
| | 233w | | | |
| | 207 vw | | | |
| 200 w | 200 w | | | |
| | 145 w | | | |
| | 137 w | | | |

^aFrequencies for pure $\text{Mg}_3(\text{VO}_4)_2$, ^bFrequencies for an 18VMgO catalyst

Table 7.6: Comparison of Raman frequencies of the $\text{Mg}_3(\text{VO}_4)_2$ phase of 19VMgO

The Raman frequencies for 14VMgO, 16VMgO, 19VMgO, 24VMgO, 35VMgO, 49VMgO, 60VMgO, V_2O_5 and MgO are shown in Table 7.7. Full spectra are shown in Appendix 3.

| V_2O_5 (cm^{-1}) | MgO (cm^{-1}) | 60VMgO (cm^{-1}) | 49VMgO (cm^{-1}) | 35VMgO (cm^{-1}) | 24VMgO (cm^{-1}) | 19VMgO (cm^{-1}) | 16VMgO (cm^{-1}) | 14VMgO (cm^{-1}) |
|---------------------------|----------------------|-------------------------|-------------------------|-------------------------|-------------------------|-------------------------|-------------------------|-------------------------|
| | 3687 | 3622 | 3658 | 3650 | 3658 | | | |
| | 3652 | | | | | | | |
| | 1104 | 1085 | 1090 | 1106 | | 1113 | | |
| 992 | | | | | | | | |
| | | 857 | 860 | 868 | 864 | 863 | 861 | 863 |
| | | | | 827 | 827 | 824 | | |
| 694 | | | | 678 | 677 | | | |
| 521 | | | | | | | | |
| 478 | | | | | | | | |
| | | | | | | 469 | | |
| | 450 | | | | | 449 | | |
| 406 | | | | | | 410 | | |
| | | 351 | 349 | 357 | 353 | 351 | | |
| | | | | | | 328 | | |
| 306 | | | | | | | | |
| 284 | 276 | 261 | 250 | 271 | 259 | 276 | | |
| 196 | | | | 227 | | 200 | | |

Table 7.7: Raman Frequencies for 14VMgO, 16VMgO, 19VMgO, 24VMgO, 35VMgO, 49VMgO, 60VMgO, V_2O_5 and MgO.

All VMgO catalysts show a strong broad band centered around 860 cm^{-1} and a medium band around 350 cm^{-1} indicating the presence of magnesium orthovanadate [23,24]. Bands for the pyrovanadate and metavanadate phases are not observed, although the presence of these phases in the VMgO catalysts cannot be ruled out by Raman spectroscopy as many bands for these phases could have been obscured by the broad band centered at 860 cm^{-1} . As the wt % vanadium decreases from 60VMgO to 19VMgO, the broad band at 860 cm^{-1} resolves into two bands, around 860 cm^{-1} and 827 cm^{-1} . Furthermore, as the wt % MgO increases from 60 VMgO to 24VMgO, the band around 3650 cm^{-1} increases noticeably. The weak (w) band around 1100 cm^{-1} also becomes more noticeable. These bands are attributed to MgO present in the catalysts. The Raman spectrum for 16VMgO shows a weak to medium intensity band at 861 cm^{-1} . No other bands are clearly distinguishable. The spectrum for 14VMgO is similar to that of 16VMgO except that the band around 860 cm^{-1} has a much lower intensity.

7.2.7 Fourier transform infrared spectroscopy (FTIR)

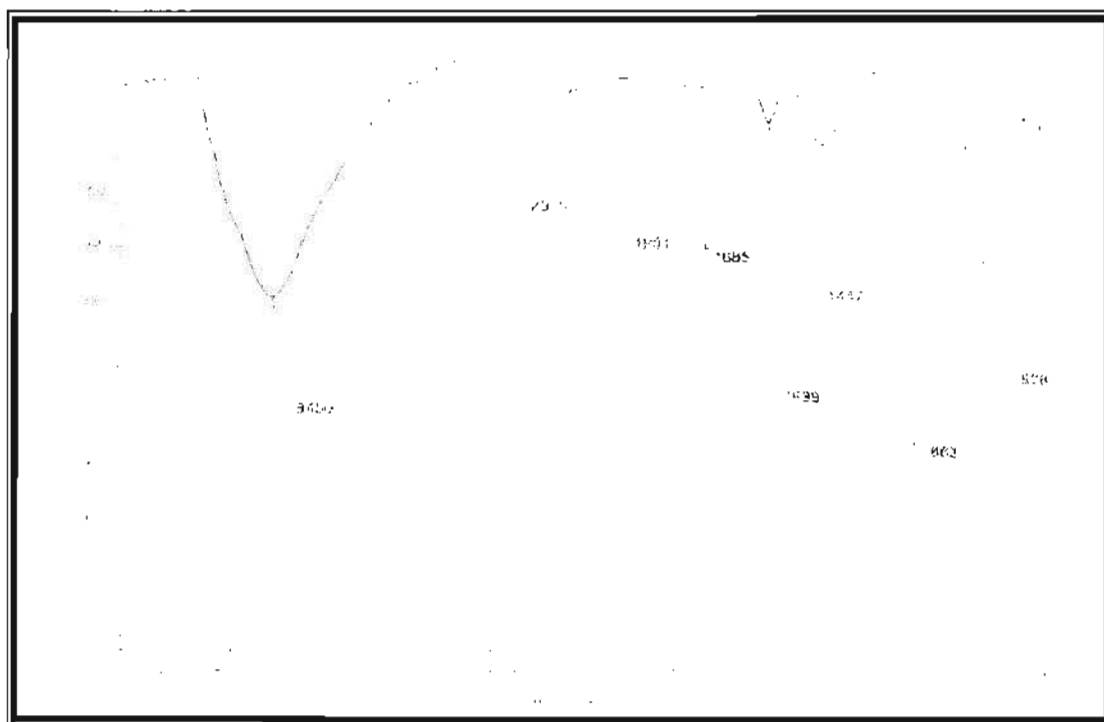


Figure 7.5: FTIR spectrum of 19VMgO

The FTIR spectrum for the 19VMgO catalyst is shown above (Figure 7.5). The strong broad bands at 863 and 676 cm^{-1} are characteristic of magnesium orthovanadate [14,18,21,26-28]. The former band is assigned to the ν_3 antisymmetric stretching of $(\text{VO}_4)^{3-}$ anions, whilst the latter band can be assigned to V-O-V stretching [14,23]. The FTIR spectrum of V_2O_5 is

shown in **Appendix 3**. The strong band at 1020 cm^{-1} observed for V_2O_5 is characteristic of $\text{V}=\text{O}$ stretching. This band is absent from the 19VMgO spectrum. This indicates that V_2O_5 has completely reacted with MgO in this catalyst. The band at 1020 cm^{-1} does not appear in any of the synthesized VMgO catalysts. The FTIR spectra of all VMgO catalysts are given in **Appendix 3**. In VMgO catalysts with low vanadium loading (14VMgO and 16VMgO) the band centered around 680 cm^{-1} cannot be discriminated due to the strong Mg-O vibration in that region. This band is observed in VMgO catalysts with a vanadium loading of 19 % or more. The intense band around 863 cm^{-1} is present in all FTIR spectra.

The IR bands in the $1400\text{ to }1560\text{ cm}^{-1}$ region indicate the presence of magnesium carbonate or hydrogen carbonate. CO_2 easily adsorbs onto basic magnesium vanadate after calcination [19]. In IR spectra obtained under an inert atmosphere, it has been shown that the doublet band at $2300\text{ to }2400\text{ cm}^{-1}$ is indicative of weakly adsorbed gaseous CO_2 being released from the surface of VMgO catalysts [19]. In the present VMgO FTIR spectra, the doublet probably arises from both atmospheric CO_2 present in the sample chamber (since no evacuation was done) as well as the release of weakly adsorbed CO_2 . The broad band in the $3000\text{ to }4000\text{ cm}^{-1}$ region confirms the presence of water (as also revealed by the band at 1640 cm^{-1}) and surface hydroxyl groups [19]. Bands corresponding to magnesium metavanadate and magnesium pyrovanadate are absent from the FTIR spectra of all VMgO catalysts [18,23-25,28]. The broad bands present in the FTIR spectra of all VMgO catalysts are consistent with the non-crystalline nature of these catalysts.

7.2.8 X-ray induced photoelectron spectroscopy (XPS)

The surface composition of a fresh and an aged 19VMgO catalyst was determined by XPS analysis. Surface atomic ratios are shown in **Table 7.8** below. XPS spectra are shown in **Appendix 3**.

| 19VMgO | C_{1s} (eV) | O_{1s} (eV) | $\text{V}_{2p}^{3/2}$ (eV) | Mg_{2p} (eV) | $(\text{Mg}/\text{O})_{\text{XPS}}$ | $(\text{V}/\text{O})_{\text{XPS}}$ | $(\text{Mg}/\text{V})_{\text{XPS}}$ |
|--------|-------------------------|-------------------------|-------------------------------|--------------------------|-------------------------------------|------------------------------------|-------------------------------------|
| Unused | 284.7 | 530.0 | 517.2 515.4 | 49.4 | 0.75 | 0.09 | 8.23 |
| Aged | 284.8 | 530 | 517.4 515.3 | 49.4 | 0.77 | 0.12 | 7.94 |

Table 7.8: Binding energy and surface atomic ratio's for 19VMgO

The binding energy of oxygen, vanadium and magnesium were consistent with previously reported results [19,28]. In **Table 7.8**, it can be seen that the $(\text{Mg}/\text{V})_{\text{XPS}}$ ratio was found to be much larger than the theoretical ratio of the orthovanadate phase ($\text{Mg}/\text{V}=1.5$). Gao *et al.* [29] indicate that this suggests that the surface consists of mainly magnesium and limited amounts of magnesium supported vanadium atoms rather than the stoichiometric orthovanadate phase [29]. Sam *et al.* [18] concluded that a superficial enrichment of magnesium occurs on the crystals of magnesium orthovanadate. The $(\text{Mg}/\text{V})_{\text{XPS}}$ ratio (8.2) for the unused catalyst was lower than that determined by chemical analysis (9.7) indicating an enrichment of vanadium on the surface with respect to the bulk catalyst. The $(\text{Mg}/\text{V})_{\text{XPS}}$ ratio was even lower for the aged catalyst (**Table 7.8**).

The $\text{V}_{2p}^{3/2}$ peak was deconvoluted into two bands (**Figure 7.6**), corresponding to V^{5+} and V^{4+} for higher and lower energies, respectively [19,25,28]. Accordingly, the ratio of $\text{V}^{5+}/\text{V}^{4+}$ was determined to be 3.2 for the unused catalyst and 3.0 for the aged catalyst. This may indicate that the catalyst is reduced under reaction conditions, although it must be noted that small amounts of reduced vanadium species may be produced during XPS measurements, probably due to the high vacuum under which samples have been pretreated [28]. The definitive presence of V^{4+} in VMgO catalysts has been confirmed by electron spin resonance (ESR) examination [19]. However, ESR is a sensitive bulk study and not a surface characterization technique.

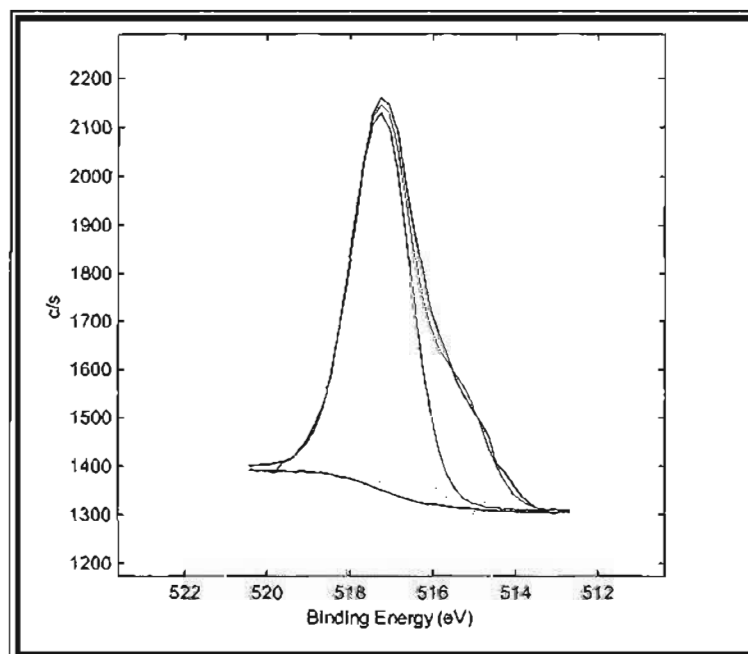


Figure 7.6: XPS spectrum of 19VMgO showing $\text{V}_{2p}^{3/2}$ peak deconvolution

7.2.9 Scanning electron microscopy (SEM)

The SEM images of freshly synthesized 19VMgO, aged 19VMgO and their MgO and V₂O₅ precursors are shown below in Figures 7.7-7.10. SEM images for other catalysts are given in Appendix 3.

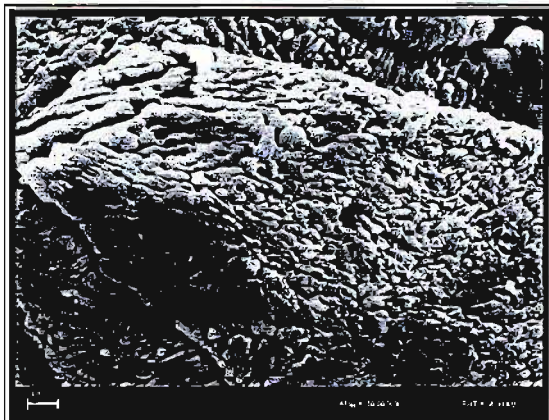


Figure 7.7: SEM image of V₂O₅



Figure 7.8: SEM image of MgO

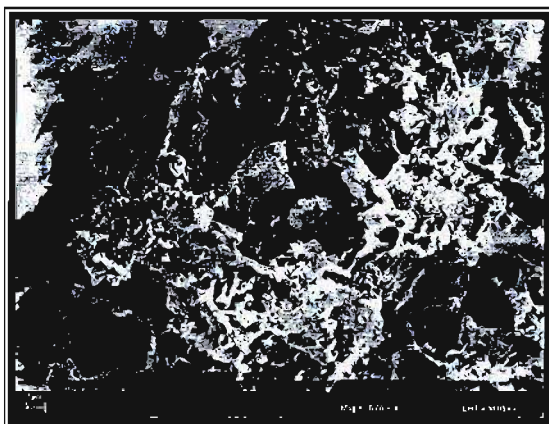


Figure 7.9: SEM image of unused 19VMgO

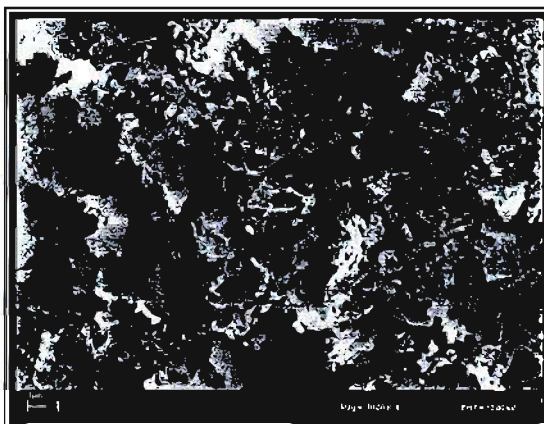


Figure 7.10: SEM image of aged 19VMgO

The SEM image of V₂O₅ shows a well-defined layered structure (Figure 7.7). Images of V₂O₅ under higher magnification are consistent with a crystalline structure. Pure MgO appears as porous and fluffy particles, exhibiting a definitive platelet-like structure (Figure 7.8). The addition of small amounts of vanadium to MgO resulted in samples containing particles of less uniform size and shape. 14VMgO and 16VMgO retain most of the platelet structure of MgO (Appendix 3). 19VMgO exhibited a fair amount of platelet character (Figure 7.9) and this morphology was still retained in the aged catalyst (Figure 7.10). Not much of the platelet structure is observed in 24VMgO, whilst 35VMgO is clearly dissimilar to MgO (Appendix 3). SEM images of 19VMgO and catalysts with higher vanadium loadings appear to contain particles, which are not well-formed crystals but very porous material. This is consistent with the high surface areas of these catalysts. Images of 35VMgO, 49VMgO and 60VMgO show broken up and irregular shaped porous particles (Appendix 3).

Close examination of the SEM images of the aged 19VMgO catalyst showed that a few porous rod shaped particles were present (Figure 7.11). These rod shaped particles were not observed in the unused catalyst (Figure 7.12). EDS analysis performed on the rod shaped particles showed that they were composed of vanadium, magnesium and oxygen. The magnesium to vanadium atomic ratio was close to 1.5. This is in full agreement with the magnesium orthovanadate atomic ratio. Similar structures have been previously observed, albeit in fresh VMgO catalysts [14]. No new phases were observed in the XRD spectrum of the aged 19VMgO catalyst. Furthermore, there did not appear to be any improvement in the crystallinity of the orthovanadate phase in the x-ray diffractogram. High magnification SEM images of the rod shaped particles showed that they were spongy and porous in nature (Appendix 3).

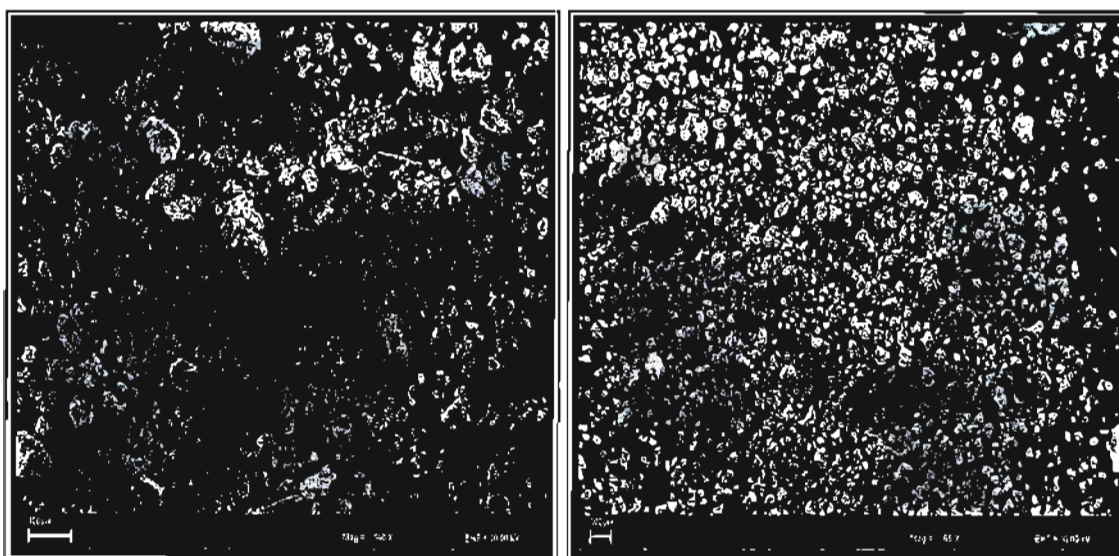


Figure 7.11: SEM image of aged 19VMgO Figure 7.12: SEM image of unused 19VMgO

Elemental maps for 19VMgO are shown in Appendix 3. Vanadium appeared to be evenly dispersed without any significant agglomeration.

7.3 Catalyst characterization: Promoted VMgO

19VMgO was promoted with small amounts of MoO₃, Sb₂O₃, TeO₂, Nb₂O₅, Bi₂O₃ and Cs₂O. Approximately 0.5, 1, 2.5 and 5 weight percent of promoter was added to 19VMgO. The synthesis details have been previously discussed (**Chapter 6.2**). The physico-chemical characteristics of all synthesized promoted VMgO catalysts are shown in **Tables 7.9** and **7.10**. All promoted catalysts had a constant magnesium to vanadium atomic ratio of 9.6. The vanadium to promoter atomic ratio was determined by ICP-AES and EDS. The atomic ratios obtained by the latter technique were significantly higher probably because it is a semi-quantitative technique and can be susceptible to matrix and particle shape effects.

In all promoted catalysts the BET surface areas were lower than unpromoted 19VMgO. Usually surface area decreased with an increase in the amount of promoter added. The loss in BET surface area ranged between 4.4 to 21.0 percent of that of unpromoted 19VMgO.

XRD analyses of these catalysts showed the presence of magnesium oxide and magnesium orthovanadate. The x-ray diffractograms of promoted catalysts closely resembled that of unpromoted 19VMgO (**Appendix 4**). No new phases were detected. The identification of any new phases in the promoted catalysts was difficult due to the concentration of promoter used being well below the detection limits of most techniques.

FTIR spectra of promoted catalysts indicated the presence of the magnesium orthovanadate phase. FTIR spectra of promoted VMgO closely resembled that of unpromoted VMgO (**Appendix 4**). The very strong and broad bands around 680 and 860 cm⁻¹ are consistent with the presence of magnesium orthovanadate. These broad bands are likely to obscure any metal-oxygen vibrations that are frequently encountered in that region. The band at 860 cm⁻¹ was clearly present in the FTIR spectra of all promoted catalysts. The band at 680 cm⁻¹ was clearly observed for all promoted catalysts except those containing bismuth and molybdenum. In bismuth and molybdenum promoted catalysts, the band at 680 cm⁻¹ appeared to be obscured by the intense magnesium oxide vibration (**Appendix 4**).

SEM images and elemental maps for promoted VMgO are shown in **Appendix 4**. The morphology of the promoted catalysts resembles that of the unpromoted catalyst. Promoted catalysts appear to have a very porous and platelet morphology. As the promoter loading increases, there appears to be a small but noticeable loss in the platelet structure of promoted catalysts. Elemental maps indicated that promoters were well dispersed in all catalysts except for those containing high loadings of niobium.

| Promoter (P) | Catalyst | BET (m ² /g) | MgO (wt %) (ICP) | V ₂ O ₅ (wt %) (ICP) | P (wt %) (ICP) | (Mg/V) _{ICP} (atomic) | (Mg/P) _{ICP} (atomic) | (V/P) _{ICP} (atomic) | (V/P) _{EDS} (atomic) |
|--------------------------------|-----------|-------------------------|------------------|--|----------------|--------------------------------|--------------------------------|-------------------------------|-------------------------------|
| - | 19VMgO | 184.9 | 81.1 | 18.9 | 0.00 | 9.7 | - | - | - |
| MoO ₃ | 0.5MoVMgO | 169.7 | 80.6 | 18.9 | 0.5 | 9.6 | 575.3 | 59.8 | 79.7 |
| | 1MoVMgO | 162.5 | 80.3 | 18.8 | 0.9 | 9.6 | 318.4 | 33.0 | 44.2 |
| | 2.5MoVMgO | 163.3 | 79.2 | 18.6 | 2.2 | 9.6 | 128.5 | 13.4 | 17.8 |
| | 5MoVMgO | 158.4 | 77.3 | 18.2 | 4.5 | 9.6 | 61.3 | 6.4 | 8.7 |
| Sb ₂ O ₃ | 0.5SbVMgO | 180.1 | 80.6 | 18.9 | 0.5 | 9.6 | 582.5 | 60.5 | 103.5 |
| | 1SbVMgO | 172.4 | 80.1 | 18.8 | 1.1 | 9.6 | 263.1 | 27.4 | 58.7 |
| | 2.5SbVMgO | 169.1 | 79.0 | 18.5 | 2.5 | 9.6 | 114.2 | 11.9 | 22.4 |
| | 5SbVMgO | 160.9 | 76.9 | 18.1 | 5.0 | 9.6 | 55.6 | 5.8 | 11.0 |
| TeO ₂ | 0.5TeVmgO | 176.2 | 80.6 | 18.9 | 0.5 | 9.6 | 637.9 | 66.3 | 107.0 |
| | 1TeVmgO | 177.1 | 80.0 | 18.8 | 1.2 | 9.6 | 263.8 | 27.5 | 44.4 |
| | 2.5TeVmgO | 161.1 | 79.0 | 18.5 | 2.5 | 9.6 | 119.3 | 12.4 | 15.3 |
| | 5TeVmgO | 150.7 | 77.1 | 18.1 | 4.8 | 9.6 | 63.6 | 6.6 | 9.0 |

Table 7.9: Physico-chemical characteristics of unpromoted and promoted VMgO catalyst

| Promoter (P) | Catalyst | BET (m ² /g) | MgO (wt %) (ICP) | V ₂ O ₅ (wt %) (ICP) | P (wt %) (ICP) | (Mg/V) _{ICP} (atomic) | (Mg/P) _{ICP} (atomic) | (V/P) _{ICP} (atomic) | (V/P) _{EDS} (atomic) |
|--------------------------------|-----------|-------------------------|------------------|--|----------------|--------------------------------|--------------------------------|-------------------------------|-------------------------------|
| - | 19VMgO | 184.9 | 81.1 | 18.9 | 0.00 | 9.7 | - | - | - |
| Nb ₂ O ₅ | 0.5NbVMgO | 177.9 | 80.6 | 18.9 | 0.5 | 9.6 | 530.8 | 55.2 | 67.4 |
| | 1NbVMgO | 178.0 | 80.2 | 18.8 | 1.0 | 9.6 | 264.1 | 27.4 | 44.1 |
| | 2.5NbVMgO | 152.1 | 79.0 | 18.5 | 2.5 | 9.6 | 104.1 | 10.8 | 16.8 |
| | 5NbVMgO | 148.9 | 76.9 | 18.1 | 5.0 | 9.6 | 50.6 | 5.3 | 8.2 |
| Bi ₂ O ₃ | 0.5BiVMgO | 171.8 | 80.7 | 18.9 | 0.4 | 9.6 | 1166.1 | 121.0 | 147.7 |
| | 1BiVMgO | 169.4 | 80.3 | 18.8 | 0.9 | 9.6 | 515.7 | 53.5 | 71.6 |
| | 2.5BiVMgO | 161.1 | 79.3 | 18.6 | 2.1 | 9.6 | 218.3 | 22.7 | 35.2 |
| | 5BiVMgO | 150.6 | 77.2 | 18.1 | 4.7 | 9.6 | 94.9 | 9.9 | 14.5 |
| Cs ₂ O | 0.5CsVMgO | 180.2 | 80.6 | 18.9 | 0.5 | 9.6 | 563.7 | 58.6 | 84.8 |
| | 1CsVMgO | 172.3 | 80.3 | 18.8 | 0.9 | 9.6 | 312.0 | 32.4 | 56.1 |
| | 2.5CsVMgO | 165.5 | 79.0 | 18.5 | 2.5 | 9.6 | 110.5 | 11.5 | 19.7 |
| | 5CsVMgO | 154.9 | 77.1 | 18.1 | 4.8 | 9.6 | 56.2 | 5.8 | 11.3 |

Table 7.10: Physico-chemical characteristics of unpromoted and promoted VMgO catalysts

7.4 Non-catalytic reactor studies

7.4.1 Introduction

Paraffins are stable molecules. Relatively high temperatures are required for their catalytic oxidative dehydrogenation. At these temperatures gas-phase reactions may occur. These non-catalytic homogeneous reaction pathways may significantly supplement heterogeneous catalytic reactions. Homogeneous pathways may result in side reactions and/or they may take part in the main route and play an important role in the formation of desired products [30]. Usually, homogeneous gas-phase reactions result in non-selective oxidation and the control of these reactions will yield better selectivity towards desired products.

In order to study the effect of the catalyst alone, the contribution of the gas-phase reactions must also be eliminated or greatly reduced. Quartz particles have been successfully used to limit the extent of homogeneous reactions [31-34]. Lemonidou [35] showed that at 580 °C the conversion of butane in air (equimolar) in an empty reactor was 62 %. This conversion dropped to 2.5 % in the presence of quartz chips. Lemonidou [35] indicated that a high surface to volume ratio (S/V) diminished the extent of homogeneous reactions through chain termination reactions of free radicals. It has also been shown that inert packing material can provide a feasible method for isolating and studying the effect of a catalyst alone in oxidative dehydrogenation reactions [33].

7.4.2 Homogeneous reactions

Catalytic reactors were fully packed with 24 grit carborundum to minimize the contribution of homogeneous reactions. The use of a smaller carborundum particle size would have yielded a higher S/V ratio and thus an even lower homogeneous reaction contribution. However, the pressure drop across the reactors would have become significant. The use of 24 grit carborundum resulted in a minimum pressure differential across the reactors, whilst effectively minimizing homogeneous reaction pathways.

n-Hexane and *n*-octane were fed through stainless steel reactors filled only with carborundum. The dimensions for these reactors are given in **Chapter 6.7** and **Appendix 1**. The extent of non-catalytic homogeneous reactions was examined under similar conditions used for catalytic runs. The results are shown in **Figures 7.13** and **7.14**.

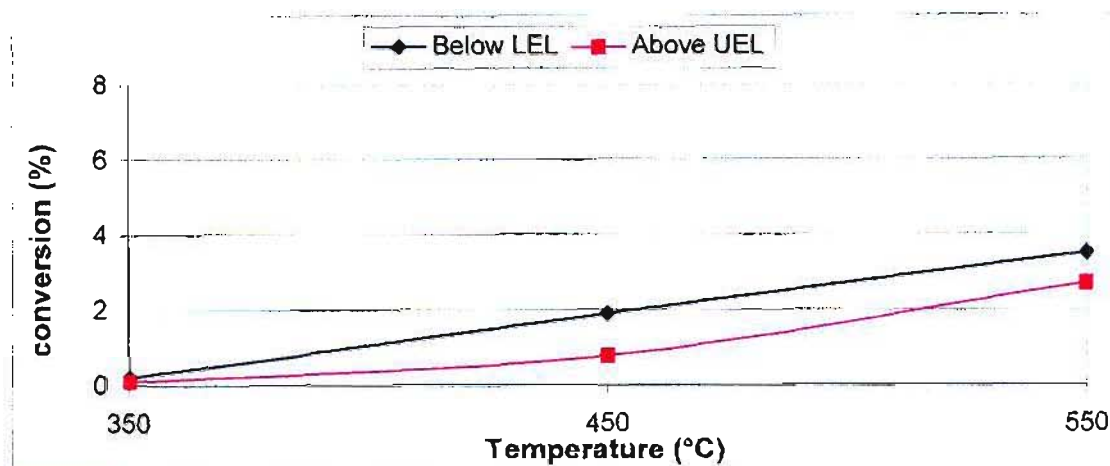


Figure 7.13: Effect of temperature on the non-catalytic conversion of *n*-hexane in carborundum filled reactors. Feed compositions of 0.6 % (below LEL) and 7.8 % (above UEL) *n*-hexane in air were used. The flow rate of the feed used was 100 ml/min.

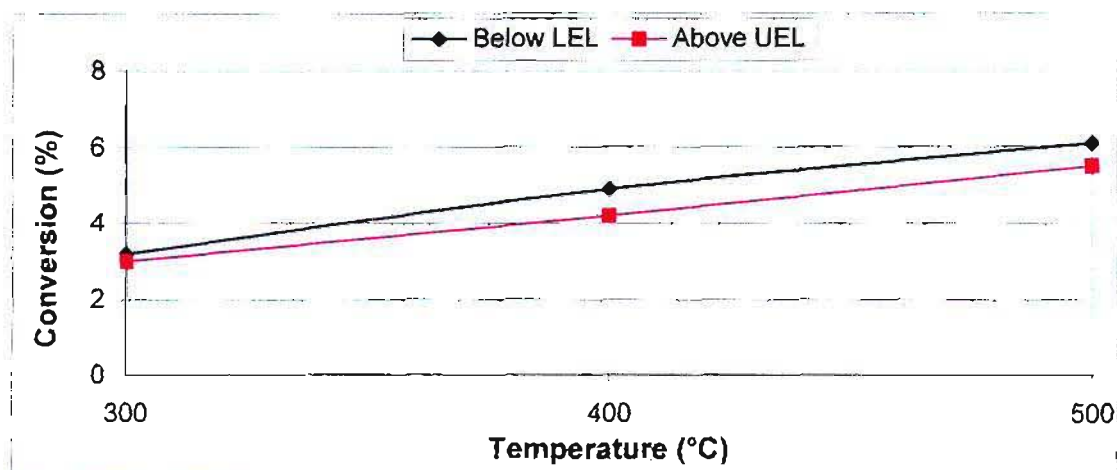


Figure 7.14: Effect of temperature on the non-catalytic conversion of *n*-octane in carborundum filled reactors. Feed compositions of 1.0 % (below LEL) and 7.0 % (above UEL) *n*-octane in air were used. The flow rate of the feed used was 100 ml/min.

Figures 7.13 and 7.14 shows that non-catalytic reactions increase with temperature. The results indicate that homogeneous reactions are more apparent for *n*-octane than for *n*-hexane. This is in agreement with longer carbon chain paraffins being more reactive. The results also indicate that homogeneous reactions at these temperatures are slightly higher below the LEL i.e. when more oxygen is present. This is attributed to a higher probability of forming oxygen radicals when oxygen rich feeds are used [33]. The product spectrum for the non-catalytic oxidation of *n*-hexane included olefins, oxygenates, cracked products, benzene and carbon oxides. The product spectrum for octane oxidation comprised of olefins, aromatics, oxygenates cracked products and mainly carbon oxides.

7.4.3 Conclusion

Filling reactors with carborundum provides a feasible method for isolating and studying the effect of a catalyst as homogeneous reactions in *n*-hexane and *n*-octane oxidation are greatly diminished under these conditions. It is still important to bear in mind that homogeneous reactions become increasingly important with increasing reaction temperatures.

Another important reaction pathway is heterogeneous-homogeneous reactions i.e. catalyst induced homogeneous reactions. It is well known that gas-phase free radicals may be generated on the surface of a catalyst [36]. These radicals may desorb into the gas-phase and participate in homogeneous gas-phase reactions. These heterogeneous-homogeneous reaction pathways contribute to the total effect of a catalyst. In general, the extent of the contributions of heterogeneous-homogeneous pathways is not understood and often controversial [33,37-40]. The contribution from heterogeneous-homogeneous reactions was not evaluated in this study.

Recently, heterogeneous-homogeneous reactions pathways were proposed for the partial oxidation of *n*-hexane [41]. Here, short-contact-time reactors containing a single layer of a platinum-rhodium catalyst were used to produce mainly C₆ oxygenates and C₃₋₆ olefins. Benzene, propane and propene (products of the present study) were not reported as observable products.

7.5 References:

- 1) Hutchings, G. J., *Catalytic Activation and Functionalisation of Light Alkanes*, Kluwer Academic Publishers, Netherlands, 1998, pp. 125-156.
- 2) Baerns, M. and Buyevskaya, O., *Catal. Today*, **45**, 1998, 13.
- 3) Mamedov, E. A. and Corberan, V. C., *Appl. Catal. A*, **127**, 1995, 1.
- 4) Blasco, T. and Lopez Nieto, J. M., *Appl. Catal. A*, **157**, 1997, 117.
- 5) Lee, J. S., Oyama, S. T., *Catal. Rev. Sci. Eng.*, **30**, 1998, 249.
- 6) Madeira, L. M. and Portela, M. F., *Catal. Rev. Sci. Eng.*, **44**, 2002, 247.
- 7) Kung, H. H., *Adv. Catal.*, **40**, 1994, 1.
- 8) Albonetti, S., Cavani, F. and Trifiro, F., *Catal. Rev. Sci. Eng.*, **38**, 1996, 413.
- 9) Cavani, F. and Trifiro, F., *Appl. Catal. A*, **88**, 1992, 115.
- 10) Cavani, F. and Trifiro, F., *Catal. Today*, **24**, 1995, 307.
- 11) Cavani, F. and Trifiro, F., *Catal. Today*, **51**, 1999, 561.
- 12) Mamedov, E. A., *Appl. Catal. A*, **116**, 1994, 49.
- 13) Lemonidou, A. A., Tjatjopoulos, G. J. and Vasalos, I. A., *Catal. Today*, **45**, 1998, 65.
- 14) Chaar, M. A., Patel, D., Kung, M. C. and Kung, H. H., *J. Catal.*, **105**, 1987, 483.
- 15) Dejoz, A., Lopez Nieto, J. M., Marquez, F. and Vazquez, M. I., *Appl. Catal. A*, **180**, 1999, 83.
- 16) Burrows, A., Kiely, C. J., Perregaard, J., Hojlund-Nielsen, P. E., Vorbeck, G., Calvino, J. J. and Lopez-Cartes, C., *Catal. Lett.*, **57** 1999, 121.
- 17) Blasco, T., Lopez Nieto, J. M., Dejoz, A. and Vasquez, M. I., *J. Catal.*, **157**, 1995, 271.
- 18) Siew Hew Sam, D., Soenen, V. and Volta, J. C., *J. Catal.*, **123**, 1990, 417.
- 19) Tellez, C., Abon, M., Dalmon, J. A., Mirodatos, C. and Santamaria, J., *J. Catal.*, **195**, 2000, 113.
- 20) Nakamura, K., Kawai, K. and Fujiwara, Y., *J. Catal.*, **34**, 1974, 345.
- 21) Corma, A., Lopez Nieto, J. M. and Paredes, N., *J. Catal.*, **144**, 1993, 425.
- 22) Kung, H. H. and Kung, M. C., *Appl. Catal. A*, **157**, 1997, 105.
- 23) Hanuza, J., Jezowska-Trzebiatowska, B. and Oganowski, W., *J. Mol. Catal.*, **29**, 1985, 109.
- 24) Lopez Nieto, J. M., Dejoz, A. and Vazquez, M. I., *Appl. Catal. A*, **132**, 1995, 41.
- 25) Gao, X., Ruiz, P., Xin, Q., Guo, X. and Delmon, B., *Catal. Lett.*, **23**, 1994, 321.
- 26) Corma, A., Lopez Nieto, J. M. and Paredes, N., *Appl. Catal. A*, **97**, 1993, 159.
- 27) Solsona, B., Dejoz, A., Vazquez, M. I., Marquez, F. and Lopez Nieto, J. M., *Appl. Catal. A*, **208**, 2001, 99.

- 28) Gao, X., Ruiz, P., Xin, X., Guo, B. and Delmon, J., *J. Catal.*, **148**, 1994, 56.
- 29) Pantazidis, A., Burrows, A., Kiely, C. J. and Mirodatos, C., *J. Catal.*, **177**, 1998, 325.
- 30) Vislovskiy, V.P., Suleimanov, T. E., Sinev, M. Y., Tulenin, Y. P., Margolis, L. Y. and Corberan, V.C., *Catal. Today*, **61**, 2000, 287.
- 31) Hatano, M., Hinson, P. G., Vines, K. S. and Lunsford, J. H., *J. Catal.*, **124**, 1990, 557.
- 32) Kalenik, Z. and Wolf, E. E., *J. Catal.*, **124**, 1990, 566.
- 33) Burch, R. and Crabb, E. M., *Appl. Catal. A.*, **97**, 1993, 49.
- 34) Morales, E. and Lunsford, J. H., *J. Catal.*, **118**, 1989, 255.
- 35) Lemonidou, A. A. and Stambouli, A. E., *Appl. Catal. A*, **171**, 1998, 325.
- 36) Driscoll, D. J., Campbell, K. D. and Lunsford, J.H., *Adv. Catal.*, **35**, 1987, 139.
- 37) Martin, G. A., Bates, A., Ducarme, V. and Mirodatos, C., *Appl. Catal. A*, **47**, 1989, 287.
- 38) Hatano, M., Hinson, P. G., Vines, K. S. and Lunsford, J. H., *J. Catal.*, **124**, 1990, 557.
- 39) Yates, D. J. C. and Zlotin, N. E., *J. Catal.*, **124**, 1990, 562.
- 40) Kalenik, Z. and Wolf, E. E., *J. Catal.*, **124**, 1990, 566.
- 41) O'Connor, R. P. and Schmidt, L. D., *Chem. Eng. Sci.*, **55**, 2000, 5693.

CHAPTER 8: Oxidative Dehydrogenation of *n*-Hexane

8.1 Catalyst testing below the lower explosive limit

Magnesium oxide, vanadium pentoxide and magnesium vanadium oxide catalysts were synthesized as described in Chapter 6.2. These catalysts were tested on a 0.6 % *n*-hexane in air feed in a fixed bed reactor as described in Chapter 6.5. A feed flow rate of 100 ml/min was used. The volume of the catalyst bed was 1.6 ml. This corresponded to a gas hourly space velocity (GHSV) of 3750 h⁻¹. The results for *n*-hexane ODH over pure magnesium oxide and vanadium pentoxide are shown in Figure 8.1 below:

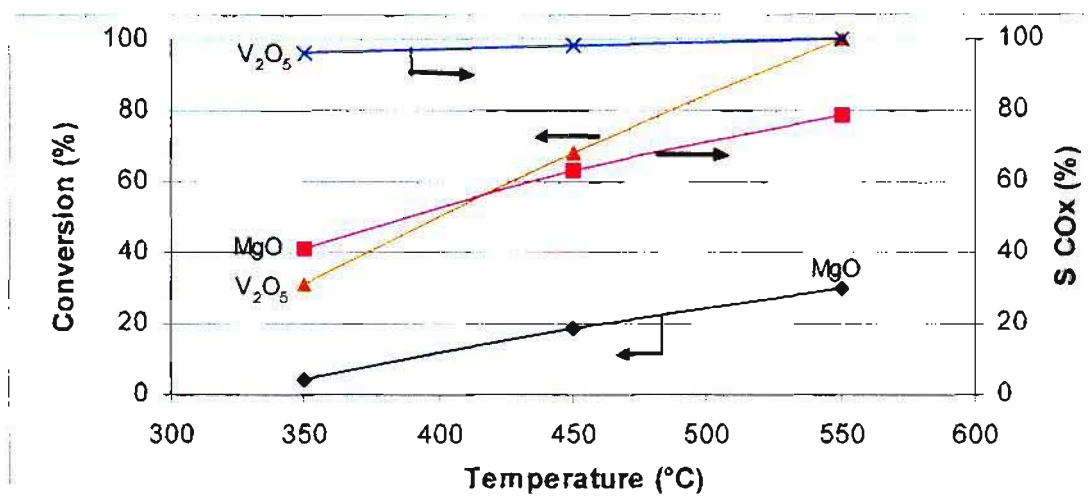


Figure 8.1: Effect of temperature on conversion and selectivity in *n*-hexane ODH over MgO and V₂O₅.

Under the conditions tested, V₂O₅ is quite active for *n*-hexane oxidation. Total oxidation is strongly favoured. MgO is noticeably less active but its selectivity towards total oxidation appears to be lower. The product spectrum included mainly cracked products and to a lesser extent olefins and isomers of hexane.

Tables 8.1 – 8.7 show the effect of temperature on conversion and selectivity in *n*-hexane ODH over vanadium magnesium oxide catalysts with different vanadium loadings. Catalysts testing began at 300 °C and ended either at 550 °C or until 100 percent conversion of *n*-hexane was achieved. At low temperatures and conversions, carbon oxides are the only carbon containing products formed. As the temperature increases benzene is formed and selectivity towards CO_x decreases. At high conversions it was possible to observe and accumulate small amounts of water.

| Temperature (°C) | C _{Hexane} (%) | S _{Benzene} (%) | S _{COx} (%) |
|---------------------|----------------------------|-----------------------------|-------------------------|
| 300 | 8.1 | 0 | 100 |
| 350 | 21.3 | 0.1 | 99.9 |
| 400 | 33.0 | 1.1 | 98.9 |
| 450 | 62.0 | 2.0 | 98.0 |
| 500 | 83.0 | 1.0 | 99.0 |
| 550 | 95.0 | 0.1 | 99.9 |

Table 8.1: *n*-Hexane ODH over 14VMgO

| Temperature (°C) | C _{Hexane} (%) | S _{Benzene} (%) | S _{COx} (%) |
|---------------------|----------------------------|-----------------------------|-------------------------|
| 300 | 19.1 | 0 | 100 |
| 350 | 61.6 | 1.1 | 98.9 |
| 400 | 83.0 | 4.4 | 95.6 |
| 425 | 96.0 | 6.5 | 93.5 |
| 435 | 98.1 | 7.1 | 92.9 |
| 450 | 100 | 5.4 | 94.6 |

Table 8.2: *n*-Hexane ODH over 16VMgO

| Temperature (°C) | C _{Hexane} (%) | S _{Benzene} (%) | S _{COx} (%) |
|---------------------|----------------------------|-----------------------------|-------------------------|
| 300 | 19.3 | 6.8 | 93.2 |
| 350 | 65.0 | 8.8 | 91.2 |
| 400 | 96.1 | 14.8 | 85.2 |
| 415 | 96.3 | 15.0 | 85.0 |
| 430 | 98.5 | 15.6 | 84.4 |
| 445 | 99.4 | 17.7 | 82.3 |
| 450 | 100 | 17.1 | 82.9 |

Table 8.3: *n*-Hexane ODH over 19VMgO

| Temperature (°C) | C _{Hexane} (%) | S _{Benzene} (%) | S _{COx} (%) |
|---------------------|----------------------------|-----------------------------|-------------------------|
| 300 | 9.2 | 0 | 100 |
| 350 | 44.1 | 3.9 | 96.1 |
| 400 | 61.8 | 6.0 | 94.0 |
| 425 | 83.3 | 9.4 | 90.6 |
| 450 | 96.1 | 12.4 | 87.6 |
| 465 | 99.4 | 15.5 | 84.5 |
| 475 | 100 | 14.3 | 85.7 |

Table 8.4: *n*-Hexane ODH over 24VMgO

| Temperature (°C) | C _{Hexane} (%) | S _{Benzene} (%) | S _{COx} (%) |
|---------------------|----------------------------|-----------------------------|-------------------------|
| 300 | 7.9 | 0 | 100 |
| 350 | 21.6 | 0 | 100 |
| 400 | 50.8 | 4.2 | 95.8 |
| 430 | 70.9 | 6.2 | 93.8 |
| 440 | 75.0 | 6.9 | 93.1 |
| 450 | 81.8 | 8.0 | 92.0 |
| 470 | 90.2 | 9.8 | 90.2 |
| 490 | 95.4 | 11.6 | 88.4 |
| 510 | 98.6 | 13.2 | 86.8 |
| 525 | 99.9 | 14.3 | 85.7 |
| 535 | 100 | 13.4 | 86.6 |

Table 8.5: *n*-Hexane ODH over 35VMgO

| Temperature (°C) | C _{Hexane} (%) | S _{Benzene} (%) | S _{COx} (%) |
|---------------------|----------------------------|-----------------------------|-------------------------|
| 300 | 4.9 | 0.0 | 100 |
| 350 | 11.0 | 0.0 | 100 |
| 400 | 15.1 | 1.0 | 99.0 |
| 450 | 33.2 | 3.4 | 96.6 |
| 500 | 46.0 | 5.9 | 94.1 |
| 550 | 66.0 | 5.8 | 94.2 |

Table 8.6: *n*-Hexane ODH over 49VMgO

| Temperature (°C) | C _{Hexane} (%) | S _{Benzene} (%) | S _{COx} (%) |
|---------------------|----------------------------|-----------------------------|-------------------------|
| 300 | 3.1 | 0 | 100 |
| 350 | 8.0 | 0 | 100 |
| 400 | 15.0 | 0.2 | 99.8 |
| 450 | 27.0 | 1.2 | 98.8 |
| 500 | 37.2 | 1.6 | 98.4 |
| 550 | 52.1 | 2.1 | 97.9 |

Table 8.7: *n*-Hexane ODH over 60VMgO

As temperatures close to the upper limit of testing were reached, the selectivity towards benzene started to decrease and a corresponding increase in CO_x was observed. At elevated temperatures, the thermal stability of benzene decreases and it can be consecutively oxidized to CO_x. The thermal stability of benzene over VMgO catalysts is shown in **Chapter 10**.

Interestingly, the ODH of *n*-hexane over VMgO's yielded a very simple FID GC trace containing just benzene and unreacted *n*-hexane, if it was present. Not even trace amounts of other organic products were observed with the FID detector. This effect has been observed before for *n*-pentane oxidation over a vanadyl pyrophosphate catalyst [1,2]. When the fuel to air ratio is low i.e. below the LEL, the surface of the catalyst is not saturated with adsorbed species. Catalytic sites are accessible and available and consequently the probability of adsorbed intermediates desorbing into the gas-phase is low [2]. When the surface is saturated with intermediates i.e. above the UEL, the situation is changed and the catalysis becomes nonselective in terms of the number of different products formed. This was the case when a much higher fuel to air ratio was used (**Chapter 8.2**).

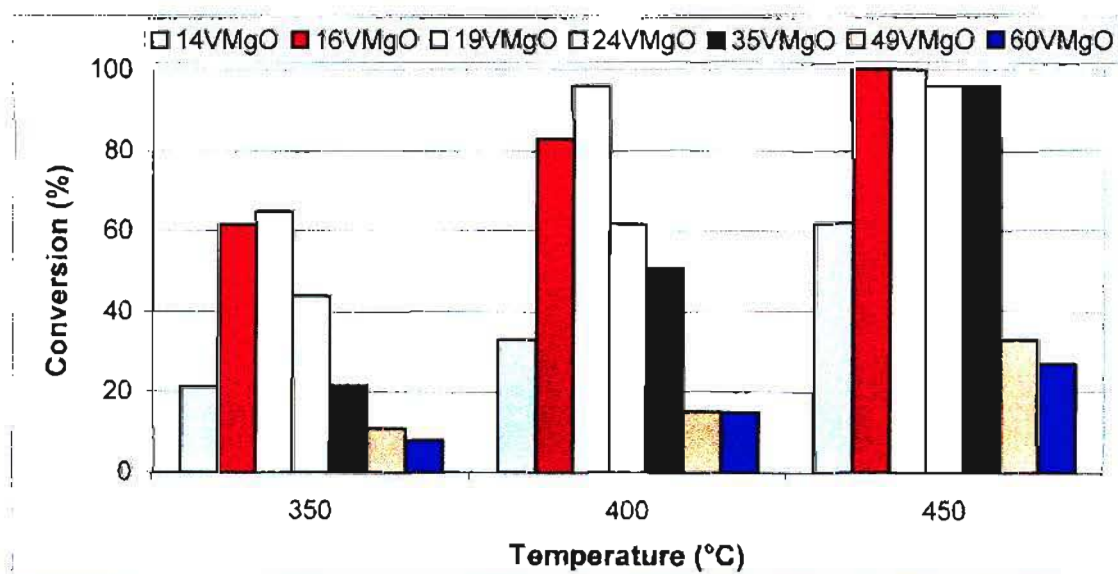


Figure 8.2: Effect of temperature on *n*-hexane conversion

Figure 8.2 shows the conversion of *n*-hexane at 350, 400 and 450 °C. Complete conversion of *n*-hexane occurs at 450 °C with 16VMgO and 19VMgO. *n*-Hexane conversion is higher over 19VMgO than any other catalyst at any temperature where 100 percent conversion has not been attained. **Figure 8.3** shows the temperature required for a 20 % conversion of *n*-hexane. The data indicates that 19VMgO is the most active catalyst for a 20 % conversion of *n*-hexane. 19VMgO even showed higher activity than pure V₂O₅. It was observed that the addition of limited amounts of vanadium to MgO to form VMgO resulted in an increase in catalytic activity. Loadings above 19 weight % resulted in an evident drop in activity.

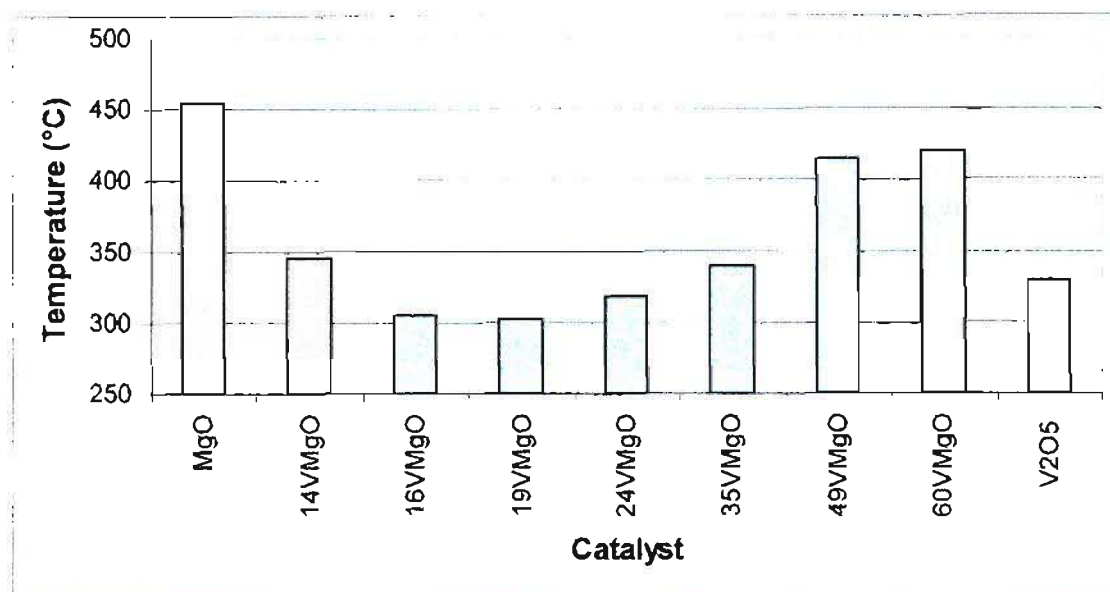


Figure 8.3: Temperature required for a 20% *n*-hexane conversion

Catalyst activity is dependent on three contributing factors i.e. surface area, the density of active sites and the specific reactivity of active sites. In **Table 8.8** below the activities of all catalysts tested are normalized for surface area. It can be seen that the conversion per surface area tends to increase with increasing vanadium content. This indicates that the specific activity of VMgO catalysts is dependent on the density of vanadium atoms. Increasing the vanadium content resulted in catalysts with higher specific activity. This is in agreement with vanadium atoms acting as active sites for *n*-hexane ODH.

| Catalyst | Surface area (m ² /g) | Conversion (%) ^a | Conversion (m ⁻²) ^b |
|-------------------------------|----------------------------------|-----------------------------|--|
| MgO | 132.3 | 12.0 | 0.15 ^c |
| 14VMgO | 183.4 | 21.3 | 0.29 |
| 16VMgO | 188.6 | 61.6 | 0.82 |
| 19VMgO | 184.9 | 65.0 | 0.88 |
| 24VMgO | 133.2 | 44.1 | 0.83 |
| 35VMgO | 53.2 | 21.6 | 1.00 |
| 49VMgO | 22.7 | 11.0 | 1.21 |
| 60VMgO | 8.9 | 8.0 | 2.24 |
| V ₂ O ₅ | 4.2 | 25.0 | 9.87 ^c |

^a 0.6% hexane in air feed ^b Catalyst weight = 0.4 g ^c Catalyst weight = 0.6 g

Table 8.8: Specific activity for MgO, V₂O₅ and VMgO catalysts at 350 °C

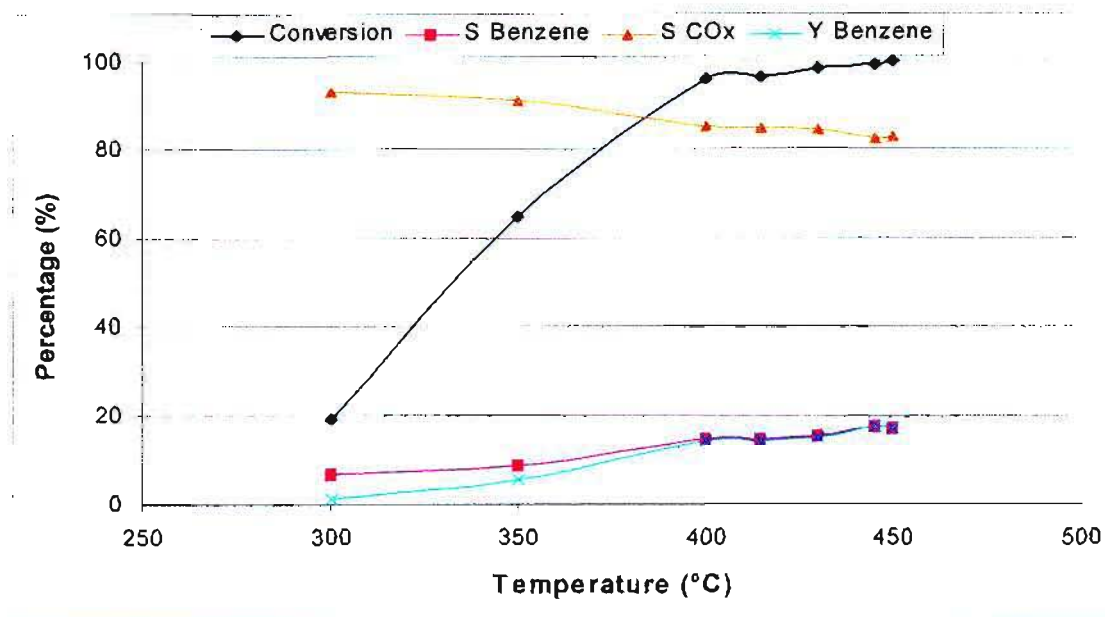


Figure 8.4: Effect of temperature on *n*-hexane conversion, selectivity to benzene, selectivity to COx and yield of benzene for 19VMgO

The maximum yield of benzene is $17.6 (\pm 0.4) \%$ at $445 \text{ }^\circ\text{C}$ (**Figure 8.4**). At this temperature the selectivity to benzene is $17.7 (\pm 0.4) \%$ and *n*-hexane conversion is $99.4 (\pm 0.4) \%$. **Figure 8.5** below shows the selectivities obtained by the VMgO catalysts at 30 % conversion. 19VMgO shows the highest selectivity towards benzene. At comparable conversions 19VMgO is at least twice as selective as any other VMgO catalyst tested. It is thus concluded that a vanadium loading around 19 % yields the best performance for *n*-hexane ODH over VMgO catalysts and under fuel lean conditions.

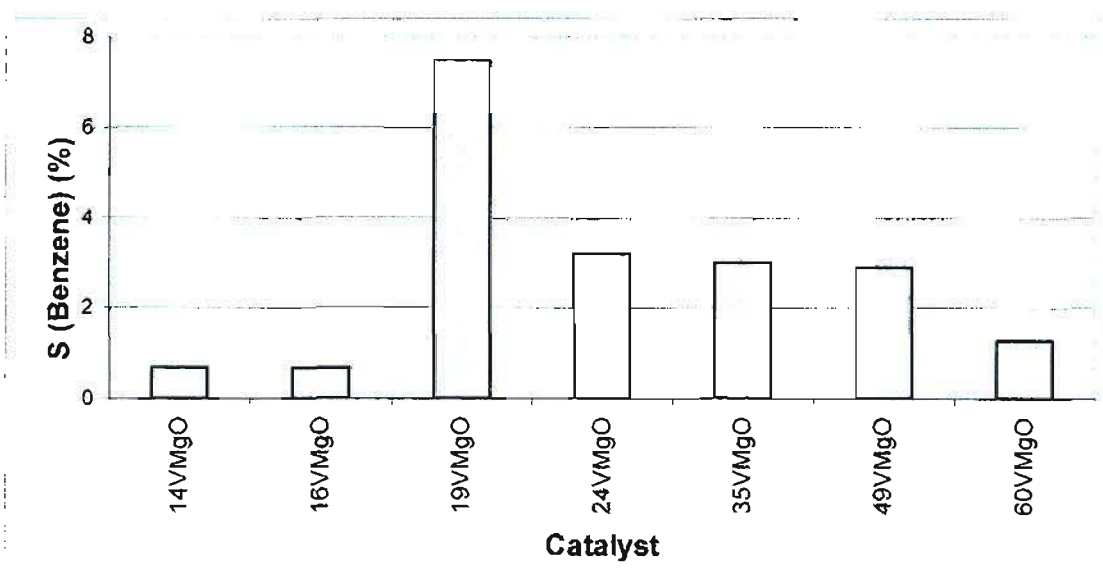


Figure 8.5: Selectivity to benzene on VMgO catalysts at 30 % conversion

8.2 Catalyst testing above the upper explosive limit

16VMgO, 19VMgO and 24VMgO were tested on a 7.8 % *n*-hexane in air feed in a fixed bed reactor. The experimental details have been previously discussed (**Chapter 6**). Catalysts were tested between 350 and 550 °C. The volume of the catalyst bed was 1.6 ml (0.4 g). A flow rate of 100 ml/min was used and this corresponded to a gas hourly space velocity of 3750 h⁻¹. The results for *n*-hexane ODH over 16VMgO, 19VMgO and 24VMgO are shown in **Tables 8.9, 8.10 and 8.11**.

Catalytic testing of the 3 catalysts below the lower explosive limit (0.6 % *n*-hexane in air) had previously yielded 4 products i.e. C₆H₆, CO₂, CO and H₂O. Testing above the upper explosive limit yielded several new products. In addition to C₆H₆, CO_x and H₂O the following products were also formed: 1-hexene, 2-hexene, propane and propene. Cavani and Trifiro [2] indicate that a high fuel to air ratio results in the surface of the catalyst becoming saturated with adsorbed species. They report that under fuel lean conditions pentane oxidation over vanadyl pyrophosphate yields maleic anhydride, phthalic anhydride and CO_x. Under fuel rich conditions other products, which did not appear for low *n*-pentane concentrations in the feed, were observed. On a saturated catalyst surface, catalytic sites are scarce. The catalytic reaction then becomes nonselective because intermediate olefinic species desorb into the gas-phase. These desorbed species may then undergo further transformations in the gas-phase [2]. Desorbed species may also be readsorbed.

It is well known that the surface of a catalyst is in dynamic interaction with the gas-phase [2,3]. Under fuel lean (below LEL) conditions the gas-phase has high oxidizing power. The converse is also true. In this way the oxidation state of vanadium in VMgO catalysts is influenced. In oxidation catalysis, a more oxidized catalytic surface usually results in more active but less selective catalysts [2]. Catalysts operating above the UEL are thus expected to be less active and more selective. The results shown in **Tables 8.9, 8.10 and 8.11** for *n*-hexane ODH under fuel rich conditions are in full agreement.

| Temp (°C) | C (%) | S (C ₆ H ₆) | Y (C ₆ H ₆) | S (Hexenes) | S (C ₃ H ₈) | S (C ₃ H ₆) | S (COx) | Y (Hexenes) | Y (C ₃ H ₈) | Y (C ₃ H ₆) | Y (COx) | TDS |
|-----------|-------|------------------------------------|------------------------------------|-------------|------------------------------------|------------------------------------|---------|-------------|------------------------------------|------------------------------------|---------|------|
| 350 | 28.3 | 0 | 0 | 0 | 0 | 0 | 100 | 0 | 0 | 0 | 28.3 | 0 |
| 400 | 41.4 | 8.4 | 3.5 | 4.4 | 0 | 0 | 87.2 | 1.8 | 0 | 0.0 | 36.1 | 12.8 |
| 425 | 47.9 | 12.5 | 6.0 | 4.6 | 0 | 0 | 82.9 | 2.2 | 0 | 0.0 | 39.7 | 17.1 |
| 450 | 51.2 | 12.9 | 6.6 | 4.8 | 0 | 0 | 82.3 | 2.5 | 0 | 0.0 | 42.1 | 17.7 |
| 475 | 50.3 | 15.3 | 7.7 | 4.1 | 1.6 | 0.8 | 78.1 | 2.1 | 0.8 | 0.4 | 39.3 | 20.2 |
| 500 | 56.2 | 18.7 | 10.5 | 4.0 | 2.9 | 0.4 | 74.0 | 2.3 | 1.6 | 0.2 | 41.6 | 23.2 |
| 525 | 56.8 | 25.0 | 14.2 | 3.8 | 5.6 | 3.0 | 62.5 | 2.2 | 3.2 | 1.8 | 35.5 | 31.9 |
| 550 | 59.7 | 21.4 | 12.8 | 3.7 | 7.9 | 4.0 | 63.0 | 2.2 | 4.7 | 2.4 | 37.6 | 29.1 |

Table 8.9: The effect of temperature on conversion, selectivity and yield in *n*-hexane ODH over 16VMgO

| Temp (°C) | C (%) | S (C ₆ H ₆) | Y (C ₆ H ₆) | S (Hexenes) | S (C ₃ H ₈) | S (C ₃ H ₆) | S (COx) | Y (Hexenes) | Y (C ₃ H ₈) | Y (C ₃ H ₆) | Y (COx) | TDS |
|-----------|-------|------------------------------------|------------------------------------|-------------|------------------------------------|------------------------------------|---------|-------------|------------------------------------|------------------------------------|---------|------|
| 350 | 29.8 | 0 | 0 | 0 | 0 | 0 | 100 | 0 | 0 | 0 | 29.8 | 0 |
| 400 | 56.3 | 8.5 | 4.8 | 4.8 | 0.9 | 0 | 85.8 | 1.6 | 0.5 | 0 | 48.3 | 13.3 |
| 425 | 59.9 | 14.1 | 8.4 | 4.6 | 0.8 | 0 | 80.5 | 2.1 | 0.5 | 0 | 48.2 | 18.7 |
| 450 | 56.3 | 17.5 | 9.8 | 4.0 | 1.1 | 0.2 | 77.2 | 2.6 | 0.6 | 0.1 | 43.5 | 21.6 |
| 475 | 61.7 | 19.8 | 12.2 | 3.9 | 1.9 | 1.1 | 73.2 | 2.4 | 1.2 | 0.7 | 45.2 | 24.9 |
| 500 | 65.3 | 21.4 | 14.0 | 4.0 | 3.5 | 2.0 | 69.2 | 2.6 | 2.3 | 1.3 | 45.2 | 27.4 |
| 525 | 67.1 | 29.2 | 19.6 | 3.9 | 7.3 | 3.9 | 55.7 | 2.6 | 4.9 | 2.6 | 37.4 | 37.0 |
| 550 | 68.8 | 26.0 | 17.9 | 3.7 | 10.3 | 5.1 | 55.1 | 2.5 | 7.1 | 3.5 | 37.9 | 34.8 |

Table 8.10: The effect of temperature on conversion, selectivity and yield in *n*-hexane ODH over 19VMgO

| Temp (°C) | C (%) | S (C ₆ H ₆) | Y (C ₆ H ₆) | S (Hexenes) | S (C ₃ H ₈) | S (C ₃ H ₆) | S (COx) | Y (Hexenes) | Y (C ₃ H ₈) | Y (C ₃ H ₆) | Y (COx) | TDS |
|-----------|-------|------------------------------------|------------------------------------|-------------|------------------------------------|------------------------------------|---------|-------------|------------------------------------|------------------------------------|---------|------|
| 350 | 27.3 | 0 | 0.0 | 0 | 0 | 0 | 100 | 0.0 | 0.0 | 0.0 | 27.3 | 0 |
| 400 | 49.4 | 6.4 | 3.2 | 5.8 | 0 | 0 | 87.8 | 2.9 | 0.0 | 0.0 | 43.4 | 12.2 |
| 425 | 53.6 | 8.5 | 4.6 | 5.7 | 0.8 | 0 | 85.0 | 3.1 | 0.4 | 0.0 | 45.6 | 14.2 |
| 450 | 56.3 | 10.2 | 5.7 | 5.2 | 1.5 | 1.0 | 82.1 | 2.9 | 0.8 | 0.6 | 46.2 | 16.4 |
| 475 | 55.7 | 15.9 | 8.9 | 5.0 | 2.0 | 1.1 | 76.0 | 2.8 | 1.1 | 0.6 | 42.3 | 22.0 |
| 500 | 58.1 | 19.3 | 11.2 | 4.4 | 4.2 | 2.8 | 69.3 | 2.6 | 2.4 | 1.6 | 40.2 | 26.5 |
| 525 | 59.1 | 24.7 | 14.6 | 4.2 | 5.5 | 3.8 | 61.8 | 2.5 | 3.3 | 2.3 | 36.5 | 32.7 |
| 550 | 62.0 | 20.7 | 12.9 | 4.2 | 8.5 | 4.4 | 62.2 | 2.6 | 5.3 | 2.7 | 38.6 | 29.3 |

Table 8.11: The effect of temperature on conversion, selectivity and yield in *n*-hexane ODH over 24VMgO

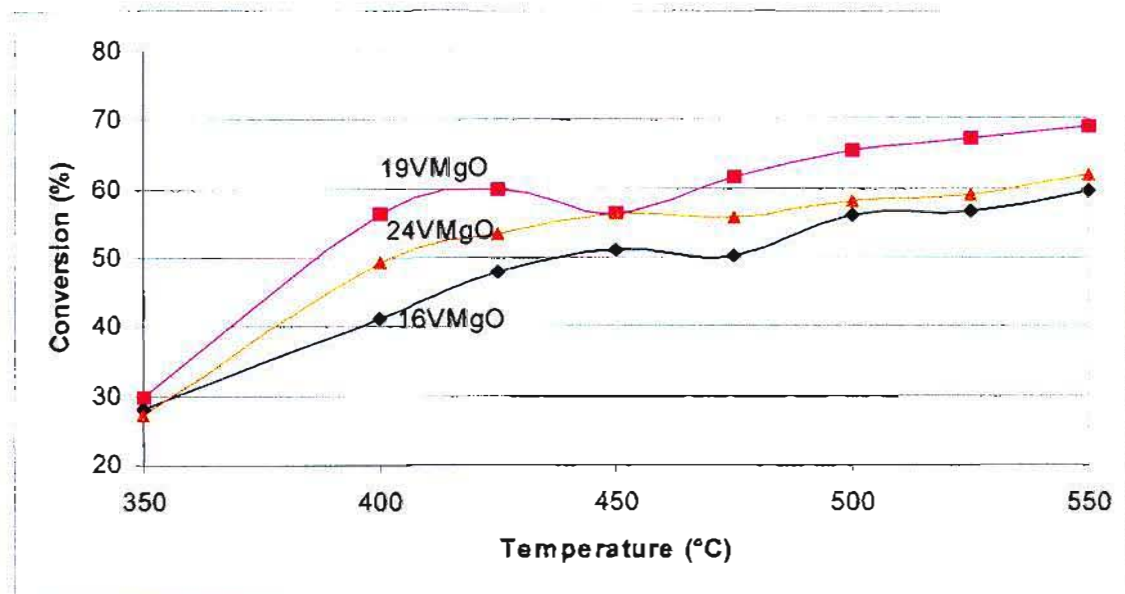


Figure 8.6: Effect of temperature on conversion in *n*-hexane ODH

In **Figure 8.6** above it can be seen that 19VMgO again gives higher *n*-hexane conversion at a specific temperature. In all 3 catalysts conversion increases rapidly from 350 °C to about 425 °C and then stabilizes over a few degrees Celcius. At 450 °C there is a drop in conversion with 19VMgO. The conversion in 24VMgO and 16VMgO also drops albeit at a slightly higher temperature. After this point conversion increases slowly. This latter increase in conversion is accompanied by an increase in cracking products. Oxygen conversion was difficult to accurately determine with the analytical system used due to the inefficient separation of oxygen and nitrogen. Nevertheless, the absence of oxygen in the analysis of the product stream was conspicuous. Complete oxygen conversion was observed at 475 °C for 16VMgO and 24 VMgO. For 19VMgO complete oxygen conversion was observed at 450 °C.

Figures 8.7, 8.8 and 8.9 show the effect of temperature on selectivity for 16VMgO, 19VMgO and 24VMgO. At 350 °C, CO_x is formed exclusively over all catalysts. Benzene and hexenes start to form at 400 °C. Propane and propene form at temperatures greater than 425 °C. The selectivity to benzene increases with temperature in all catalysts until a maximum is reached at 525 °C. Above this temperature benzene is unstable and consecutive oxidation of benzene to CO_x becomes strongly favoured. At 550 °C, selectivity to CO_x was observed to increase.

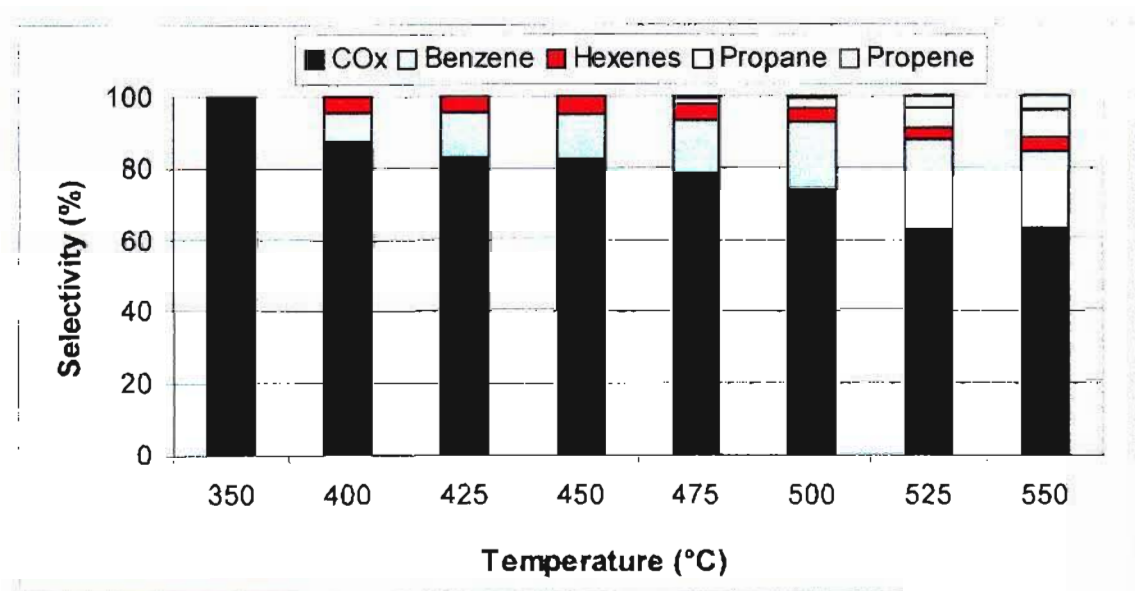


Figure 8.7: Effect of temperature on selectivity in *n*-hexane ODH over 16VMgO

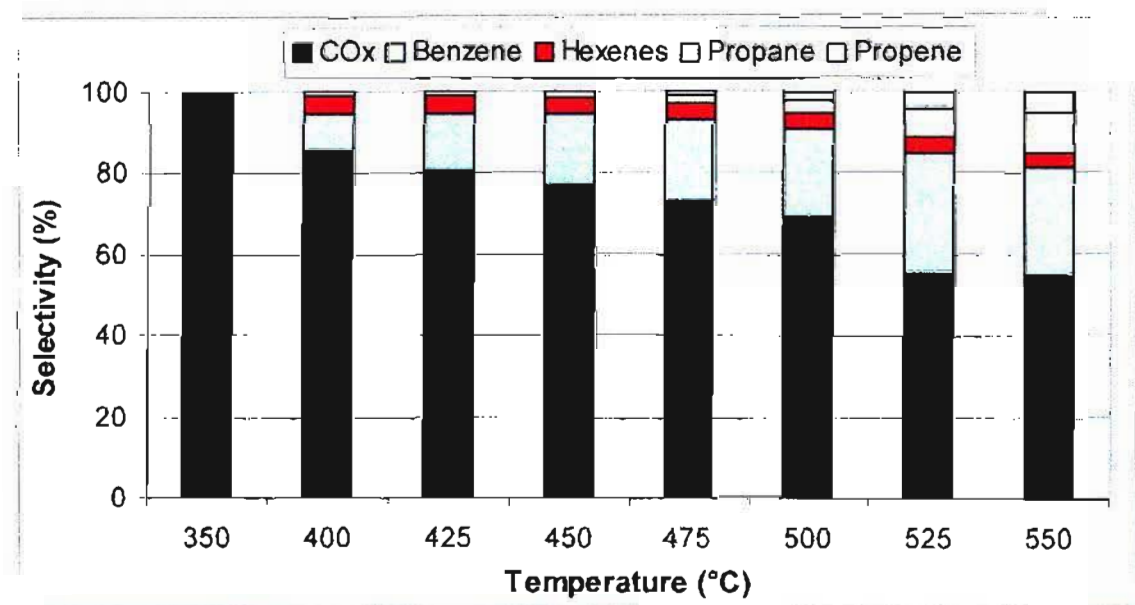


Figure 8.8: Effect of temperature on selectivity in *n*-hexane ODH over 19VMgO

In all three catalysts 1-hexene and 2-hexene are produced at 400 °C. No 3-hexene was observed. The ratio of 2-hexene to 1-hexene was usually close to two. The selectivity to hexenes slowly decreased with increasing temperature. At higher temperatures propane and propene are produced. Typically, the selectivity to propane close to double that of propene and this ratio increased with temperature probably because propene is more reactive than propane. At 550 °C, the selectivity to propane over 19VMgO was over 10 % and the selectivity to propene was close to 5 %.

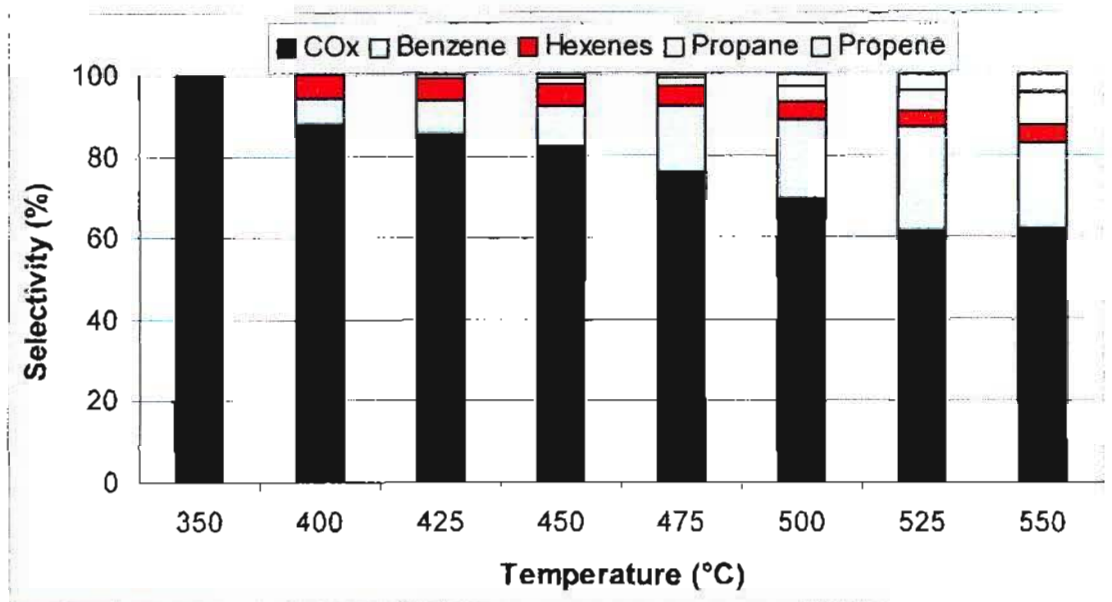


Figure 8.9: Effect of temperature on selectivity in *n*-hexane ODH over 24VMgO

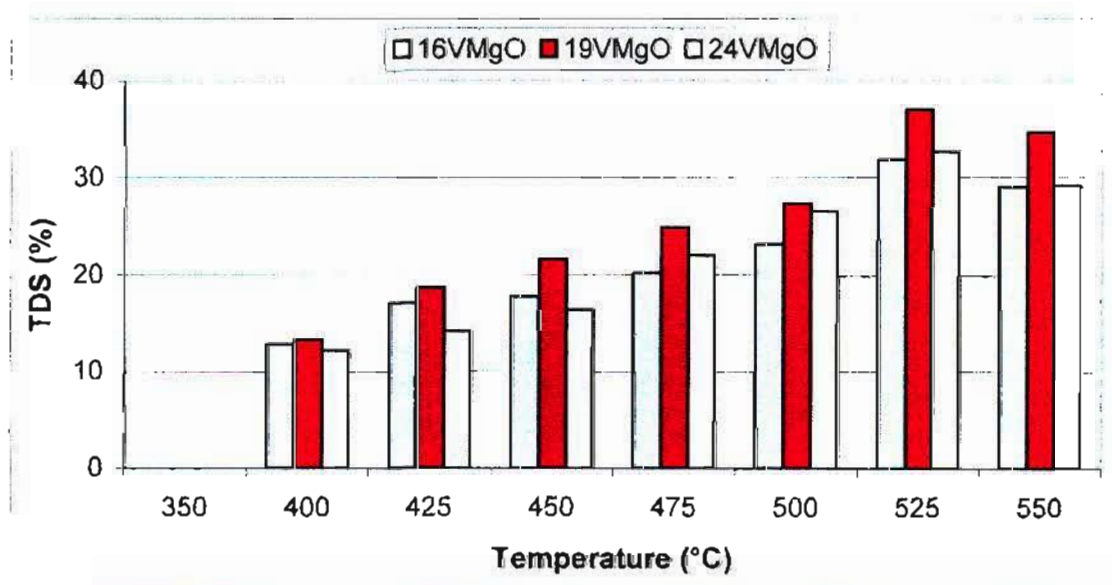


Figure 8.10: Effect of temperature on the total dehydrogenation selectivity (TDS) in *n*-hexane ODH over 16VMgO, 19VMgO and 24VMgO

Figure 8.10 above shows that the overall selectivity to dehydrogenation (benzene, hexenes and propene) increases with temperature and peaks at 525 °C. The highest selectivity at any particular temperature was obtained with 19VMgO. Figure 8.11 shows the highest selectivity to benzene and total dehydrogenation obtained by the three catalysts tested. For 16VMgO the highest selectivity to benzene was 25.0 (± 0.4) % and its highest TDS was 31.9 (± 0.4) %. For 19VMgO the highest selectivity to benzene was 29.2 (± 0.4) % and its highest TDS was 37.0 (± 0.4) %.

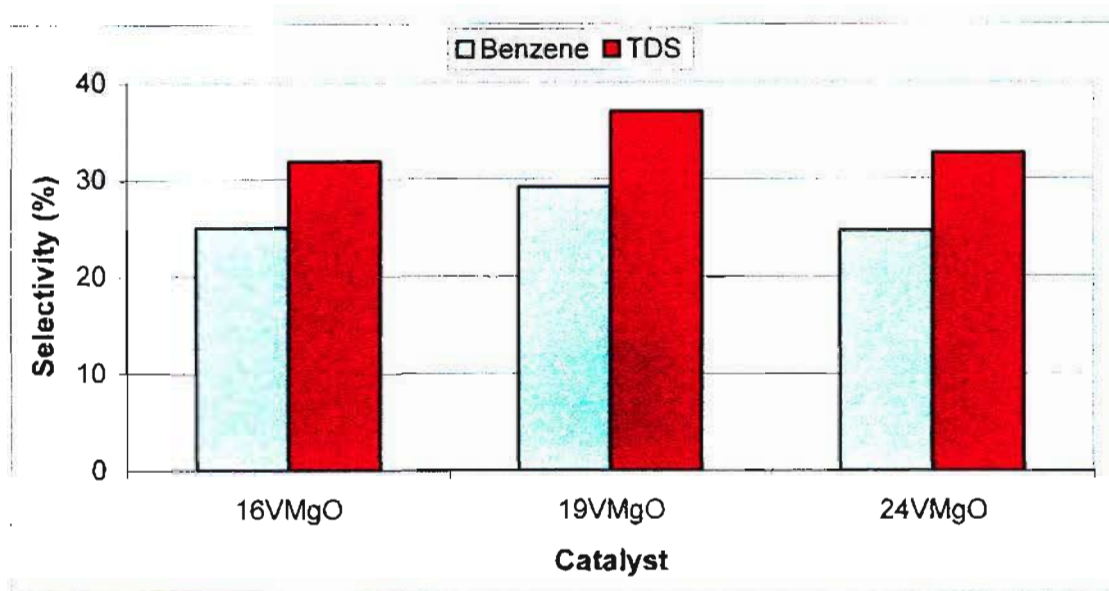


Figure 8.11: Highest selectivity to benzene and highest selectivity to dehydrogenation products (benzene+hexenes+propene) obtained with 16VMgO, 19VMgO and 24VMgO.

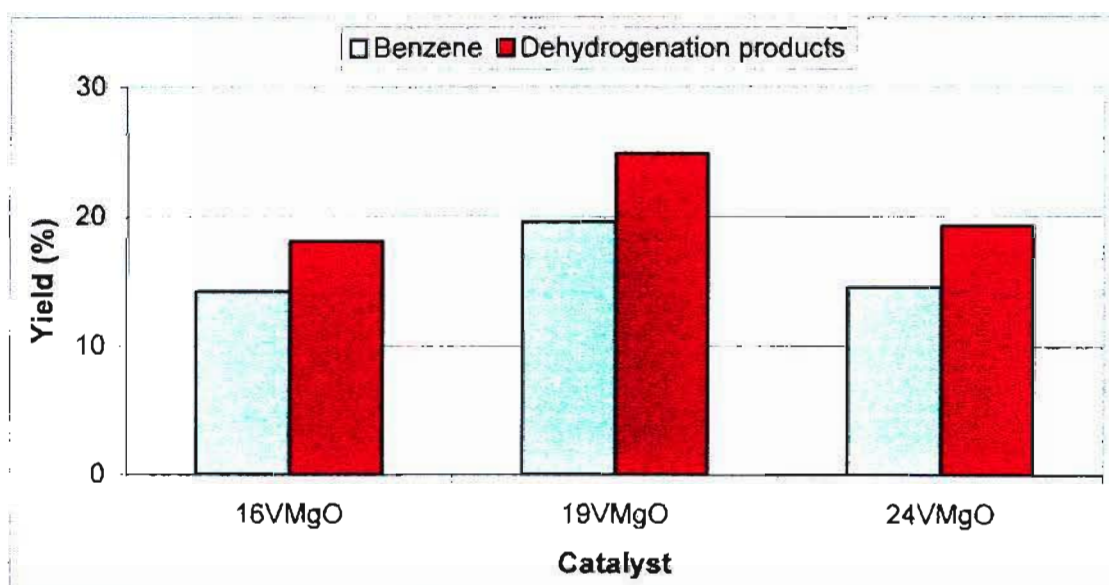


Figure 8.12: Highest yield obtained for benzene and highest yield obtained for dehydrogenation (benzene+hexenes+propene) with 16VMgO, 19VMgO and 24VMgO.

The highest selectivity to benzene with 24VMgO was 24.7 (\pm 0.4) % and the highest TDS attained was 32.7 (\pm 0.4) %. **Figure 8.12** shows the highest yields to benzene and dehydrogenation achieved by 16VMgO, 19VMgO and 24VMgO. The overall highest yield to benzene was 19.6 (\pm 0.4) % and the highest yield to dehydrogenated products was 24.8 (\pm 0.4) %. These yields were obtained with 19VMgO at 525 °C.

8.3 Variation in gas hourly space velocity (GHSV)

The effect of variations in the gas hourly space velocity was investigated using 19VMgO. This effect was studied above the UEL with a 7.8 % *n*-hexane in air feed. The GHSV was varied by changing the flow rate of the feed. Flow rates of 80, 100, 125, 150 ml/min were investigated. A constant catalyst volume of 1.6 ml was used. GHSV's were varied at a constant temperature of 525 °C.

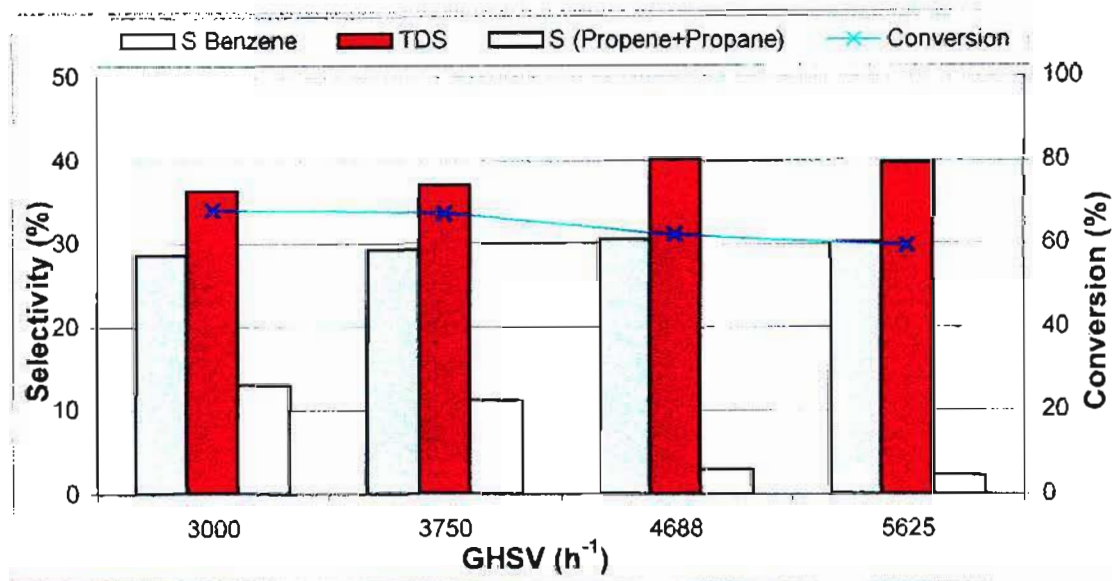


Figure 8.13: Effect of GHSV on *n*-hexane conversion, benzene selectivity, TDS and propane and propene selectivity obtained with 19VMgO.

In **Figure 8.13** above, it can be seen that the amount of *n*-hexane converted decreases with an increase in the gas hourly space velocity. The selectivity to benzene increased slightly with increasing GHSV. This slight increase is most likely due to the lower residence time of benzene on the catalyst surface, which would save it from consecutive oxidation. The total selectivity to dehydrogenated products also increases and then appears to level off at approximately 40 %. The most noticeable change is in the selectivity to propane and propene, which are most likely cracked products. The selectivity of these products decreased with increasing GHSV. With increasing GHSV, the residence time in the reactor is reduced and thus the extent of secondary or consecutive reactions is reduced. Looking at the selectivity towards these products at comparable conversion suggests that this is the case (**Table 8.10**).

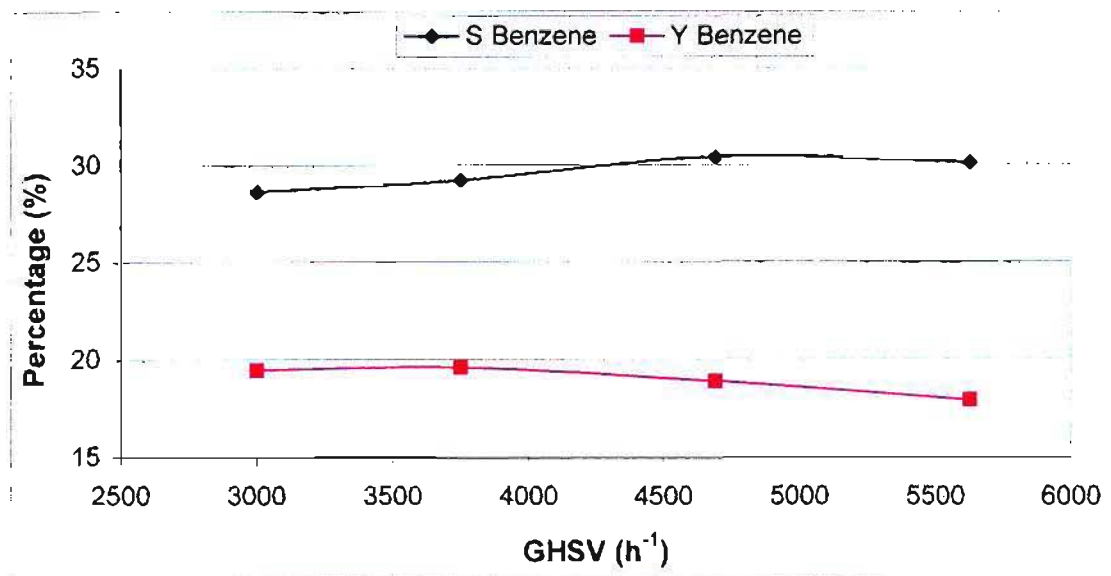


Figure 8.14: Effect of GHSV on the yield and selectivity towards benzene

Figure 8.14 shows that the highest selectivity to benzene obtained over 19VMgO was 30.4 (± 0.4) % at a GHSV of 4688 h⁻¹ at 525 °C. The yield of benzene was observed to decrease with increasing gas hourly space velocities. The highest yield of benzene was 19.6 (± 0.4) % and this was obtained at a GHSV of 3750 h⁻¹ at 525 °C.

8.4 *n*-Hexane ODH in the flammable region

The UEL of *n*-hexane is 7.7 % and its LEL is 1.2 % in air at 20 °C and atmospheric pressure. The flammable region expands with temperature and pressure. Feed compositions within the flammable region may result in a fire or explosion (**Chapter 6.7**). Nevertheless, operation of oxidation processes within the explosion limits has become possible through careful reactor design and proper safety precautions.

VMgO catalysts tested for *n*-hexane ODH show good activity below the LEL. The same catalysts tested above the UEL exhibited much better selectivity towards desired products but lower activity. Testing under more stoichiometric conditions could lead to an intermediate performance and this may result in a higher yield. Moreover, it has been observed that the oxidative dehydrogenation of paraffins within the flammable region resulted in much higher oxidative dehydrogenation selectivity [4].

Feed compositions of 3.1 and 5.5 % *n*-hexane in air were tested over 19VMgO. A constant GHSV of 4688 h⁻¹ and a constant reaction temperature of 525 °C was used. The same catalyst was used for the duration of the investigation.

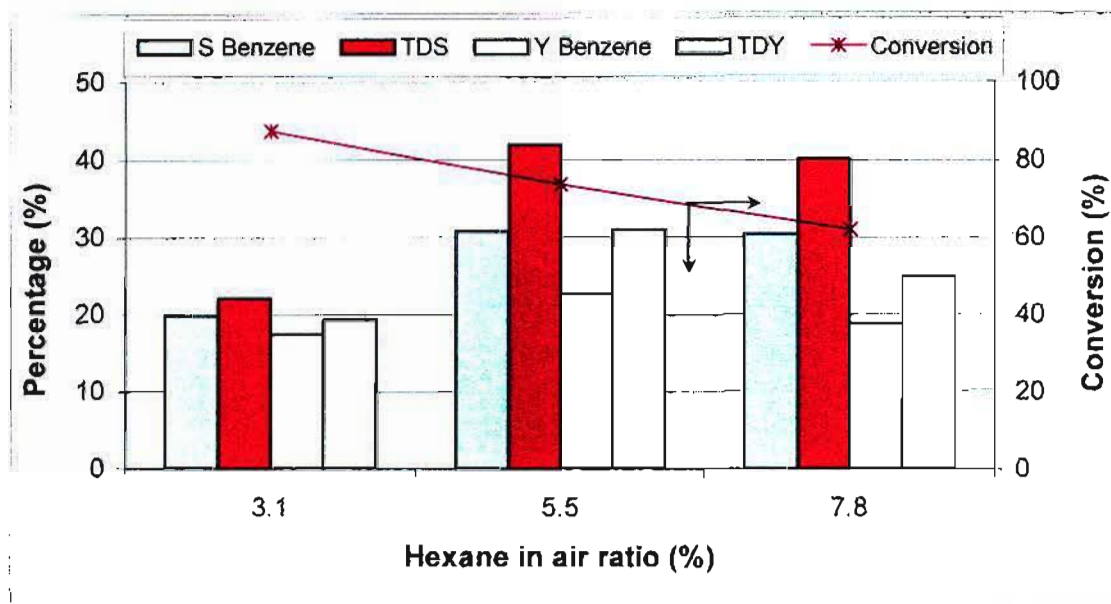


Figure 8.15: Effect of variation in the *n*-hexane to air ratio on conversion, selectivity and yield

Figure 8.15 above shows the increase in conversion with a decreasing *n*-hexane in air ratio. Changing the feed composition from 7.8 % to 5.5 % resulted in higher yields of benzene as well as the total dehydrogenated products. In the case of benzene, the yield increase is due to the increased conversion. The selectivity to benzene was similar with both feed compositions. The increase in yield to total dehydrogenated product was due to both an increase in conversion as well as selectivity. TDS increased by 2.0 (± 0.4) %.

A conversion of over 80 % was achieved with the 3.1 % *n*-hexane in air feed. There was a drop in both benzene selectivity as well as the selectivity to total dehydrogenation. The low selectivity with the 3.1 % hexane in air feed is consistent with the stronger oxidizing nature of this feed. The surface of the catalyst would be in a higher oxidizing state and therefore more active but less selective. Additionally, variation in the paraffin to oxidant ratio is known to cause a restructuring or reconstruction of the surface of the catalyst. Pantazidis *et al.* [5] reported evidence for surface reconstruction during ODH of propane over a VMgO catalyst. It was shown that dispersed vanadia surface units undergo a reversible order – disorder restructuring depending on their exposure to reducing or oxidizing atmospheres. This could have led to the poor catalytic performance obtained with the 3.1 % *n*-hexane in air feed (**Figure 8.15**).

8.5 Promoted VMgO

A promoter is any substance that is added to a catalyst to enhance its activity, selectivity or stability. They are usually added in relatively small amounts. A discussion on promoters is found in **Chapter 1.4**.

The catalytic behaviour of vanadium oxide catalysts in the selective oxidation of paraffins is strongly dependent on the redox properties of vanadium species as well as the acid – base properties of both the support and the catalyst [6-8]. The addition of promoters has been reported to modify the redox properties of vanadium as well as the acid – base properties of the catalyst and support [8-10]. According to Dejoz *et al.* [7], the formulation of optimal catalysts for selective oxidation should include the presence of metallic elements capable of easily changing their valence states according to the reduction – oxidation steps of the reaction.

19VMgO was promoted with approximately 0.5, 1.0, 2.5 and 5.0 weight percent of MoO₃, Sb₂O₃, Cs₂O, Nb₂O₅, Bi₂O₃ and TeO₂. The synthesis of these catalysts was previously discussed (**Chapter 6.2**). The physico-chemical characteristics of these catalysts are given in **Chapter 7.3**. Promoted catalysts were tested on a 7.8 % *n*-hexane in air feed. A GHSV of 3750 h⁻¹ was used. Catalysts were tested from 450 to 550 °C in 25 °C increments.

8.5.1 Molybdenum oxide (MoO₃)

Catalysts containing molybdenum oxide are active for the oxidation of paraffins [8]. Metal molybdates have been shown to be selective catalysts for ODH reactions [7,8,10-12]. Usually catalysts containing vanadium are preferred over molybdenum catalytic systems, as vanadium catalysts allow for reactions to be carried out at lower temperatures than with molybdenum catalytic systems and in this way vanadium catalysts usually show better selectivity to desired products. Nonetheless, molybdenum has been used in the formulation of good catalysts for selective ODH of paraffins [7,11,13-15].

Tables 8.12 – 8.15 show the catalytic results obtained for *n*-hexane ODH over 0.5MoVMgO, 1MoVMgO, 2.5MoVMgO and 5MoVMgO.

| Temp (°C) | C (%) | S (C ₆ H ₆) | Y (C ₆ H ₆) | S (Hexenes) | S (C ₃ H ₈) | S (C ₃ H ₆) | S (COx) | Y (Hexenes) | Y (C ₃ H ₈) | Y (C ₃ H ₆) | Y (COx) | TDS |
|-----------|-------|------------------------------------|------------------------------------|-------------|------------------------------------|------------------------------------|---------|-------------|------------------------------------|------------------------------------|---------|------|
| 450 | 55.0 | 18.1 | 10.0 | 3.6 | 2.0 | 1.1 | 75.2 | 2.0 | 1.1 | 0.6 | 41.4 | 22.8 |
| 475 | 58.0 | 20.8 | 12.1 | 3.4 | 2.7 | 1.4 | 71.7 | 2.0 | 1.6 | 0.8 | 41.6 | 25.6 |
| 500 | 61.5 | 21.2 | 13.0 | 3.0 | 3.5 | 2.2 | 70.1 | 1.8 | 2.2 | 1.4 | 43.1 | 26.4 |
| 525 | 63.4 | 29.1 | 18.4 | 3.0 | 8.3 | 4.0 | 55.6 | 1.9 | 5.3 | 2.5 | 35.2 | 36.1 |
| 550 | 66.1 | 24.6 | 16.3 | 2.5 | 11.0 | 5.6 | 56.3 | 1.6 | 7.3 | 3.7 | 37.2 | 32.7 |

Table 8.12: The effect of temperature on conversion, selectivity and yield in *n*-hexane ODH over 0.5MoVMgO

| Temp (°C) | C (%) | S (C ₆ H ₆) | Y (C ₆ H ₆) | S (Hexenes) | S (C ₃ H ₈) | S (C ₃ H ₆) | S (COx) | Y (Hexenes) | Y (C ₃ H ₈) | Y (C ₃ H ₆) | Y (COx) | TDS |
|-----------|-------|------------------------------------|------------------------------------|-------------|------------------------------------|------------------------------------|---------|-------------|------------------------------------|------------------------------------|---------|------|
| 450 | 55.0 | 18.4 | 10.1 | 2.9 | 2.2 | 0.8 | 75.7 | 1.6 | 1.2 | 0.4 | 41.6 | 22.1 |
| 475 | 56.9 | 21.3 | 12.1 | 2.7 | 3.1 | 1.1 | 71.8 | 1.5 | 1.8 | 0.6 | 40.9 | 25.1 |
| 500 | 60.0 | 22.2 | 13.3 | 2.1 | 3.9 | 1.6 | 70.2 | 1.3 | 2.3 | 1.0 | 42.1 | 25.9 |
| 525 | 62.1 | 29.8 | 18.5 | 2.0 | 8.0 | 4.3 | 55.9 | 1.2 | 5.0 | 2.7 | 34.7 | 36.1 |
| 550 | 64.0 | 24.4 | 15.6 | 1.9 | 11.3 | 5.7 | 56.7 | 1.2 | 7.2 | 3.6 | 36.3 | 32.0 |

Table 8.13: The effect of temperature on conversion, selectivity and yield in *n*-hexane ODH over 1MoVMgO

| Temp (°C) | C (%) | S (C ₆ H ₆) | Y (C ₆ H ₆) | S (Hexenes) | S (C ₃ H ₈) | S (C ₃ H ₆) | S (COx) | Y (Hexenes) | Y (C ₃ H ₈) | Y (C ₃ H ₆) | Y (COx) | TDS |
|-----------|-------|------------------------------------|------------------------------------|-------------|------------------------------------|------------------------------------|---------|-------------|------------------------------------|------------------------------------|---------|------|
| 450 | 57.1 | 21.0 | 12.0 | 1.9 | 2.0 | 1.0 | 74.1 | 1.1 | 1.1 | 0.6 | 42.3 | 23.9 |
| 475 | 61.9 | 23.7 | 14.7 | 1.8 | 2.9 | 1.4 | 70.2 | 1.1 | 1.8 | 0.9 | 43.5 | 26.9 |
| 500 | 64.2 | 25.5 | 16.4 | 1.7 | 4.8 | 2.0 | 66.0 | 1.1 | 3.1 | 1.3 | 42.4 | 29.2 |
| 525 | 66.5 | 32.1 | 21.3 | 1.5 | 10.0 | 3.9 | 52.5 | 1.0 | 6.7 | 2.6 | 34.9 | 37.5 |
| 550 | 67.2 | 28.0 | 18.8 | 1.1 | 12.2 | 6.0 | 52.7 | 0.7 | 8.2 | 4.0 | 35.4 | 35.1 |

Table 8.14: The effect of temperature on conversion, selectivity and yield in *n*-hexane ODH over 2.5MoVMgO

| Temp (°C) | C (%) | S (C ₆ H ₆) | Y (C ₆ H ₆) | S (Hexenes) | S (C ₃ H ₈) | S (C ₃ H ₆) | S (COx) | Y (Hexenes) | Y (C ₃ H ₈) | Y (C ₃ H ₆) | Y (COx) | TDS |
|-----------|-------|------------------------------------|------------------------------------|-------------|------------------------------------|------------------------------------|---------|-------------|------------------------------------|------------------------------------|---------|------|
| 450 | 46.0 | 18.0 | 8.3 | 1.1 | 3.3 | 1.1 | 76.5 | 0.5 | 1.5 | 0.5 | 35.2 | 20.2 |
| 475 | 48.2 | 19.4 | 9.4 | 1.0 | 3.6 | 1.3 | 74.7 | 0.5 | 1.7 | 0.6 | 36.0 | 21.7 |
| 500 | 49.8 | 22.1 | 11.0 | 1.0 | 5.5 | 2.2 | 69.2 | 0.5 | 2.7 | 1.1 | 34.5 | 25.3 |
| 525 | 53.1 | 25.4 | 13.5 | 0.7 | 11.3 | 5.5 | 57.1 | 0.4 | 6.0 | 2.9 | 30.3 | 31.6 |
| 550 | 55.0 | 22.4 | 12.3 | 0.9 | 13.0 | 5.9 | 57.8 | 0.5 | 7.2 | 3.2 | 31.8 | 29.2 |

Table 8.15: The effect of temperature on conversion, selectivity and yield in *n*-hexane ODH over 5MoVMgO

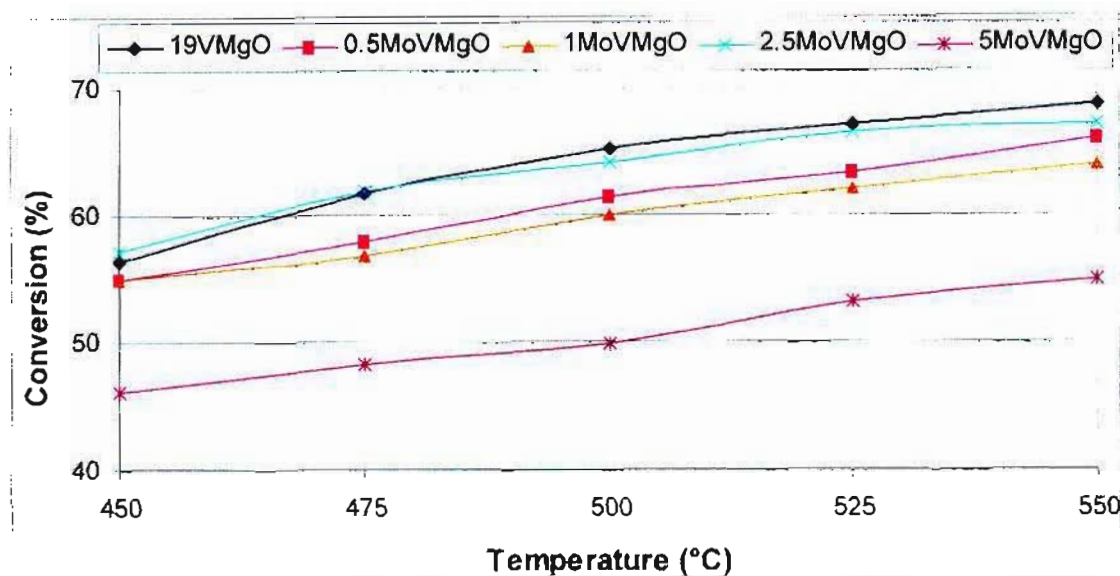


Figure 8.16: Effect of temperature on conversion in *n*-hexane ODH over 19VMgO and molybdenum promoted 19VMgO

Figure 8.16 above shows the effect of temperature on conversion in *n*-hexane ODH over 19VMgO and molybdenum promoted VMgO catalysts. 2.5MoVMgO shows better activity compared to the other molybdenum promoted catalysts. Its specific activity is better than that of unpromoted 19VMgO. At 550 °C, the specific activities of 19VMgO, 0.5MoVMgO, 1MoVMgO, 2.5MoVMgO and 5MoVMgO were $0.93 (\pm 0.02)$, $0.97 (\pm 0.02)$, $0.98 (\pm 0.02)$, $1.03 (\pm 0.02)$ and $0.87 (\pm 0.02) \text{ m}^{-2}$ respectively. Dejoz *et al.* [7] have reported on a VMgO catalyst containing 23.8 wt % V_2O_5 and 3.65 wt % MoO_3 being more active for butane ODH than the corresponding unpromoted catalyst.

Figure 8.17 shows the effect of temperature on the selectivity to benzene over 19VMgO and molybdenum promoted VMgO catalysts. 2.5MoVMgO was more selective to benzene at any given temperature compared to unpromoted 19VMgO and the other molybdenum promoted catalysts. The highest selectivity to benzene was obtained at 525 °C. At lower temperatures, all of the molybdenum promoted catalysts showed equal or better selectivity towards benzene compared to the unpromoted catalyst. At 550 °C only 2.5MoVMgO showed better selectivity to benzene than unpromoted 19VMgO.

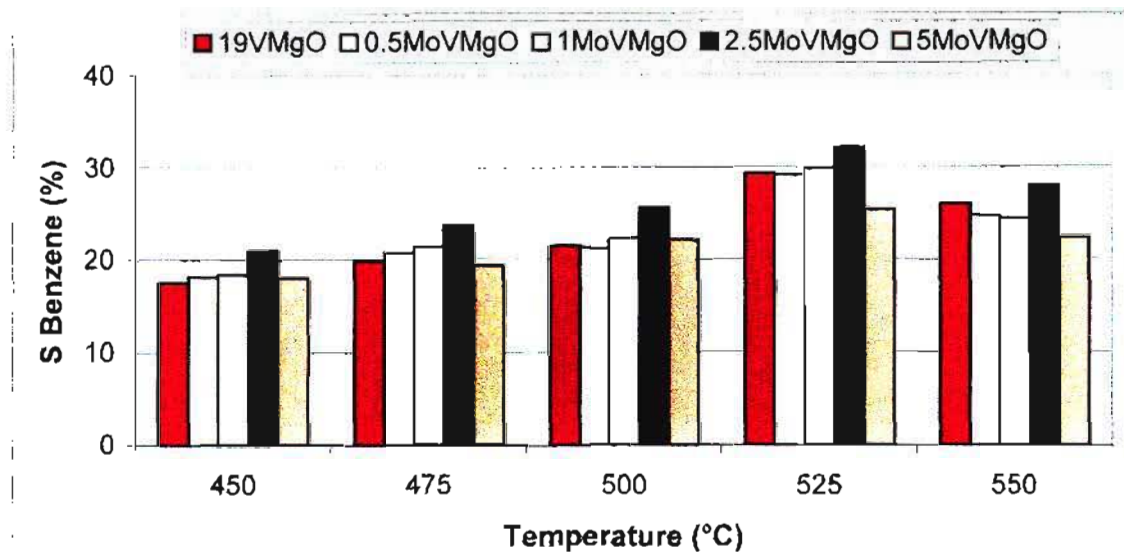


Figure 8.17: Effect of temperature on the selectivity to benzene over 19VMgO and molybdenum promoted 19VMgO catalysts

Figure 8.18 below compares the conversion of *n*-hexane, selectivity and yield of benzene and the total ODH selectivity and yield obtained at 525 °C for 19VMgO and molybdenum promoted 19VMgO. 2.5MoVMgO showed better selectivity and yield of benzene as well as better TDS at a comparable conversion to 19VMgO. The selectivity to benzene was 32.1 (± 0.5) % with 2.5MoVMgO compared to 29.1 (± 0.5) % with 19VMgO.

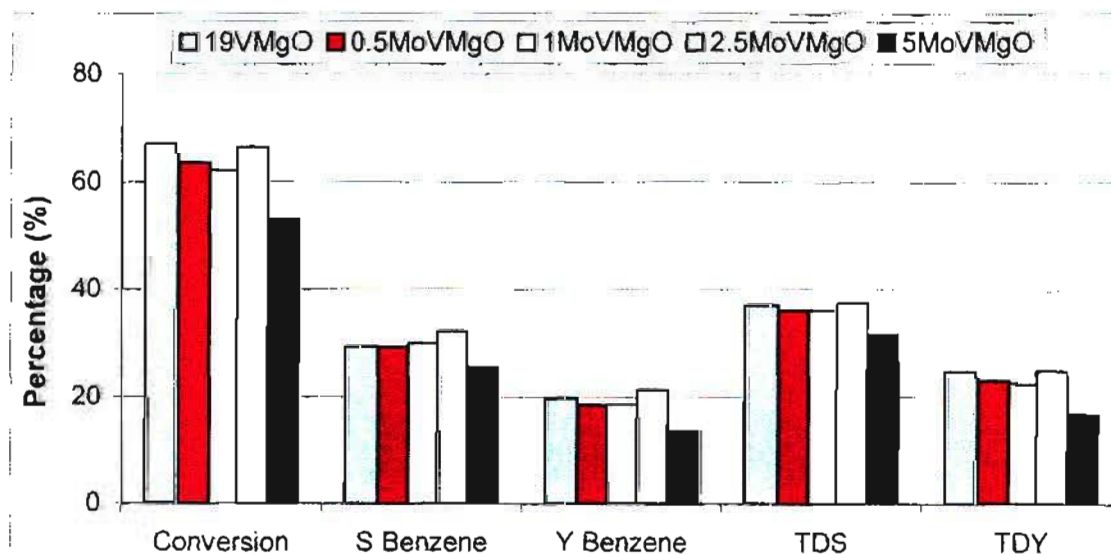


Figure 8.18: Conversion of *n*-hexane, selectivity to benzene, total ODH selectivity (TDS), yield of benzene and the total ODH yield obtained with 19VMgO and molybdenum promoted 19VMgO catalysts at 525 °C.

The highest TDS obtained at 525 °C was about 37 % and this was approximately the same for both 2.5MoVMgO and 19VMgO. 2.5MoVMgO gave a higher benzene yield of 21.3 (\pm 0.4) % compared to 19.6 (\pm 0.4) % for the unpromoted catalyst.

The promotion of VMgO catalysts with molybdenum oxide could result in the substitution of Mo^{6+} into the V^{5+} cation sites because Mo^{6+} has a similar ionic radius and tetrahedral coordination as the V^{5+} in magnesium orthovanadate [11]. Harding *et al.* [11] studied the effect of incorporating molybdenum oxide into magnesium orthovanadate. They detected the formation $\text{Mg}_{2.5}\text{VMoO}_8$ which had a similar structure to $\text{Mg}_3(\text{VO}_4)_2$. In both structures vanadium is tetrahedrally coordinated and vanadium tetrahedra are isolated from one another. $\text{Mg}_{2.5}\text{VMoO}_8$ was shown to have a selectivity to ODH products similar to that of pure $\text{Mg}_3(\text{VO}_4)_2$ during the oxidative dehydrogenation of *n*-butane.

No molybdenum phases were detected in the molybdenum promoted catalysts synthesized and tested in this study, probably due to low levels of promoter used (**Chapter 7.3**). Dejoz *et al.* [7] detected MgMoO_4 in a 17.3 wt % molybdenum promoted VMgO catalyst. In catalysts with lower loadings this phase was barely detectable or undetected. Dejoz *et al.* [7] have also reported a more selective catalyst for butane ODH. They found that the incorporation of molybdenum into VMgO catalysts favoured a selectivity and a yield to ODH products (especially butadiene) higher than that of an unpromoted VMgO catalyst. They claim that the incorporation of MoO_3 decreases both the amount and the reducibility of vanadium species. In addition to this, the amount of non-selective sites in VMgO, which are related to vanadium-free magnesia on the surface, are reduced with the addition of MoO_3 [7]. In this way selectivity to desired products is enhanced.

According to Dejoz *et al.* [7] the addition of MoO_3 to VMgO could also result in the formation of new acid sites related to Mo^{6+} sites and this would alter the acid – base properties of these catalysts. They were not able to conclusively observe an increase in the number of acid sites during pyridine adsorption FTIR experiments [7]. The presence of these sites in molybdenum promoted VMgO catalysts may explain the poor ODH selectivity obtained by Bhattacharyya *et al.* [15] when they promoted a 24VMgO catalyst with MoO_3 such that the vanadium to molybdenum weight ratio was 10:1.

8.5.2 Cesium oxide (Cs₂O)

Alkaline and alkaline-earth promoters are widely used to enhance the catalytic efficiency of many heterogeneous catalysts [16]. Both the nature of promoter used and its concentration affects the behaviour of the final catalyst [12,17,18]. The addition of alkaline promoters can decrease the acidity and increase the basicity of the surface of a catalyst [16]. A basic surface will favour the desorption of ODH products and in this way save them from subsequent deeper oxidation [19]. Usually, promotion with alkaline metals results in a decrease in catalytic activity. This is attributed to both a decrease in surface area as well as the lower paraffin – surface interaction [17].

Table's 8.16 – 8.19 show the catalytic results obtained for *n*-hexane ODH over 0.5CsVMgO, 1CsVMgO, 2.5CsVMgO and 5CsVMgO.

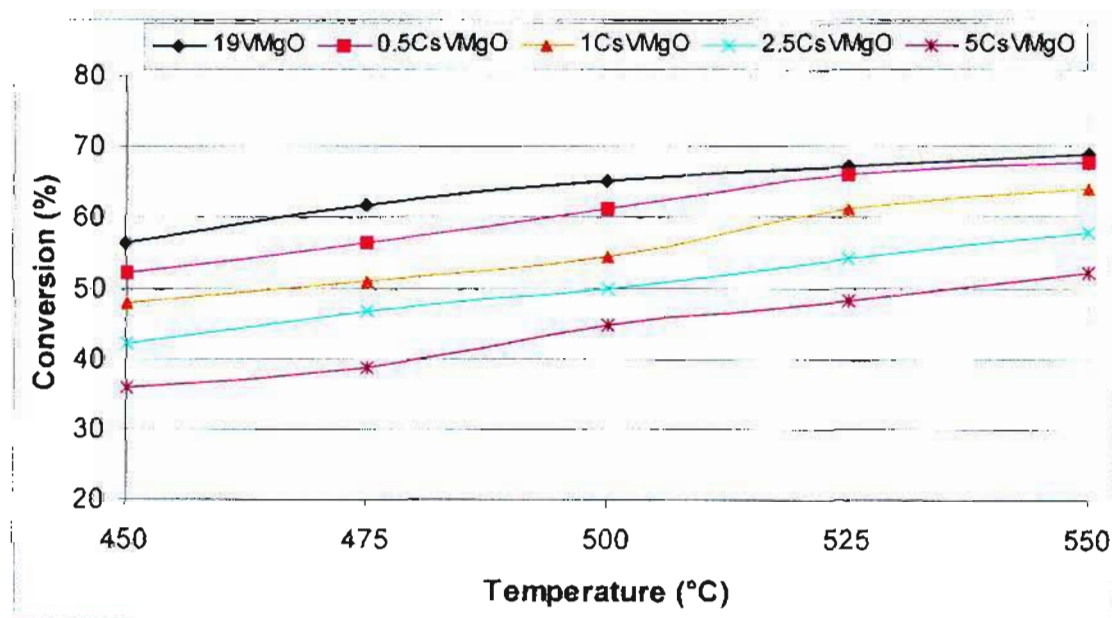


Figure 8.19: Effect of temperature on conversion in *n*-hexane ODH over 19VMgO and cesium promoted 19VMgO

In Figure 8.19 above, it can be seen that the cesium promoted catalysts show a lower conversion at a specific temperature relative to unpromoted VMgO. The lower activity of promoted catalysts with higher cesium loading can be attributed to both a decrease in surface area as well as lower *n*-hexane – surface interactions [16,17]. In addition to this, Grabowski *et al.* [20] proposed that the decreased activity of alkaline promoted catalysts may be due to the blocking of paraffin activation sites and that the extent of this effect is dependent on the ionic radius of the alkaline cation. The specific activity at 525 °C decreased as follows: 19VMgO ($0.90 \pm 0.02 \text{ m}^{-2}$) \approx 0.5CsVMgO \approx 1CsVMgO > 2.5CsVMgO ($0.82 \pm 0.02 \text{ m}^{-2}$) > 5CsVMgO ($0.78 \pm 0.02 \text{ m}^{-2}$).

| Temp (°C) | C (%) | S (C ₆ H ₆) | Y (C ₆ H ₆) | S (Hexenes) | S (C ₃ H ₈) | S (C ₃ H ₆) | S (COx) | Y (Hexenes) | Y (C ₃ H ₈) | Y (C ₃ H ₆) | Y (COx) | TDS |
|-----------|-------|------------------------------------|------------------------------------|-------------|------------------------------------|------------------------------------|---------|-------------|------------------------------------|------------------------------------|---------|------|
| 450 | 52.2 | 17.0 | 8.9 | 5.4 | 1.1 | 0.4 | 76.1 | 2.8 | 0.6 | 0.2 | 39.7 | 22.8 |
| 475 | 56.4 | 19.1 | 10.8 | 5.1 | 1.4 | 0.6 | 73.8 | 2.9 | 0.8 | 0.3 | 41.6 | 24.8 |
| 500 | 61.1 | 21.0 | 12.8 | 5.0 | 2.6 | 1.1 | 70.3 | 3.1 | 1.6 | 0.7 | 43.0 | 27.1 |
| 525 | 66.2 | 29.4 | 19.5 | 4.6 | 5.2 | 2.9 | 57.9 | 3.0 | 3.4 | 1.9 | 38.3 | 36.9 |
| 550 | 67.8 | 27.2 | 18.4 | 3.6 | 8.4 | 5.3 | 55.5 | 2.4 | 5.7 | 3.6 | 37.6 | 36.1 |

Table 8.16: The effect of temperature on conversion, selectivity and yield in *n*-hexane ODH over 0.5CsVMgO

| Temp (°C) | C (%) | S (C ₆ H ₆) | Y (C ₆ H ₆) | S (Hexenes) | S (C ₃ H ₈) | S (C ₃ H ₆) | S (COx) | Y (Hexenes) | Y (C ₃ H ₈) | Y (C ₃ H ₆) | Y (COx) | TDS |
|-----------|-------|------------------------------------|------------------------------------|-------------|------------------------------------|------------------------------------|---------|-------------|------------------------------------|------------------------------------|---------|------|
| 450 | 47.8 | 17.1 | 8.2 | 5.1 | 0 | 0 | 77.8 | 2.4 | 0 | 0 | 37.2 | 22.2 |
| 475 | 50.9 | 19.5 | 9.9 | 4.9 | 0 | 0 | 75.6 | 2.5 | 0 | 0 | 38.5 | 24.4 |
| 500 | 54.4 | 22.4 | 12.2 | 4.6 | 1.1 | 0.4 | 71.5 | 2.5 | 0.6 | 0.2 | 38.9 | 27.4 |
| 525 | 61.3 | 30.3 | 18.6 | 4.5 | 3.9 | 2.5 | 58.8 | 2.8 | 2.4 | 1.5 | 36.0 | 37.3 |
| 550 | 64.2 | 29.2 | 18.7 | 4.0 | 5.7 | 4.4 | 56.7 | 2.6 | 3.7 | 2.8 | 36.4 | 37.6 |

Table 8.17: The effect of temperature on conversion, selectivity and yield in *n*-hexane ODH over 1CsVMgO

| Temp (°C) | C (%) | S (C ₆ H ₆) | Y (C ₆ H ₆) | S (Hexenes) | S (C ₃ H ₈) | S (C ₃ H ₆) | S (COx) | Y (Hexenes) | Y (C ₃ H ₈) | Y (C ₃ H ₆) | Y (COx) | TDS |
|-----------|-------|------------------------------------|------------------------------------|-------------|------------------------------------|------------------------------------|---------|-------------|------------------------------------|------------------------------------|---------|------|
| 450 | 42.1 | 16.9 | 7.1 | 5.9 | 0 | 0 | 77.2 | 2.5 | 0 | 0 | 32.5 | 22.8 |
| 475 | 46.7 | 22.4 | 10.5 | 6.1 | 0 | 0 | 71.5 | 2.8 | 0 | 0 | 33.4 | 28.5 |
| 500 | 49.9 | 26.7 | 13.3 | 5.3 | 1.4 | 0.6 | 66.0 | 2.6 | 0.7 | 0.3 | 32.9 | 32.6 |
| 525 | 54.2 | 32.3 | 17.5 | 4.9 | 2.9 | 2.1 | 57.8 | 2.7 | 1.6 | 1.1 | 31.3 | 39.3 |
| 550 | 57.8 | 30.8 | 17.8 | 4.1 | 5.0 | 4.4 | 55.7 | 2.4 | 2.9 | 2.5 | 32.2 | 39.3 |

Table 8.18: The effect of temperature on conversion, selectivity and yield in *n*-hexane ODH over 2.5CsVMgO

| Temp (°C) | C (%) | S (C ₆ H ₆) | Y (C ₆ H ₆) | S (Hexenes) | S (C ₃ H ₈) | S (C ₃ H ₆) | S (COx) | Y (Hexenes) | Y (C ₃ H ₈) | Y (C ₃ H ₆) | Y (COx) | TDS |
|-----------|-------|------------------------------------|------------------------------------|-------------|------------------------------------|------------------------------------|---------|-------------|------------------------------------|------------------------------------|---------|------|
| 450 | 36.0 | 16.5 | 5.9 | 6.6 | 0 | 0 | 76.9 | 2.4 | 0 | 0 | 27.7 | 23.1 |
| 475 | 38.9 | 20.4 | 7.9 | 5.7 | 0 | 0 | 73.9 | 2.2 | 0 | 0 | 28.7 | 26.1 |
| 500 | 44.7 | 25.2 | 11.3 | 5.4 | 1.2 | 0.4 | 67.8 | 2.4 | 0.5 | 0.2 | 30.3 | 31.0 |
| 525 | 48.2 | 27.4 | 13.2 | 5.0 | 3.0 | 1.8 | 62.8 | 2.4 | 1.4 | 0.9 | 30.3 | 34.2 |
| 550 | 52.2 | 29.1 | 15.2 | 4.2 | 4.7 | 2.9 | 59.1 | 2.2 | 2.5 | 1.5 | 30.9 | 36.2 |

Table 8.19: The effect of temperature on conversion, selectivity and yield in *n*-hexane ODH over 5CsVMgO

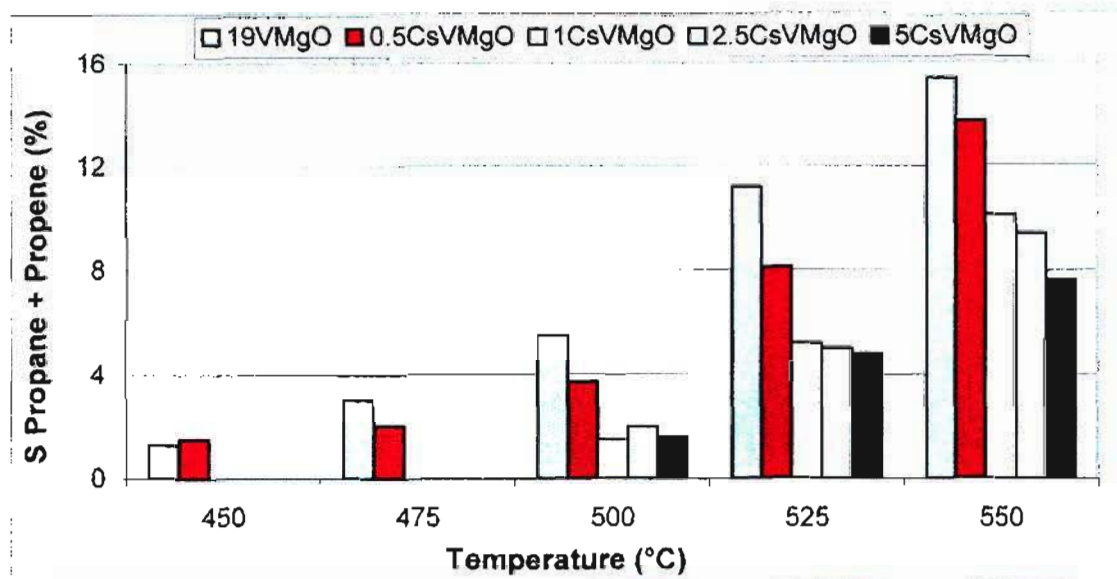


Figure 8.20: Effect of temperature on the selectivity to cracked products

In **Figure 8.20** above, the effect of temperature on the selectivity to the cracked products (propane and propene) is shown. The selectivity to propane and propene is generally much lower on cesium promoted catalysts compared to unpromoted 19VMgO. The selectivity to cracked products was usually observed to decrease with an increase in weight % of cesium.

Figure 8.21 compares the selectivity to hexenes, selectivity to benzene, total ODH selectivity, yield of benzene and the total ODH yield obtained with 19VMgO and cesium promoted VMgO catalysts at 525 °C. 2.5CsVMgO gave the highest selectivity to benzene i.e. 32.3 (\pm 0.5) %. The selectivity to benzene obtained with the unpromoted catalyst was 29.2 (\pm 0.4) %. 0.5CsVMgO and 1CsVMgO also gave higher selectivities to benzene than the unpromoted catalyst. 5CsVMgO gave lower selectivity to benzene than unpromoted 19VMgO. The highest TDS of 39.3 (\pm 0.4) % was also obtained with 2.5CsVMgO. The TDS for 19VMgO, 0.5CsVMgO and 1CsVMgO were comparable, whilst that of 5VMgO was lower. According to Madeira and Portela [16] an excess of promoter usually leads to drastic deterioration in catalytic performance. This effect is called the ‘overdoping effect’ [16]. The effect was clearly shown in a study with a 6 weight % cesium promoted NiMoO₄ catalyst [17]. Here the selectivity to oxidative dehydrogenation products increased with 1CsNiMoO₄ and 3CsNiMoO₄ but markedly decreased with 6CsNiMoO₄ during butane ODH.

The yields of benzene and dehydrogenated products decreased with an increase of cesium in the promoted catalysts. This was due to the lower *n*-hexane conversion obtained on promoted catalysts. The selectivity to hexenes was slightly higher with cesium promoted catalysts compared to unpromoted 19VMgO. At 525 °C the selectivity to hexenes was 3.9 (\pm 0.4) %

with 19VMgO compared to 4.9 (\pm 0.4) % with 2.5CsVMgO. At comparable conversions, 2.5CsVMgO was the more selective catalyst (Table 8.10 and Tables 8.16-8.19).

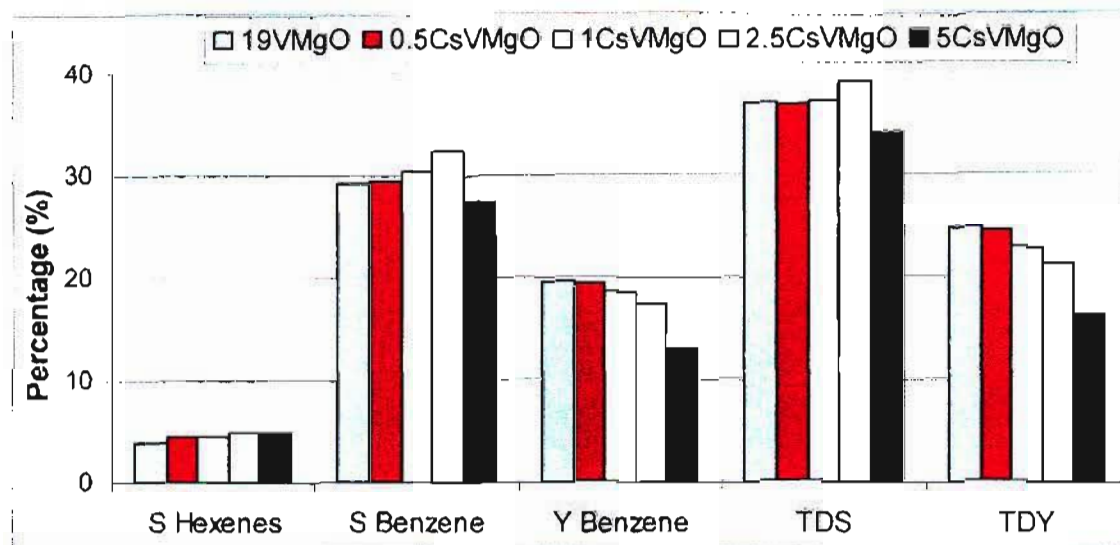


Figure 8.21: Selectivity to hexenes, selectivity to benzene, total ODH selectivity (TDS), yield of benzene and the total ODH yield

No new phases were observed in the x-ray diffractograms of the cesium promoted catalysts. Nevertheless, promotion of 19VMgO with small amounts of cesium had a noticeable effect on catalytic performance. In general activity decreased according to the sequence 19VMgO > 0.5CsVMgO > 1CsVMgO > 2.5CsVMgO > 5CsVMgO (Tables 8.16 – 8.19). The lower activity was due in part to the lower surface areas of the cesium promoted catalysts. Cesium promotion usually results in a decrease in the number of acid sites and an increase in the number of basic sites [6,16]. Consequently, the observed lower activity can be attributed to lower *n*-hexane – surface interactions [16,17]. Additionally, less acid sites will result in lower selectivity to cracked products. Furthermore, the enhanced basicity of cesium promoted catalysts may favour the desorption of ODH products and this may account for their enhanced selectivity [6,16,19,21].

The addition of alkaline metals to supported vanadia catalysts has been shown to decrease the reducibility of vanadium species and this may also influence the selectivity to ODH products [6,16,20,22]. The addition of alkaline metals may also block unselective sites that favour the formation of CO_x and in this way show enhanced selectivity to ODH products [20,23]. In addition to this, it has been reported that cesium promotion results in a decrease in the amount and electronegative character of the oxygen associated with deep oxidation sites [21]. At 525 °C, the observed TDS and selectivity to benzene decreased according to the sequence 2.5CsVMgO > 0.5CsVMgO > 1CsVMgO > 19VMgO > 5CsVMgO.

8.5.3 Antimony oxide (Sb_2O_3)

Vanadium catalysts containing antimony oxides are commonly studied as ammoxidation catalysts [3,8]. In ammoxidation reactions, it is generally accepted that olefins are intermediates [3,25]. Catalysts containing Vanadium and antimony have also been shown to catalyze the ODH of ethane to ethene [25]. These catalysts have also been used for the ODH of *n*-butane and isopentane [26].

Table's 8.20 – 8.23 show the catalytic results obtained for *n*-hexane ODH over 0.5SbVMgO, 1SbVMgO, 2.5SbVMgO and 5SbVMgO.

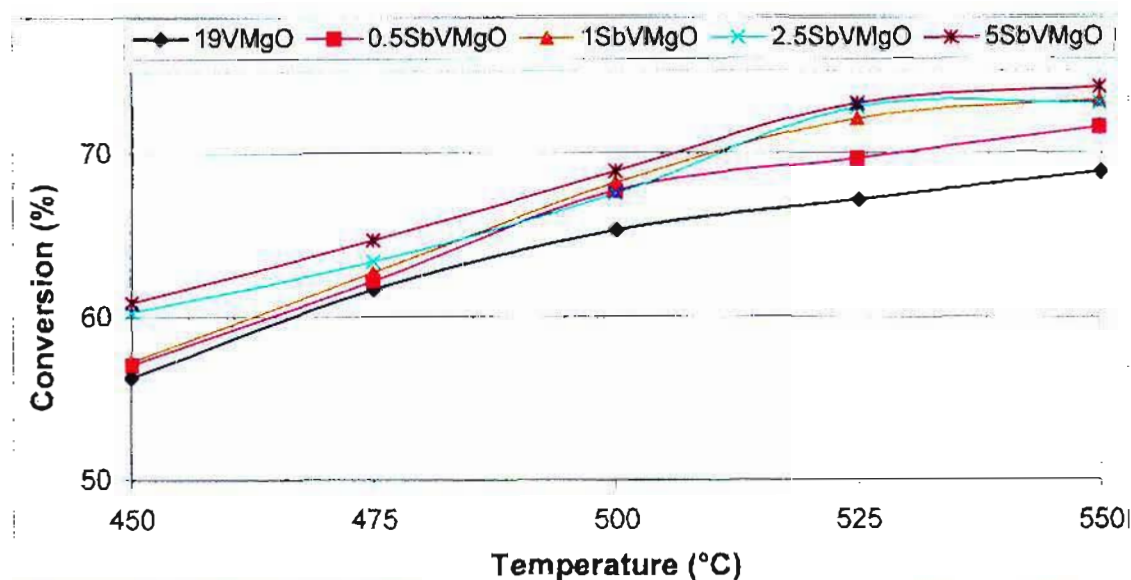


Figure 8.22: Effect of temperature on conversion in *n*-hexane ODH over 19VMgO and antimony promoted 19VMgO

In Figure 8.22 above, it can be seen that higher conversions were obtained with the antimony promoted catalysts compared to unpromoted 19VMgO at any particular temperature. The specific activity at 525 °C increased with antimony loading. The specific activities of 19VMgO, 0.5SbVMgO, 1SbVMgO, 2.5SbVMgO and 5SbVMgO were $0.90 (\pm 0.02)$, $0.97 (\pm 0.02)$, $1.05 (\pm 0.02)$, $1.08 (\pm 0.02)$ and $1.13 (\pm 0.02) \text{ m}^{-2}$ respectively.

Antimony oxide is a known spillover oxygen donor phase (Chapter 2.6) [27]. When supported VOx are promoted with antimony, the amount of reactive oxygen is increased and reduction – oxidation cycles of vanadium ions proceed more efficiently. Spillover oxygen species are capable of reoxidizing vanadium active sites rapidly, thereby keeping them in a high oxidation state and preventing the destruction of these sites [27,28]. Spillover oxygen is also responsible for effectively inhibiting the formation of carbonaceous deposits [27].

| Temp (°C) | C (%) | S (C ₆ H ₆) | Y (C ₆ H ₆) | S (Hexenes) | S (C ₃ H ₈) | S (C ₃ H ₆) | S (COx) | Y (Hexenes) | Y (C ₃ H ₈) | Y (C ₃ H ₆) | Y (COx) | TDS |
|-----------|-------|------------------------------------|------------------------------------|-------------|------------------------------------|------------------------------------|---------|-------------|------------------------------------|------------------------------------|---------|------|
| 450 | 57.1 | 17.3 | 9.9 | 6.2 | 0 | 0 | 76.5 | 3.5 | 0 | 0 | 43.7 | 23.5 |
| 475 | 62.2 | 20.3 | 12.6 | 5.8 | 1.0 | 0.4 | 72.5 | 3.6 | 0.6 | 0.2 | 45.1 | 26.5 |
| 500 | 67.7 | 22.4 | 15.2 | 5.1 | 2.6 | 1.3 | 68.6 | 3.5 | 1.8 | 0.9 | 46.4 | 28.8 |
| 525 | 69.7 | 30.1 | 21.0 | 4.6 | 5.3 | 2.6 | 57.4 | 3.2 | 3.7 | 1.8 | 40.0 | 37.3 |
| 550 | 71.6 | 26.8 | 19.2 | 4.5 | 8.5 | 4.4 | 55.8 | 3.2 | 6.1 | 3.2 | 40.0 | 35.7 |

Table 8.20: The effect of temperature on conversion, selectivity and yield in *n*-hexane ODH over 0.5SbVMgO

| Temp (°C) | C (%) | S (C ₆ H ₆) | Y (C ₆ H ₆) | S (Hexenes) | S (C ₃ H ₈) | S (C ₃ H ₆) | S (COx) | Y (Hexenes) | Y (C ₃ H ₈) | Y (C ₃ H ₆) | Y (COx) | TDS |
|-----------|-------|------------------------------------|------------------------------------|-------------|------------------------------------|------------------------------------|---------|-------------|------------------------------------|------------------------------------|---------|------|
| 450 | 57.3 | 18.2 | 10.4 | 7.3 | 0 | 0 | 74.5 | 4.2 | 0 | 0 | 42.7 | 25.5 |
| 475 | 62.7 | 21.1 | 13.2 | 7.0 | 1.1 | 0.4 | 70.4 | 4.4 | 0.7 | 0.3 | 44.1 | 28.5 |
| 500 | 68.2 | 23.4 | 16.0 | 6.3 | 2.3 | 1.1 | 66.9 | 4.3 | 1.6 | 0.8 | 45.6 | 30.8 |
| 525 | 72.1 | 31.5 | 22.7 | 5.1 | 4.7 | 2.0 | 56.7 | 3.7 | 3.4 | 1.4 | 40.9 | 38.6 |
| 550 | 73.2 | 26.0 | 19.0 | 4.4 | 6.9 | 3.3 | 59.4 | 3.2 | 5.1 | 2.4 | 43.5 | 33.7 |

Table 8.21: The effect of temperature on conversion, selectivity and yield in *n*-hexane ODH over 1SbVMgO

| Temp (°C) | C (%) | S (C ₆ H ₆) | Y (C ₆ H ₆) | S (Hexenes) | S (C ₃ H ₈) | S (C ₃ H ₆) | S (COx) | Y (Hexenes) | Y (C ₃ H ₈) | Y (C ₃ H ₆) | Y (COx) | TDS |
|-----------|-------|------------------------------------|------------------------------------|-------------|------------------------------------|------------------------------------|---------|-------------|------------------------------------|------------------------------------|---------|------|
| 450 | 60.3 | 18.1 | 10.9 | 7.7 | 0 | 0 | 74.2 | 4.6 | 0 | 0 | 44.7 | 25.8 |
| 475 | 63.4 | 20.3 | 12.9 | 6.5 | 0.9 | 0.4 | 71.9 | 4.1 | 0.6 | 0.3 | 45.6 | 27.2 |
| 500 | 67.5 | 22.7 | 15.3 | 6.1 | 2.2 | 1.1 | 67.9 | 4.1 | 1.5 | 0.7 | 45.8 | 29.9 |
| 525 | 72.8 | 28.7 | 20.9 | 5.3 | 4.8 | 2.5 | 58.7 | 3.9 | 3.5 | 1.8 | 42.7 | 36.5 |
| 550 | 73.0 | 24.1 | 17.6 | 4.7 | 7.0 | 3.5 | 60.7 | 3.4 | 5.1 | 2.6 | 44.3 | 32.3 |

Table 8.22: The effect of temperature on conversion, selectivity and yield in *n*-hexane ODH over 2.5SbVMgO

| Temp (°C) | C (%) | S (C ₆ H ₆) | Y (C ₆ H ₆) | S (Hexenes) | S (C ₃ H ₈) | S (C ₃ H ₆) | S (COx) | Y (Hexenes) | Y (C ₃ H ₈) | Y (C ₃ H ₆) | Y (COx) | TDS |
|-----------|-------|------------------------------------|------------------------------------|-------------|------------------------------------|------------------------------------|---------|-------------|------------------------------------|------------------------------------|---------|------|
| 450 | 60.9 | 17.6 | 10.7 | 4.9 | 0 | 0 | 77.5 | 3.0 | 0 | 0 | 47.2 | 22.5 |
| 475 | 64.7 | 19.3 | 12.5 | 4.5 | 1.3 | 0.8 | 74.1 | 2.9 | 0.8 | 0.5 | 47.9 | 24.6 |
| 500 | 68.9 | 22.3 | 15.4 | 4.1 | 3.1 | 1.7 | 68.8 | 2.8 | 2.1 | 1.2 | 47.4 | 28.1 |
| 525 | 73.0 | 26.1 | 19.1 | 3.9 | 6.4 | 3.4 | 60.2 | 2.8 | 4.7 | 2.5 | 43.9 | 33.4 |
| 550 | 74.0 | 21.8 | 16.1 | 3.7 | 7.9 | 4.2 | 62.4 | 2.7 | 5.8 | 3.1 | 46.2 | 29.7 |

Table 8.23: The effect of temperature on conversion, selectivity and yield in *n*-hexane ODH over 5SbVMgO

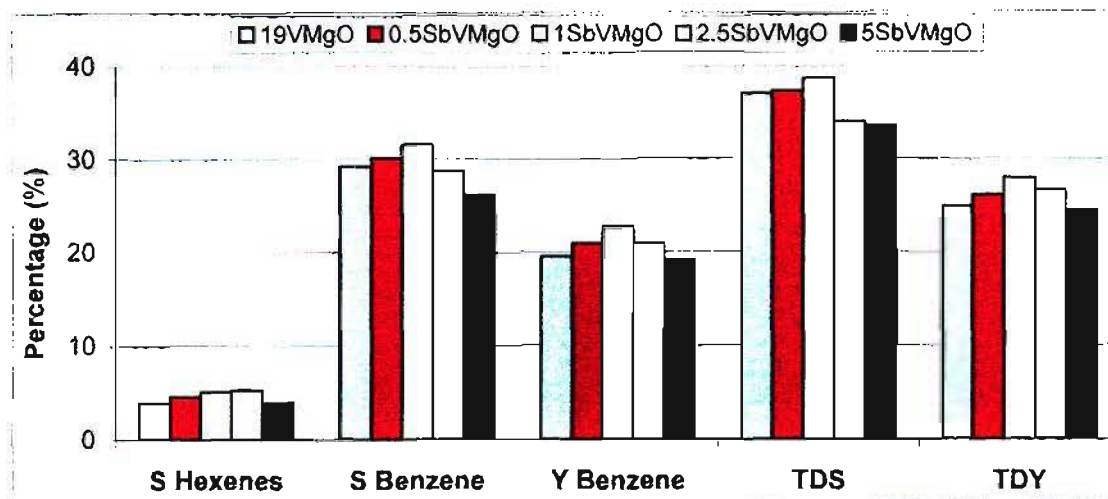


Figure 8.23: Selectivity to hexenes, selectivity to benzene, TDS, yield of benzene and the TDY obtained with 19VMgO and antimony promoted 19VMgO catalysts at 525 °C

In **Figure 8.23** above, it can be seen that promoting 19VMgO with antimony (up to 2.5 weight %) resulted in catalysts that were more selective to benzene, hexenes and to the total ODH products produced. Higher yields were also obtained with the more selective catalysts. The highest selectivities were obtained with 1SbVMgO at 525 °C. At 525 °C, 1SbVMgO had a selectivity to hexenes, benzene and a TDS of 5.1 (\pm 0.5), 31.5 (\pm 0.4) and 38.6 (\pm 0.4) % respectively, whilst unpromoted 19VMgO gave corresponding selectivities of 3.9 (\pm 0.4), 29.2 (\pm 0.5) and 37.0 (\pm 0.4) %. The yield of benzene and the TDY obtained with 1SbVMgO was 22.7 (\pm 0.4) and 27.8 (\pm 0.4) % respectively, and this was higher than the corresponding 19.6 (\pm 0.4) and 24.8 (\pm 0.4) % obtained with unpromoted 19VMgO. At a conversion of about 62 %, the selectivity to dehydrogenated products was higher with 0.5SbVMgO, 1SbVMgO and 2.5SbVMgO compared to 19VMgO.

Stern *et al.* have previously reported on obtaining favourable selectivity by promoting VMgO with antimony [14]. They report that in the ODH of butane, promoting a VMgO catalyst with antimony resulted in a catalyst that was twice as selective to ODH products compared to the unpromoted catalyst. They attributed the improved performance of promoted catalysts to the formation of MgVSb ternary phases [14]. Although no new phases were observable in the XRD diffractograms of the antimony promoted catalysts (**Appendix 4**) used in the current study, the existence of ternary phases or a secondary redox active VSbO₄ phase cannot be excluded. It is believed that ternary MgVSb phases can structurally isolate vanadium active sites and thereby prevent over oxidation of reacting molecules [14]. The higher selectivity to ODH products may also be due to intimate phase cooperation between the binary and ternary phases if present in the promoted catalysts [14].

8.5.4 Niobium oxide (Nb_2O_5)

There has been much interest in studying the association of niobium with vanadium in mixed oxide catalysts for mild oxidation of paraffins [29-33]. Niobium oxide itself is a selective catalyst, but the addition of vanadium improves its activity while maintaining good selectivity [8]. Niobium is often used in the formulation of selective multi-component oxide catalysts [3,30]. In addition to being used as a promoter, niobium oxide has been used successfully as a support for preparing supported metal oxide catalysts for ODH reactions [34,35].

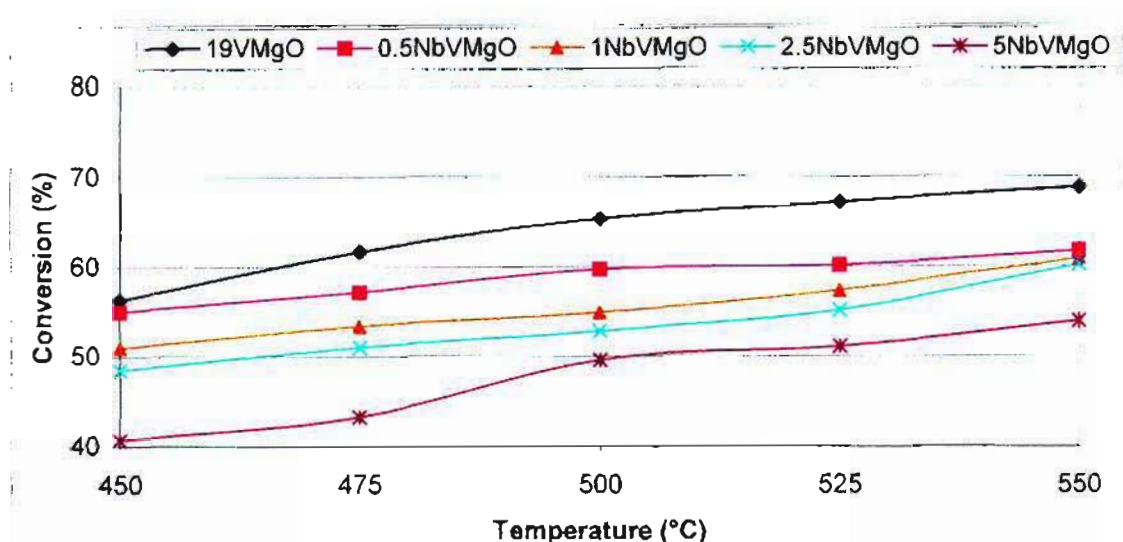


Figure 8.24: Effect of temperature on conversion in *n*-hexane ODH over 19VMgO and niobium promoted VMgO

Figure 8.24 above compares the conversions obtained with 19VMgO and niobium promoted 19VMgO. Niobium promoted catalysts exhibited a lower *n*-hexane conversion than unpromoted VMgO at a given temperature. The conversion at any given temperature decreased with an increase in the weight % of Nb_2O_5 . The lower conversions in niobium promoted catalysts are in part due to the lower surface areas of these catalysts. Both 0.5NbVMgO and 1NbVMgO have very similar surface areas of approximately $178 \text{ m}^2/\text{g}$. This suggests that the difference in catalytic activity between niobium promoted and unpromoted VMgO is not entirely due to differences in surface area. The specific activity at 525 °C decreased according to the following sequence: $19\text{VMgO} \approx 2.5\text{NbVMgO} > 0.5\text{NbVMgO} \approx 5\text{NbVMgO} > 1\text{NbVMgO}$. Sathler and Eon [36] reported that the decrease in activity in a vanadium niobium oxide catalyst compared to a vanadium oxide catalyst is approximately proportional to the decrease in the vanadium concentration on the surface. Contrary to this, Farias *et al.* [31] have reported that promoting a VPO catalyst with niobium creates defects that are responsible for *n*-butane activation. These defects were observed at the periphery of the $(\text{VO})_2\text{P}_2\text{O}_7$ phase.

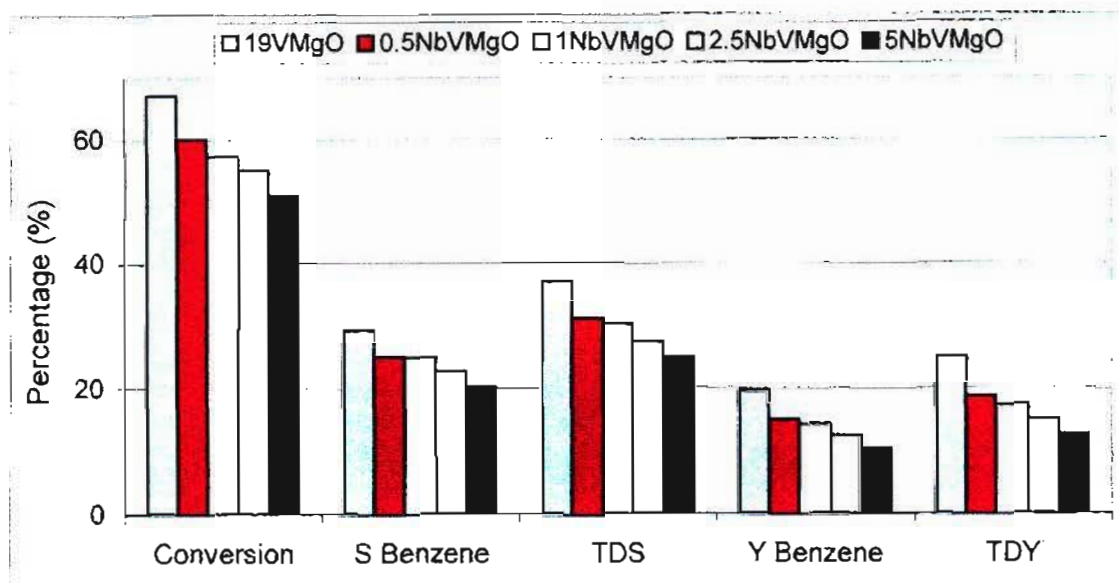


Figure 8.25: Conversion of *n*-hexane, selectivity to benzene, total ODH selectivity (TDS), yield of benzene and the total ODH yield obtained with 19VMgO and niobium promoted VMgO catalysts at 525 °C

Figure 8.25 compares the conversions, selectivities and yields obtained with 19VMgO and niobium promoted 19VMgO at 525 °C. Unpromoted 19VMgO showed better catalytic performance compared to the niobium promoted catalysts. Both the selectivity and the yield to benzene and ODH products decreased with an increase in the weight % of niobium. At 525 °C, the yield to benzene and the TDY obtained with unpromoted 19VMgO is almost twice that obtained with 5NbVMgO. At comparable conversions, the selectivity to ODH products was observed to decrease with increasing niobium oxide loading.

The superior selectivities exhibited by VMgO catalysts have been attributed to the difficulty in reducing the lattice V-O-Mg oxygen [37,38]. Since the strength of the niobium – oxygen bond is greater than that of a vanadium – oxygen bond, catalysts containing V-O-Nb bonds are expected to be more selective for ODH [33]. This was confirmed for propane ODH [32], but not observed for *n*-hexane in this work. Presuming the niobium promoted 19VMgO catalysts contains these V-O-Nb bonds; it is not clear why the observed selectivities to dehydrogenated products in *n*-hexane ODH are lower.

8.5.5 Bismuth oxide (Bi_2O_3)

A very selective catalytic system comprising of VMgO together with bismuth oxide has been patented for the ODH of alkylaromatics and paraffins [39]. Bismuth together with nickel oxide has also been patented for the selective ODH of paraffins [40]. Vanadium bismuth oxide catalysts have been reported for the selective ODH of propane [41] and multi-component catalysts containing vanadium and bismuth have exhibited good catalytic properties in the ODH of *n*-butane [42].

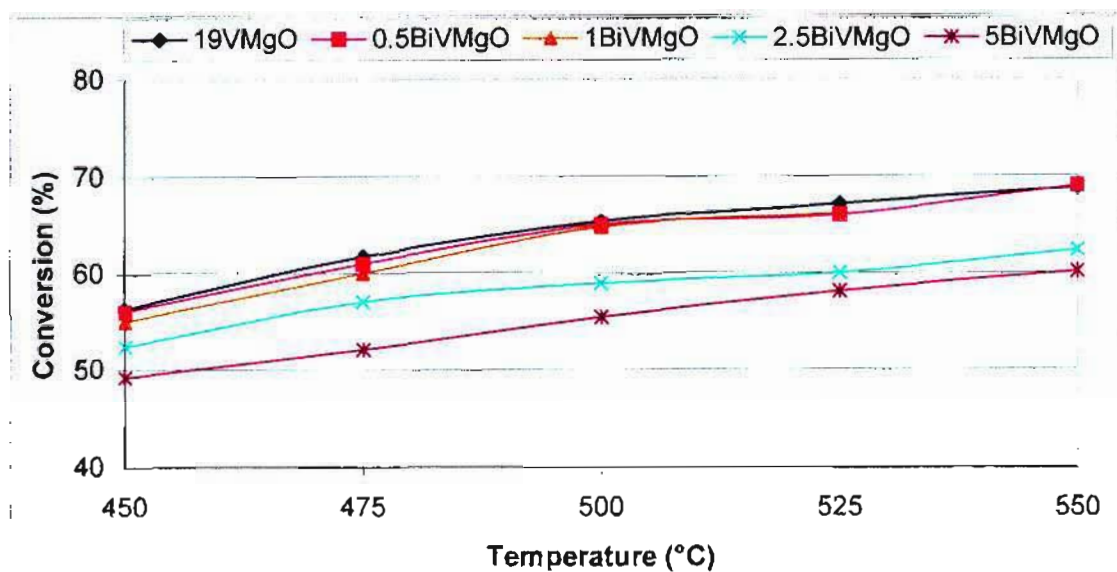


Figure 8.26: Effect of temperature on conversion in *n*-hexane ODH over 19VMgO and bismuth promoted VMgO

Figure 8.26 above compares the conversions obtained with 19VMgO and bismuth promoted 19VMgO. The conversions obtained with 0.5BiVMgO and 1BiVMgO were comparable to that of unpromoted 19VMgO per temperature. 2.5BiVMgO and 5BiVMgO gave lower conversions at similar temperatures. The specific activities at 525 °C for all these catalysts were similar (approximately 0.9 m^{-2}).

Figure 8.27 compares the conversions, selectivities and yields obtained with 19VMgO and bismuth promoted 19VMgO at 525 °C. The catalytic properties of 0.5BiVMgO and 1BiVMgO are similar to those of unpromoted 19VMgO. 2.5BiVMgO and 5BiVMgO exhibited much lower selectivities and yields to ODH products than unpromoted 19VMgO. At comparable conversions, the selectivity to ODH products decreased according to the following sequence: 19VMgO > 0.5BiVMgO \approx 1BiVMgO > 2.5BiVMgO > 5BiVMgO.

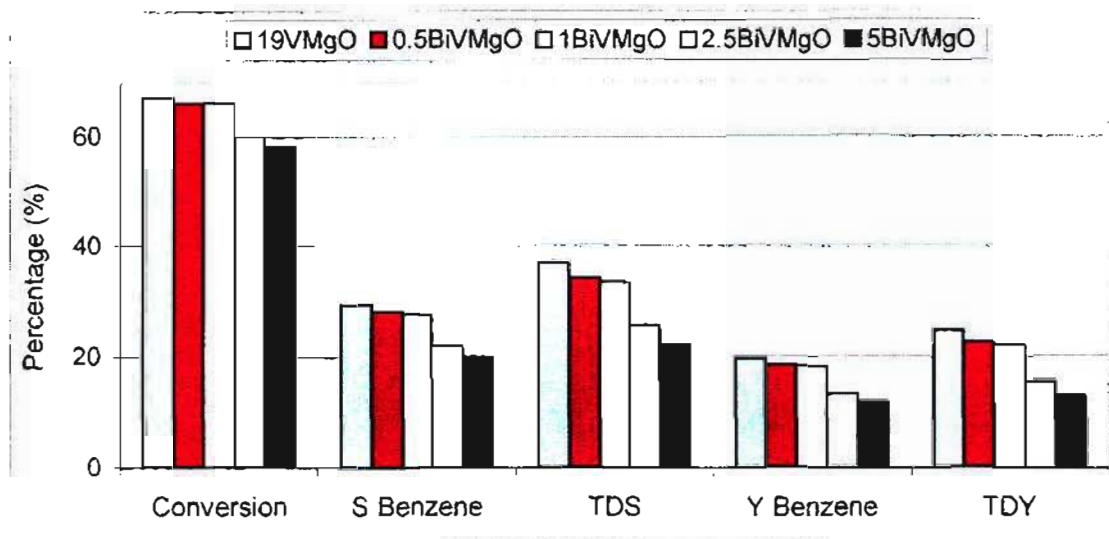


Figure 8.27: Conversion of *n*-hexane, selectivity to benzene, total ODH selectivity (TDS), yield of benzene and the total ODH yield obtained with 19VMgO and bismuth promoted VMgO catalysts at 525 °C

The negative promotional effects observed with these catalysts may be due to the increased oxygen mobility in the lattice. Hanna [43] found that bismuth could promote oxygen mobility in the lattice. The mobility of lattice oxygen atoms is a known selectivity determining factor [8,16]. Higher oxygen mobility can favour overoxidation of products. In addition to this, promoters with large ionic radii are known to cause a distortion of the active vanadium phase [44]. Bismuth induced distortion of the vanadyl pyrophosphate phase was shown to lead to enhanced activity and selectivity to ODH products [45]. A structurally deformed magnesium orthovanadate phase may favour over oxidation.

8.5.6 Tellurium oxide (TeO₂)

Tellurium and vanadium are found in multi-component oxide catalysts selective for ODH reactions [46,47]. For propane ODH over these catalysts, it is believed that surface V⁵⁺ sites are responsible for abstracting a methylene hydrogen atom and Te⁴⁺ sites are responsible for methyl hydrogen abstraction from propane [47,48]. Te⁴⁺ sites are also capable of α -hydrogen abstraction once the olefin has formed [47]. A major drawback of tellurium catalysts is tellurium's volatility when it is in the Te⁴⁺ state [48]. This shortcoming can be circumvented by co-feeding volatile tellurium compounds continuously or intermittently, directly into the reactor. Zeolite supported tellurium (Te⁰) catalysts have been shown to be active and selective catalysts for the non-oxidative aromatization of *n*-hexane [49].

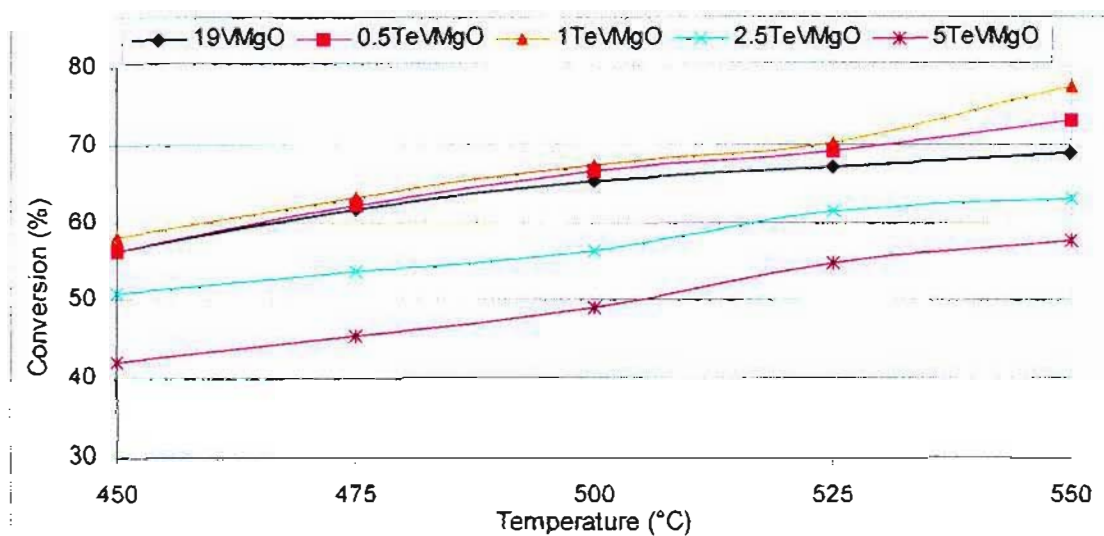


Figure 8.28: Effect of temperature on conversion in *n*-hexane ODH over 19VMgO and tellurium promoted VMgO

Figure 8.28 above shows the effect of temperature on conversions of *n*-hexane over 19VMgO and tellurium promoted 19VMgO. Conversions obtained with 0.5TeVMgO, 1.0TeVMgO and unpromoted 19VMgO were similar at lower temperatures. At higher temperatures, higher conversions were obtained with 0.5TeVMgO and 1.0TeVMgO. 5TeVMgO exhibited the lowest conversion at each temperature. The specific activity at 525 °C decreased as follows: 1.0TeVMgO ($0.99 (\pm 0.02) \text{ m}^{-2}$) \approx 0.5TeVMgO ($0.99 (\pm 0.02) \text{ m}^{-2}$) > 2.5TeVMgO ($0.95 (\pm 0.02) \text{ m}^{-2}$) > 5.0TeVMgO ($0.91 (\pm 0.02) \text{ m}^{-2}$) \approx 19VMgO ($0.90 (\pm 0.02) \text{ m}^{-2}$).

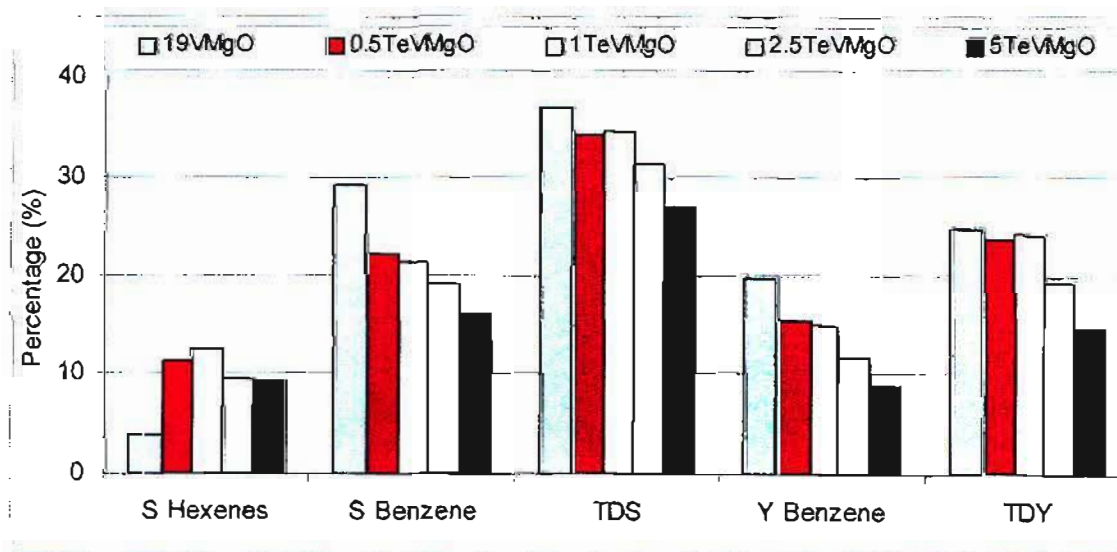


Figure 8.29: Selectivity to hexenes, selectivity to benzene, TDS, yield of benzene and TDY's obtained with 19VMgO and tellurium promoted VMgO catalysts at 525 °C

Figure 8.29 shows the selectivities and yields obtained with 19VMgO and tellurium promoted 19VMgO at 525 °C. Tellurium promoted catalysts favour the formation of mono – olefins i.e. 1-hexene and 2-hexene. At 525 °C, the selectivity to hexenes is at least twice that of unpromoted 19VMgO. The highest selectivity to hexenes was 12.4 (\pm 0.6) % and this was obtained with 1TeVMgO at 525 °C. The conversion of *n*-hexane at this temperature was 57.3 (\pm 0.4) %. Unpromoted 19VMgO gave a selectivity to hexenes of 4.0 (\pm 0.4) % at a similar conversion. The selectivity to benzene and the TDS was lower with tellurium promoted catalysts compared to unpromoted 19VMgO. At 525 °C, TDS decreased according to the sequence 19VMgO > 0.5TeVMgO \approx 1TeVMgO > 2.5TeVMgO > 5TeVMgO.

Lower yields of benzene and total dehydrogenated products were obtained with tellurium promoted catalysts. At 525 °C, the TDY obtained with 19 VMgO was 24.8 (\pm 0.4) %, whilst the TDY obtained with 0.5TeVMgO, 1TeVMgO, 2.5TeVMgO and 5TeVMgO were 23.6 (\pm 0.4), 24.3 (\pm 0.4), 19.3 (\pm 0.4) and 14.7 (\pm 0.4) % respectively.

Although no binary and/or ternary tellurium phases could be identified in these catalysts, due to their concentrations being below the detection limits of the applied characterization techniques, their existence cannot be precluded. These phases, if present, could account for the differences in observed selectivity with these catalysts. It is unclear why tellurium oxide promotion resulted in a suppression of aromatization and an increase in mono – olefin formation. It may be that the overall reaction pathway is augmented by non – oxidative dehydrogenation reactions on Te⁴⁺ sites. This might account for the higher activity of 0.5TeVMgO and 1.0TeVMgO at high temperatures compared to unpromoted 19VMgO. Since activity does not increase with increasing tellurium concentration, other factors that are at present not clear, must be involved. The presence of active ternary and binary tellurium phases (if present) could also account for the enhanced activity.

8.6 Conclusion

VMgO catalysts characterized by magnesium orthovanadate and magnesium oxide phases were shown to be active for the ODH of *n*-hexane. Good selectivity to ODH products was obtained with these catalysts. The product profile obtained during catalytic runs included 1-hexene, 2-hexene, benzene, propane, propene, water and CO_x. Oxygenated compounds other than CO_x were not observed.

19VMgO was the most selective catalyst below the LEL of hexane. The activity of catalysts tested decreased according to the sequence: 19VMgO > 16VMgO > 24VMgO > V₂O₅ > 35VMgO > 14VMgO > 49VMgO > 60 VMgO > MgO (based on temperature required for a 20 % *n*-hexane conversion). The specific activity (conversion per m²) was dependent on the amount of vanadium present in each catalyst tested. This suggests that vanadium atoms act as active sites for *n*-hexane ODH. Catalytic testing below the LEL of hexane resulted in the formation of benzene, water and CO_x only. The highest yield of benzene obtained was 18 %. This was achieved with 19VMgO at 445 °C and at a conversion of 99 %.

In catalytic tests above the UEL of *n*-hexane, propane, propene, 1-hexene and 2-hexene, which were not observed in catalytic tests below the LEL, were additionally formed. Catalysts were less active but more selective when tested above the UEL of *n*-hexane. This was ascribed to the dynamic interaction between the catalyst surface and the gas-phase. Above the UEL, the surface of the catalyst is in contact with a reducing environment. This results in a lower average vanadium oxidation state, which was observed to be beneficial for ODH selectivity. 19VMgO was again the most active and selective catalyst tested. 19VMgO gave a selectivity to benzene of 29 % and a TDS of 32 % at 525 °C. A maximum benzene yield of 20 % and a TDY of 25 % was obtained.

The effect of GHSV on catalytic performance was investigated and it was found that higher space velocities resulted in a slight improvement in the selectivity to benzene and dehydrogenated product. The selectivity to propane and propene was notably lower with higher GHSV's. The effect of the *n*-hexane to air ratio was also investigated and the best results were obtained within the flammability region. Catalytic testing with a feed composition of 5.5 % *n*-hexane in air resulted in a selectivity to benzene of 31 % and a TDS of 42 %. This corresponded to a benzene yield of 23 % and a TDY of 31 %.

19VMgO was promoted with 0.5, 1.0, 2.5 and 5.0 weight % of MoO₃, Sb₂O₃, Cs₂O, Nb₂O₅, Bi₂O₃ and TeO₂. 2.5MoVMgO showed better catalytic performance compared to unpromoted 19VMgO. The highest selectivity to benzene obtained with 2.5MoVMgO was 32 %, which was better than the 29 % achieved with 19VMgO. The corresponding yield of benzene obtained with 2.5MoVMgO was 21 %, which was comparable to the 20 % obtained with 19VMgO.

Cesium promoted catalysts also showed higher selectivity for dehydrogenation than 19VMgO. The observed TDS and selectivity to benzene decreased according to the sequence 2.5CsVMgO > 0.5CsVMgO > 1CsVMgO > 19VMgO > 5CsVMgO. 2.5CsVMgO gave a benzene selectivity of 32 % and a TDS of 39 %.

Promotion of 19VMgO with antimony resulted in catalysts, which were slightly more active and selective. Activity decreased according to the sequence 5SbVMgO > 1SbVMgO ≈ 2.5SbVMgO > 0.5SbVMgO > 19VMgO. The selectivity to benzene and the TDS at 525 °C decreased according to the sequence 1SbVMgO > 0.5SbVMgO > 19VMgO > 2.5SbVMgO > 5SbVMgO. At 525 °C, 1SbVMgO gave a selectivity to hexenes, benzene and a TDS of 5, 32 and 39 % respectively, whilst unpromoted 19VMgO gave corresponding selectivities of 4, 29 and 37 %.

Niobium and bismuth promotion of 19VMgO resulted in a negative effect on catalytic performance. These catalysts favour total oxidation probably through blocking selective ODH sites and/or through the formation of binary and ternary phases that are unselective. Bismuth promotion may have resulted in an increase in lattice oxygen mobility, which probably favoured CO_x formation. Additionally, these promoters could modify the local structure of the orthovanadate phase on the surface, consequently reducing activity and selectivity to ODH products.

The overall catalytic performance obtained with tellurium promoted catalysts was lower than that of 19VMgO. At higher temperatures higher conversions were obtained with 0.5TeVMgO and 1TeVMgO probably due to non – oxidative dehydrogenation. Higher selectivities to mono – olefins were obtained with tellurium promoted catalysts. At comparable conversions, the selectivity to hexenes was at least twice that of 19VMgO.

8.7 Reference:

- 1) Cavani, F., Colombo, A., Giuntoli, F., Gobbi, E., Trifiro, F. and Vazquez, P., *Catal. Today*, **32**, 1996, 125.
- 2) Cavani, F. and Trifiro, F., *Catal. Today*, **51**, 1999, 561.
- 3) Mamedov, E. A., *Appl. Catal. A*, **116**, 1994, 49.
- 4) Mahomed, A. S., PhD Thesis, University of Kwazulu-Natal, 2005.
- 5) Pantazidis, A., Burrows, A., Kiely, C. J. and Mirodatos, C., *J. Catal.*, **177**, 1998, 325.
- 6) Blasco, T. and Lopez Nieto, J. M., *Appl. Catal. A*, **157**, 1997, 117.
- 7) Dejoz, A., Lopez Nieto, J. M., Marquez, F. and Vazquez, M. I., *Appl. Catal. A*, **180**, 1999, 83.
- 8) Albonetti, S., Cavani, F. and Trifiro, F., *Catal. Rev. Sci. Eng.*, **38**, 1996, 413.
- 9) Vedrine, J. C., *Stud. Surf. Sci. Catal.*, **110**, 1997, 61.
- 10) Yoon, Y. S., Fijikawa, N., Ueda, W., Moro-oka, Y. and Lee, K. W., *Catal. Today*, **24**, 1995, 327.
- 11) Harding, W. D., Hung, H. H., Kozhevnikov, V.L. and Poeppeleir, K. R., *J. Catal.*, **144**, 1993, 597.
- 12) Martin-Aranda, R. M., Portela, M. F., Machira, L. M., Freire, M. and Oliveira, M., *Appl. Catal. A*, **127**, 1995, 201.
- 13) Oganowski, W., Hanuza, J., Druhis, H., Mista, W. and Macalik, L., *Appl. Catal. A*, **136**, 1996, 143.
- 14) Stern, D. L., Michaels, J. N., DeCaul, L. and Grasselli, R. K., *Appl. Catal. A*, **153**, 1997, 21.
- 15) Bhattacharyya, D., Bej, S. K. and Rao, M. S., *Appl. Catal. A*, **87**, 1992, 29.
- 16) Madeira, L. M. and Portela, M. F., *Catal. Rev. Sci. Eng.*, **44**, 2002, 247.
- 17) Maldonado-Hodar, F. J., Madeira, L. M., Portela, M. F., Martin-Aranda, R. M. and Freire, F., *J. Mol. Catal. A*, **111**, 1996, 313.
- 18) Jones, C., Leonard, J. J. and Sofranco, J. A., *J. Catal.*, **103**, 1987, 311.
- 19) Chaar, M. A., Patel, D., Kung, M. C. and Kung, H. H., *J. Catal.*, **105**, 1987, 483.
- 20) Grabowski, R., Grzybowska, B., Samson, K., Sloczynski, J., Stoch, J. and Wcislo, K., *Appl. Catal. A*, **125**, 1995, 129.
- 21) Madeira, L. M. And Portela, M. F., *Appl. Catal. A*, **281**, 2005, 179.
- 22) Owens, L. And Kung, H. H., *J. Catal.*, **148**, 1994, 587.
- 23) Lemonidou, A. A., Nalbandian, L. and Vasalos, I. A., *Catal. Today*, **61**, 2000, 333.
- 24) Centi, G., Grasselli, R. K. And Trifiro, F., *Catal. Today*, **13**, 1992, 661.

- 25) Juarez Lopez, R., Godjayeva, N. S., Corberan, V. C., Fierro, J. L. G. and Mamedov, E.A., *Appl. Catal. A*, **124**, 1995, 281.
- 26) Rizayev, R. G., Talyshinskiy, R. M., Seifullayeva, J. M. Guseinova, E. M., Panteleyeva, Y. A. and Mamedov, E. A., *Stud. Surf. Sci. Catal.*, **82**, 1994, 125.
- 27) Weng, L. T. and Delmon, B., *Appl. Catal. A*, **81**, 1992, 141.
- 28) Weng, L. T. Ruiz, P. and Delmon, B., *Stud. Surf. Sci. Catal.*, **72**, 1992, 399.
- 29) Ciambelli, P., Lisi, L., Russo, G., Viparelli, P. and Volta, J. C., *Appl. Catal. A*, **184**, 1999, 291.
- 30) Thorsteinson, E. M., Wilson, T. P., Young, F. G. and Kasai, P. H., *J. Catal.*, **52**, 1978, 116.
- 31) Duarte, A. M. D., Gonzalez, W. A., Oliveira, P. G. P., Eon, J. G., Herrmann, J. M., Aouine, M., Loidant, S. and Volta, J. C., *J. Catal.*, **208**, 2002, 238.
- 32) Ross, J. R. H., Smits, K. and Seshan, K., *Catal. Today*, **16**, 1993, 503.
- 33) Sarzi-Amade, M., Morselli, S., Moggi, P., Maione, A., Ruiz, P. and Devillers, M., *Appl. Catal. A*, **284**, 2005, 11.
- 34) Wachs, I. E., Chen, Y., Jehng, J. M., Briand, L. E. and Tanaka, T., *Catal. Today*, **78**, 2003, 13.
- 35) Cherian, M., Rao, M. S. and Deo, G., *Catal. Today*, **78**, 2003, 397.
- 36) Sathler, M. N. B. and Eon, J. G., *Braz. J. Chem. Eng.*, **15**, 1998, 1.
- 37) Owen, O. S., Kung, M. C. and Kung, H. H., *Catal. Lett.*, **12**, 1992, 45.
- 38) Cavani, F. and Trifiro, F., *Catal. Today*, **24**, 1995, 307.
- 39) US patent 6586360
- 40) US patent 6541418
- 41) Concepcion, P., Lopez Nieto, J. M. and Perez-Pariente, J., *Catal. Lett.*, **28**, 1994, 9.
- 42) Mamedov, E. A. and Corberan, V. C., *Appl. Catal. A*, **127**, 1995, 1.
- 43) Hanna, T. A., *Coord. Chem. Rev.*, **248**, 2004, 429.
- 44) Haber, J., Zazhigalov, V. A., Stoch, J., Bogutskaya, L. V. and Bacherikova, I. V., *Catal. Today*, **33**, 1997, 39.
- 45) Lopez Nieto, J. M., Zazhigalov, V. A., Solsona, B. and Bacherikova, I. V., *Stud. Surf. Sci. Catal.*, **130**, 2000, 1853.
- 46) Lopez Nieto, J. M., Botella, P., Concepcion, P., Dejoz, A. and Vazquez, M. I., *Catal. Today*, **91**, 2004, 241.
- 47) Xie, Q., Chen, L., Weng, W. and Wan, H., *J. Mol. Catal. A*, **240**, 2005, 191.
- 48) Grasselli, R. K., *Appl. Catal. A*, **57**, 1990, 149.
- 49) Miale, J. N. and Weisz, P. B., *J. Catal.*, **20**, 1971, 288.

Chapter 9: Oxidative Dehydrogenation of *n*-Octane

9.1 Introduction

Longer chain paraffins are more easily activated than those with less carbon – hydrogen bonds. It was therefore expected that *n*-octane would be more reactive than *n*-hexane. Lower temperatures for *n*-octane activation could save dehydrogenated products from further oxidation. It was previously shown that the oxidation of *n*-octane over hydrotalcite – like catalysts yielded olefins, ethylbenzene and styrene as products [1].

19VMgO showed relatively good selectivity with *n*-hexane yielding mono – olefins and benzene as useful products. If the transformation of *n*-octane over 19VMgO proceeded *via* mechanistically similar pathways to those in *n*-hexane ODH, the expected product profile would include octenes and ethylbenzene/styrene as useful products. Indeed this was the observed outcome.

Styrene, in particular, is a highly desired product. Although styrene has limited direct use, it is nonetheless a key monomer in the petrochemical industry [2]. More than 90 % of styrene is produced by the dehydrogenation of ethylbenzene over potassium promoted iron catalysts [3,4]. The problems with this synthetic route are typical for dehydrogenation reactions i.e. reaction is equilibrium limited and strongly endothermic. Current research solutions to these problems include oxygen-assisted dehydrogenation and membrane catalysis (Chapter 2.5). The direct ODH of *n*-octane to styrene represents an attractive synthetic route from an economic and process point of view. Styrene was expected to be relatively stable over a basic non-oxygen inserting catalyst like VMgO; coupled with the lower temperatures required for *n*-octane activation, relatively good selectivity was expected. Catalysts were thus tested with the intent of optimizing the selectivity and yield of styrene.

9.2 Catalyst testing

A feed composition of 7.0 % *n*-octane in air was used. 19VMgO was tested in the 300 to 450 °C temperature range at a constant GHSV of 4287 h⁻¹. A low flow rate of air (10 – 20 ml / min) was passed over 19VMgO from room temperature to 300 °C. Whilst maintaining a steady air flow, the HPLC pump was switched on to the required LHSV. During this period the composition of the feed quickly moves from below the lower explosion limit to well above the upper explosion limit leaving 19VMgO in a significantly reduced state. The flow rate of air was then carefully increased to the desired composition ensuring that the catalyst bed temperature did not rise appreciably.

19VMgO was active at 300 °C. The product profile included octenes, octadienes, octatrienes, benzene, ethylbenzene (EB), styrene (STY), *o*-xylene, CO_x and water. Lower olefins and cracked products were also observed with increasing temperatures.

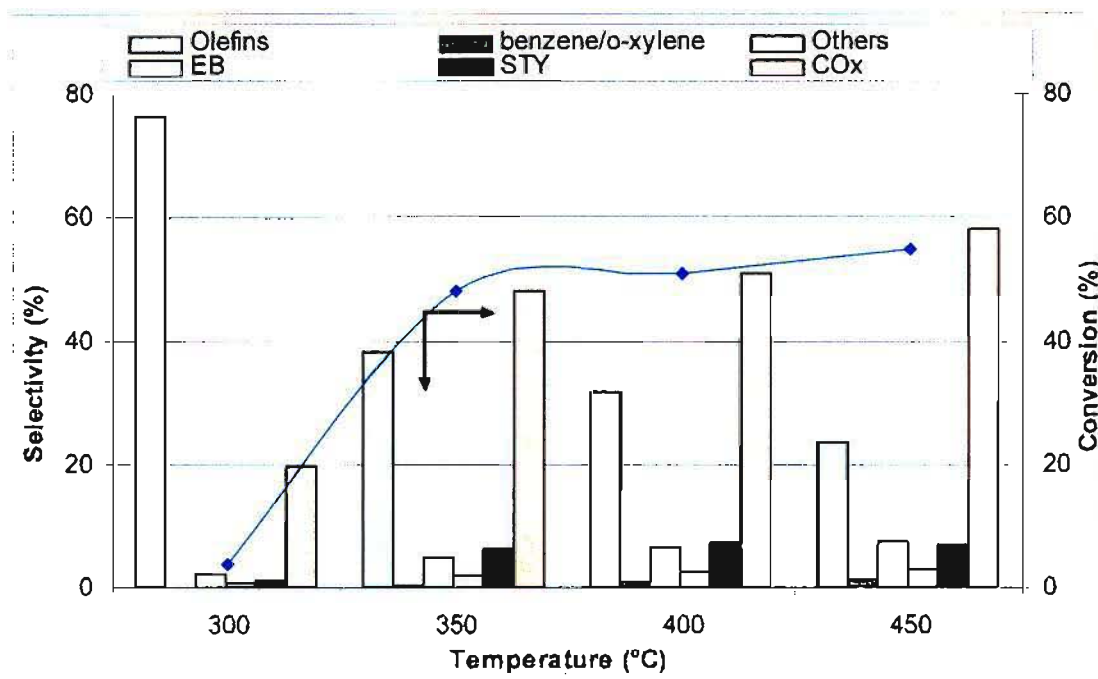


Figure 9.1: Effect of temperature on selectivity and conversion in *n*-octane ODH over 19VMgO (Others = methylheptane, heptane, cracked products and unknowns)

In **Figure 9.1** above it can be seen that the conversion of *n*-octane increases rapidly from 300 to 350 °C. After 350 °C, *n*-octane conversion increased slowly, as most of the oxygen was used up. As the temperature increases from 300 to 400 °C, the selectivity to the aromatics benzene, *o*-xylene, ethylbenzene (EB) and styrene (STY) increases. The increased selectivity is due to the higher activation energy of formation of aromatics compared to that of CO_x [5,6]. In addition to this, the relative stability of the aromatics could explain the increase in selectivity with temperature [5]. The highest selectivity to styrene was about 7 % and this was obtained at 400 °C.

Figure 9.2 shows the variation of selectivity to ODH products with *n*-octane conversion. The selectivity to olefins (mainly 2-,3-,4-octene) was high (almost 80 %) at low conversions. As the conversion increased, selectivity to olefins decreased. The selectivity to CO_x increased with increasing conversion. The selectivity to aromatics was also observed to increase with conversion. The selectivity to styrene increased with conversion and then decreased slightly. This decrease is probably due to its further oxidation with increasing temperatures.

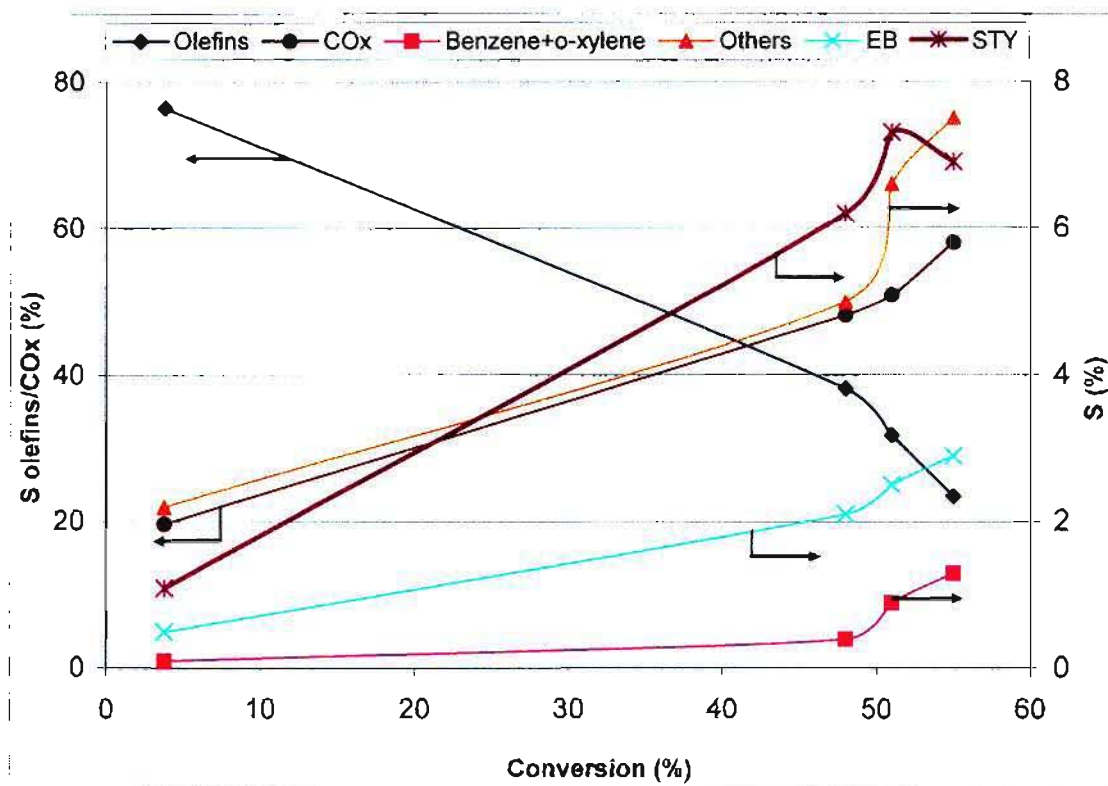


Figure 9.2: Variation of selectivity to ODH products with *n*-octane conversion

9.3 Variation in gas hourly space velocity (GHSV)

The effect of varying the GHSV on styrene selectivity and *n*-octane conversion is shown in Figure 9.3 below:

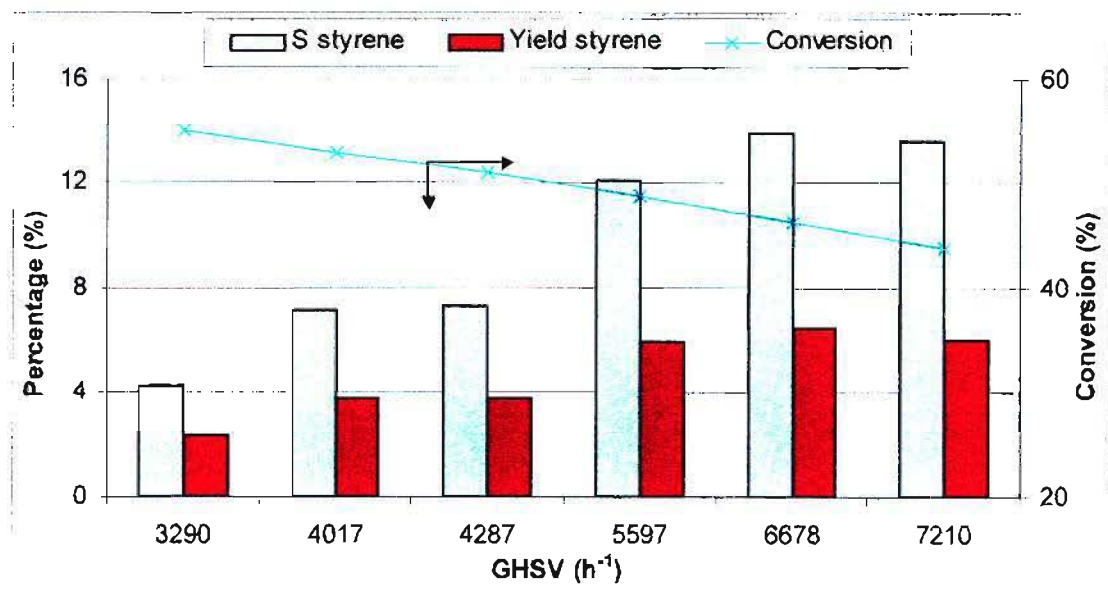


Figure 9.3: Effect of GHSV on *n*-octane conversion and styrene selectivity and yield

The GHSV was varied at a constant feed composition of 7.0 % *n*-octane in air and at a constant temperature of 400 °C. In **Figure 9.3** it can be seen that as the GHSV increased, conversion decreased. The selectivity to styrene increased up to a GHSV of 6678 h⁻¹. The use of high GHSV's resulted in decreased residence times of styrene on the surface of 19VMgO saving it from consecutive oxidation. A maximum styrene selectivity of 14 % was obtained with a GHSV of 6678 h⁻¹. The yield of styrene at this GHSV was 7 %.

9.4 Variation in the *n*-octane to air feed ratio

The effect of changing the paraffin to oxidant feed ratio on the surface of a catalyst was previously discussed and variation in the *n*-hexane to air feed ratio was shown to result in a change in selectivity to ODH products (**Chapter 8**). The feed ratio was lowered from 7.0 % *n*-octane in air to ratios within the flammable region. A constant temperature of 400 °C and a space velocity of 6678 h⁻¹ was used.

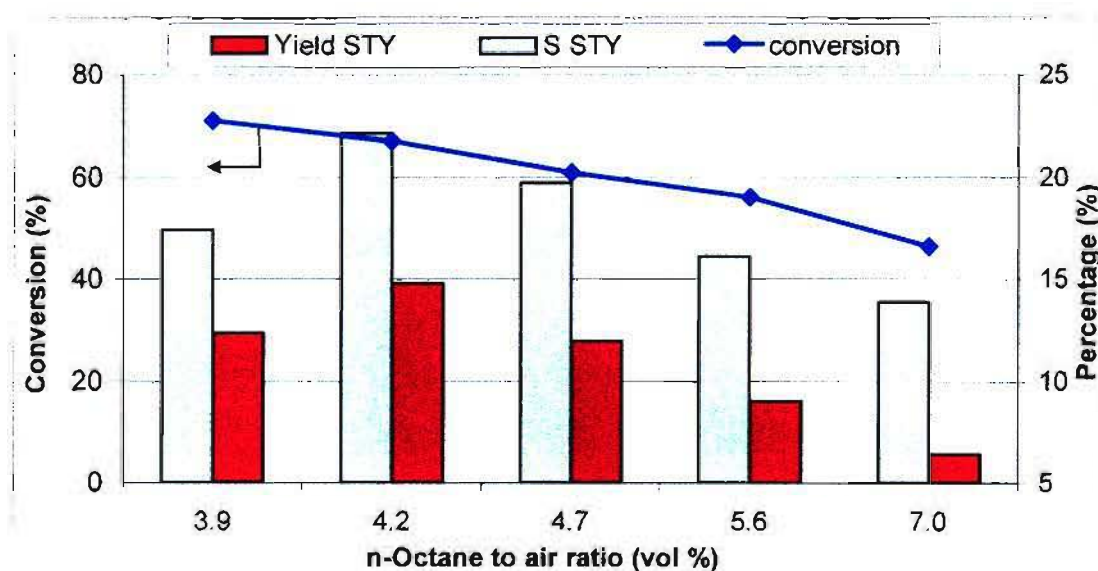


Figure 9.4: Effect of *n*-octane to air feed ratio on conversion, selectivity and yield of styrene

In **Figure 9.5** it can be seen that as the volume % of air increased in the feed, the conversion of *n*-octane increased. More oxygen is available to participate in catalytic reactions and hence the conversion increases. The selectivity and yield of styrene was also observed to increase with a decrease in the *n*-octane to air feed ratio to 4.2 %. A maximum styrene selectivity of 22 % and a corresponding yield of 15 % were obtained with a *n*-octane to air feed ratio of 4.2 %. This improved selectivity to styrene suggests that the interaction between the reacting feed and the catalyst surface is critical to catalytic performance. As discussed previously,

Pantazidis *et al.* [7] have showed the ability of various oxidizing or reducing environments to induce different restructuring of catalytic surfaces and consequently this can result in different catalytic performance.

9.5 Promoted 19VMgO

2.5MoVMgO, 2.5CsVMgO and 1SbVMgO had previously shown enhanced catalytic performance for *n*-hexane ODH (Chapter 8.5). These catalysts were tested with *n*-octane. A *n*-octane to air feed ratio of 4.2 % was used. Catalysts were tested at 400 °C. A gas hourly space velocity of 6678 h⁻¹ was used.

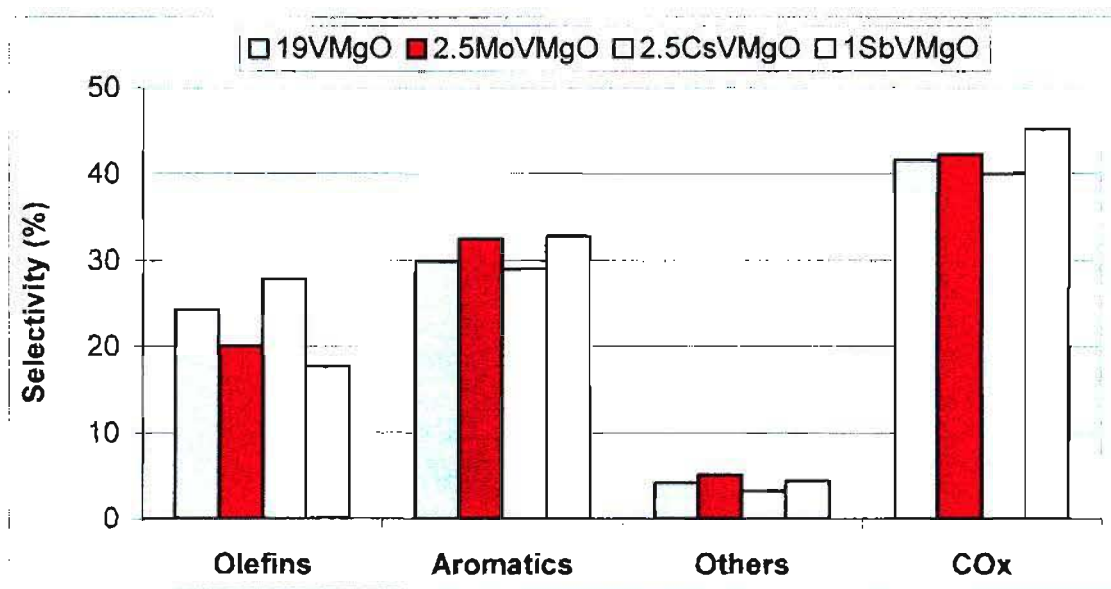


Figure 9.5: Selectivity to products observed during *n*-octane ODH of 19VMgO and promoted 19VMgO (Others = Mainly cracked products, trace water soluble products (acetaldehyde and acetone) and unknowns)

Figure 9.5 shows the selectivity to products formed. At 400 °C the conversions achieved by these catalysts were approximately 67 %, 70 %, 61 and 74 % for 19VMgO, 2.5MoVMgO, 2.5CsVMgO and 1SbVMgO respectively. Antimony and molybdenum promotion resulted in higher COx and aromatic selectivity compared to 19VMgO at 400 °C. The selectivity to olefins was much lower with these catalysts than with 19VMgO. The cesium promoted catalyst was observed to exhibit the opposite trend with higher selectivities to olefins than 19VMgO. This increase in selectivity is probably due to the decreased conversion as well as the favoured desorption of olefins on cesium promoted catalysts.

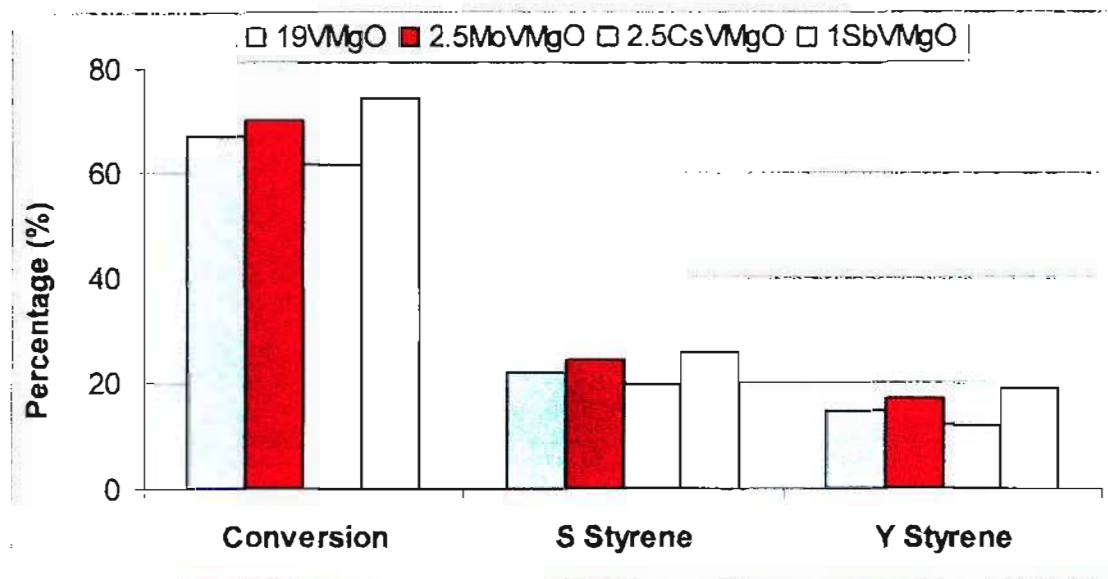


Figure 9.6: Comparison of *n*-octane conversion, styrene selectivity and styrene yield obtained with 19VMgO and molybdenum, cesium and antimony promoted 19VMgO

In **Figure 9.6** it can be seen that the highest selectivity and yield to styrene was obtained with 1SbVMgO. The selectivity and yield to styrene was 26 and 19 % respectively. At 400 °C, the selectivity and yield to styrene decreased according to the sequence: 1SbVMgO > 2.5MoVMgO > 19VMgO > 2.5 CsVMgO. The activity of the catalysts tested followed the same sequence.

9.6 Conclusion

VMgO and promoted VMgO catalysts were shown to be active for the ODH of *n*-octane. Olefins and aromatics were the main organic products produced. The selectivity to aromatics i.e. benzene, *o*-xylene, ethylbenzene and styrene increased from 300 to 400 °C. The increased selectivity is due to both the higher activation energy of formation of aromatics compared to that of CO_x as well as the relative stability of the aromatics [5,6]. After 400 °C, the aromatics become increasingly less stable and overoxidation to CO_x occurs. The same effect was observed for *n*-hexane ODH (**Chapter 8.2**). At 350 °C, CO_x was formed exclusively from *n*-hexane. As the temperature increased, the selectivity to CO_x decreased and the selectivity to benzene increased. At 550 °C, benzene oxidation to CO_x becomes significant and the overall selectivity to CO_x was then observed to increase. Although the unusual decrease in CO_x selectivity for *n*-hexane is readily observed, this is not the case for *n*-octane ODH. This is

mainly due to the initial high selectivity to octenes. The selectivity to octenes significantly decreases with increasing temperature and this contributes to the increasing COx selectivity.

The selectivity and yield of styrene was enhanced by the optimization of the *n*-octane to air feed ratio as well as the gas hourly space velocity. A feed ratio of 4.2 % *n*-octane in air and a GHSV of 6678 h⁻¹ yielded the best results of the study. At 400 °C, 19VMgO gave a styrene selectivity of 22 % and a yield of 15 %. Promotion of 19VMgO with antimony, molybdenum and cesium resulted in a change in selectivity. 1SbVMgO and 2.5MoVMgO gave a selectivity and yield of styrene higher than that of unpromoted 19VMgO. 2.5CsVMgO gave higher selectivity to olefins compared to that of unpromoted 19VMgO. A maximum styrene selectivity and yield of 26 and 19 % respectively was obtained with 1SbVMgO.

9.7 References:

- 1) Mahomed, A. S., PhD Thesis, University of Kwazulu-Natal, 2005.
- 2) Yoo, J.S, *Appl. Catal. A*, **142**, 1996, 19.
- 3) Cavani, F. and Trifiro, F., *Appl. Catal. A*, **133**, 1995, 219.
- 4) Meima, G. R. And Menon, P. G., *Appl. Catal. A*, **2001**, 239.
- 5) Lemonidou, A. A, Tjatjopoulos, G. J. and Vasalos, I. A., *Catal. Today*, **45**, 1998, 65.
- 6) Corma, A., Lopez Nieto, J. M., Paredes, N., Dejoz, A and Vazquez, I., *New Developments in Selective Oxidation II*, Studies in Surface Science and Catalysis, Elsevier Science, Amsterdam, **82**, 1994, p. 113.
- 7) Pantazidis, A., Burrows, A., Kiely, C. J. and Mirodatos, C., *J. Catal.*, **177**, 1998, 325.

CHAPTER 10: Mechanistic Studies

10.1 Introduction

Hutchings and Taylor [1] have described a simplified approach for designing oxidation catalysts. A key criterion of their design approach is the stability of products over a chosen catalyst. Good catalysts are those that do not catalyse the oxidation of the required product under the reaction condition. The stability of the major product benzene was evaluated over 19VMgO. Minor products (hexenes) and plausible reaction intermediates were also fed into the reactor in an attempt to elucidate or assess feasible catalytic reaction pathways.

10.2 Stability of benzene over 19VMgO

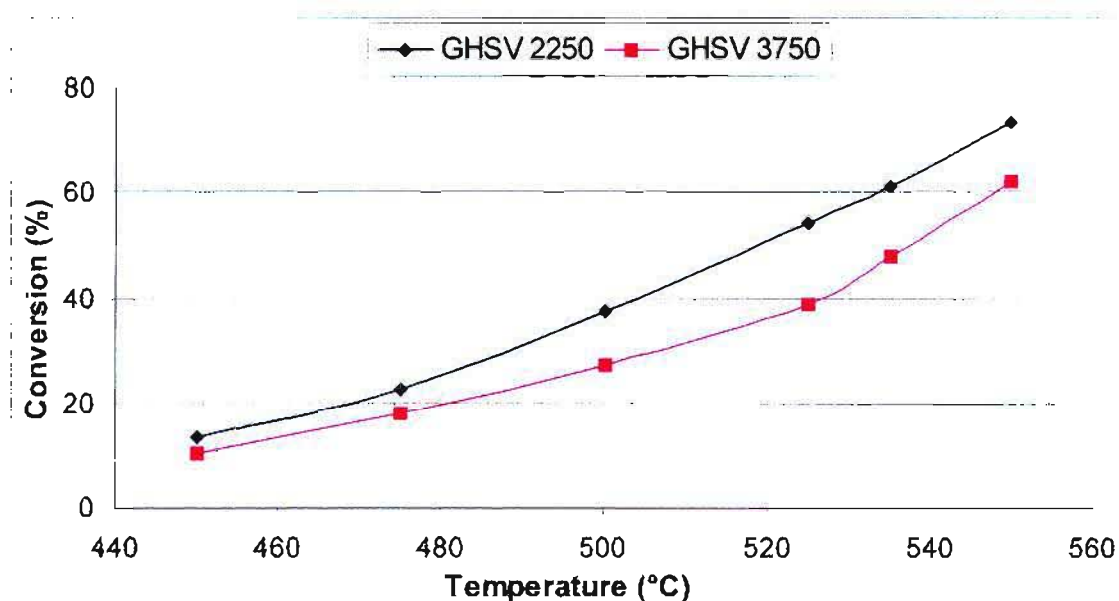


Figure 10.1: Effect of temperature on the conversion of benzene over 19VMgO

A 1 % benzene in air feed was tested over 19VMgO. Gas hourly space velocities of 2250 and 3750 h^{-1} were used to determine the effect of contact time on benzene conversion. In **Figure 10.1** it can be seen that the use of a higher space velocity reduces the amount of benzene oxidized. Less time spent by benzene molecules on the surface of 19VMgO results in a lower conversion. At temperatures higher than 500 °C a significant amount of benzene is oxidized i.e. at least 25 %. At 525 °C, almost 40 % of benzene was oxidized when a space velocity of 3750 h^{-1} was used. **Figure 10.1** probably indicates the maximum instability of benzene. Under reactions conditions the stability of benzene may be partially favoured by the unavailability of catalytic sites as well as a lower amount of oxidant available for its combustion.

10.3 Reaction network and mechanism

10.3.1 Homogeneous gas-phase reactions

The contribution of gas-phase reactions in this study was previously shown to be small (Chapter 7.4). A gas-phase reaction involves the formation of free radicals. The initial step is considered to be the hydrogen atom abstraction of the paraffin to form an alkyl radical [2]. An oxygen molecule can react directly with the paraffin, forming an alkyl radical and a hydroperoxy radical, or a radical such as a hydroxyl radical could desorb from the catalyst surface and abstract a hydrogen atom from the paraffin (Figure 10.2) [2].

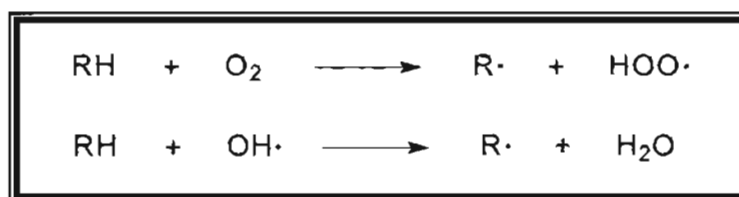


Figure 10.2: Alkyl radical formation [2]

Alkyl radicals that form can dehydrogenate oxidatively to form olefins [2]

10.3.2 Heterogeneous reactions

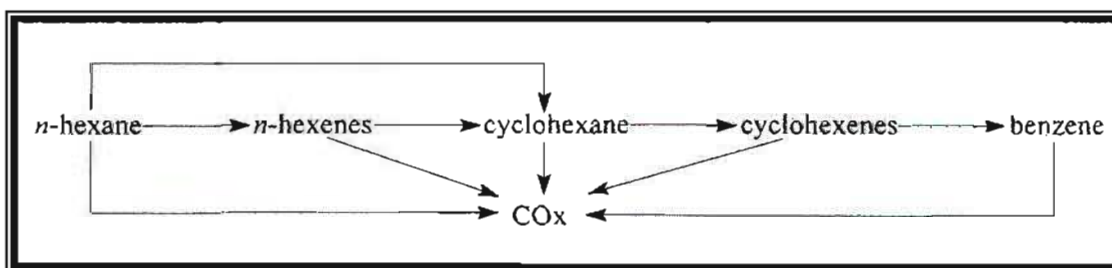


Figure 10.3: Proposed reaction network in oxidative dehydrogenation of *n*-hexane

Figure 10.3 shows the possible reaction pathways during the ODH of *n*-hexane leading to the formation of benzene. There are three primary steps forming hexenes, cyclohexane and CO_x. CO_x are formed directly from *n*-hexane, intermediate products and from the final benzene product itself. If the rates of the consecutive reactions to benzene are rapid then its selectivity will be high (presuming that benzene itself is only slowly oxidised to CO_x). If the rates of the consecutive steps leading to benzene are slow then these steps will favour deep oxidation to CO_x. Olefins that have desorbed may be subsequently readsorbed on unselective oxidizing sites resulting in the formation of carbon oxides. In VMgO catalysts the basic nature of the surface facilitates the desorption of olefins from the catalyst surface. In addition to this, the

basic surface ensures that the interaction between a desorbed olefin and the catalyst surface is low. Furthermore, the basicity of VMgO catalysts has been correlated to the absence of oxygenated organic products [3]. The low residence times of olefins on the catalyst surface does not favour oxygen insertion.

The following 3 different mechanisms have been proposed for ODH of paraffins:

- 1) A Mars-van Krevelen mechanism where selective reactions take place on partially reduced sites and deep oxidation on highly oxidised sites [4].
- 2) A dual – site Mars-van Krevelen mechanism in which different sites catalyze the formation of selective and unselective ODH products [5].
- 3) A Mars-van Krevelen mechanism which operates for selective dehydrogenation and a Langmuir-Hinshelwood mechanism for deep oxidation [6].

According to the Mars-van Krevelen mechanism, the oxidation of paraffins proceeds by two steps (**Chapter 2.6**):

- 1) The reactant paraffin molecule initially reduces an oxidized surface site.
- 2) The reduced surface site is subsequently reoxidized by gas-phase molecular oxygen.

10.3.2.1 Mechanism of 1-hexene and 2-hexene formation

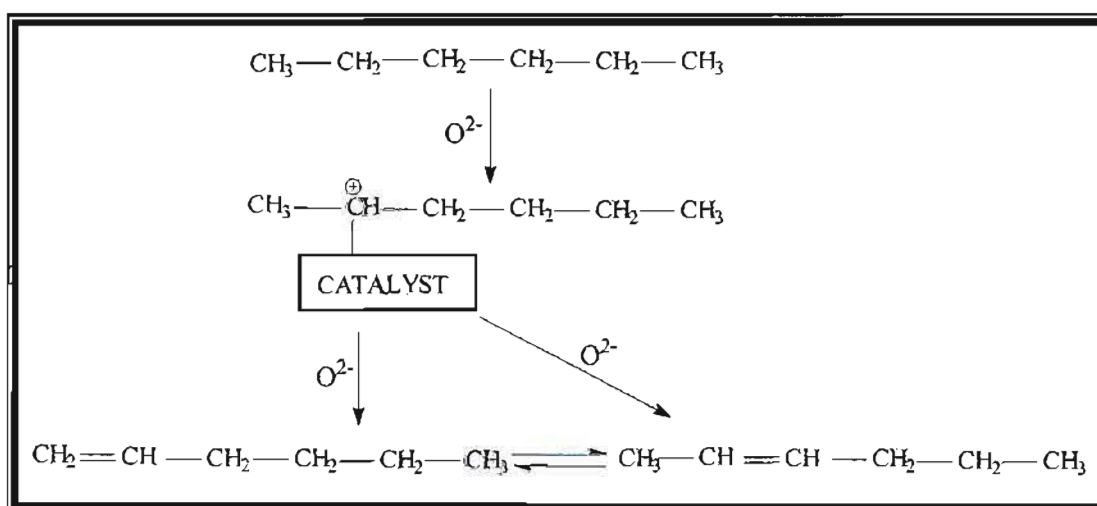


Figure 10.4: Mechanism of 1-hexene and 2-hexene formation [7]

It is generally accepted that the activation step and rate limiting step in paraffin ODH is the irreversible hydrogen abstraction from a secondary carbon to give an adsorbed alkyl radical [8-11]. The alkyl radical that forms is very reactive. The removal of another hydrogen atom then leads to olefins (**Figure 10.4**). The adsorbed olefin can undergo further

transformation or it can desorb into the gas-phase. The active centre on VMgO catalysts for C-H bond activation is believed to be a $V^{5+} - O^{2-}$ couple, which is considered to be an acid – base pair [12]. It is still unclear as to whether it is the nucleophilicity/basicity of the oxygen or the electrophilicity/acidity of the vanadium atom that is responsible for C-H bond cleavage.

Centi and Trifiro [13] believe that a concerted attack of both Lewis acid and base centres on VPO catalysts leads to the contemporaneous removal of two hydrogen atoms from butane resulting in adsorbed butene. At variance with this mechanism, Busca *et al.* [14] believe that nucleophilic oxygen species are responsible for paraffin activation, leading to the formation of a surface hydroxyl group.

The general consensus is that ODH on VMgO catalysts proceeds *via* the reduction of tetrahedrally coordinated V^{5+} ions, although the oxidation state of the reduced vanadium cation is contentious [8]. In this study only V^{5+} and V^{4+} cations were observed by XPS analysis of the used 19VMgO catalyst suggesting a $V^{5+} \leftrightarrow V^{4+}$ redox cycle.

10.3.2.2 Oxidative dehydrocyclisation of *n*-hexane to benzene

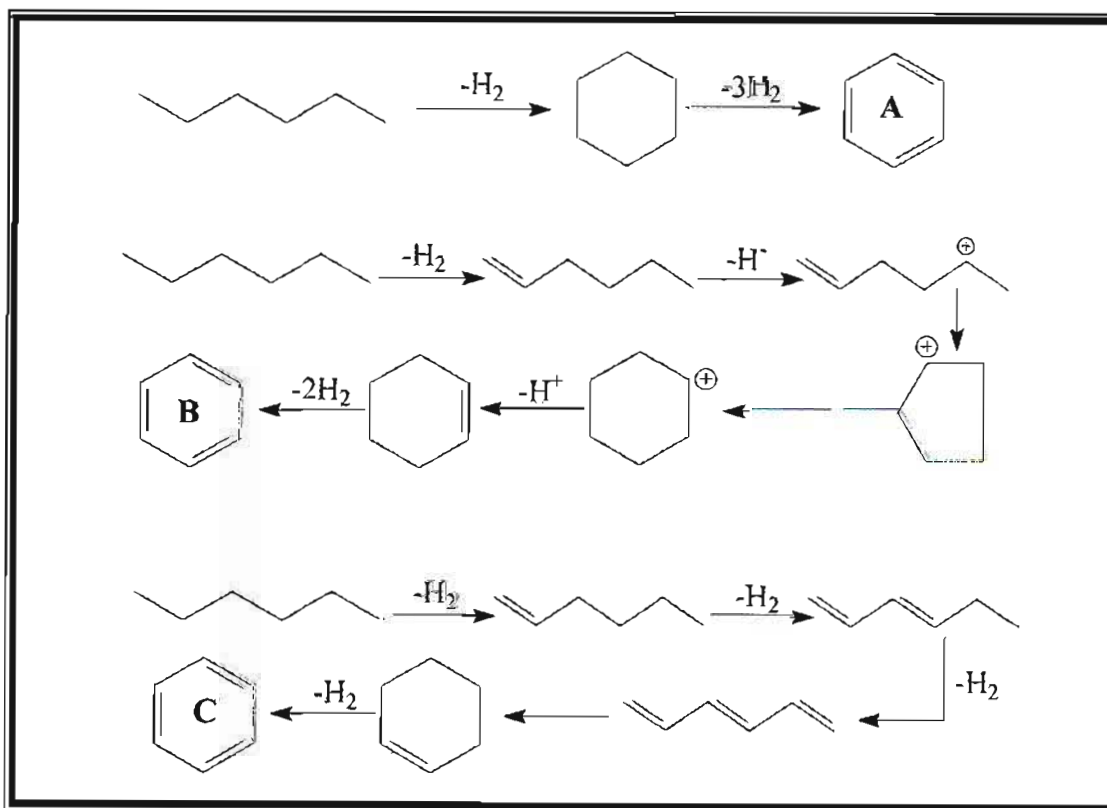


Figure 10.5: Proposed mechanisms for the cyclisation of *n*-hexane [15,16]

Possible cyclisation mechanisms for *n*-hexane are shown in **Figure 10.5** above:

- A) 1,6 ring closure to cyclohexane followed by ODH to benzene [16].
- B) 1,5 ring closure, followed by ring expansion to cyclohexane and ODH to benzene [16].
- C) ODH of hexane to hexenes, hexadienes, hexatrienes, followed by thermal ring closure and ODH to benzene [15].

To assess the feasibility of pathways B and C, selected intermediates were used as feeds. A feed composition of approximately 1 % intermediate in air was fed over 19VMgO at 400 °C. A gas hourly space velocity of 3750 h⁻¹ was used. The major and minor products observed are shown in **Table 10.1** below:

| Intermediate | Major products observed | Minor products observed |
|--------------------|-------------------------|-------------------------|
| 1-Hexene | CO _x | Benzene |
| 2-hexene | CO _x | |
| Methylcyclopentane | CO _x | |
| Cyclohexane | Benzene, Cyclohexene | CO _x |
| Cyclohexene | Benzene | CO _x |

Table 10.1: Major and minor products observed by feeding intermediates over 19VMgO

The results shown in **Table 10.1** suggests that the direct 1,6 ring closure mechanism is most likely the dominant pathway to benzene. When 1-hexene was fed into the reactor only trace amounts of benzene was observed, suggesting that this was not a significant reaction pathway. When 2-hexene was fed into the reactor only CO_x was observed. No isomerization products were observed consistent with the weakly acidic character of 19VMgO. C₅ to C₆ ring expansion is usually catalysed by acid catalysts [16]. The lack of isomerization activity with 19VMgO suggests that ring expansion pathways would not be a favourable route to benzene.

10.4 Conclusion

It is proposed that in the ODH of *n*-hexane over VMgO catalysts, 1,6 oxidative dehydrocyclisation is the major pathway to benzene. Similarly it can be envisaged that 1,6 ring closure in *n*-octane ODH is probably the major pathway to ethylbenzene and styrene whilst *o*-xylene would be produced *via* 2,7 ring closure. It must be noted that *n*-hexane and *n*-octane molecules are big enough to interact simultaneously with two adjacent vanadium sites and the cyclisation mechanism may be facilitated in this manner [10,17].

There is still uncertainty regarding the extent of the contribution from successive dehydrogenation of *n*-hexane and *n*-octane followed by thermal ring closure to produce aromatics. In butane oxidation, butene and butadiene are likely intermediates, but no olefins are observed among the reaction products [18]. Investigations using butenes as feeds resulted in very poor selectivities to maleic anhydride [19].

10.5 References:

- 1) Hutchings, G. J. and Taylor, S. H., *Catal. Today*, **49**, 1999, 105.
- 2) O'Connor, R. P. and Schmidt, L. D., *Chem. Eng. Sci.*, **55**, 2000, 5693.
- 3) Albonetti, S., Cavani, F. and Trifiro, F., *Catal. Rev. Sci. Eng.*, **38**, 1996, 413.
- 4) Mamedov, E. A. and Corberan, V. C., *Appl. Catal. A*, **127**, 1995, 1.
- 5) Tellez, C., Menendez, M. and Santamaria, J., *J. Catal.*, **183**, 1999, 210.
- 6) Stern, D. L. and Grasselli, R. K., *J. Catal.*, **167**, 1997, 560.
- 7) Lopez Nieto, J. M., Concepcion, P., Dejoz, A., Melo, F., Knozinger, H. and Vazquez, M. I., *Catal. Today*, **61**, 2000, 361.
- 8) Tellez, C., Abon, M., Dalmon, J. A., Mirodatos, C. and Santamaria, J., *J. Catal.*, **195**, 2000, 113.
- 9) Blasco, T., Lopez Nieto, J. M., Dejoz, A. and Vazquez, A., *J. Catal.*, **157**, 1995, 271.
- 10) Michalakos, P. M., Kung, M. C., Jahan, I. And Kung, H. H., *J. Catal.*, **140**, 1993, 226.
- 11) Grzybowska-Swierkosz, B., *Appl. Catal. A*, **157**, 1997, 409.
- 12) Grzybowska-Swierkosz, B., *Ann. Rep. Prog. Chem.*, **96**, 2000, 297.
- 13) Centi, G. and Trifiro, F., *Catal. Today*, **3**, 1988, 51.
- 14) Finocchio, E., Ramis, G., Busca, G., Lorenzelli, V. and Willey, R. J., *Catal. Today*, **28**, 1996, 381.
- 15) Klepel, C., Breitkopf, C. and M. Standke, *J. Mol. Catal. A*, **210**, 2004, 211.
- 16) Meriaudeau, P. and Naccache, C., *Catal. Rev. Sci. Eng.*, **39**, 1997, 5.
- 17) Blasco, T. and Lopez Nieto, J. M., *Appl. Catal. A*, **157**, 1997, 117.
- 18) Cavani, F. and Trifiro, F., *Catal. Today*, **36**, 1997, 431.
- 19) Centi, G., *Catal. Lett.*, **22**, 1993, 53.

Chapter 11: Summary and Conclusion

Vanadium magnesium mixed oxide catalysts were synthesized and tested for the ODH of *n*-hexane and *n*-octane. Four parallel horizontal reactors were designed and constructed for *n*-hexane ODH. Two vertical reactors were used for *n*-octane ODH. VMgO catalysts with variable vanadium loadings were synthesized and characterized by XRD, ICP, BET surface area, FTIR, LRS and SEM. A MgO catalyst containing a 19 weight percent loading of vanadium was further characterized by DSC-TGA and XPS. Magnesium oxide and magnesium orthovanadate were found to be the only phases present in all catalysts. 19VMgO was promoted with approximately 0.5, 1, 2.5 and 5 weight percent of MoO₃, Sb₂O₃, TeO₂, Nb₂O₅, Bi₂O₃ and Cs₂O. All promoted catalysts were tested on *n*-hexane. Promoted catalysts, which showed enhanced performance, were tested on *n*-octane.

The product profile observed for *n*-hexane ODH over VMgO included benzene, 1-hexene, 2-hexene, propane, propene, CO_x and H₂O. A VMgO catalyst with a vanadium loading of 19 weight percent resulted in the best catalytic performance. This confirmed that the coexistence of definitive amounts of MgO and Mg₃(VO₄)₂ was beneficial for the increased production of olefins and aromatics. It is believed that phase cooperation between the two phases present on the catalyst surface results in enhanced catalytic performance.

The optimization of process variables such as temperature, *n*-hexane to air feed ratio and gas hourly space velocity resulted in a selectivity and yield of benzene of 31 and 23 % respectively. The total dehydrogenation selectivity was 42 % and the yield of dehydrogenated product was 31 %. This was obtained with a *n*-hexane to air feed ratio of 5.5 % and a GHSV of 4688 h⁻¹ at 525 °C with 19VMgO. These results reflect that the paraffin to oxidant ratio is crucial to the control of selectivity in paraffin oxidation. It was shown that when oxygen is limited, the surface of the catalyst becomes saturated with reactive paraffin molecules and this leads to nonselective reactions. Additionally, the lack of oxygen in the reactor can lead to an atypical decrease in the selectivity to CO_x. An increase in heterogeneous-homogeneous reactions which give olefins, which can rapidly cyclise, could also account for the observed increase in selectivity to benzene with increasing temperature.

Promoted catalysts were tested on a 7.8 % *n*-hexane in air feed using a GHSV of 3750 h⁻¹. Under these conditions unpromoted 19VMgO gave a benzene selectivity and yield of 29 and 20 % respectively. 2.5MoVMgO gave a benzene selectivity and yield of 32 % and 21 %. Selectivity to benzene of 32 % was also obtained with 2.5CsVMgO and 1SbVMgO. Niobium

and bismuth promotion of 19VMgO resulted in a negative effect on catalytic performance. Tellurium promoted catalysts favoured the formation of mono – olefins. At comparable conversions, the selectivity to hexenes was at least twice that of unpromoted 19VMgO.

n-Octane ODH over 19VMgO resulted in the formation of octenes, octadienes, octatrienes, benzene, ethylbenzene, styrene, *o*-xylene, CO_x and water. Styrene, in particular, was considered to be a highly desired product as the direct conversion of *n*-octane to styrene has potential to be an attractive commercial process. Optimization of process conditions resulted in a maximum styrene selectivity and yield of 22 % and 15 % respectively. This was achieved with a *n*-octane to air feed ratio of 4.2 % and a GHSV of 6678 h⁻¹ at 400 °C. Under these conditions 1SbVMgO gave a maximum styrene selectivity and yield of 26 % and 19 % respectively.

It is proposed that the mechanism of oxidative dehydrocyclisation proceeds *via* 1,6 ring closure to form benzene during *n*-hexane ODH and ethylbenzene / styrene during *n*-octane ODH.

APPENDIX 1: EXPERIMENTAL

Carbon Balance

n-Hexane ODH:

Reactants and products were analyzed by two online GC's. One GC was equipped with a flame ionisation detector (FID) and the other with a thermal conductivity detector (TCD). Organic reactants and products were analyzed with the FID and CO_x was analyzed with the TCD.

Calibration gases containing different concentrations were used to obtain a plot of peak area vs moles of *n*-hexane. This graph was used to determine the moles of *n*-hexane, once the peak area was obtained from the GC trace. Calibration graphs of peak area vs moles were also obtained for all organic products using standards. Calibration gases were also used to obtain plots of peak area vs moles of CO_x and from these plots the moles of CO_x could then be readily determined if the peak area was known.

Usually CO_x selectivity was taken as the difference of all other products. Nevertheless, carbon balances were regularly referenced by analyzing the CO_x. Referenced carbon balances were found to be between 96 and 100 %.

n-Octane ODH

In *n*-octane ODH, the feed and the tail gas were analyzed online. The liquid condensates from the knock-out pot were analyzed off line. This condensate usually contained an aqueous layer and an organic layer. These layers were separated, weighed and analyzed in the FID GC by manual injection of 0.5 μl of sample.

Summary of catalytic testing results:

n-Hexane ODH: *n*-Hexane to air = 0.06% and GHSV = 3750 h⁻¹

| Temperature (°C) | C _{Hexane} (%) | S _{Benzene} (%) | S _{COx} (%) | Temperature (°C) | C _{Hexane} (%) | S _{Benzene} (%) | S _{COx} (%) |
|------------------|-------------------------|--------------------------|----------------------|------------------|-------------------------|--------------------------|----------------------|
| 300 | 8.1 | 0 | 100 | 300 | 19.1 | 0 | 100 |
| 350 | 21.3 | 0.1 | 99.9 | 350 | 61.6 | 1.1 | 98.9 |
| 400 | 33.0 | 1.1 | 98.9 | 400 | 83.0 | 4.4 | 95.6 |
| 450 | 62.0 | 2.0 | 98.0 | 425 | 96.0 | 6.5 | 93.5 |
| 500 | 83.0 | 1.0 | 99.0 | 435 | 98.1 | 7.1 | 92.9 |
| 550 | 95.0 | 0.1 | 99.9 | 450 | 100 | 5.4 | 94.6 |

n-Hexane ODH over 14VMgO

n-Hexane ODH over 16VMgO

| Temperature (°C) | C _{Hexane} (%) | S _{Benzene} (%) | S _{COx} (%) | Temperature (°C) | C _{Hexane} (%) | S _{Benzene} (%) | S _{COx} (%) |
|------------------|-------------------------|--------------------------|----------------------|------------------|-------------------------|--------------------------|----------------------|
| 300 | 19.3 | 6.8 | 93.2 | 300 | 9.2 | 0 | 100 |
| 350 | 65.0 | 8.8 | 91.2 | 350 | 44.1 | 3.9 | 96.1 |
| 400 | 96.1 | 14.8 | 85.2 | 400 | 61.8 | 6.0 | 94.0 |
| 415 | 96.3 | 15.0 | 85.0 | 425 | 83.3 | 9.4 | 90.6 |
| 430 | 98.5 | 15.6 | 84.4 | 450 | 96.1 | 12.4 | 87.6 |
| 445 | 99.4 | 17.7 | 82.3 | 465 | 99.4 | 15.5 | 84.5 |
| 450 | 100 | 17.1 | 82.9 | 475 | 100 | 14.3 | 85.7 |

n-Hexane ODH over 19VMgO

n-Hexane ODH over 24VMgO

| Temperature (°C) | C _{Hexane} (%) | S _{Benzene} (%) | S _{COx} (%) | Temperature (°C) | C _{Hexane} (%) | S _{Benzene} (%) | S _{COx} (%) |
|------------------|-------------------------|--------------------------|----------------------|------------------|-------------------------|--------------------------|----------------------|
| 300 | 7.9 | 0 | 100 | 300 | 4.9 | 0.0 | 100 |
| 350 | 21.6 | 0 | 100 | 350 | 11.0 | 0.0 | 100 |
| 400 | 50.8 | 4.2 | 95.8 | 400 | 15.1 | 1.0 | 99.0 |
| 430 | 70.9 | 6.2 | 93.8 | 450 | 33.2 | 3.4 | 96.6 |
| 440 | 75.0 | 6.9 | 93.1 | 500 | 46.0 | 5.9 | 94.1 |
| 450 | 81.8 | 8.0 | 92.0 | 550 | 66.0 | 5.8 | 94.2 |
| 470 | 90.2 | 9.8 | 90.2 | | | | |
| 490 | 95.4 | 11.6 | 88.4 | | | | |
| 510 | 98.6 | 13.2 | 86.8 | | | | |
| 525 | 99.9 | 14.3 | 85.7 | | | | |
| 535 | 100 | 13.4 | 86.6 | | | | |

n-Hexane ODH over 35VMgO

n-Hexane ODH over 49VMgO

n-Hexane ODH: *n*-Hexane to air = 7.8% and GHSV = 3750 h⁻¹

| Temp (°C) | C (%) | S (C ₆ H ₆) | Y (C ₆ H ₆) | S (Hexenes) | S (C ₃ H ₈) | S (C ₃ H ₆) | S (COx) | Y (Hexenes) | Y (C ₃ H ₈) | Y (C ₃ H ₆) | Y (COx) | TDS |
|-----------|-------|------------------------------------|------------------------------------|-------------|------------------------------------|------------------------------------|---------|-------------|------------------------------------|------------------------------------|---------|------|
| 350 | 28.3 | 0 | 0 | 0 | 0 | 0 | 100 | 0 | 0 | 0 | 28.3 | 0 |
| 400 | 41.4 | 8.4 | 3.5 | 4.4 | 0 | 0 | 87.2 | 1.8 | 0 | 0 | 36.1 | 12.8 |
| 425 | 47.9 | 12.5 | 6.0 | 4.6 | 0 | 0 | 82.9 | 2.2 | 0 | 0 | 39.7 | 17.1 |
| 450 | 51.2 | 12.9 | 6.6 | 4.8 | 0 | 0 | 82.3 | 2.5 | 0 | 0 | 42.1 | 17.7 |
| 475 | 50.3 | 15.3 | 7.7 | 4.1 | 1.6 | 0.8 | 78.1 | 2.1 | 0.8 | 0.4 | 39.3 | 20.2 |
| 500 | 56.2 | 18.7 | 10.5 | 4.0 | 2.9 | 0.4 | 74.0 | 2.3 | 1.6 | 0.2 | 41.6 | 23.2 |
| 525 | 56.8 | 25.0 | 14.2 | 3.8 | 5.6 | 3.0 | 62.5 | 2.2 | 3.2 | 1.8 | 35.5 | 31.9 |
| 550 | 59.7 | 21.4 | 12.8 | 3.7 | 7.9 | 4.0 | 63.0 | 2.2 | 4.7 | 2.4 | 37.6 | 29.1 |

The effect of temperature on conversion, selectivity and yield in *n*-hexane ODH over 16VMgO

| Temp (°C) | C (%) | S (C ₆ H ₆) | Y (C ₆ H ₆) | S (Hexenes) | S (C ₃ H ₈) | S (C ₃ H ₆) | S (COx) | Y (Hexenes) | Y (C ₃ H ₈) | Y (C ₃ H ₆) | Y (COx) | TDS |
|-----------|-------|------------------------------------|------------------------------------|-------------|------------------------------------|------------------------------------|---------|-------------|------------------------------------|------------------------------------|---------|------|
| 350 | 29.8 | 0 | 0 | 0 | 0 | 0 | 100 | 0 | 0 | 0 | 29.8 | 0 |
| 400 | 56.3 | 8.5 | 4.8 | 4.8 | 0.9 | 0 | 85.8 | 1.6 | 0.5 | 0 | 48.3 | 13.3 |
| 425 | 59.9 | 14.1 | 8.4 | 4.6 | 0.8 | 0 | 80.5 | 2.1 | 0.5 | 0 | 48.2 | 18.7 |
| 450 | 56.3 | 17.5 | 9.8 | 4.0 | 1.1 | 0.2 | 77.2 | 2.6 | 0.6 | 0.1 | 43.5 | 21.6 |
| 475 | 61.7 | 19.8 | 12.2 | 3.9 | 1.9 | 1.1 | 73.2 | 2.4 | 1.2 | 0.7 | 45.2 | 24.9 |
| 500 | 65.3 | 21.4 | 14.0 | 4.0 | 3.5 | 2.0 | 69.2 | 2.6 | 2.3 | 1.3 | 45.2 | 27.4 |
| 525 | 67.1 | 29.2 | 19.6 | 3.9 | 7.3 | 3.9 | 55.7 | 2.6 | 4.9 | 2.6 | 37.4 | 37.0 |
| 550 | 68.8 | 26.0 | 17.9 | 3.7 | 10.3 | 5.1 | 55.1 | 2.5 | 7.1 | 3.5 | 37.9 | 34.8 |

The effect of temperature on conversion, selectivity and yield in *n*-hexane ODH over 19VMgO

| Temp (°C) | C (%) | S (C ₆ H ₆) | Y (C ₆ H ₆) | S (Hexenes) | S (C ₃ H ₈) | S (C ₃ H ₆) | S (COx) | Y (Hexenes) | Y (C ₃ H ₈) | Y (C ₃ H ₆) | Y (COx) | TDS |
|-----------|-------|------------------------------------|------------------------------------|-------------|------------------------------------|------------------------------------|---------|-------------|------------------------------------|------------------------------------|---------|------|
| 350 | 27.3 | 0 | 0 | 0 | 0 | 0 | 100 | 0 | 0 | 0 | 27.3 | 0 |
| 400 | 49.4 | 6.4 | 3.2 | 5.8 | 0 | 0 | 87.8 | 2.9 | 0 | 0 | 43.4 | 12.2 |
| 425 | 53.6 | 8.5 | 4.6 | 5.7 | 0.8 | 0 | 85.0 | 3.1 | 0.4 | 0 | 45.6 | 14.2 |
| 450 | 56.3 | 10.2 | 5.7 | 5.2 | 1.5 | 1.0 | 82.1 | 2.9 | 0.8 | 0.6 | 46.2 | 16.4 |
| 475 | 55.7 | 15.9 | 8.9 | 5.0 | 2.0 | 1.1 | 76.0 | 2.8 | 1.1 | 0.6 | 42.3 | 22.0 |
| 500 | 58.1 | 19.3 | 11.2 | 4.4 | 4.2 | 2.8 | 69.3 | 2.6 | 2.4 | 1.6 | 40.2 | 26.5 |
| 525 | 59.1 | 24.7 | 14.6 | 4.2 | 5.5 | 3.8 | 61.8 | 2.5 | 3.3 | 2.3 | 36.5 | 32.7 |
| 550 | 62.0 | 20.7 | 12.9 | 4.2 | 8.5 | 4.4 | 62.2 | 2.6 | 5.3 | 2.7 | 38.6 | 29.3 |

The effect of temperature on conversion, selectivity and yield in *n*-hexane ODH over 24VMgO

n-Hexane ODH: *n*-Hexane to air = 7.8% and GHSV = 3750 h⁻¹

| Temp (°C) | C (%) | S (C ₆ H ₆) | Y (C ₆ H ₆) | S (Hexenes) | S (C ₃ H ₈) | S (C ₃ H ₆) | S (CO _x) | Y (Hexenes) | Y (C ₃ H ₈) | Y (C ₃ H ₆) | Y (CO _x) | TDS |
|-----------|-------|------------------------------------|------------------------------------|-------------|------------------------------------|------------------------------------|----------------------|-------------|------------------------------------|------------------------------------|----------------------|------|
| 450 | 55.0 | 18.1 | 10.0 | 3.6 | 2.0 | 1.1 | 75.2 | 2.0 | 1.1 | 0.6 | 41.4 | 22.8 |
| 475 | 58.0 | 20.8 | 12.1 | 3.4 | 2.7 | 1.4 | 71.7 | 2.0 | 1.6 | 0.8 | 41.6 | 25.6 |
| 500 | 61.5 | 21.2 | 13.0 | 3.0 | 3.5 | 2.2 | 70.1 | 1.8 | 2.2 | 1.4 | 43.1 | 26.4 |
| 525 | 63.4 | 29.1 | 18.4 | 3.0 | 8.3 | 4.0 | 55.6 | 1.9 | 5.3 | 2.5 | 35.2 | 36.1 |
| 550 | 66.1 | 24.6 | 16.3 | 2.5 | 11.0 | 5.6 | 56.3 | 1.6 | 7.3 | 3.7 | 37.2 | 32.7 |

The effect of temperature on conversion, selectivity and yield in *n*-hexane ODH over 0.5MoVMgO

| Temp (°C) | C (%) | S (C ₆ H ₆) | Y (C ₆ H ₆) | S (Hexenes) | S (C ₃ H ₈) | S (C ₃ H ₆) | S (CO _x) | Y (Hexenes) | Y (C ₃ H ₈) | Y (C ₃ H ₆) | Y (CO _x) | TDS |
|-----------|-------|------------------------------------|------------------------------------|-------------|------------------------------------|------------------------------------|----------------------|-------------|------------------------------------|------------------------------------|----------------------|------|
| 450 | 55.0 | 18.4 | 10.1 | 2.9 | 2.2 | 0.8 | 75.7 | 1.6 | 1.2 | 0.4 | 41.6 | 22.1 |
| 475 | 56.9 | 21.3 | 12.1 | 2.7 | 3.1 | 1.1 | 71.8 | 1.5 | 1.8 | 0.6 | 40.9 | 25.1 |
| 500 | 60.0 | 22.2 | 13.3 | 2.1 | 3.9 | 1.6 | 70.2 | 1.3 | 2.3 | 1.0 | 42.1 | 25.9 |
| 525 | 62.1 | 29.8 | 18.5 | 2.0 | 8.0 | 4.3 | 55.9 | 1.2 | 5.0 | 2.7 | 34.7 | 36.1 |
| 550 | 64.0 | 24.4 | 15.6 | 1.9 | 11.3 | 5.7 | 56.7 | 1.2 | 7.2 | 3.6 | 36.3 | 32.0 |

The effect of temperature on conversion, selectivity and yield in *n*-hexane ODH over 1MoVMgO

| Temp (°C) | C (%) | S (C ₆ H ₆) | Y (C ₆ H ₆) | S (Hexenes) | S (C ₃ H ₈) | S (C ₃ H ₆) | S (CO _x) | Y (Hexenes) | Y (C ₃ H ₈) | Y (C ₃ H ₆) | Y (CO _x) | TDS |
|-----------|-------|------------------------------------|------------------------------------|-------------|------------------------------------|------------------------------------|----------------------|-------------|------------------------------------|------------------------------------|----------------------|------|
| 450 | 57.1 | 21.0 | 12.0 | 1.9 | 2.0 | 1.0 | 74.1 | 1.1 | 1.1 | 0.6 | 42.3 | 23.9 |
| 475 | 61.9 | 23.7 | 14.7 | 1.8 | 2.9 | 1.4 | 70.2 | 1.1 | 1.8 | 0.9 | 43.5 | 26.9 |
| 500 | 64.2 | 25.5 | 16.4 | 1.7 | 4.8 | 2.0 | 66.0 | 1.1 | 3.1 | 1.3 | 42.4 | 29.2 |
| 525 | 66.5 | 32.1 | 21.3 | 1.5 | 10.0 | 3.9 | 52.5 | 1.0 | 6.7 | 2.6 | 34.9 | 37.5 |
| 550 | 67.2 | 28.0 | 18.8 | 1.1 | 12.2 | 6.0 | 52.7 | 0.7 | 8.2 | 4.0 | 35.4 | 35.1 |

The effect of temperature on conversion, selectivity and yield in *n*-hexane ODH over 2.5MoVMgO

| Temp (°C) | C (%) | S (C ₆ H ₆) | Y (C ₆ H ₆) | S (Hexenes) | S (C ₃ H ₈) | S (C ₃ H ₆) | S (CO _x) | Y (Hexenes) | Y (C ₃ H ₈) | Y (C ₃ H ₆) | Y (CO _x) | TDS |
|-----------|-------|------------------------------------|------------------------------------|-------------|------------------------------------|------------------------------------|----------------------|-------------|------------------------------------|------------------------------------|----------------------|------|
| 450 | 46.0 | 18.0 | 8.3 | 1.1 | 3.3 | 1.1 | 76.5 | 0.5 | 1.5 | 0.5 | 35.2 | 20.2 |
| 475 | 48.2 | 19.4 | 9.4 | 1.0 | 3.6 | 1.3 | 74.7 | 0.5 | 1.7 | 0.6 | 36.0 | 21.7 |
| 500 | 49.8 | 22.1 | 11.0 | 1.0 | 5.5 | 2.2 | 69.2 | 0.5 | 2.7 | 1.1 | 34.5 | 25.3 |
| 525 | 53.1 | 25.4 | 13.5 | 0.7 | 11.3 | 5.5 | 57.1 | 0.4 | 6.0 | 2.9 | 30.3 | 31.6 |
| 550 | 55.0 | 22.4 | 12.3 | 0.9 | 13.0 | 5.9 | 57.8 | 0.5 | 7.2 | 3.2 | 31.8 | 29.2 |

The effect of temperature on conversion, selectivity and yield in *n*-hexane ODH over 5MoVMgO

n-Hexane ODH: *n*-Hexane to air = 7.8% and GHSV = 3750 h⁻¹

| Temp (°C) | C (%) | S (C ₆ H ₆) | Y (C ₆ H ₆) | S (Hexenes) | S (C ₃ H ₈) | S (C ₃ H ₆) | S (COx) | Y (Hexenes) | Y (C ₃ H ₈) | Y (C ₃ H ₆) | Y (COx) | TDS |
|-----------|-------|------------------------------------|------------------------------------|-------------|------------------------------------|------------------------------------|---------|-------------|------------------------------------|------------------------------------|---------|------|
| 450 | 52.2 | 17.0 | 8.9 | 5.4 | 1.1 | 0.4 | 76.1 | 2.8 | 0.6 | 0.2 | 39.7 | 22.8 |
| 475 | 56.4 | 19.1 | 10.8 | 5.1 | 1.4 | 0.6 | 73.8 | 2.9 | 0.8 | 0.3 | 41.6 | 24.8 |
| 500 | 61.1 | 21.0 | 12.8 | 5.0 | 2.6 | 1.1 | 70.3 | 3.1 | 1.6 | 0.7 | 43.0 | 27.1 |
| 525 | 66.2 | 29.4 | 19.5 | 4.6 | 5.2 | 2.9 | 57.9 | 3.0 | 3.4 | 1.9 | 38.3 | 36.9 |
| 550 | 67.8 | 27.2 | 18.4 | 3.6 | 8.4 | 5.3 | 55.5 | 2.4 | 5.7 | 3.6 | 37.6 | 36.1 |

The effect of temperature on conversion, selectivity and yield in *n*-hexane ODH over 0.5CsVMgO

| Temp (°C) | C (%) | S (C ₆ H ₆) | Y (C ₆ H ₆) | S (Hexenes) | S (C ₃ H ₈) | S (C ₃ H ₆) | S (COx) | Y (Hexenes) | Y (C ₃ H ₈) | Y (C ₃ H ₆) | Y (COx) | TDS |
|-----------|-------|------------------------------------|------------------------------------|-------------|------------------------------------|------------------------------------|---------|-------------|------------------------------------|------------------------------------|---------|------|
| 450 | 47.8 | 17.1 | 8.2 | 5.1 | 0 | 0 | 77.8 | 2.4 | 0 | 0 | 37.2 | 22.2 |
| 475 | 50.9 | 19.5 | 9.9 | 4.9 | 0 | 0 | 75.6 | 2.5 | 0 | 0 | 38.5 | 24.4 |
| 500 | 54.4 | 22.4 | 12.2 | 4.6 | 1.1 | 0.4 | 71.5 | 2.5 | 0.6 | 0.2 | 38.9 | 27.4 |
| 525 | 61.3 | 30.3 | 18.6 | 4.5 | 3.9 | 2.5 | 58.8 | 2.8 | 2.4 | 1.5 | 36.0 | 37.3 |
| 550 | 64.2 | 29.2 | 18.7 | 4.0 | 5.7 | 4.4 | 56.7 | 2.6 | 3.7 | 2.8 | 36.4 | 37.6 |

The effect of temperature on conversion, selectivity and yield in *n*-hexane ODH over 1CsVMgO

| Temp (°C) | C (%) | S (C ₆ H ₆) | Y (C ₆ H ₆) | S (Hexenes) | S (C ₃ H ₈) | S (C ₃ H ₆) | S (COx) | Y (Hexenes) | Y (C ₃ H ₈) | Y (C ₃ H ₆) | Y (COx) | TDS |
|-----------|-------|------------------------------------|------------------------------------|-------------|------------------------------------|------------------------------------|---------|-------------|------------------------------------|------------------------------------|---------|------|
| 450 | 42.1 | 16.9 | 7.1 | 5.9 | 0 | 0 | 77.2 | 2.5 | 0 | 0 | 32.5 | 22.8 |
| 475 | 46.7 | 22.4 | 10.5 | 6.1 | 0 | 0 | 71.5 | 2.8 | 0 | 0 | 33.4 | 28.5 |
| 500 | 49.9 | 26.7 | 13.3 | 5.3 | 1.4 | 0.6 | 66.0 | 2.6 | 0.7 | 0.3 | 32.9 | 32.6 |
| 525 | 54.2 | 32.3 | 17.5 | 4.9 | 2.9 | 2.1 | 57.8 | 2.7 | 1.6 | 1.1 | 31.3 | 39.3 |
| 550 | 57.8 | 30.8 | 17.8 | 4.1 | 5.0 | 4.4 | 55.7 | 2.4 | 2.9 | 2.5 | 32.2 | 39.3 |

The effect of temperature on conversion, selectivity and yield in *n*-hexane ODH over 2.5CsVMgO

| Temp (°C) | C (%) | S (C ₆ H ₆) | Y (C ₆ H ₆) | S (Hexenes) | S (C ₃ H ₈) | S (C ₃ H ₆) | S (COx) | Y (Hexenes) | Y (C ₃ H ₈) | Y (C ₃ H ₆) | Y (COx) | TDS |
|-----------|-------|------------------------------------|------------------------------------|-------------|------------------------------------|------------------------------------|---------|-------------|------------------------------------|------------------------------------|---------|------|
| 450 | 36.0 | 16.5 | 5.9 | 6.6 | 0 | 0 | 76.9 | 2.4 | 0 | 0 | 27.7 | 23.1 |
| 475 | 38.9 | 20.4 | 7.9 | 5.7 | 0 | 0 | 73.9 | 2.2 | 0 | 0 | 28.7 | 26.1 |
| 500 | 44.7 | 25.2 | 11.3 | 5.4 | 1.2 | 0.4 | 67.8 | 2.4 | 0.5 | 0.2 | 30.3 | 31.0 |
| 525 | 48.2 | 27.4 | 13.2 | 5.0 | 3.0 | 1.8 | 62.8 | 2.4 | 1.4 | 0.9 | 30.3 | 34.2 |
| 550 | 52.2 | 29.1 | 15.2 | 4.2 | 4.7 | 2.9 | 59.1 | 2.2 | 2.5 | 1.5 | 30.9 | 36.2 |

The effect of temperature on conversion, selectivity and yield in *n*-hexane ODH over 5CsVMgO

n-Hexane ODH: *n*-Hexane to air = 7.8% and GHSV = 3750 h⁻¹

| Temp (°C) | C (%) | S (C ₆ H ₆) | Y (C ₆ H ₆) | S (Hexenes) | S (C ₃ H ₈) | S (C ₃ H ₆) | S (COx) | Y (Hexenes) | Y (C ₃ H ₈) | Y (C ₃ H ₆) | Y (COx) | TDS |
|-----------|-------|------------------------------------|------------------------------------|-------------|------------------------------------|------------------------------------|---------|-------------|------------------------------------|------------------------------------|---------|------|
| 450 | 57.1 | 17.3 | 9.9 | 6.2 | 0 | 0 | 76.5 | 3.5 | 0 | 0 | 43.7 | 23.5 |
| 475 | 62.2 | 20.3 | 12.6 | 5.8 | 1.0 | 0.4 | 72.5 | 3.6 | 0.6 | 0.2 | 45.1 | 26.5 |
| 500 | 67.7 | 22.4 | 15.2 | 5.1 | 2.6 | 1.3 | 68.6 | 3.5 | 1.8 | 0.9 | 46.4 | 28.8 |
| 525 | 69.7 | 30.1 | 21.0 | 4.6 | 5.3 | 2.6 | 57.4 | 3.2 | 3.7 | 1.8 | 40.0 | 37.3 |
| 550 | 71.6 | 26.8 | 19.2 | 4.5 | 8.5 | 4.4 | 55.8 | 3.2 | 6.1 | 3.2 | 40.0 | 35.7 |

The effect of temperature on conversion, selectivity and yield in *n*-hexane ODH over 0.5SbVMgO

| Temp (°C) | C (%) | S (C ₆ H ₆) | Y (C ₆ H ₆) | S (Hexenes) | S (C ₃ H ₈) | S (C ₃ H ₆) | S (COx) | Y (Hexenes) | Y (C ₃ H ₈) | Y (C ₃ H ₆) | Y (COx) | TDS |
|-----------|-------|------------------------------------|------------------------------------|-------------|------------------------------------|------------------------------------|---------|-------------|------------------------------------|------------------------------------|---------|------|
| 450 | 57.3 | 18.2 | 10.4 | 7.3 | 0 | 0 | 74.5 | 4.2 | 0 | 0 | 42.7 | 25.5 |
| 475 | 62.7 | 21.1 | 13.2 | 7.0 | 1.1 | 0.4 | 70.4 | 4.4 | 0.7 | 0.3 | 44.1 | 28.5 |
| 500 | 68.2 | 23.4 | 16.0 | 6.3 | 2.3 | 1.1 | 66.9 | 4.3 | 1.6 | 0.8 | 45.6 | 30.8 |
| 525 | 72.1 | 31.5 | 22.7 | 5.1 | 4.7 | 2.0 | 56.7 | 3.7 | 3.4 | 1.4 | 40.9 | 38.6 |
| 550 | 73.2 | 26.0 | 19.0 | 4.4 | 6.9 | 3.3 | 59.4 | 3.2 | 5.1 | 2.4 | 43.5 | 33.7 |

The effect of temperature on conversion, selectivity and yield in *n*-hexane ODH over 1SbVMgO

| Temp (°C) | C (%) | S (C ₆ H ₆) | Y (C ₆ H ₆) | S (Hexenes) | S (C ₃ H ₈) | S (C ₃ H ₆) | S (COx) | Y (Hexenes) | Y (C ₃ H ₈) | Y (C ₃ H ₆) | Y (COx) | TDS |
|-----------|-------|------------------------------------|------------------------------------|-------------|------------------------------------|------------------------------------|---------|-------------|------------------------------------|------------------------------------|---------|------|
| 450 | 60.3 | 18.1 | 10.9 | 7.7 | 0 | 0 | 74.2 | 4.6 | 0 | 0 | 44.7 | 25.8 |
| 475 | 63.4 | 20.3 | 12.9 | 6.5 | 0.9 | 0.4 | 71.9 | 4.1 | 0.6 | 0.3 | 45.6 | 27.2 |
| 500 | 67.5 | 22.7 | 15.3 | 6.1 | 2.2 | 1.1 | 67.9 | 4.1 | 1.5 | 0.7 | 45.8 | 29.9 |
| 525 | 72.8 | 28.7 | 20.9 | 5.3 | 4.8 | 2.5 | 58.7 | 3.9 | 3.5 | 1.8 | 42.7 | 36.5 |
| 550 | 73.0 | 24.1 | 17.6 | 4.7 | 7.0 | 3.5 | 60.7 | 3.4 | 5.1 | 2.6 | 44.3 | 32.3 |

The effect of temperature on conversion, selectivity and yield in *n*-hexane ODH over 2.5SbVMgO

| Temp (°C) | C (%) | S (C ₆ H ₆) | Y (C ₆ H ₆) | S (Hexenes) | S (C ₃ H ₈) | S (C ₃ H ₆) | S (COx) | Y (Hexenes) | Y (C ₃ H ₈) | Y (C ₃ H ₆) | Y (COx) | TDS |
|-----------|-------|------------------------------------|------------------------------------|-------------|------------------------------------|------------------------------------|---------|-------------|------------------------------------|------------------------------------|---------|------|
| 450 | 60.9 | 17.6 | 10.7 | 4.9 | 0 | 0 | 77.5 | 3.0 | 0 | 0 | 47.2 | 22.5 |
| 475 | 64.7 | 19.3 | 12.5 | 4.5 | 1.3 | 0.8 | 74.1 | 2.9 | 0.8 | 0.5 | 47.9 | 24.6 |
| 500 | 68.9 | 22.3 | 15.4 | 4.1 | 3.1 | 1.7 | 68.8 | 2.8 | 2.1 | 1.2 | 47.4 | 28.1 |
| 525 | 73.0 | 26.1 | 19.1 | 3.9 | 6.4 | 3.4 | 60.2 | 2.8 | 4.7 | 2.5 | 43.9 | 33.4 |
| 550 | 74.0 | 21.8 | 16.1 | 3.7 | 7.9 | 4.2 | 62.4 | 2.7 | 5.8 | 3.1 | 46.2 | 29.7 |

The effect of temperature on conversion, selectivity and yield in *n*-hexane ODH over 5SbVMgO

n-Octane ODH: *n*-Octane to air = 7.0% and GHSV = 4287 h⁻¹

| Temp (°C) | C (%) | S (olefin) | S (B+X) | S (Others) | S (EB) | S (STY) | S (CO _x) |
|-----------|-------|------------|---------|------------|--------|---------|----------------------|
| 300 | 3.8 | 76.4 | 0.1 | 2.2 | 0.5 | 1.1 | 19.7 |
| 350 | 48 | 38.2 | 0.4 | 5 | 2.1 | 6.2 | 48.1 |
| 400 | 51 | 31.8 | 0.9 | 6.6 | 2.5 | 7.3 | 50.9 |
| 450 | 55 | 23.4 | 1.3 | 7.5 | 2.9 | 6.9 | 58 |

Effect of temperature on selectivity and conversion in *n*-octane ODH over 19VMgO (Others = methylheptane, heptane, cracked products and unknowns)

n-Octane ODH: *n*-Octane to air = 4.2%, GHSV = 6678 h⁻¹ and temperature = 400 °C

| Catalyst | C (%) | S (STY) | Y (STY) | S (Olefins) | S (Aromatics) | S (Others) | S (CO _x) |
|----------|-------|---------|---------|-------------|---------------|------------|----------------------|
| 19VMgO | 66.9 | 22.1 | 14.7 | 24.3 | 29.9 | 4.2 | 41.6 |
| 2.5Mo | 70.1 | 24.3 | 17.3 | 20.1 | 32.5 | 5.1 | 42.3 |
| 2.5Cs | 61.4 | 19.7 | 12.0 | 27.8 | 29.0 | 3.2 | 40.0 |
| 1Sb | 74.3 | 25.6 | 19.0 | 17.7 | 32.8 | 4.4 | 45.1 |

Selectivity to products observed during *n*-octane ODH of 19VMgO and promoted 19VMgO (Others = Mainly cracked products, trace water soluble products (acetaldehyde and acetone) and unknowns)

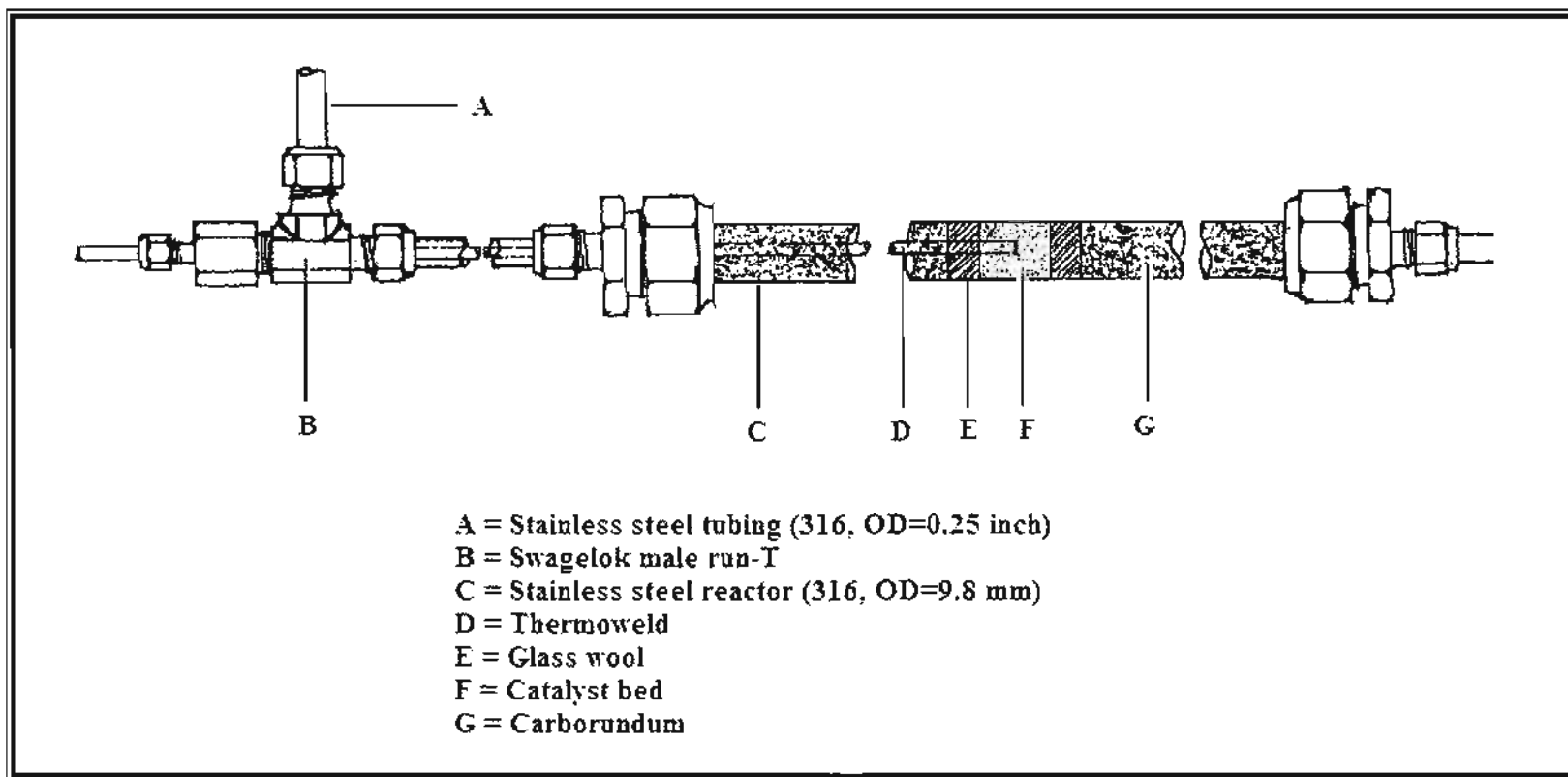


Figure 1B: Reactor tube showing feed line connection, thermoweld and catalyst bed

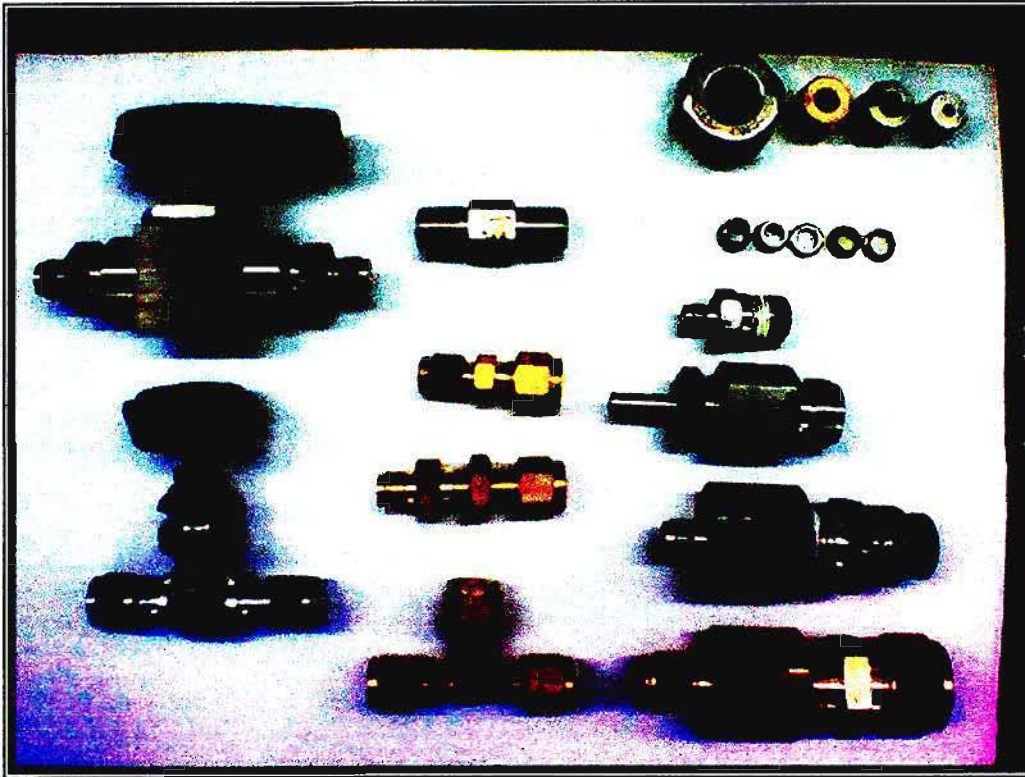


Figure 1C: Swagelok fittings used

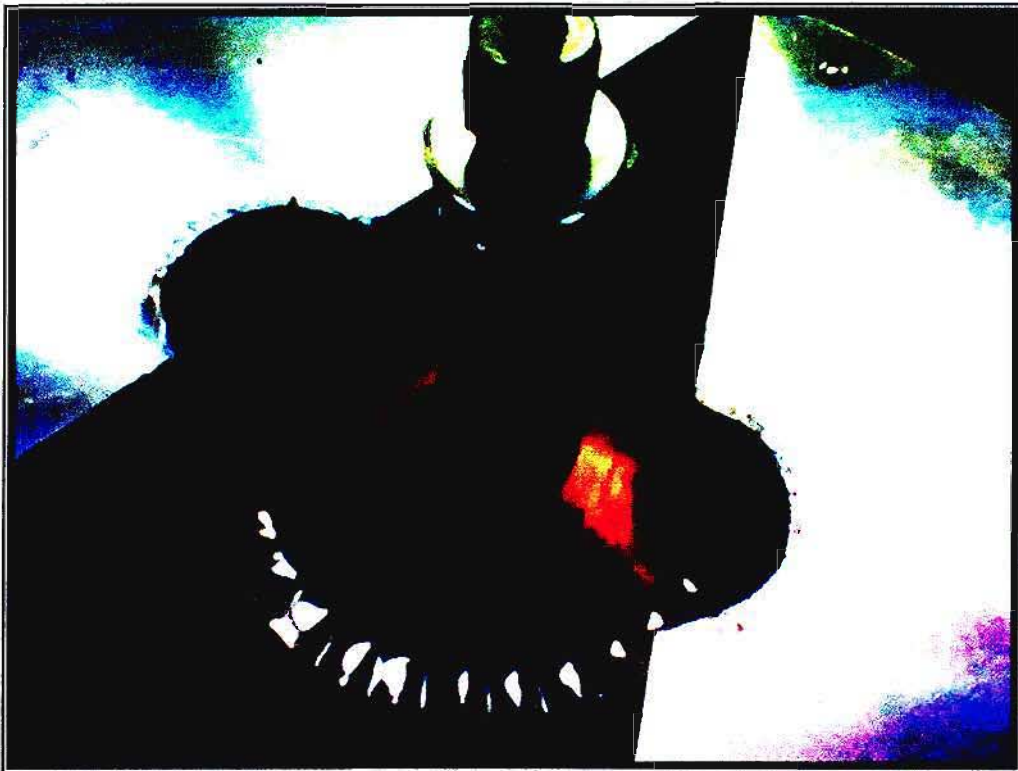


Figure 1D: Copper block surrounded by heating element



Figure 1E: Perkin Elmer XL Autosystem GC equipped with FID

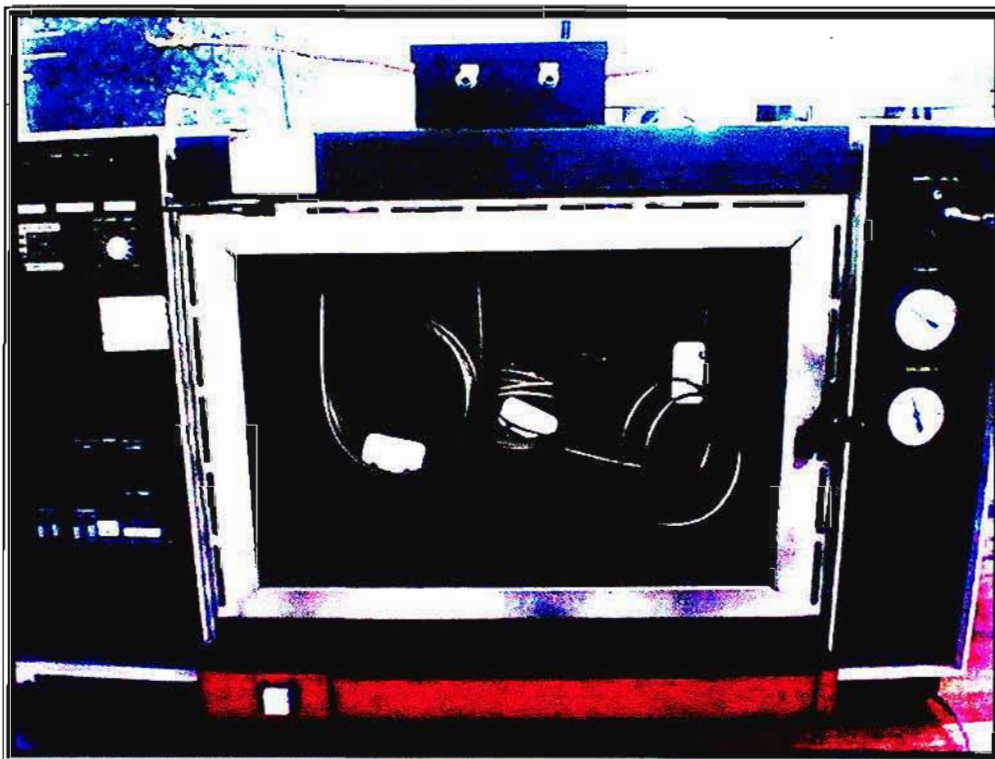


Figure 1F: Varian 3700 isothermal GC equipped with TCD

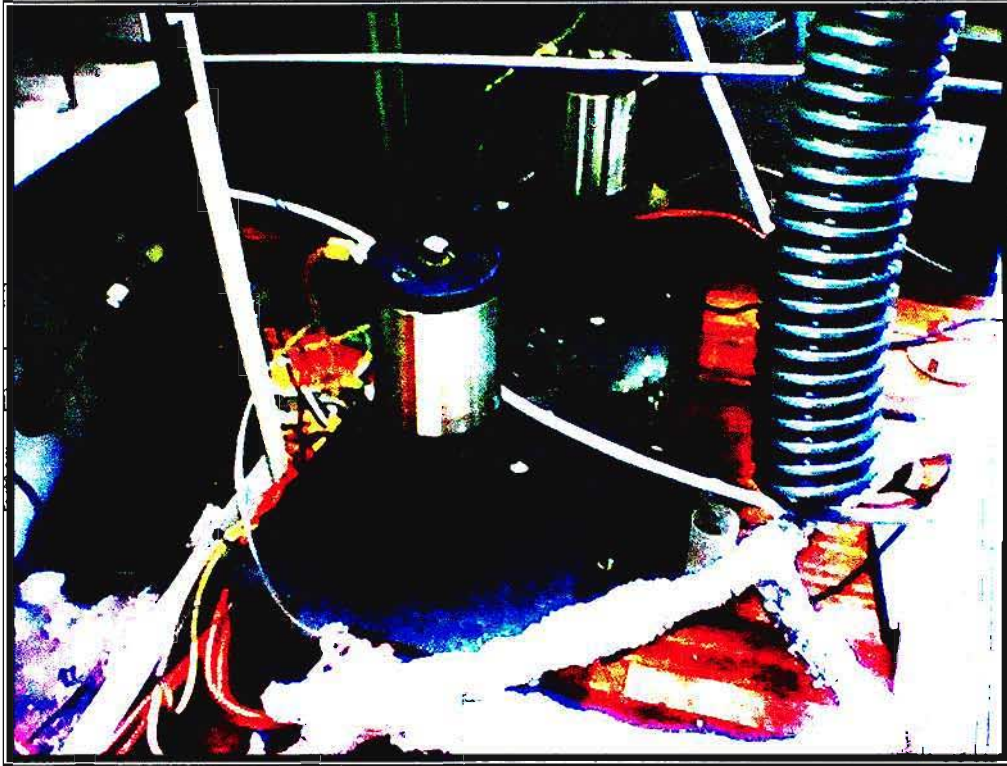


Figure 1G: Gas sampling valve box containing a 6 and a 10 port Valco Rotary Valve

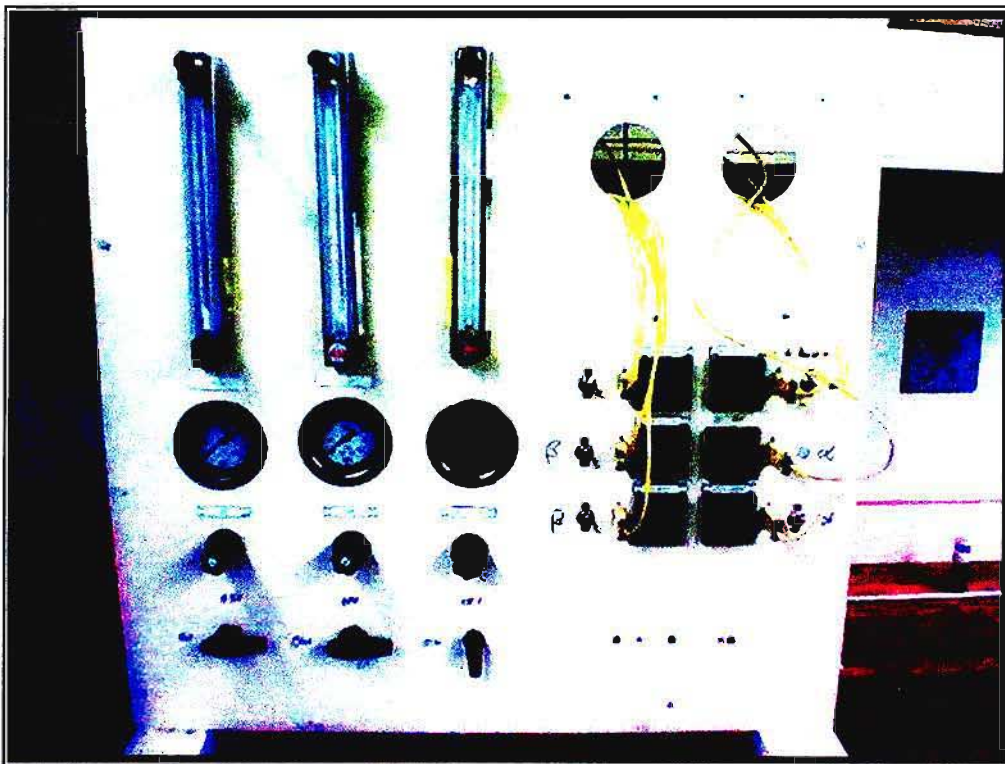


Figure 1H: Gas flow control panel containing rotameters, pressure regulators, pressure gauges and temperature controllers

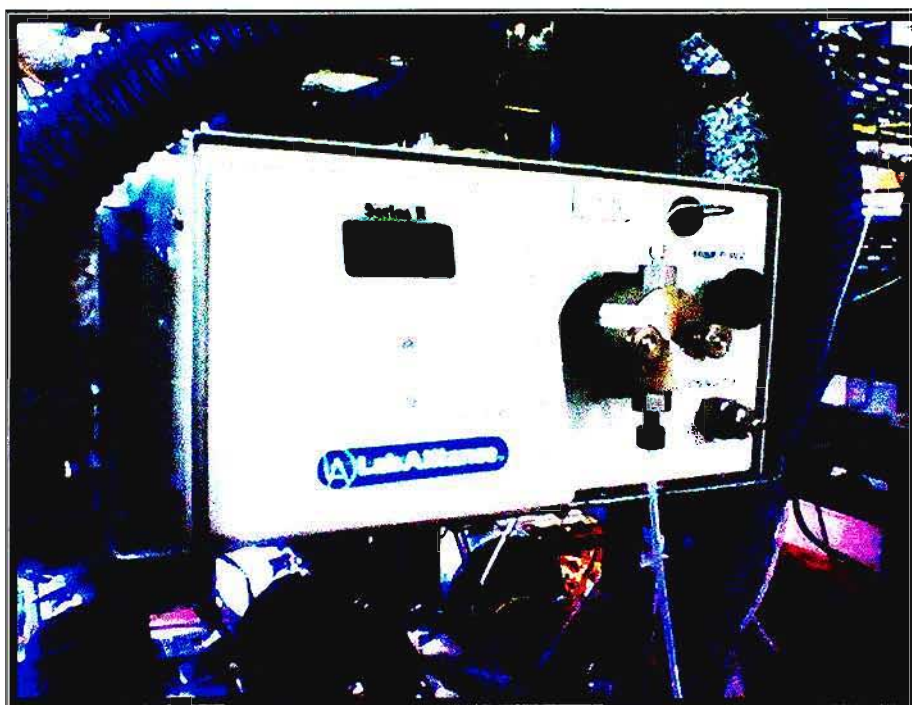


Figure 1I: HPLC pump



Figure 1J: Chiller container bubblers filled with hexane

GC parameters: Perkin Elmer XL Autosystem GC with FID

Turbochrom Method File: C:/MAINBA~1/XJC/AHEX.MTH

Channel Parameters:

Data will be collected from channel A

Channel A signal source: DetA

Channel B signal source: DetB

Analog Output: INT

Analog Output: INT

Attenuation: -4

Attenuation: 0

Offset: 0.5mV

Offset: 5.0mV

Delay Time: 0.00 min

Run time: 12.67 min

Sampling Rate: 6.2500pts/s

Carriers Parameters:

Carrier A control: Press – N2

Column A Length: 30.00 m diameter: 320um

Vacuum compensation: OFF

Split Control Mode: FLOW Setpoint: 50.2mL/m

Initial Setpoint: 5.0PSIG Initial Hold: 3.00min

Ramp 1 : 0.5 PSIG/min to 10.0 PSIG, hold for 2 min

Ramp 2: 2.0 PSIG/min to 18.0 PSIG, hold for 999.0 min

Carrier B control : Press – PSIG

Carrier B Setpoint : 0.0 PSIG

Valve configuration and settings:

Valve 1: Split ON

Valve 2: Split OFF

Valve 3: GSV OFF

Valve 4: NONE

Valve 5: NONE

Valve 6: NONE

Detector Parameters:

Detector A: FID

Detector B: NONE

Range: 20

Time constant: 200

Heated Zones:

Injector A: PSSI

Initial setpoint: 220°

Injector B: CAP

Detector A: 250°

Initial hold: 999.00min

Injector B setpoint; 200°

Detector B: 0°

Oven Programme:

Cryogenics: OFF

Initial TEMP: 55°

Initial Hold: 1.00 min

Ramp1: 15.0°/min to 200°, hold for 2.00 min

Total Run Time: 12.67 min

Maximum Temp: 300°

Equilibration Time: 0.2 min

Timed Events:

V2 set to OFF at 0.00 min

V3 set to OFF at 0.01 min

V2 set to ON at 0.02 min

V2 set to OFF at 0.08 min

V3 set to ON at 0.60min

V3 set to OFF at 0.68min

Real Time Plot Parameters:

Channel A –Pages:1 Offset: 0.0 mV Scale: 1000.0mV

Channel B – Pages: 1 Offset: 0.0mV Scale: 1000.0 mV

Processing Parameters:

Bunch Factor: 1 points

Noise Threshold: 73uV

Area Threshold: 367.0uV

Peak Separation Criteria:

Width Ratio: 0.200

Valley to Peak Ratio: 0.010

Exponential Skim Criteria

Peak Height Ratio: 5.0

Valley Height Ratio: 3.0

Adjusted Height Ratio: 4.0

Column used:

Chrompak capillary column

Coating: CP-Sil 24CB

Dimensions: Length = 30 m

OD = 0.45 mm

ID = 0.32 mm

Max temperature: 250 °C

GC parameters: Isothermal Varian 3700 with TCD

| | |
|---------------------------|----------------------------------|
| Detector temperature: | 130 °C |
| Column temperature: | 22 °C |
| Injector temperature: | 150 °C |
| TCD filament temperature: | 150 °C |
| Output: | Negative |
| Range: | 0.5 mV |
| Carrier gas: | Helium (Afrox, Instrument grade) |

Column used:

Pre-column:

| | |
|--------------------|--|
| | Stainless steel |
| Support: | Chromosorb WHPSP |
| Dimensions: | Length = 1 m OD = 1/8" ID = 2.2 mm |
| Mesh range: | 80/100 |
| Liquid phases: | OV-225 (10%) |
| Temperature range: | 20-275 °C |

Analytical Column:

| | |
|------------------|--|
| | Stainless steel |
| Support: | Carboxen™ 1000 |
| Dimensions: | Length = 2.5 m OD = 1/8" ID = 2.2 mm |
| Mesh range: | 60/80 |
| Max temperature: | 20-275 °C |

APPENDIX 2: MSDS

MSDS: Hexane

Common synonyms

n-hexane, normal hexane

Formula

C₆H₁₄

Physical properties

Form: colourless liquid with a petrol-like smell

Stability: Stable, but highly flammable

Melting point: -95 C

Flash point: -23 C

Specific gravity: 0.659

Vapour pressure: 132 mm Hg at 20 C

Boiling point: 69 C

Water solubility: negligible

Vapour density: 3 (air = 1)

Explosion limits: 1.2 - 7.7%

Antoine Equation Parameters:

| Temperature (K) | A | B | C |
|-----------------|---------|----------|---------|
| 177.70 - 264.93 | 3.45604 | 1044.038 | -53.893 |
| 286.18 - 342.69 | 4.00266 | 1171.530 | -48.784 |

Principal hazards

Hexane is very flammable. Because it is highly volatile, dangerous concentrations can develop in ambient air, creating a possible explosion risk.

Safe handling

Always wear safety glasses. Do not work in an area in which sources of ignition, such as a Bunsen burner or hot air gun, are used. Ensure good ventilation at all times - use a fume cupboard for your work if possible.

Emergency

Eye contact: Immediately flush the eye with plenty of water. If irritation persists, call for medical help.

Skin contact: Wash off with plenty of water. Remove any contaminated clothing immediately. Note that clothes soaked in hexane will present an extreme fire risk, so rapid action is essential. If the skin reddens or appears damaged, call for medical aid.

If swallowed: Call for immediate medical help.

Disposal

Hexane does not dissolve in water and must not be flushed down the drain.

Protective equipment

Safety glasses. If you need gloves, nitrile or PVA are suitable.

MSDS: **Octane**

Common synonyms

n-octane, normal octane

Formula

C₈H₁₈

Form: Colourless liquid

Stability: Stable, but very flammable

Melting point: -57 C

Flash point: 15 C

Specific gravity: 0.703

Boiling point: 126 C

Water solubility: negligible

Explosion limits: 1.0 - 6.5%

Physical properties

Antoine Equation Parametrs:

| Temperature (K) | A | B | C |
|-----------------|---------|----------|---------|
| 216.59 - 297.10 | 5.20120 | 1936.281 | -20.143 |
| 326.08 - 399.72 | 4.04867 | 1355.126 | -63.633 |

Principal hazards

Octane is very flammable. It evaporates rapidly and readily reaches a concentration in air at which an explosion is possible.

Safe handling

Wear safety glasses.

Before starting work make sure that there is nothing close at hand that might be a source of ignition. Octane may be ignited with a hot air gun, hot plate or even a hot water pipe. Make sure that you know where the fire extinguishers are kept before starting work.

Emergency

Eye contact: Immediately flush the eye with water. If irritation persists call for medical help.

Skin contact: Wash off with plenty of water. Remove any contaminated clothing. Note that clothing soaked in octane will be an EXTREME FIRE RISK; its immediate removal and storage in a safe place is essential. If the skin reddens or appears damaged, call for medical aid.

If swallowed: Call for immediate medical help.

Disposal

Octane must not be flushed down drains. There should be local rules that specify how this liquid will be stored before disposal.

Protective equipment

Safety glasses. If gloves are required use nitrile.

MSDS: Benzene

Common synonyms

None

Formula

C₆H₆

Physical properties

Form: colourless liquid
Stability: Stable, but very flammable
Melting point: 5.5 C
Water solubility: negligible
Specific gravity: 0.87

Principal hazards

Benzene is a carcinogen (cancer-causing agent).
Very flammable. The pure material, and any solutions containing it, constitute a fire risk.

Safe handling

Benzene should NOT be used at all unless no safer alternatives are available. If benzene must be used in an experiment, it should be handled at all stages in a fume cupboard. Wear safety glasses and use protective gloves.

Emergency

Eye contact: Immediately flush the eye with plenty of water. Continue for at least ten minutes and call for immediate medical help.
Skin contact: Wash off with soap and water. Remove any contaminated clothing. If the skin reddens or appears damaged, call for medical aid.
If swallowed: Call for immediate medical help.

Disposal

It is dangerous to try to dispose of benzene by washing it down a sink, since it is toxic, will not dissolve and presents a fire risk. It is probable that trying to dispose of benzene in this way will also break local environmental rules. Instead, retain in a safe place in the laboratory (well away from any source of ignition) for disposal with other flammable, non-chlorinated solvents.

Protective equipment

Safety glasses. If gloves are worn, PVA, butyl rubber and viton are suitable materials.

MSDS: Styrene

| | |
|----------------------|---|
| Common synonyms | Vinylbenzene, ethenylbenzene |
| Formula | C_8H_8 |
| Physical properties | Form: colourless oily liquid Stability: Stable in the presence of inhibitor, which is generally added to commercial product. Tends to polymerize once the inhibitor is removed, especially in the presence of radical initiators or light Melting point: -31 C Boiling point: 145 C Specific gravity: 0.91 Flash point: 31 C |
| Principal hazards | Styrene is believed to be a carcinogen (cancer-causing agent) Long-term exposure may cause <u>CNS</u> damage. |
| Safe handling | Wear safety glasses. Do not use this material in the open lab unless ventilation is very good. Normally work should be done in a fume cupboard. Use protective gloves. |
| Emergency | Eye contact: Immediately flush the eye with plenty of water. Call for medical help. Skin contact: Wash off with soap and water. Remove any contaminated clothing. If the skin reddens or appears damaged, call for medical aid. If swallowed: Call for immediate medical help |
| Disposal | Do not pour solutions containing styrene down the drains - this chemical is toxic and flammable. Store with non-chlorinated waste solvent for subsequent disposal. |
| Protective equipment | Safety glasses. PVA gloves are suggested. |

APPENDIX 3: UNPROMOTED VMgO

XRD data

Instrument: Philips PW 1130

Experimental conditions:

X-ray source : Cobalt
 Voltage : 40 kV
 Amperage : 25 mA
 Divergence slit : 1 °
 Receiver slit : 0.15 °
 Scan from : 5 °2θ
 Step size : 0.05 °2θ
 Count between steps : 2 seconds
 Used wavelength : K-Alpha (1.78897 Å)

| V ₂ O ₅ (2θ) | | | | | MgO (2θ) | | |
|------------------------------------|-------|-------|-------|-------|----------|-------|-------|
| 8.44 | 43.73 | 58.19 | 72.39 | 85.81 | 16.29 | 43.25 | 74.06 |
| 17.96 | 44.95 | 60.29 | 73.63 | 86.51 | 17.87 | 44.39 | 77.30 |
| 23.69 | 47.02 | 61.22 | 73.81 | 87.13 | 21.73 | 44.91 | 79.84 |
| 25.39 | 48.31 | 61.86 | 76.68 | 89.31 | 24.83 | 50.37 | 81.78 |
| 30.52 | 49.29 | 63.38 | 77.37 | | 29.70 | 52.37 | 89.54 |
| 36.23 | 52.38 | 65.62 | 78.60 | | 32.02 | 59.65 | |
| 37.79 | 53.37 | 66.45 | 81.38 | | 33.62 | 69.38 | |
| 38.96 | 55.57 | 69.18 | 82.16 | | 36.16 | 70.19 | |
| 40.08 | 56.29 | 69.77 | 83.07 | | 38.51 | 71.43 | |
| 42.13 | 57.41 | 71.02 | 84.02 | | 39.47 | 73.88 | |

Table 3A: 2θ values obtained for V₂O₅ and MgO

| 14VMgO 2θ | 16VMgO 2θ | 19VMgO 2θ | 24VMgO 2θ | 35VMgO 2θ | 49VMgO 2θ | 60VMgO 2θ |
|--------------|--------------|--------------|--------------|--------------|--------------|--------------|
| 44.95 | 43.33 | 41.06 | 40.77 | 40.81 | 41.18 | 41.19 |
| 50.40 | 44.95 | 43.19 | 43.25 | 41.84 | 42.00 | 42.06 |
| 52.33 | 50.36 | 44.96 | 44.88 | 43.20 | 43.25 | 42.89 |
| 73.85 | 52.35 | 50.29 | 50.30 | 44.93 | 44.90 | 44.90 |
| 77.33 | 73.85 | 52.41 | 52.24 | 50.33 | 50.44 | 50.40 |
| 79.32 | 77.32 | 73.76 | 73.80 | 52.39 | 52.30 | 52.33 |
| | 79.61 | 77.28 | 77.24 | 73.83 | 73.74 | 73.70 |
| | | | | 77.33 | 77.27 | 77.34 |
| | | | | | 79.31 | 79.31 |
| | | | | | 81.22 | 81.21 |

Table 3B: 2θ values obtained for the 14VMgO, 16VMgO, 19VMgO, 24VMgO, 35VMgO, 49VMgO and 60VMgO.

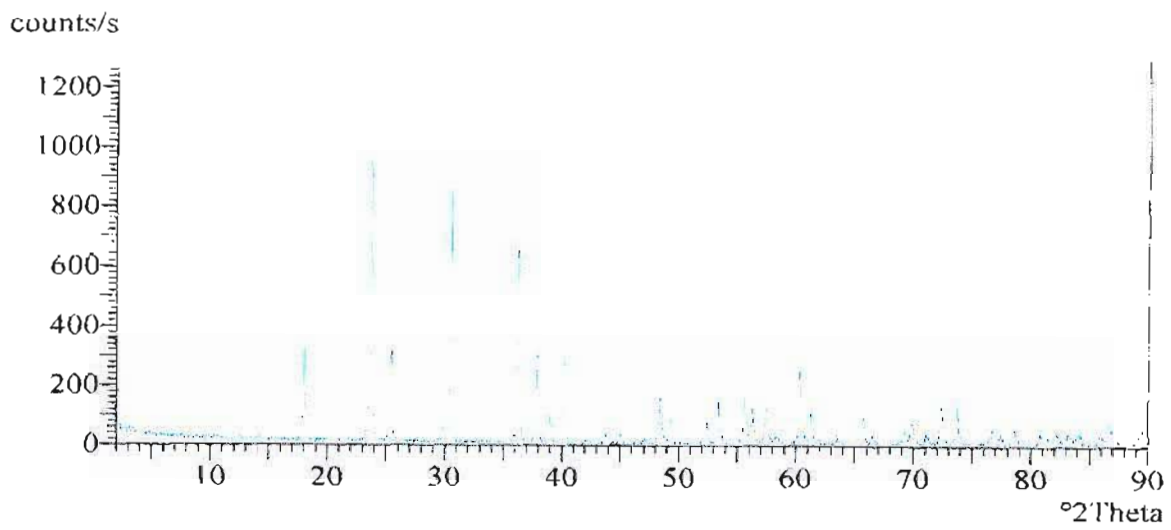


Figure 3A: XRD of V_2O_5

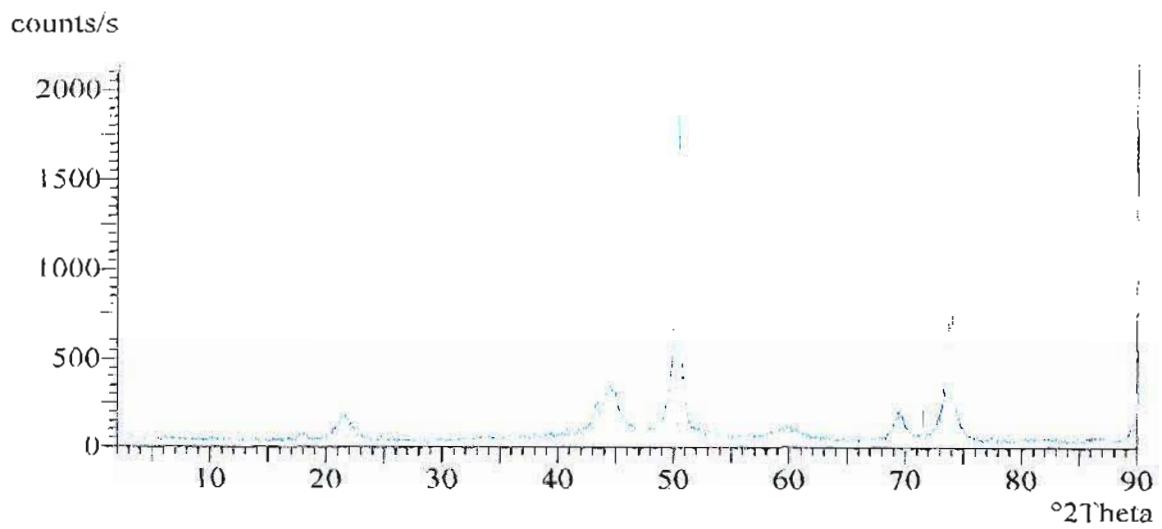


Figure 3B: XRD of MgO

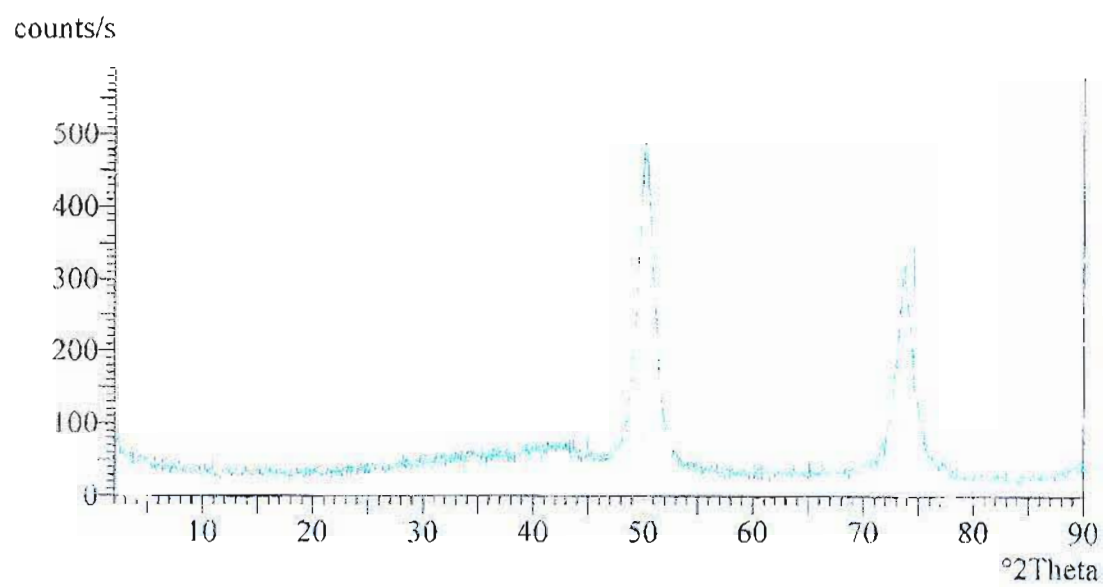


Figure 3C: XRD spectrum of 14VMgO

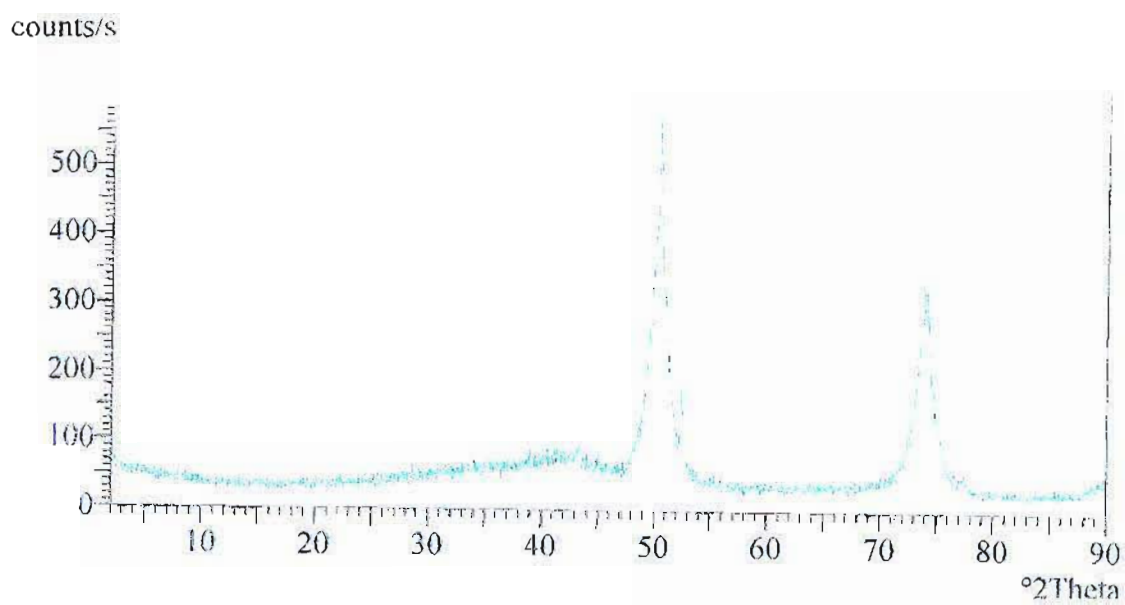


Figure 3D: XRD spectrum of 16VMgO

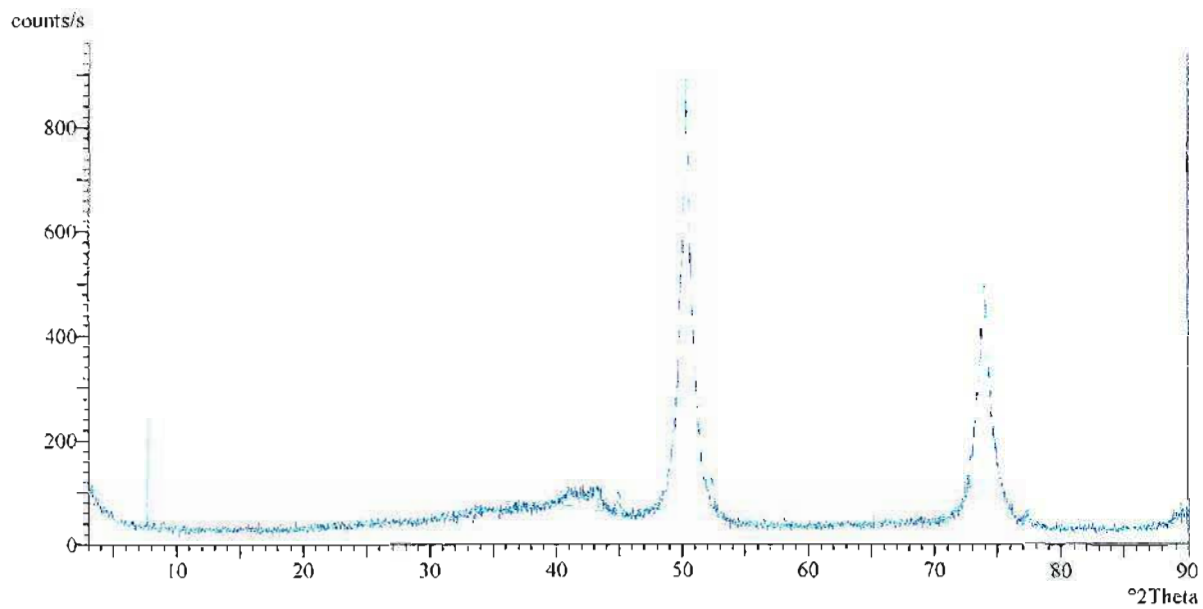


Figure 3E: XRD spectrum of 19VMgO

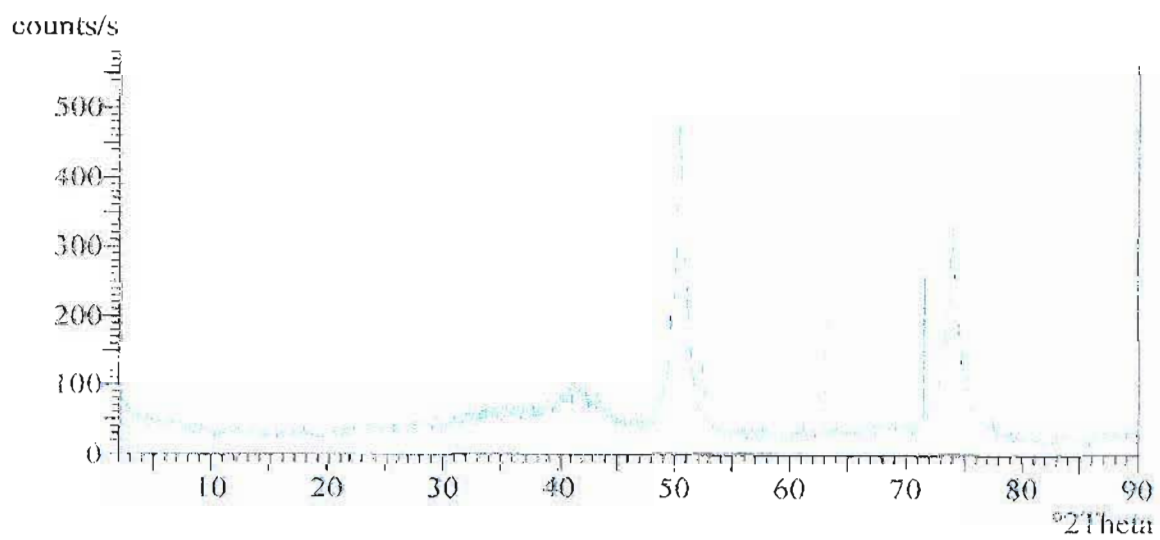


Figure 3F: XRD spectrum of 24VMgO

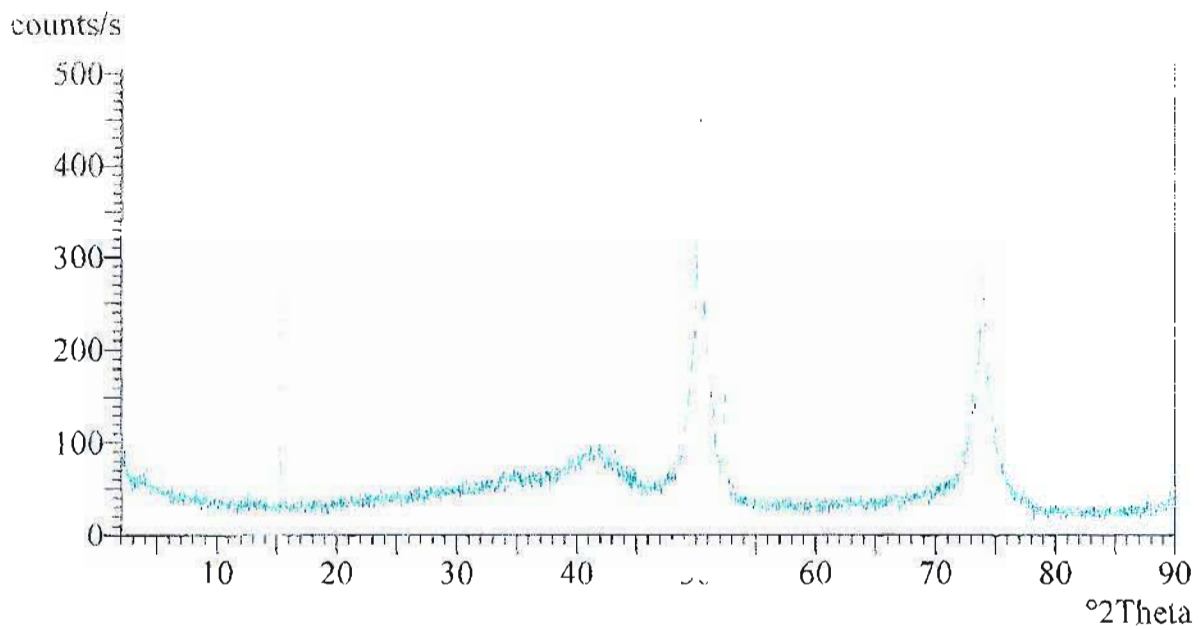


Figure 3G: XRD spectrum of 35VMgO

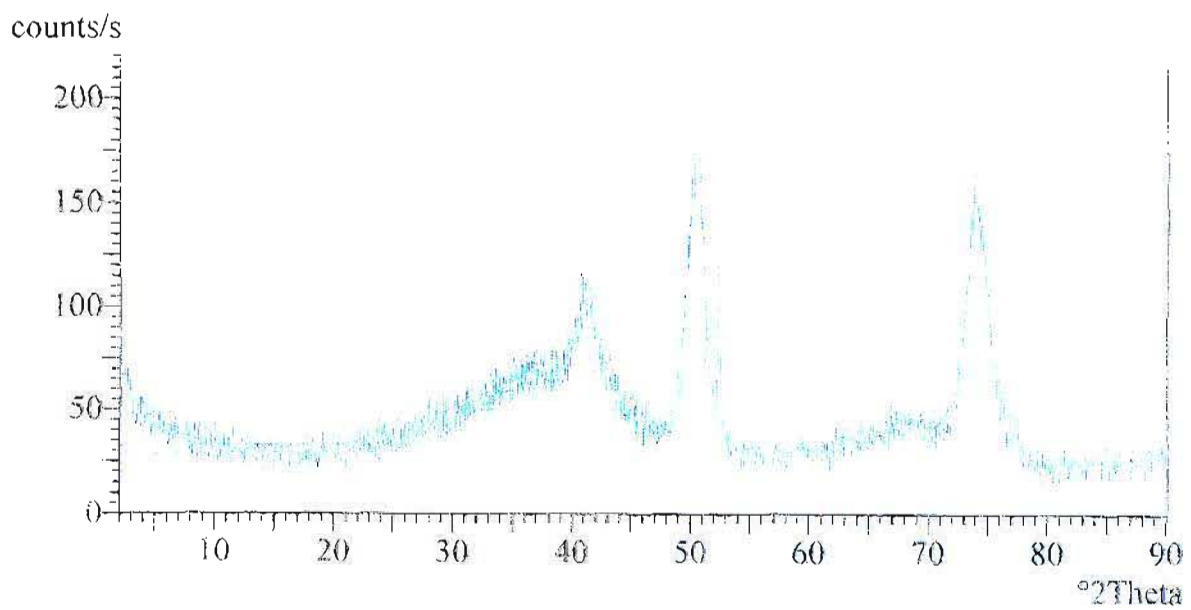


Figure 3H: XRD spectrum of 49VMgO

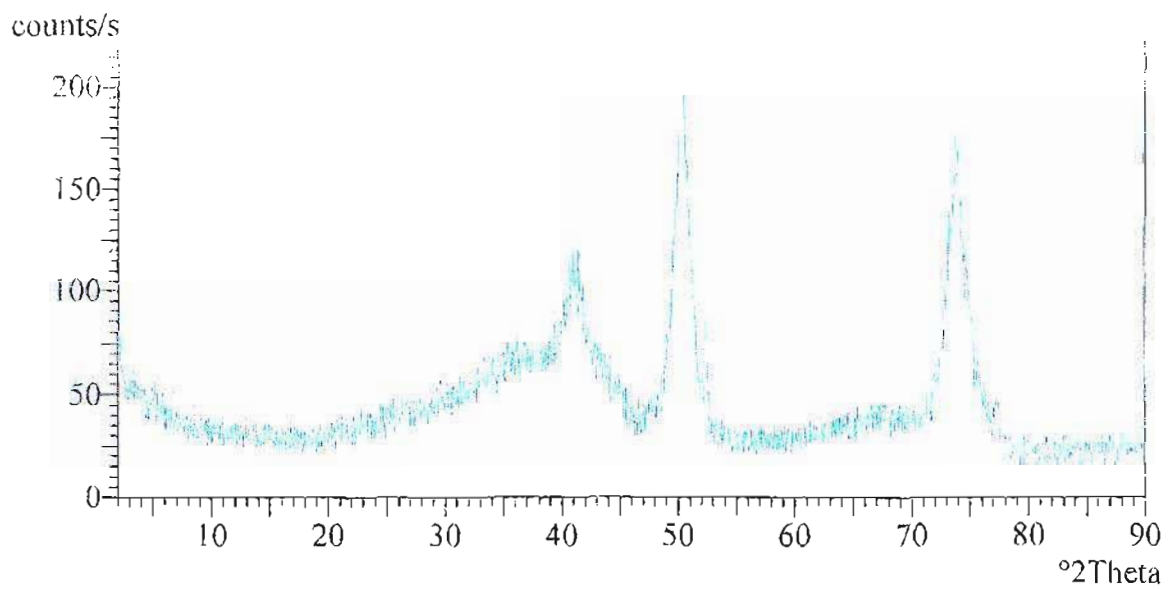


Figure 3I: XRD spectrum of 60VMgO

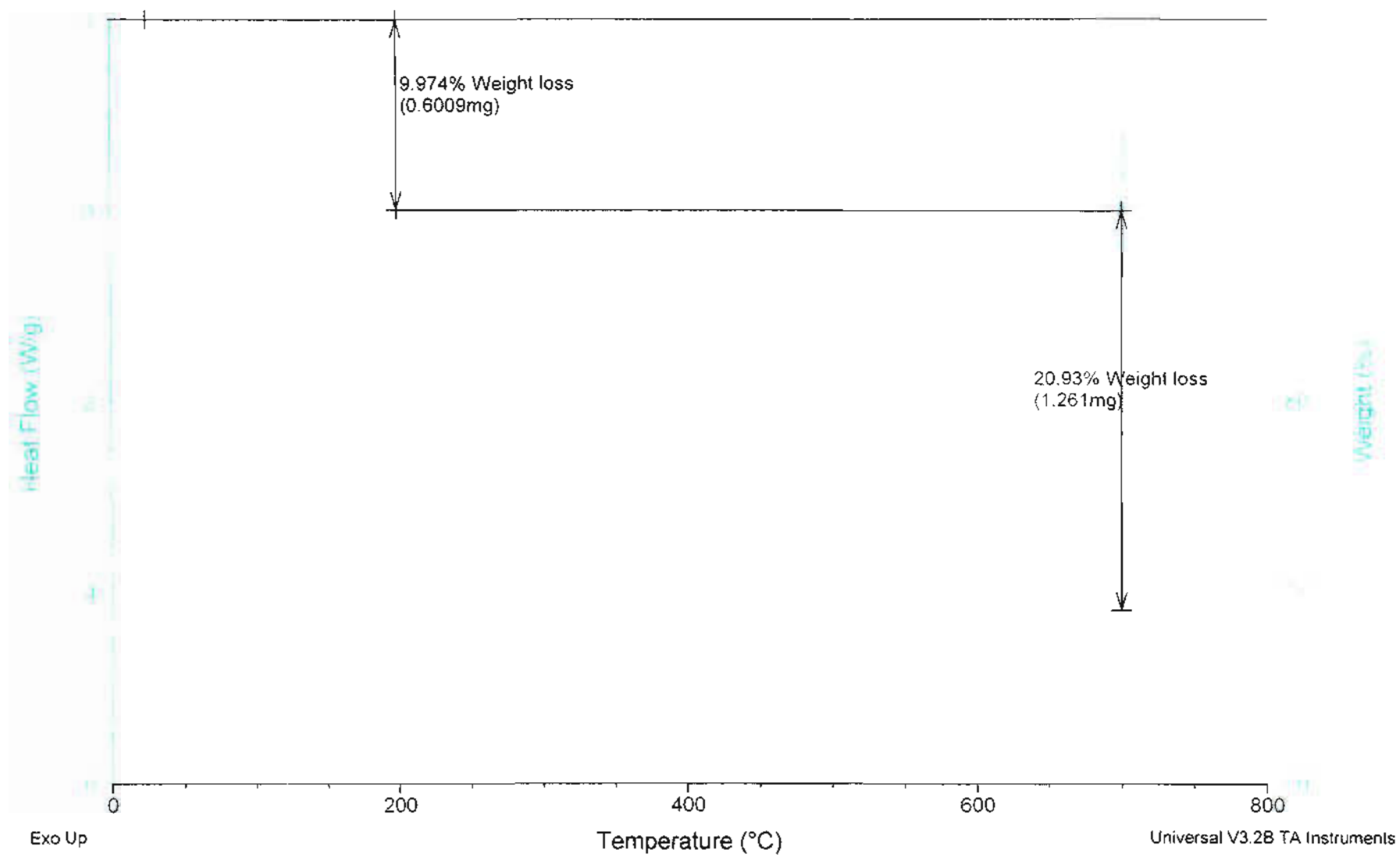


Figure 3J: DSC-TGA of 24VMgO

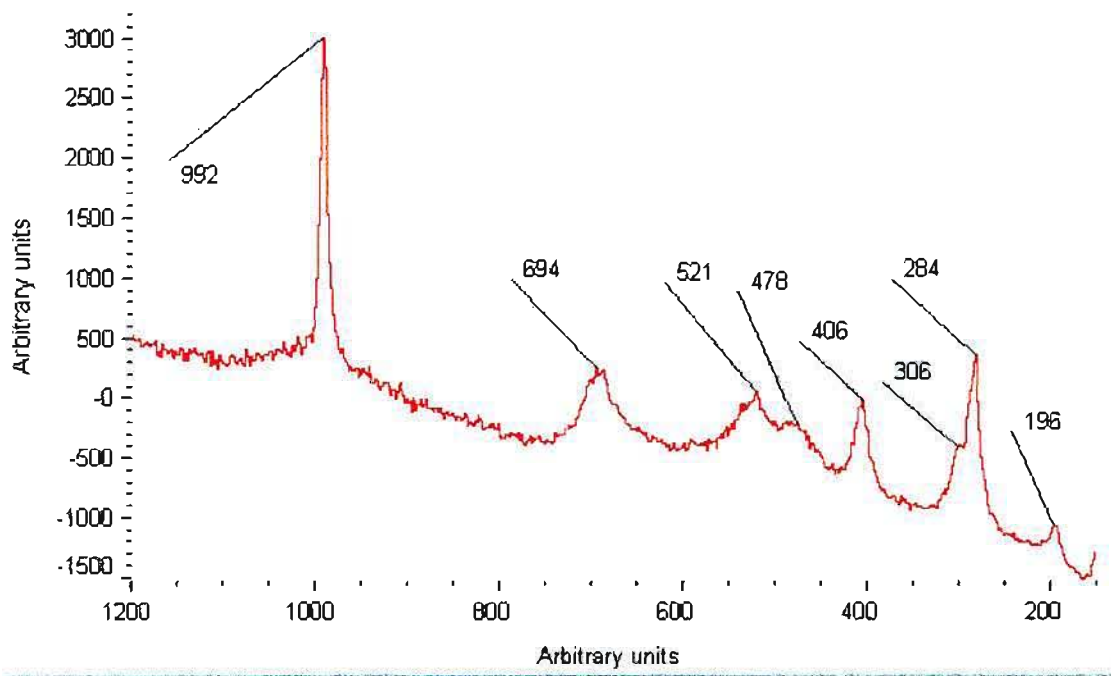


Figure 3K: Raman spectrum of V₂O₅

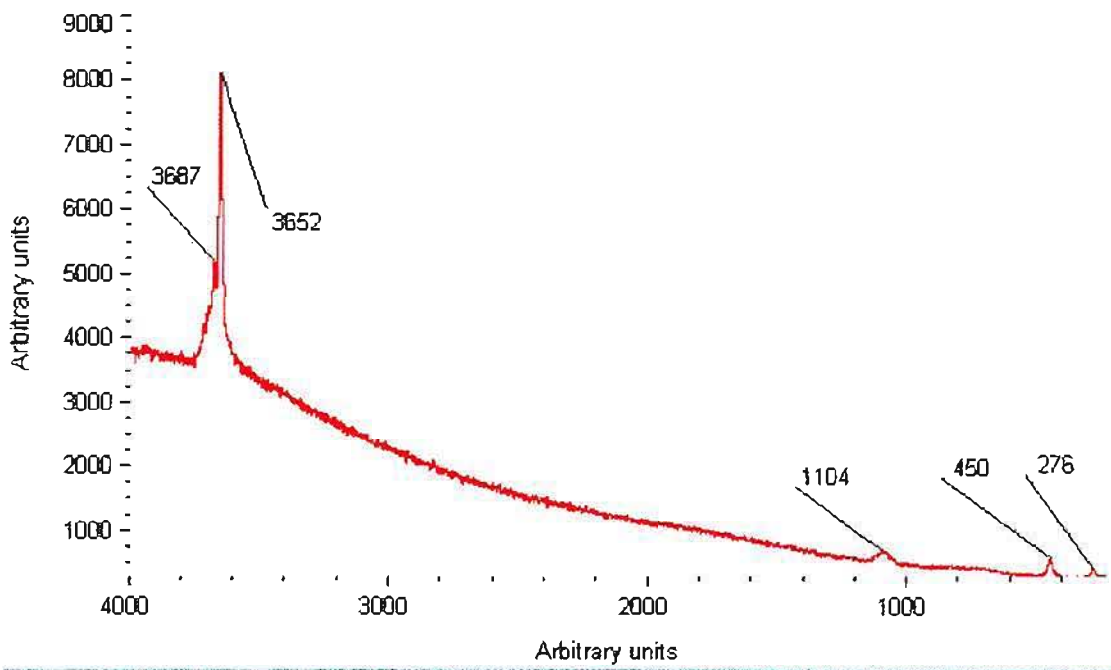


Figure 3L: Raman spectrum of MgO

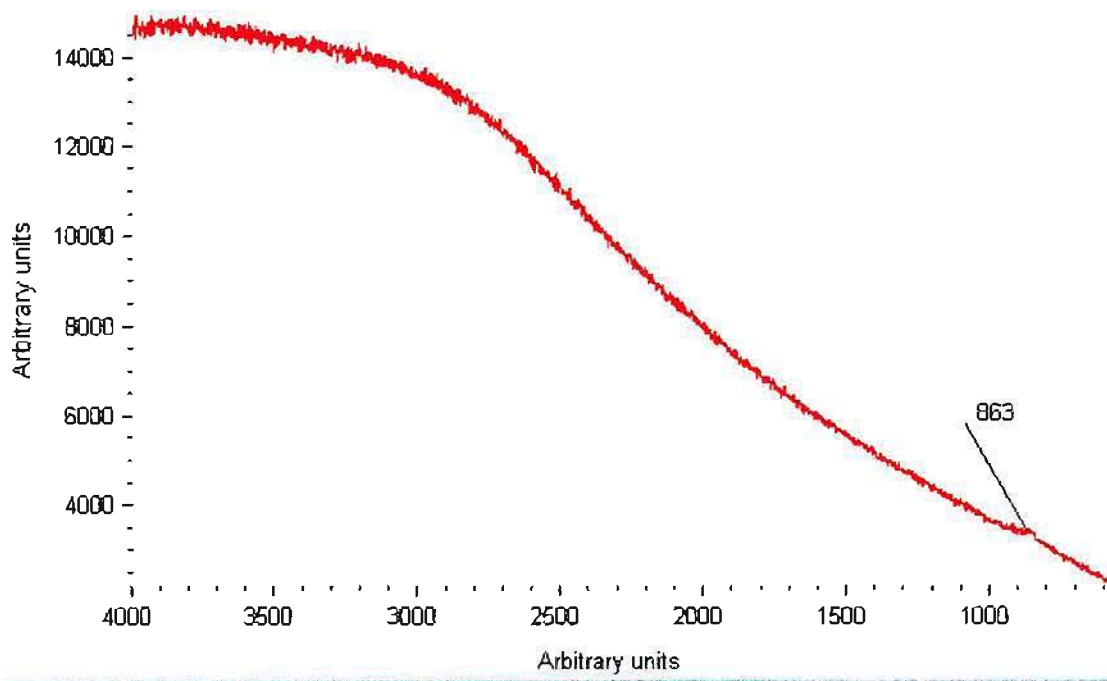


Figure 3M: Raman spectrum of 14VMgO

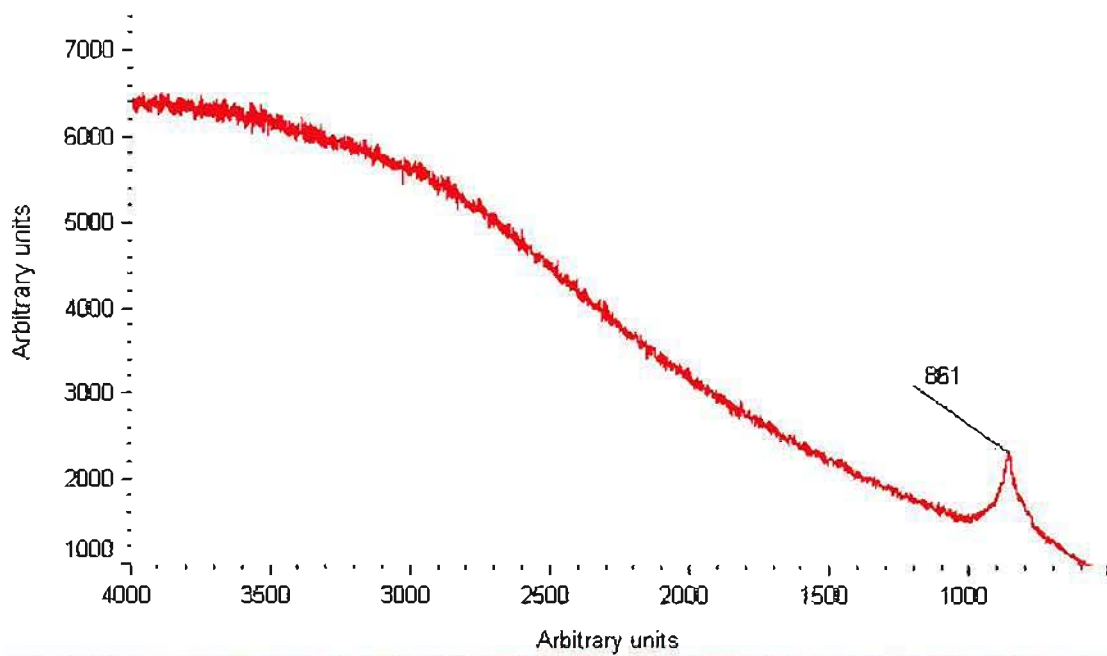


Figure 3N: Raman spectrum of 16VMgO

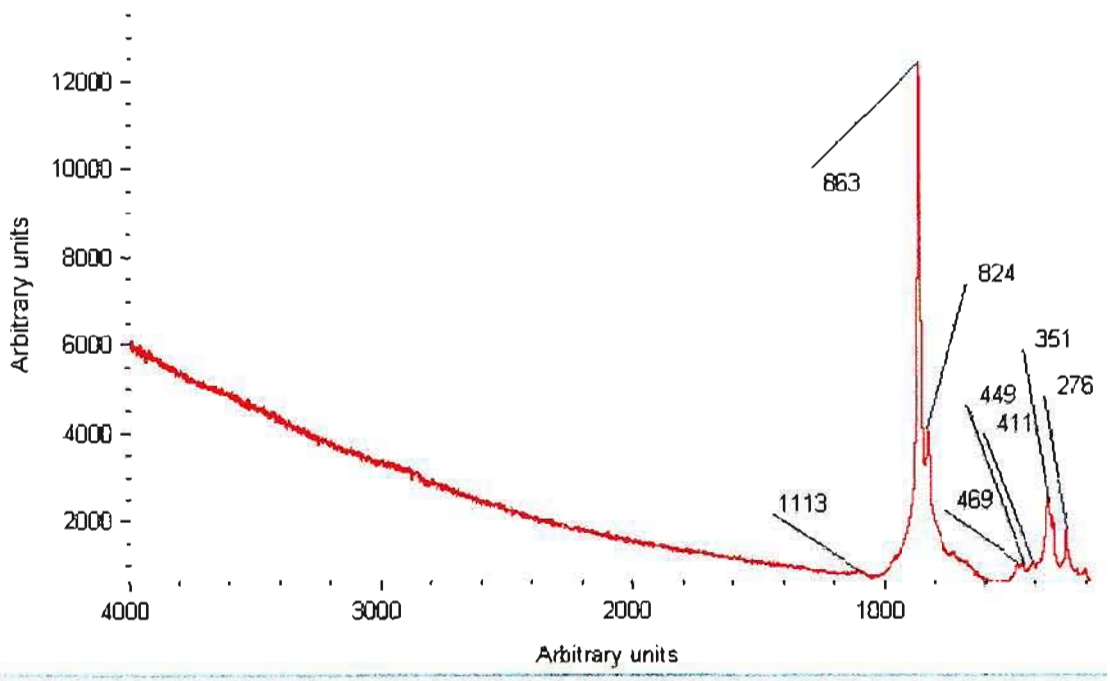


Figure 3O: Raman spectrum of 19VMgO

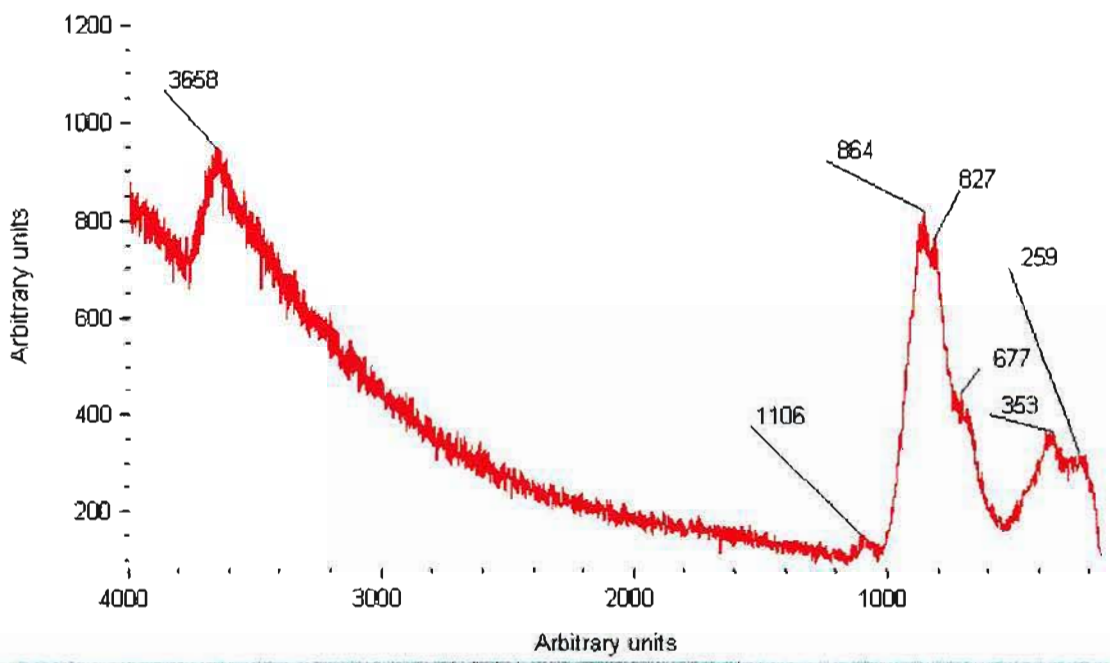


Figure 3P: Raman spectrum of 24VMgO

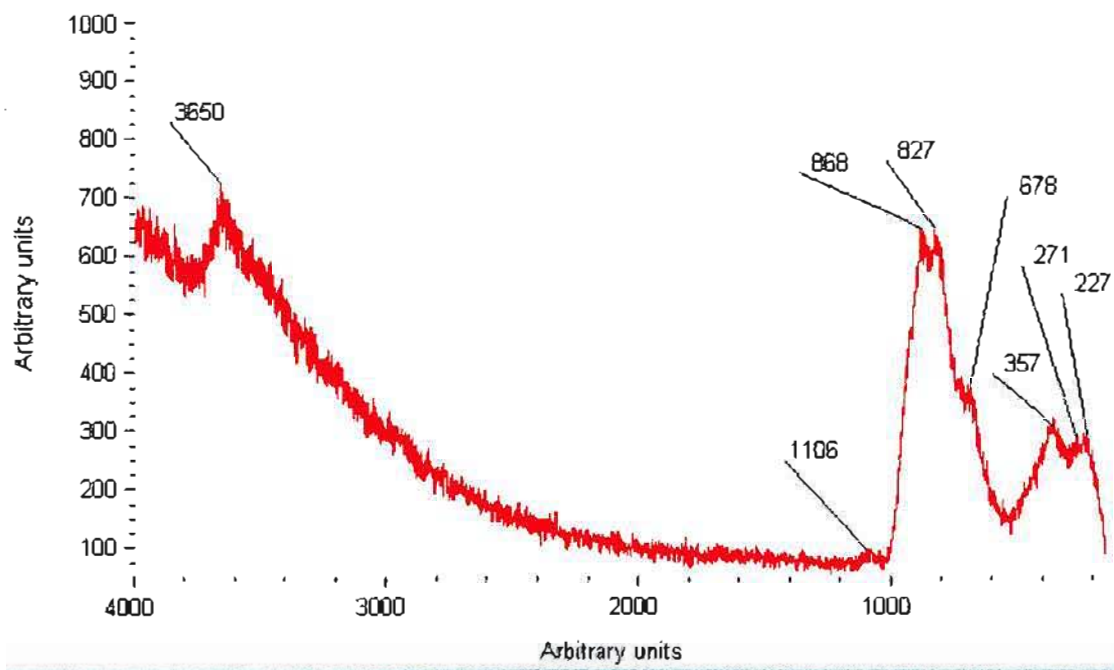


Figure 3Q: Raman spectrum of 35VMgO

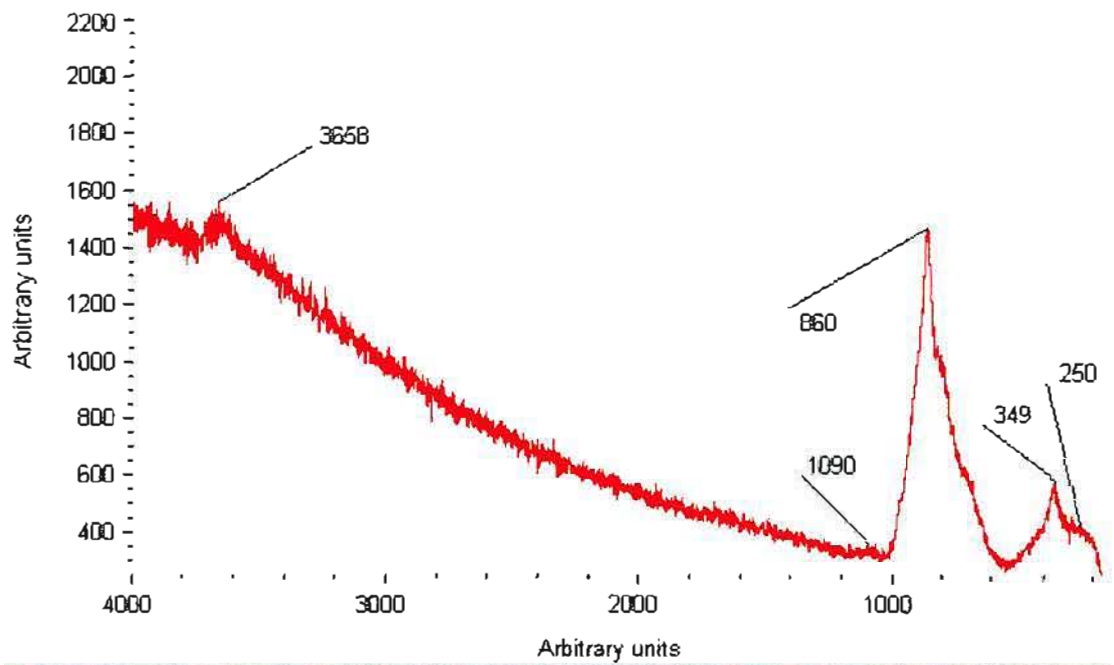


Figure 3R: Raman spectrum of 49VMgO

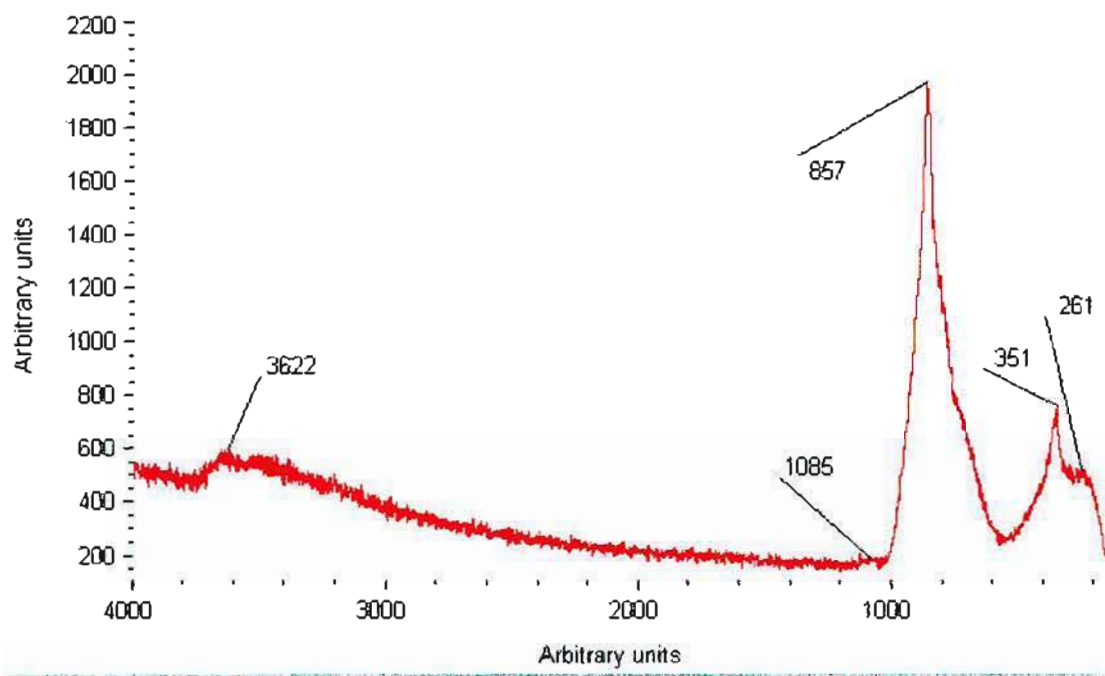


Figure 3S: Raman spectrum of 60VMgO

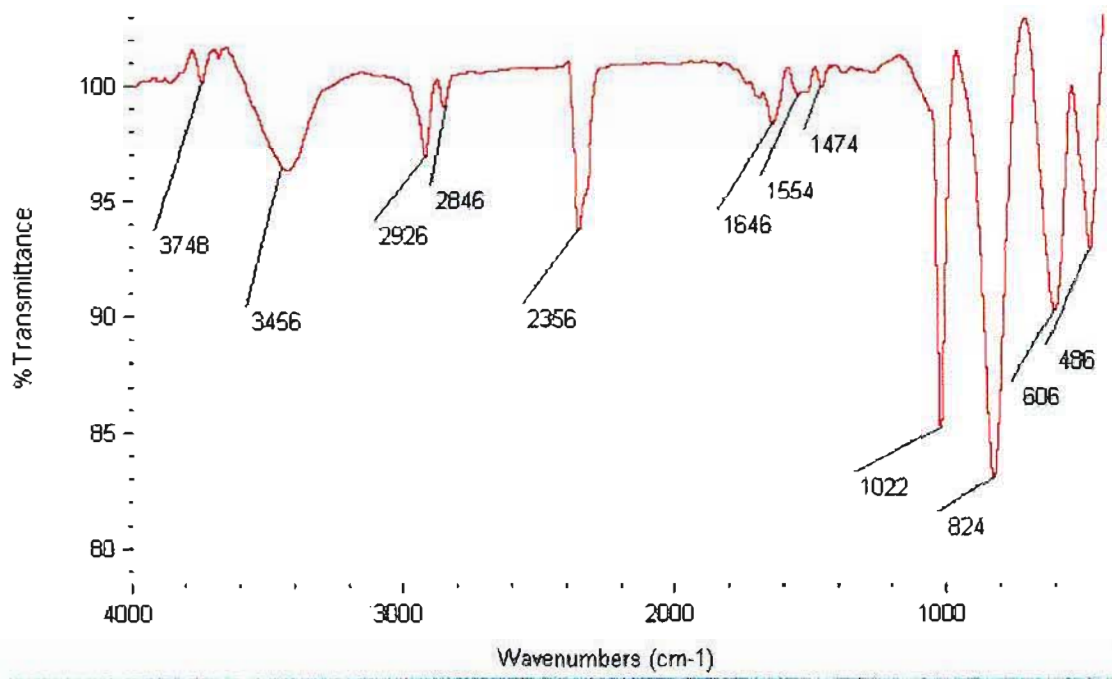


Figure 3T: FTIR spectrum of V₂O₅

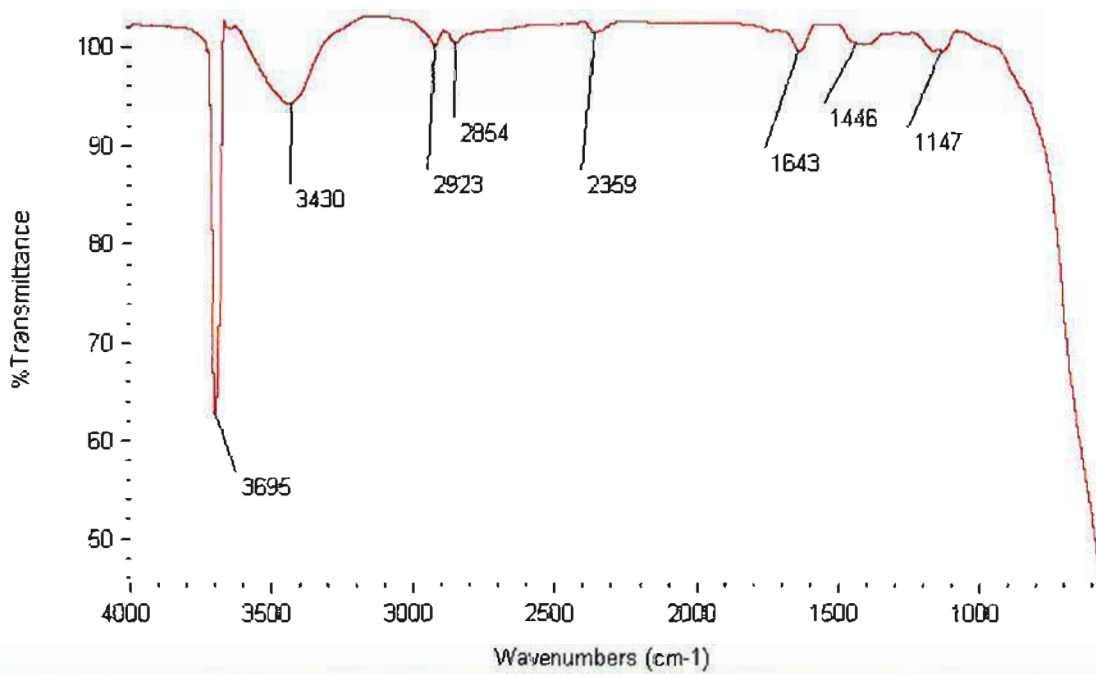


Figure 3U: FTIR spectrum of MgO

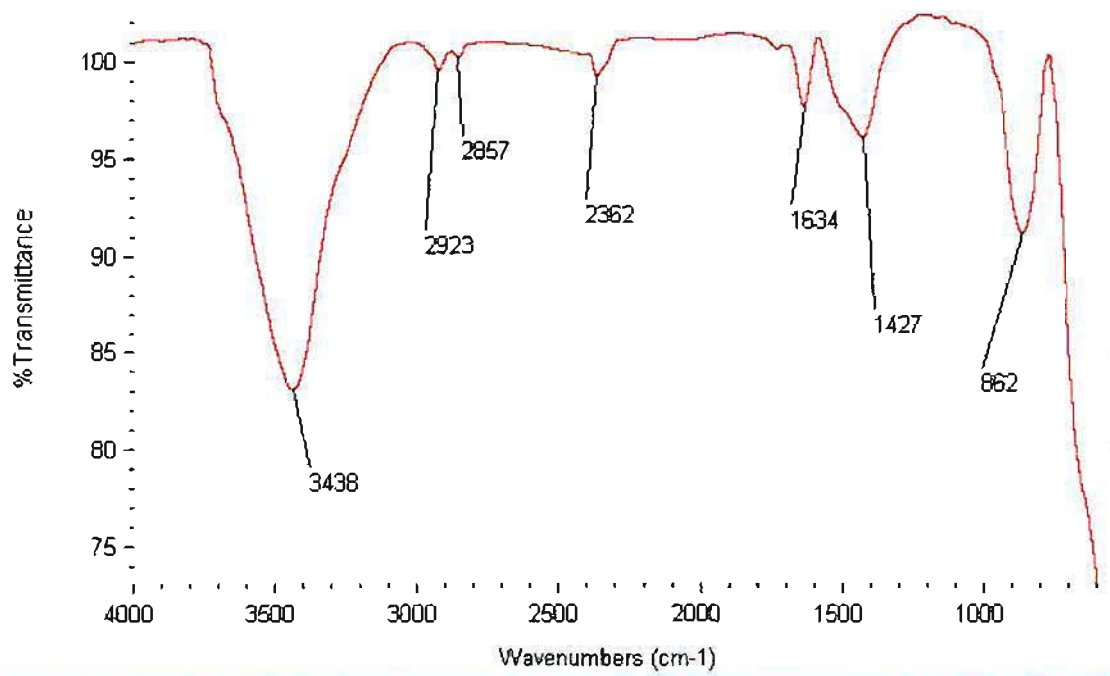


Figure 3V: FTIR spectrum of 14VMgO

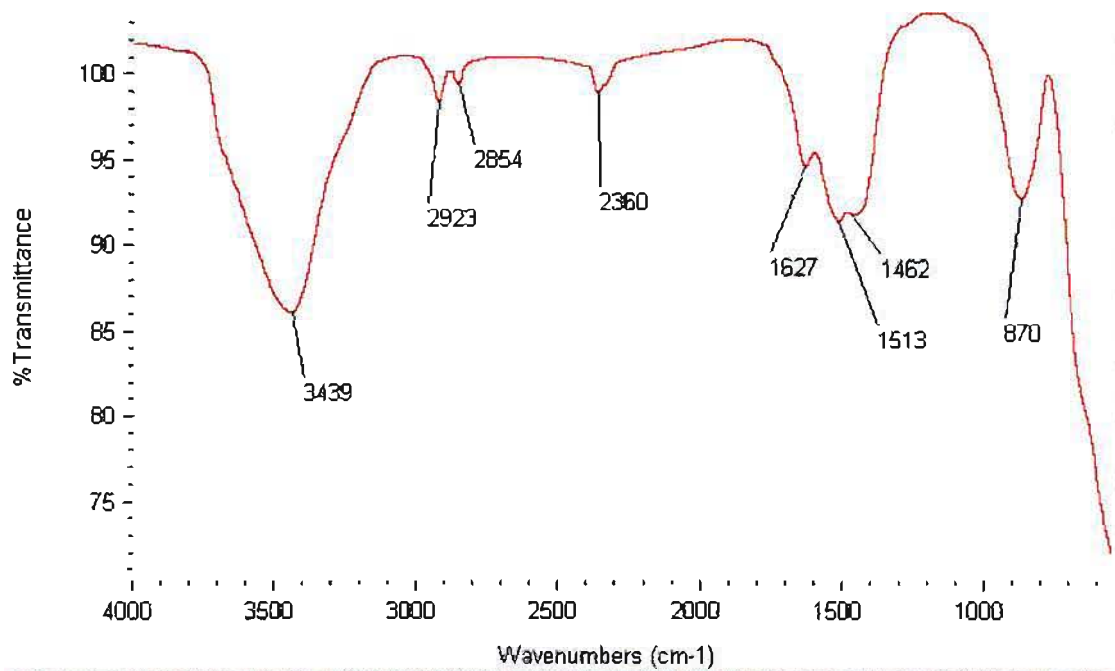


Figure 3W: FTIR spectrum of 16VMgO

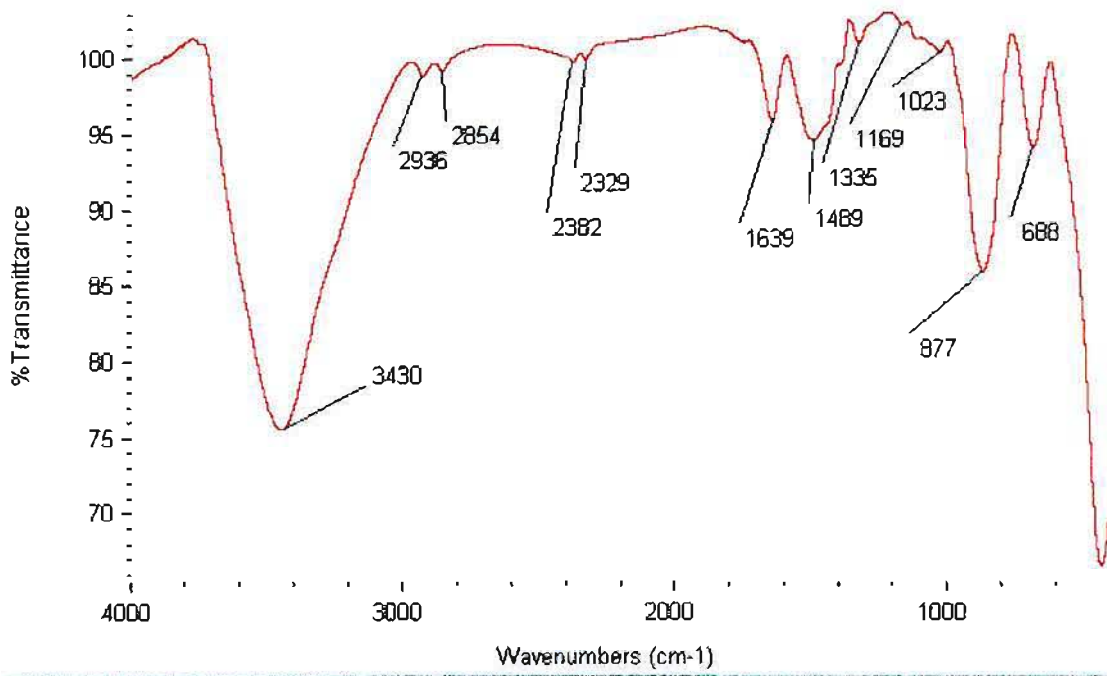


Figure 3.X: FTIR spectrum of 24VMgO

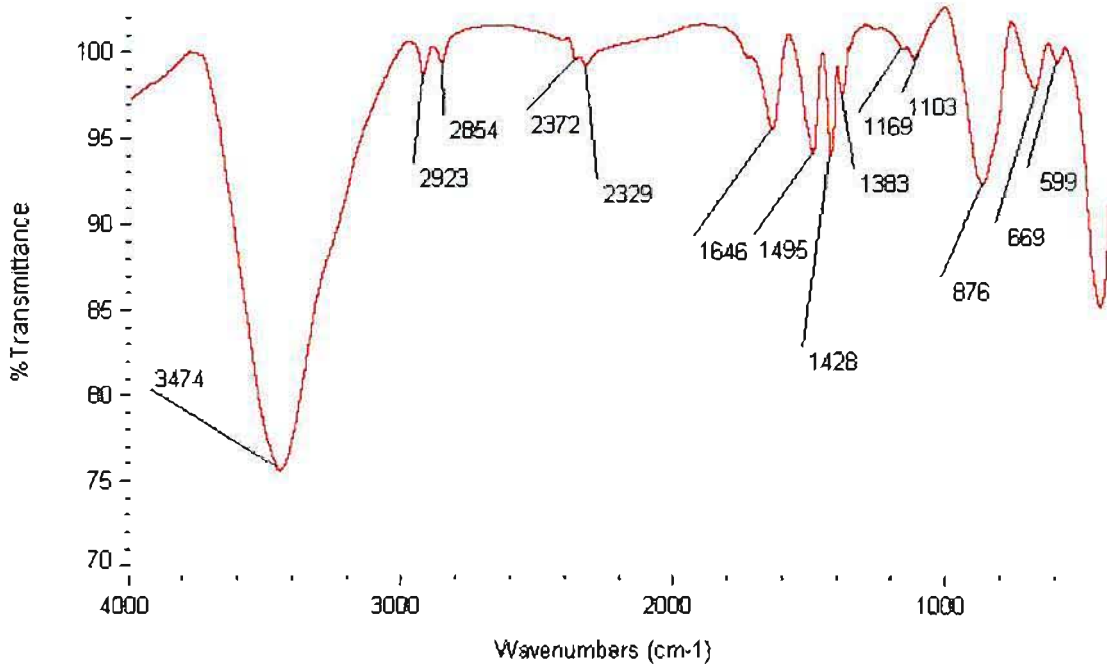


Figure 3Y: FTIR spectrum of 35VMgO

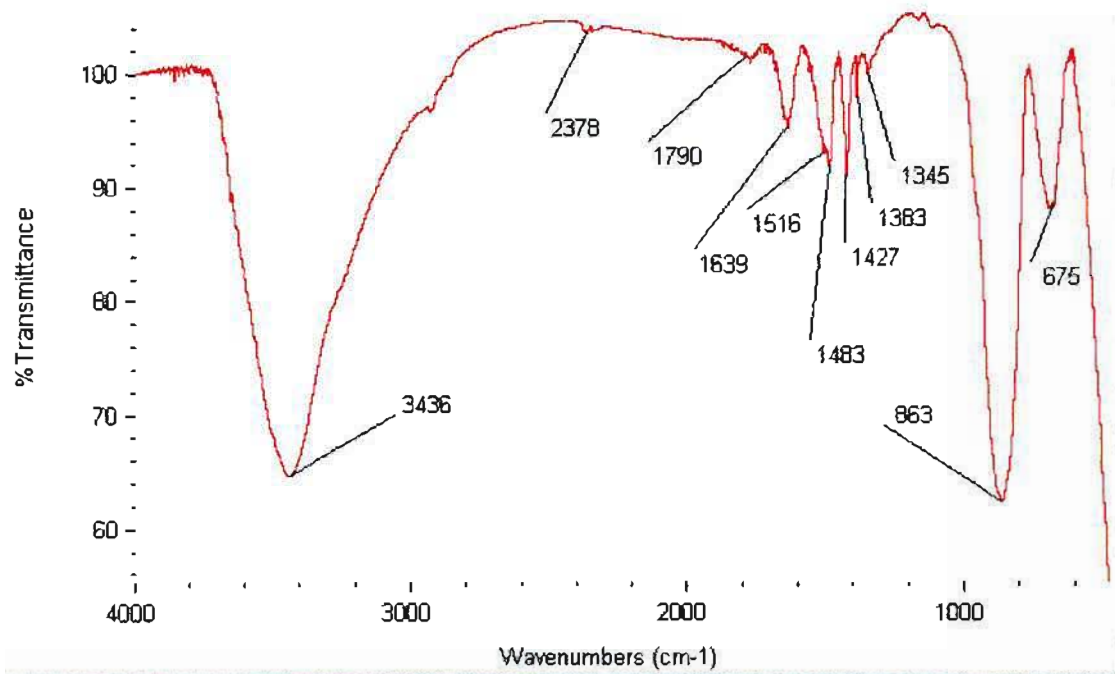


Figure 3Z: FTIR spectrum of 49VMgO

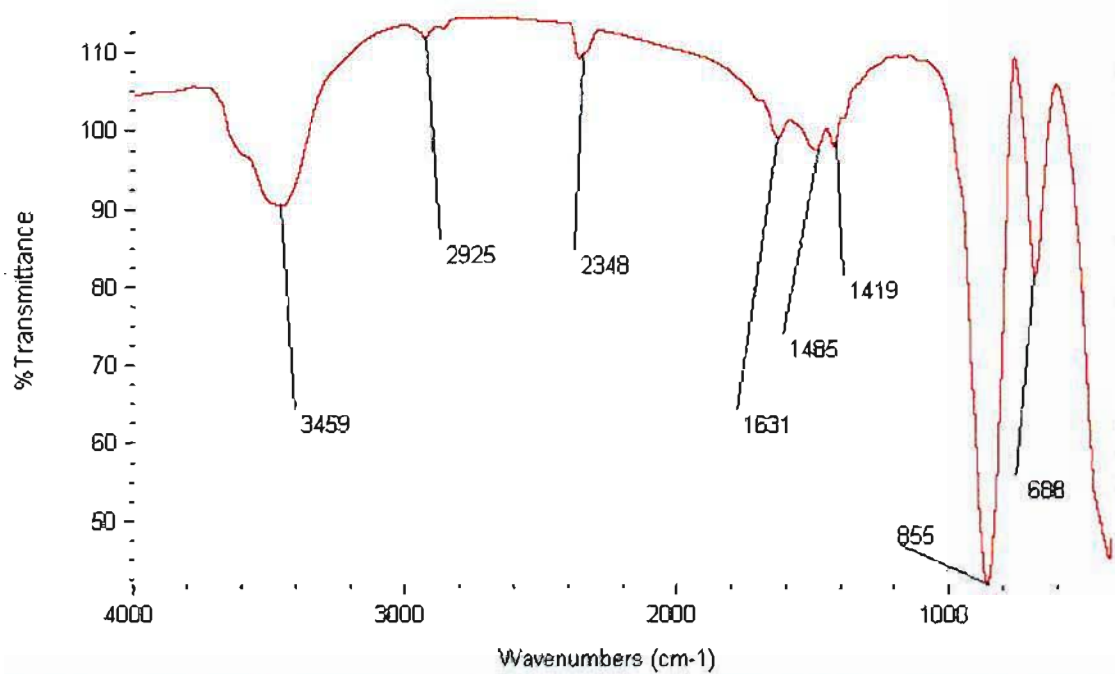


Figure 3AA: FTIR spectrum of 60VMgO

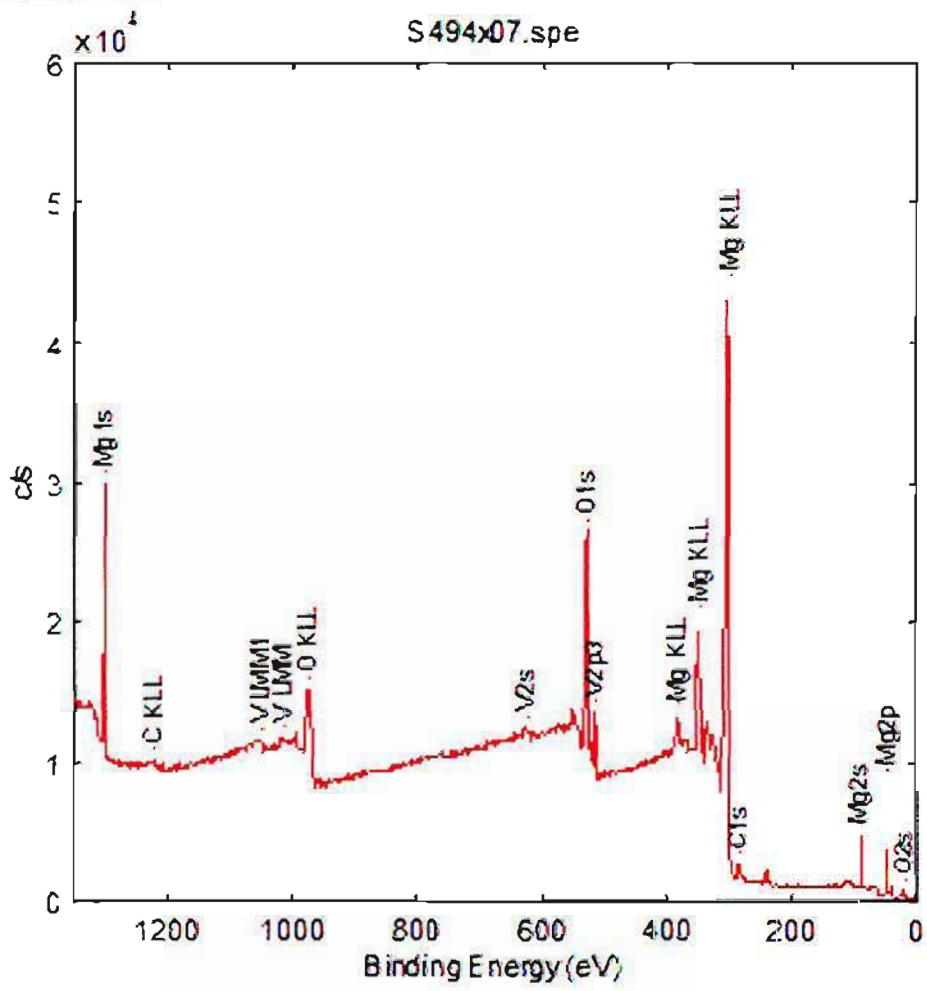


Figure 3AB: XPS of 19VMgO - Wide scan

S494x09.spe: University of Natal

CSIR-NML

4.2317e+002 max

1.35 min

C1s/Area1: JC1/1 (Shft)

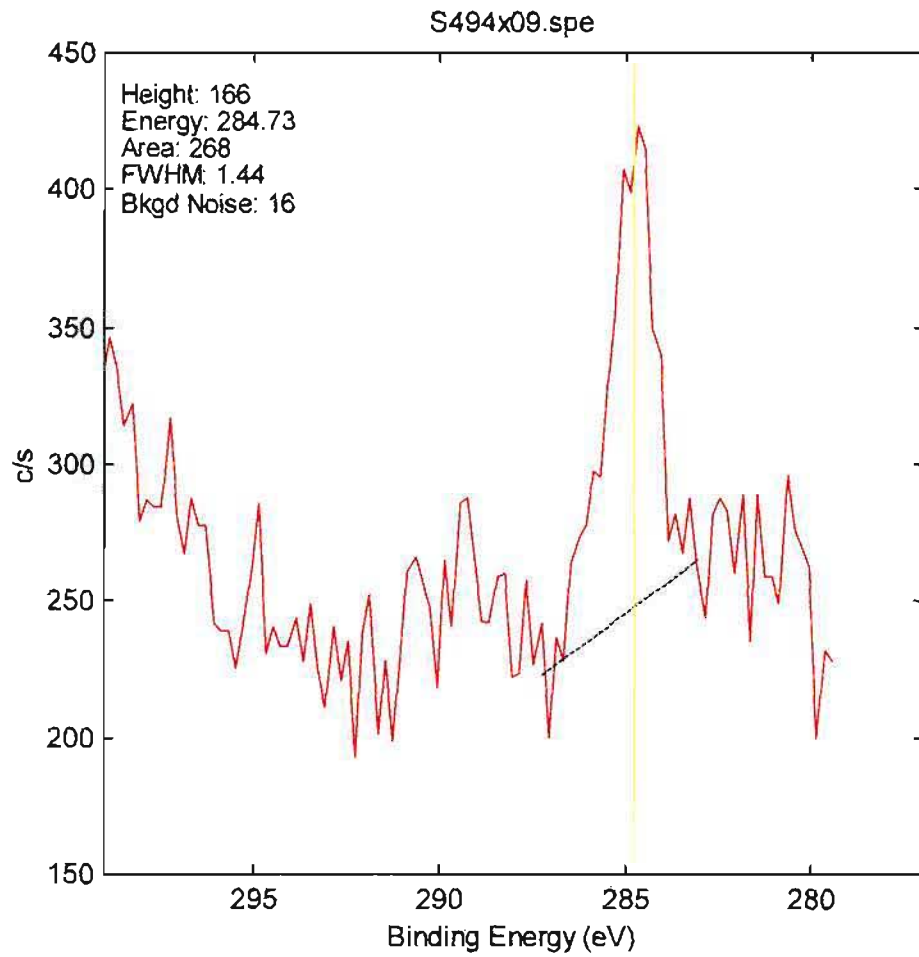


Figure 3AC: XPS of 19VMgO - Narrow scan of carbon

S494x09.spe: University of Natal CSIR-NML
2004 Jan 24 Al mono 19.3 W 100.0 μ 45.0° 23.50 eV 6.9756e+002 max 1.35 min
Mg2p/Area1: JC1/1 (Shft)

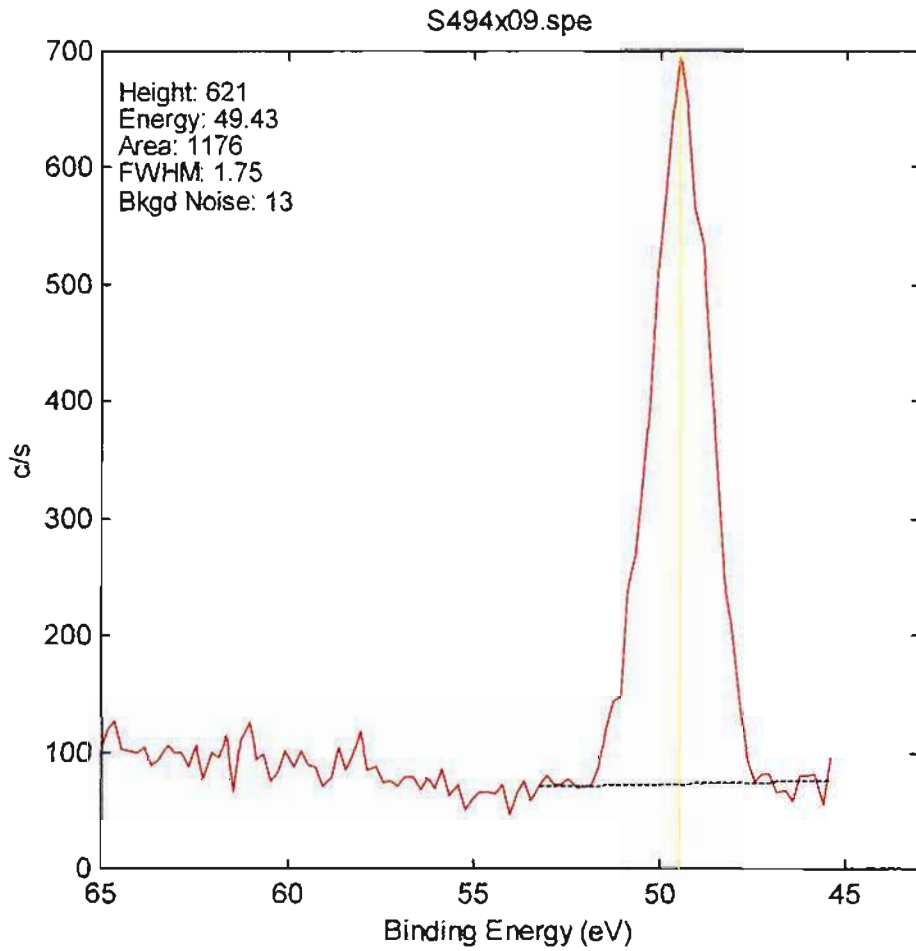


Figure 3AD: XPS of 19VMgO - Narrow scan of magnesium

S494x09.spe: University of Natal CSIR-NML
2004 Jan 24 Al mono 19.3 W 100.0 μ 45.0° 23.50 eV 4.5000e+003 max 1.35 min
O1s/Area1: JC1/1 (Shft)

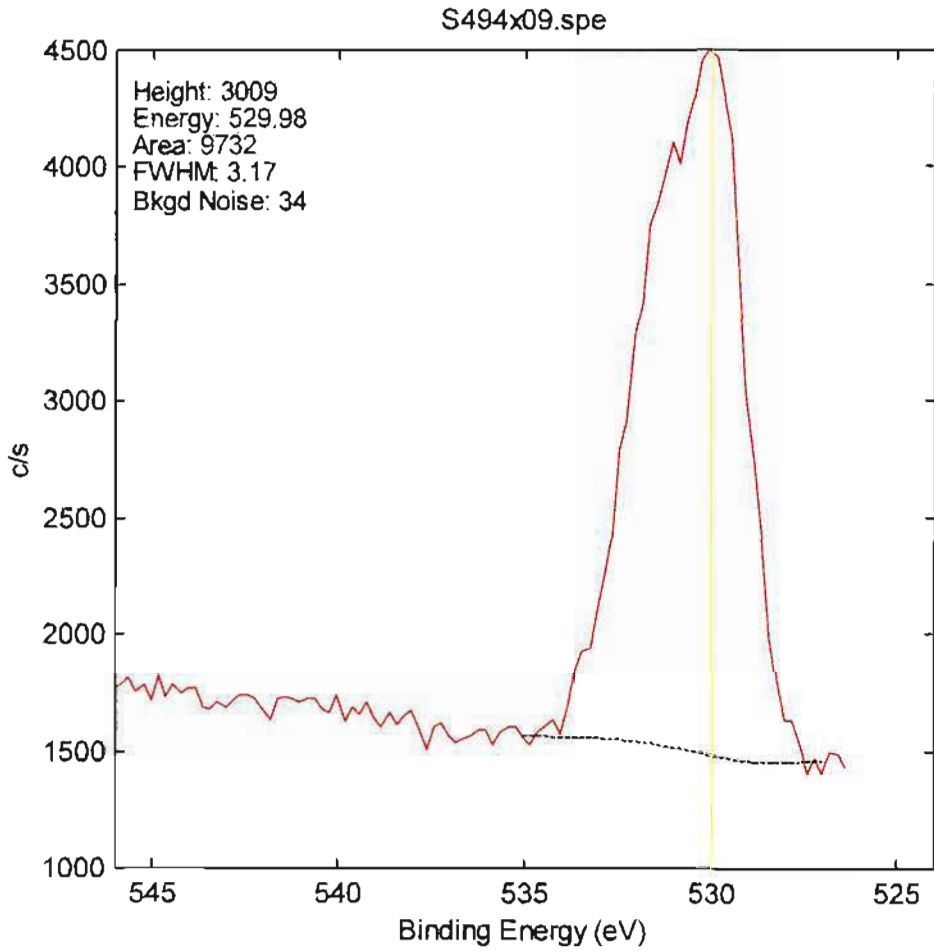


Figure 3AE: XPS of 19VMgO - Narrow scan of Oxygen

S494x09.spe: University of Natal
CSIR-NML
2.1615e+003 max 23.37 min
V2p/Area1: JC1/1 (Shft)

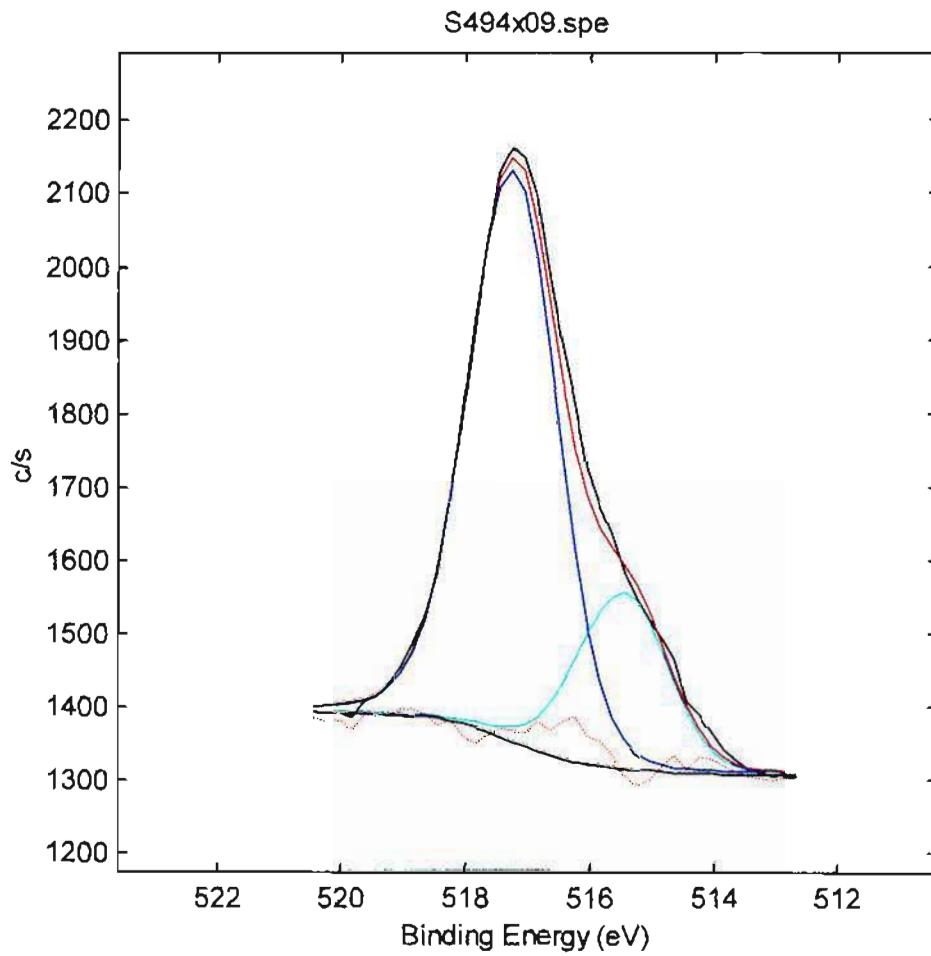


Figure 3AF: XPS of 19VMgO - Narrow scan of vanadium

S494x08.s pe: University of Natal

CSIR-NML

2004 Jan 24 Al mono 19.3 W 100.0 μ 45.0° 117.40 eV.3384e+004 max

29.72 min

SJ Area2: JC2 1

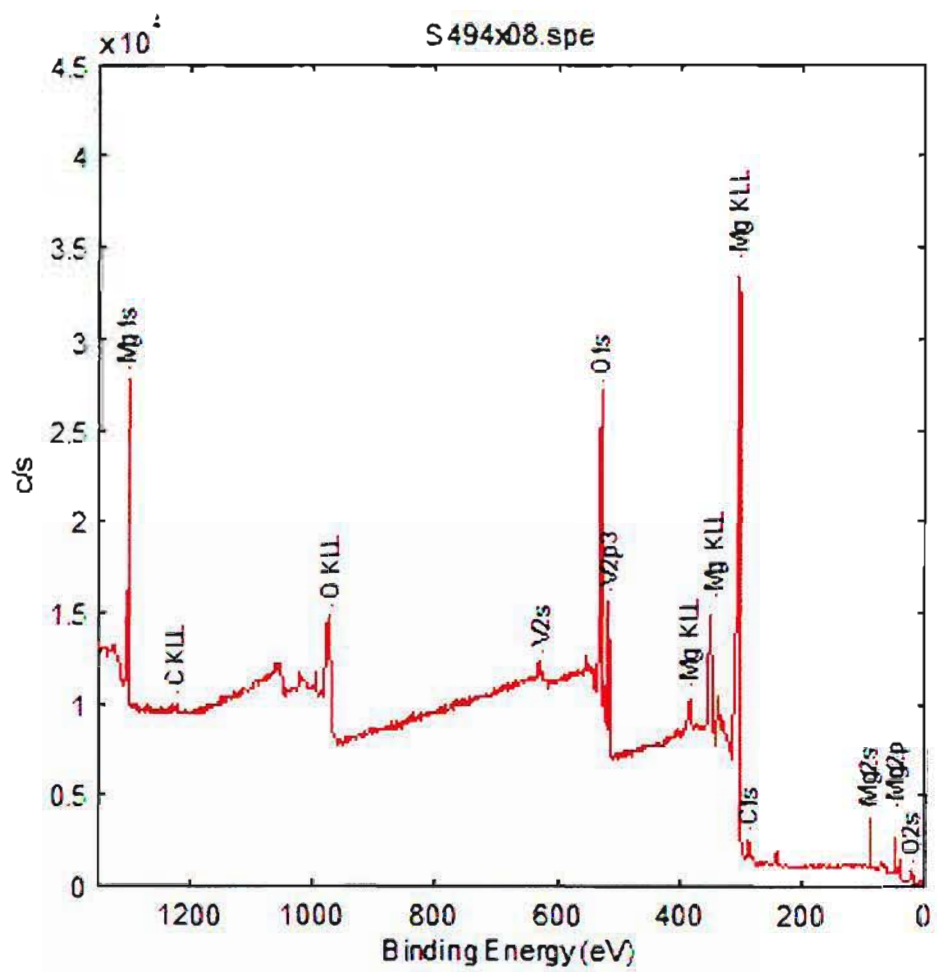


Figure 3AG: XPS of aged 19VMgO - Wide scan

S494x10.spe: University of Natal CSIR-NML
3.6585e+002 max 1.37 min
C1s/Area2: JC2/1 (Shft)

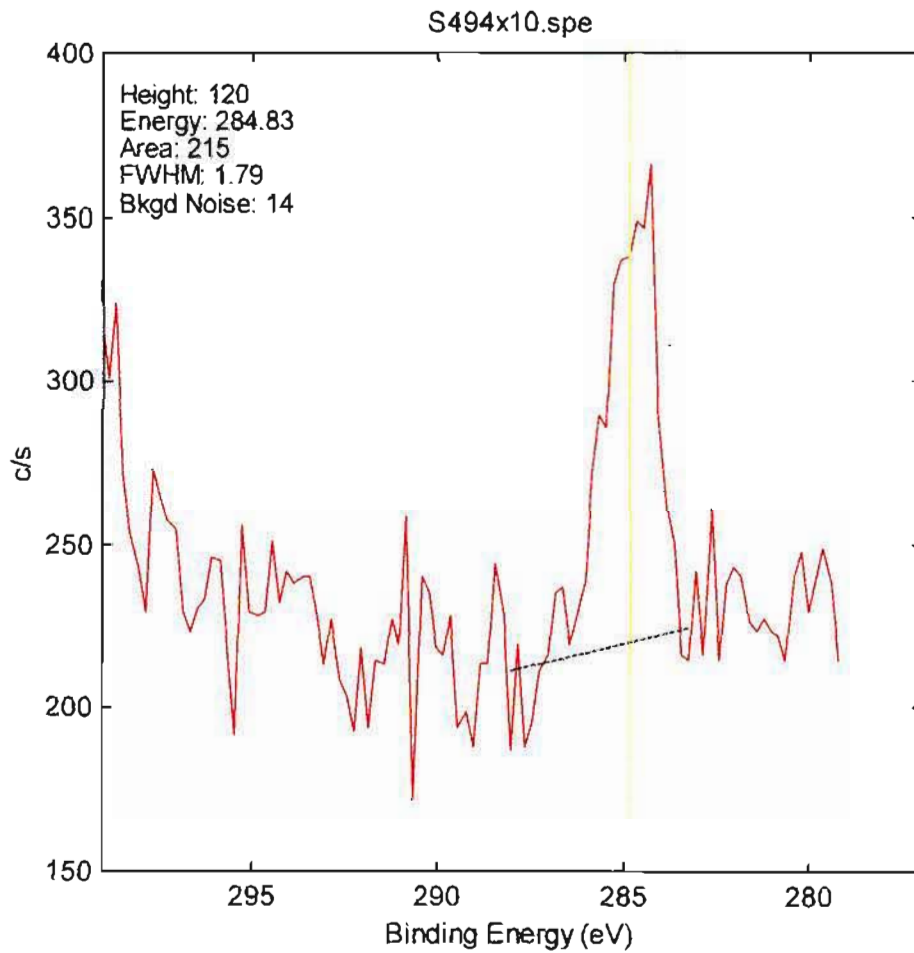


Figure 3AH: XPS of aged 19VMgO - Narrow scan of carbon

S494x10.spe: University of Natal CSIR-NML
2004 Jan 24 Al mono 19.3 W 100.0 μ 45.0° 23.50 eV 5.7073e+002 max 1.37 min
Mg2p/Area2: JC2/1 (Shft)

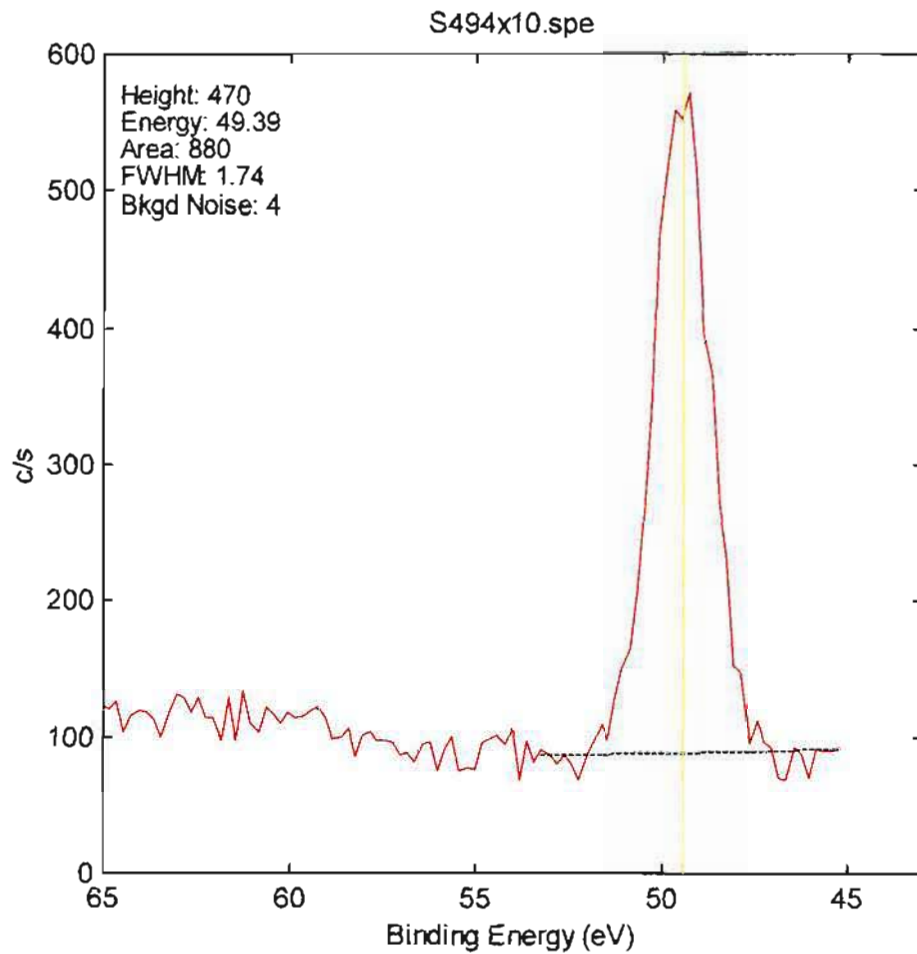


Figure A1: XPS of aged 19VMgO – Narrow scan of magnesium

S494x10.spe: University of Natal

CSIR-NML

5.1732e+003 max

1.37 min

O1s/Area2: JC2/1 (Shft)

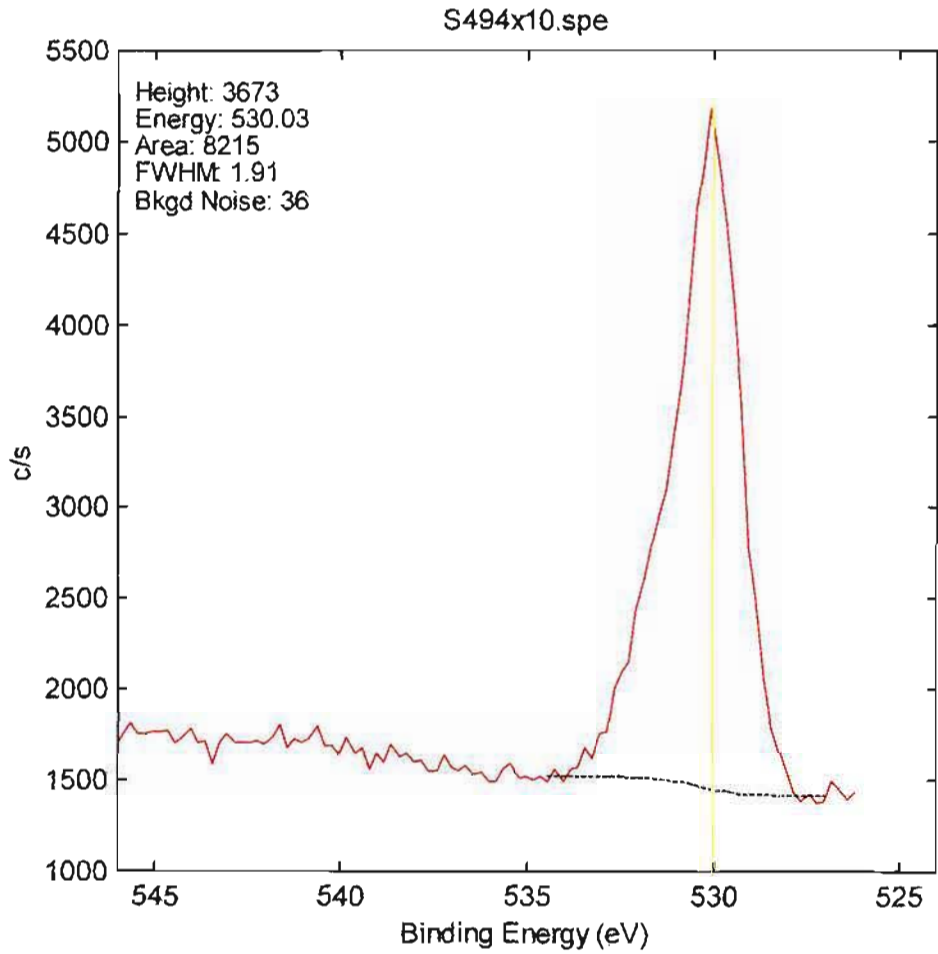


Figure 3A.J: XPS of aged 19VMgO – Narrow scan of oxygen

S494x10.spe: University of Natal
2004 Jan 24 Al mono 19.3 W 100.0 μ 45.0° 23.50 2.6729e+003 max 23.78 min
V2p/Area2: JC2/1 (Shft)

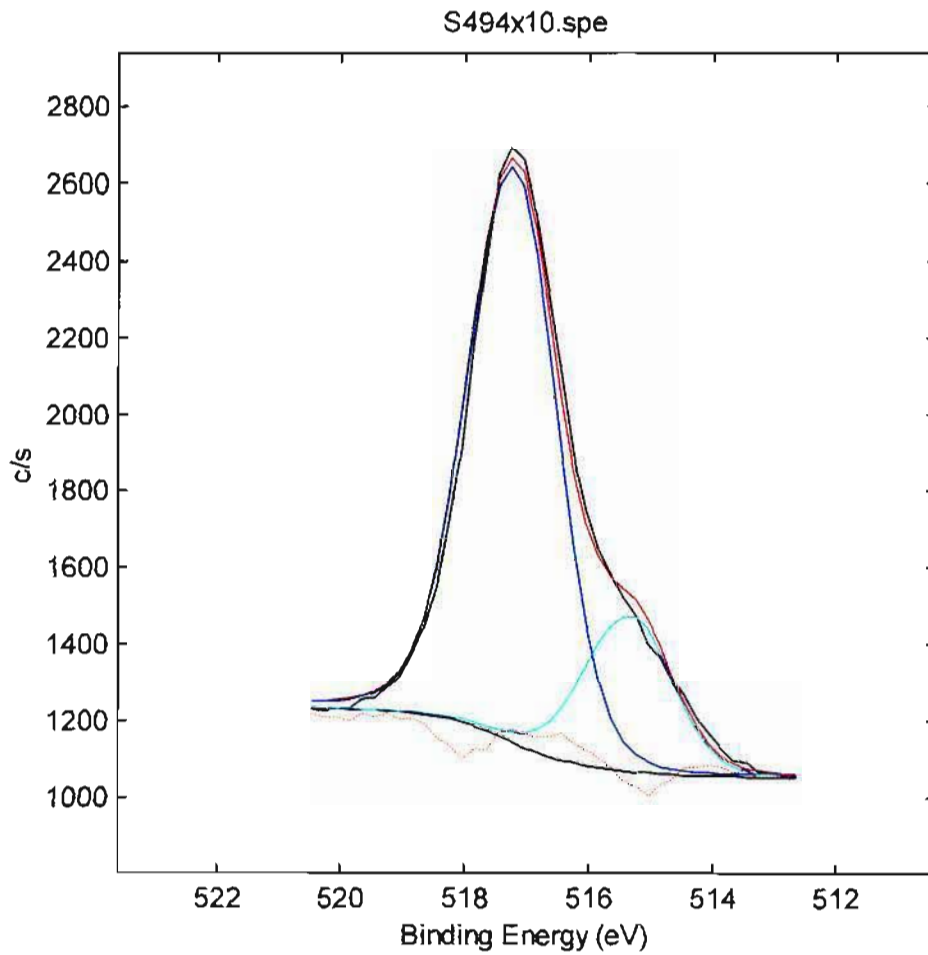


Figure 3AK: XPS of aged 19VMgO – Narrow scan of vanadium



Figure 3AL: SEM Image of V₂O₅

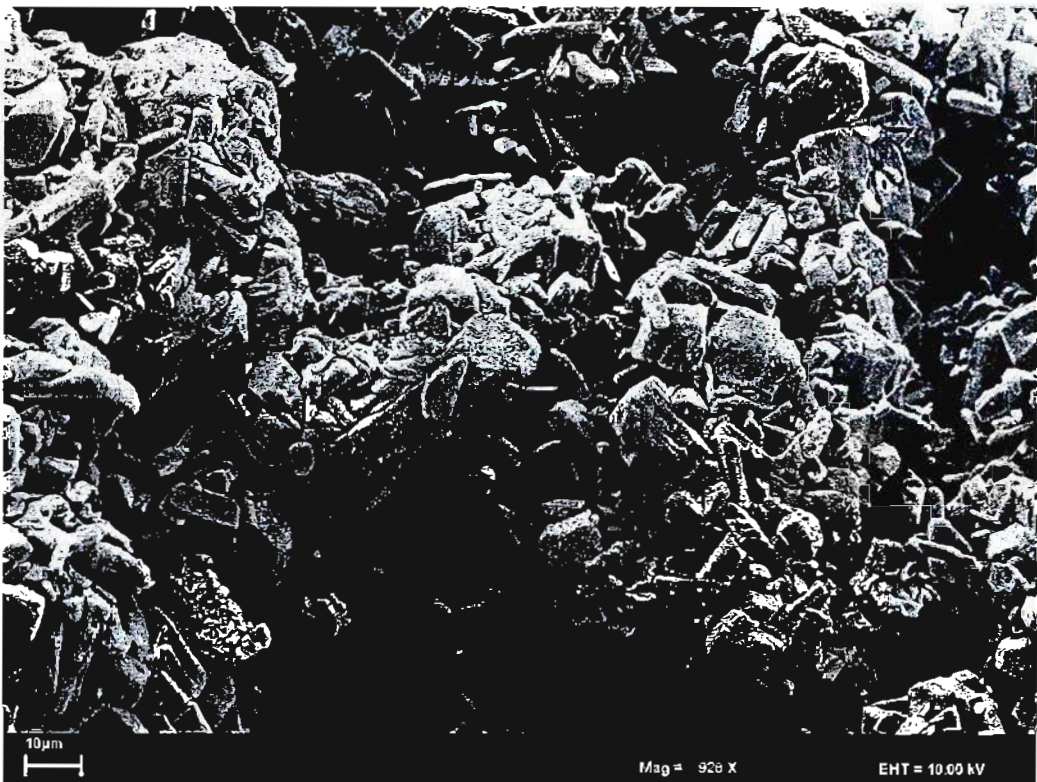


Figure 3AM: SEM Image of V₂O₅



Figure 3AN: SEM Image of V₂O₅

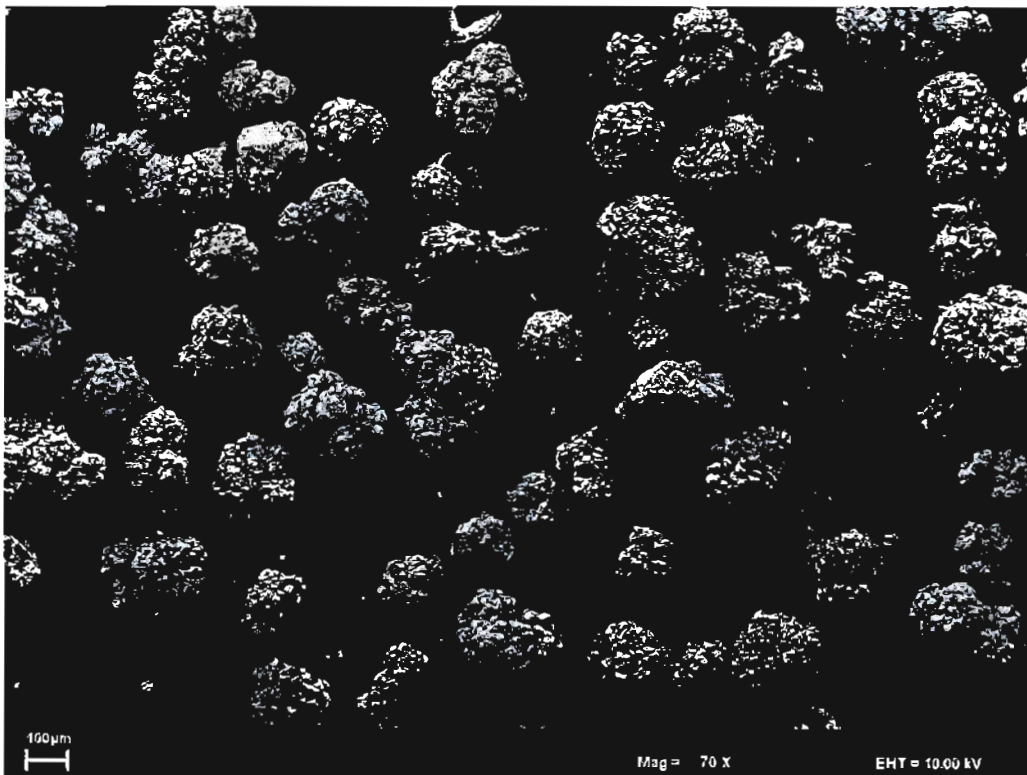


Figure 3AO: SEM Image of V₂O₅

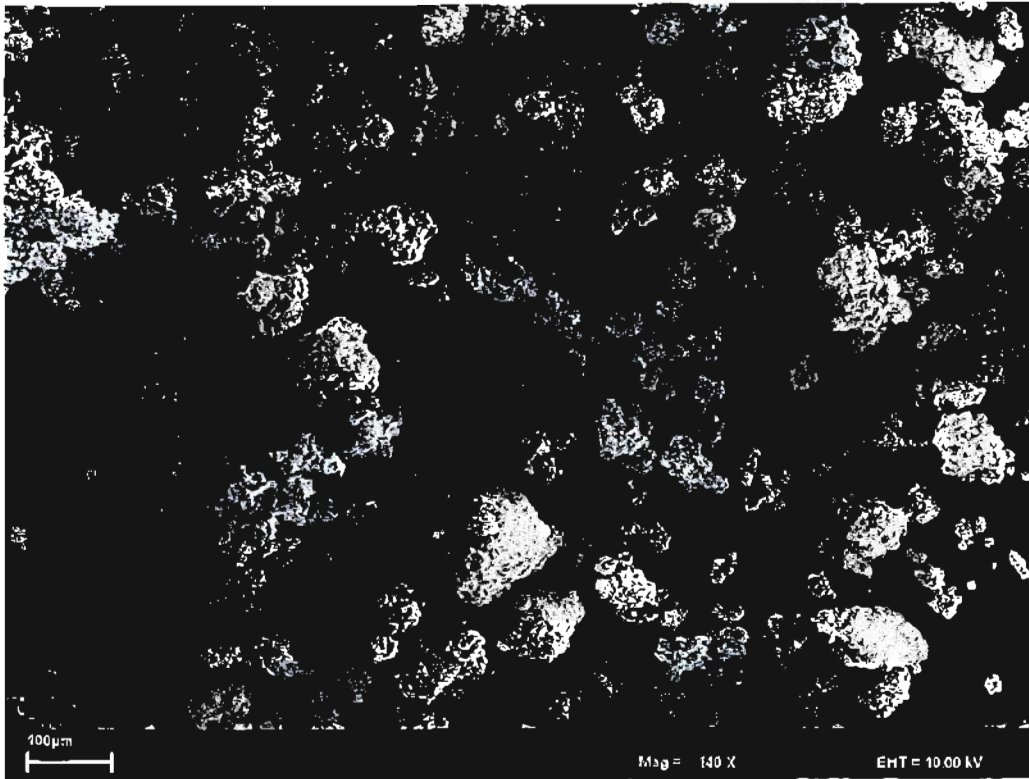


Figure 3AP: SEM image of MgO



Figure 3AQ: SEM image of MgO

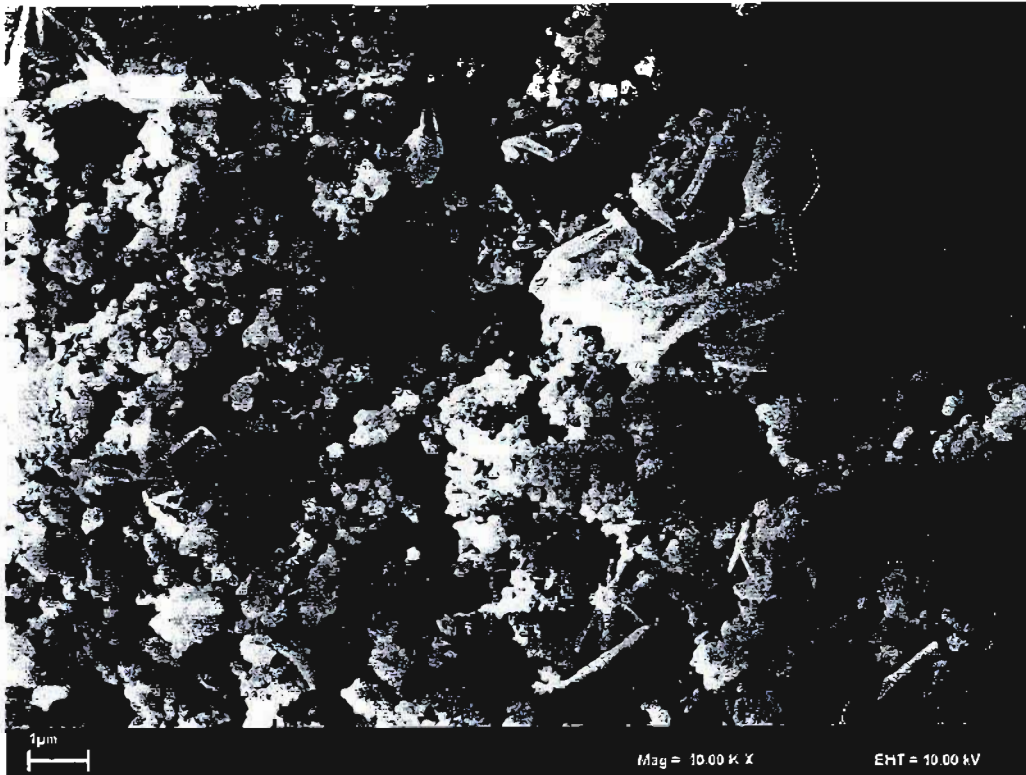


Figure 3AR: SEM image of MgO



Figure 3AS: SEM Image of MgO

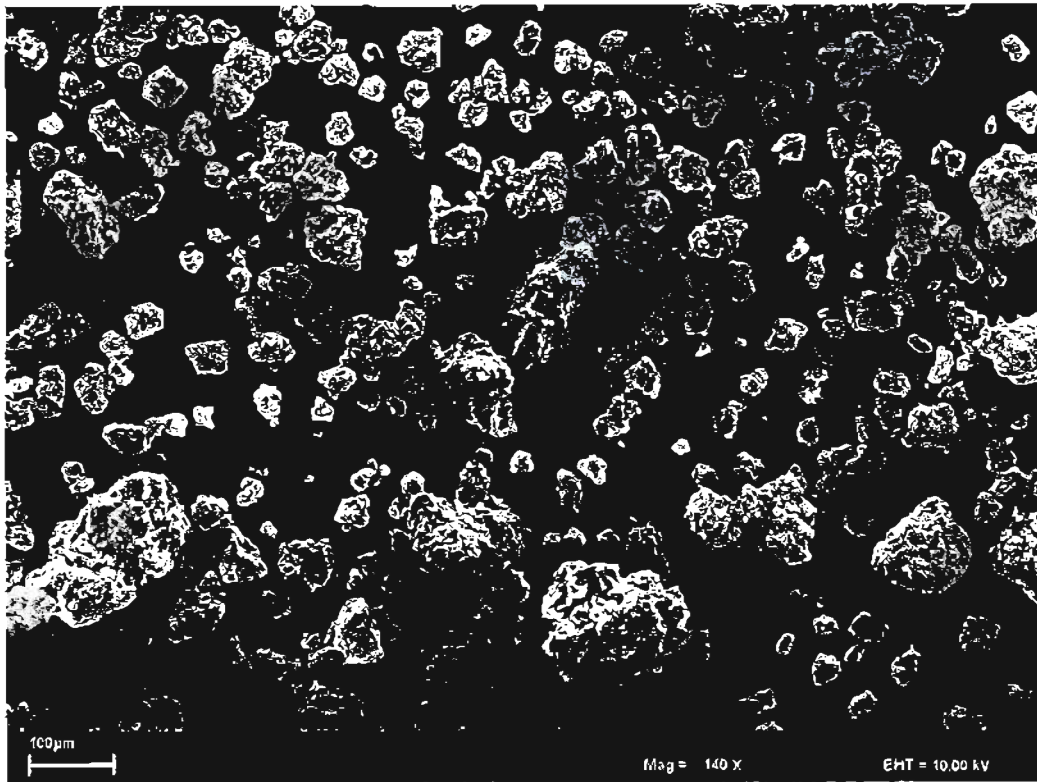


Figure 3AT: SEM image of 14VMgO

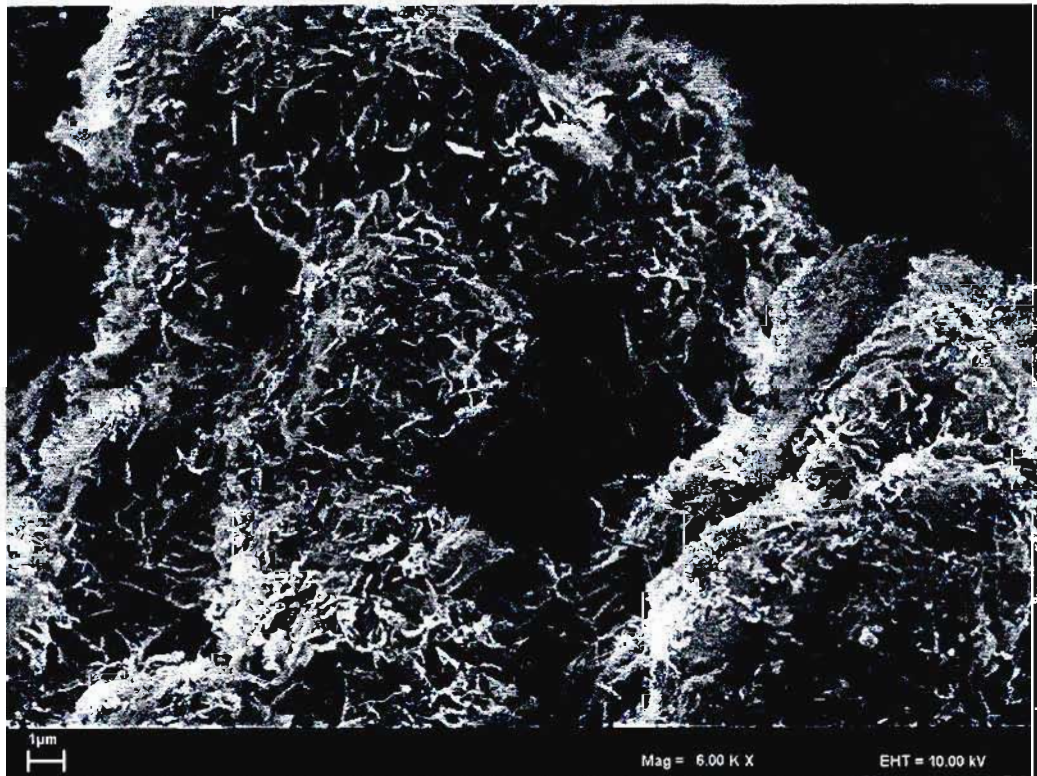


Figure 3AU: SEM image of 14VMgO

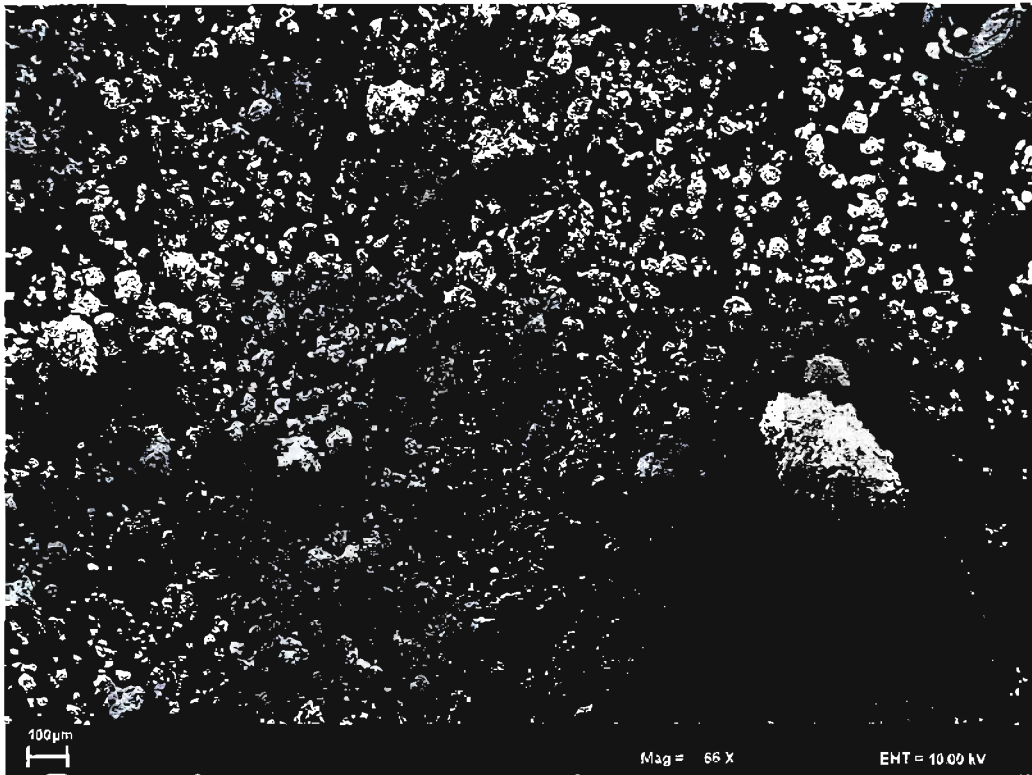


Figure 3AV: SEM image of 16VMgO

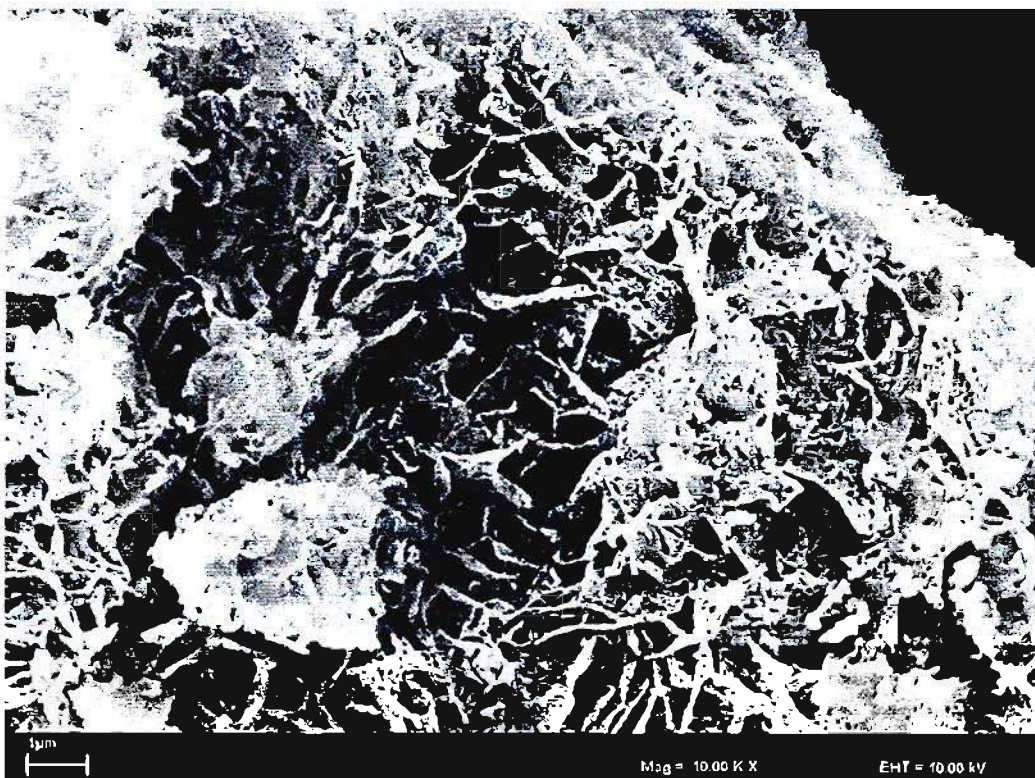


Figure 3AW: SEM image of 16VMgO

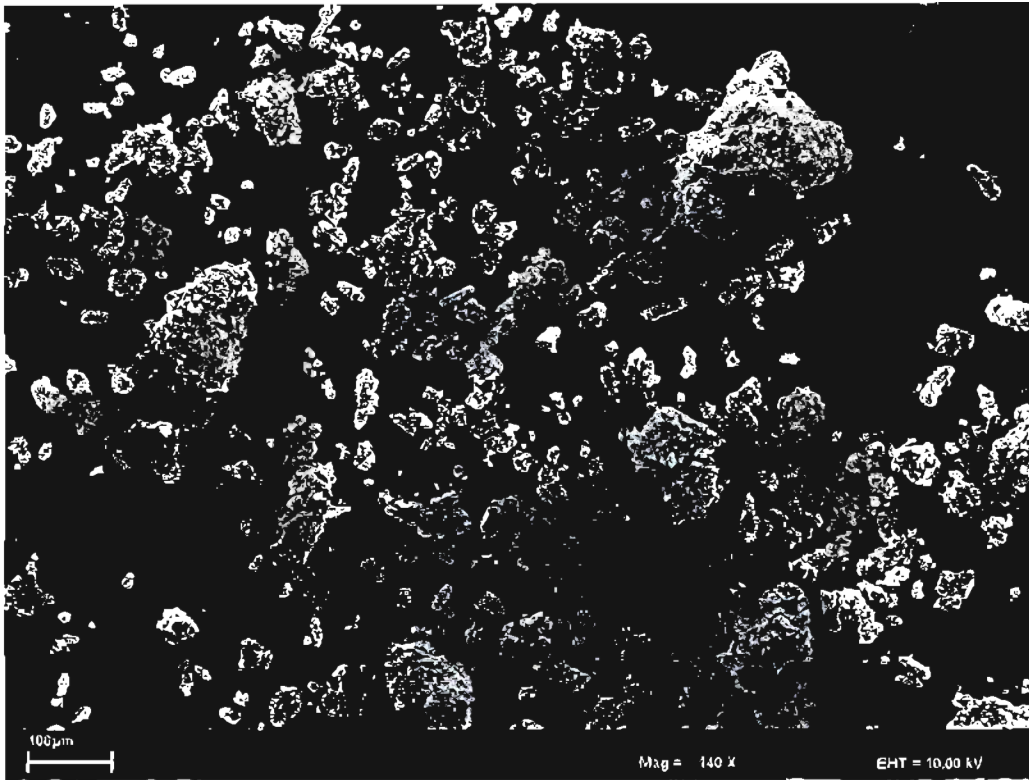


Figure 3AX: SEM image of 19VMgO

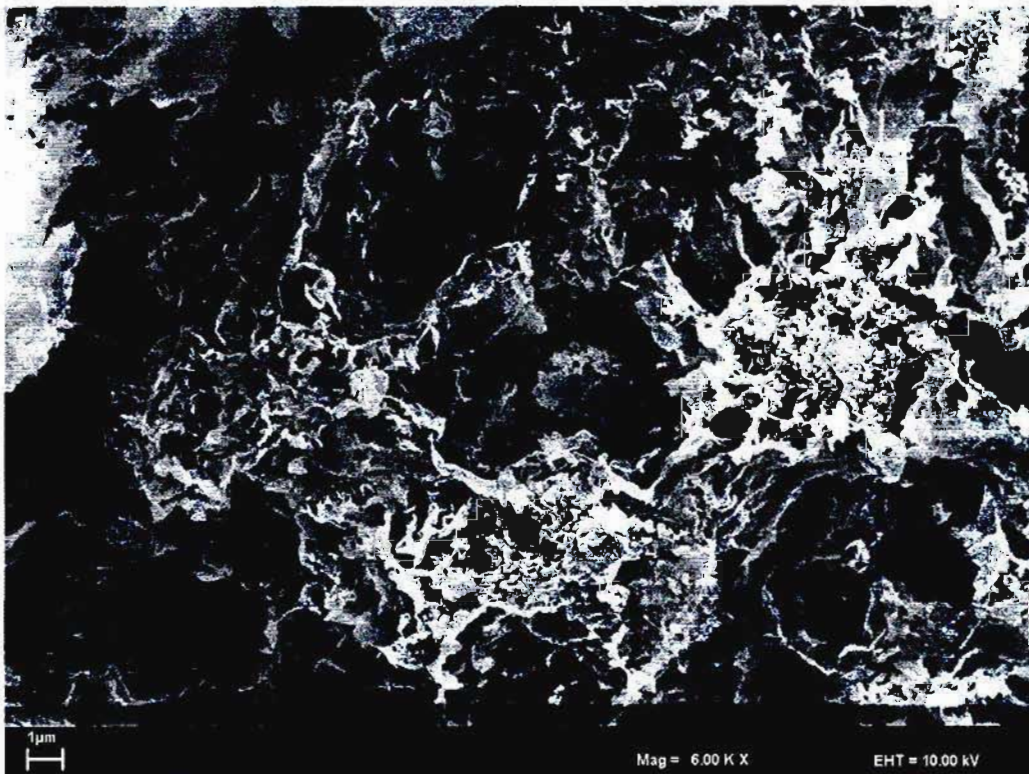


Figure 3AY: SEM image of 19VMgO

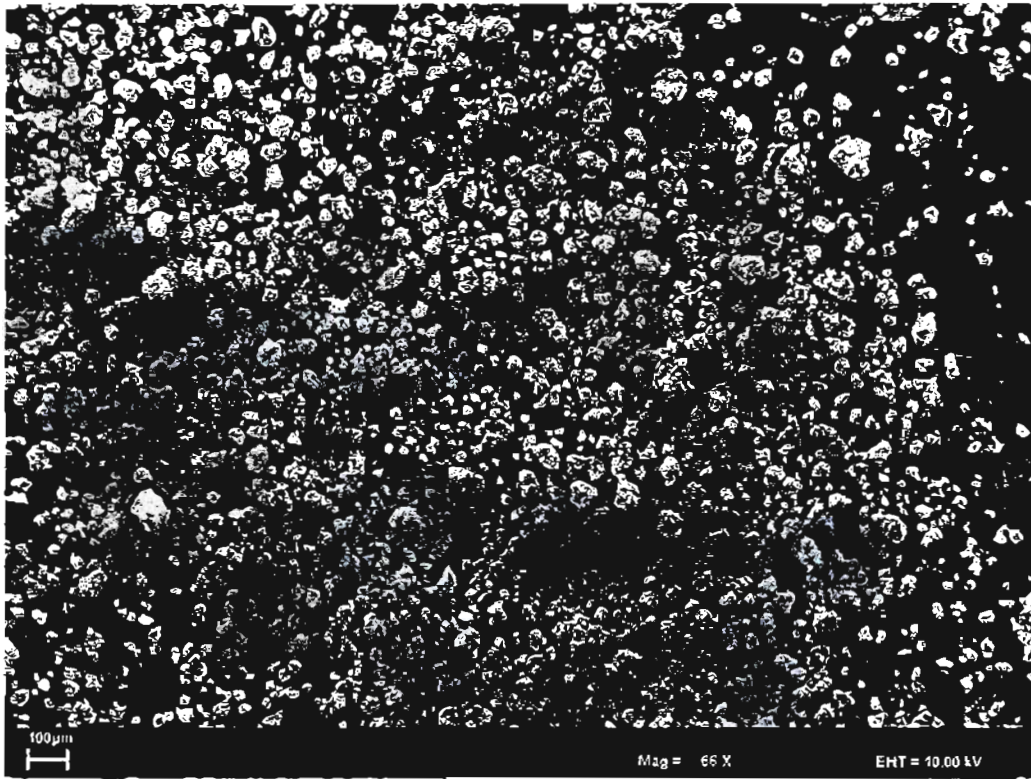


Figure 3AZ: SEM image of 24VMgO



Figure 3BA: SEM image of 24VMgO

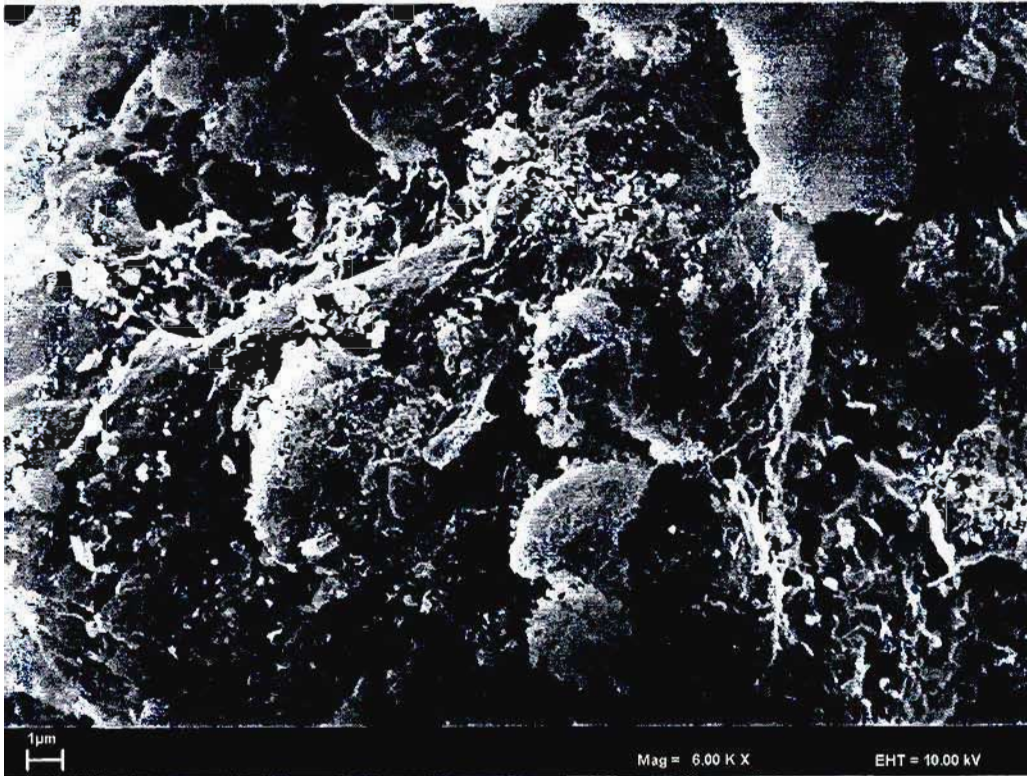


Figure 3BB: SEM image of 35VMgO



Figure 3BC: SEM image of 35VMgO

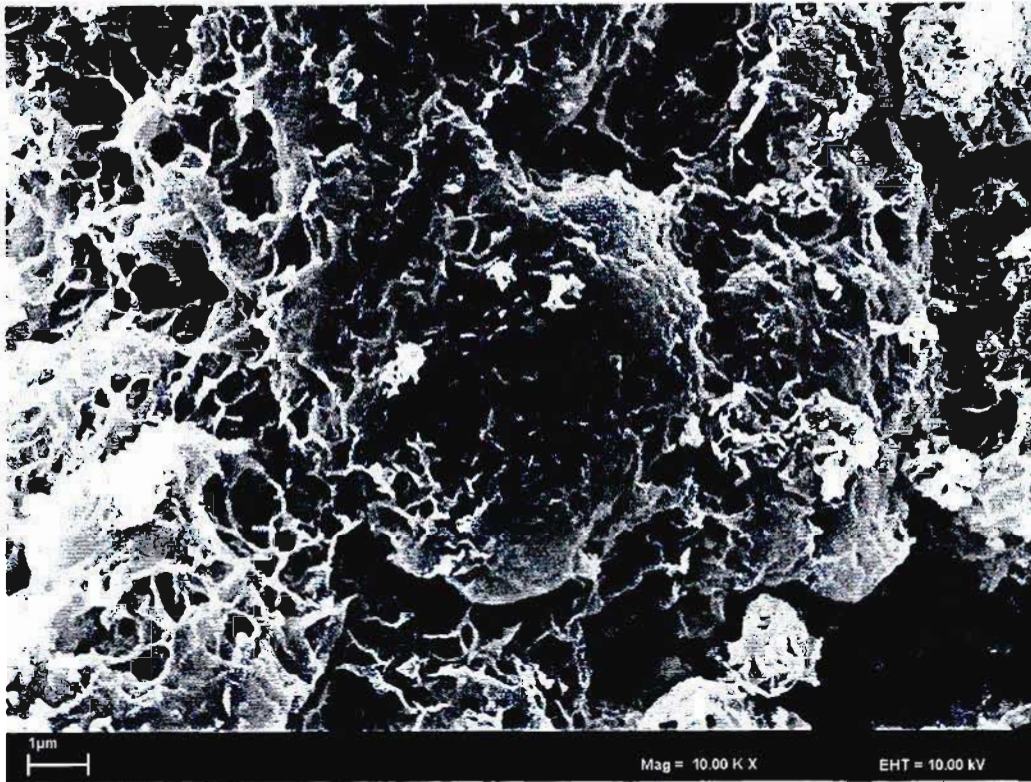


Figure 3BD: SEM image of 49VMgO

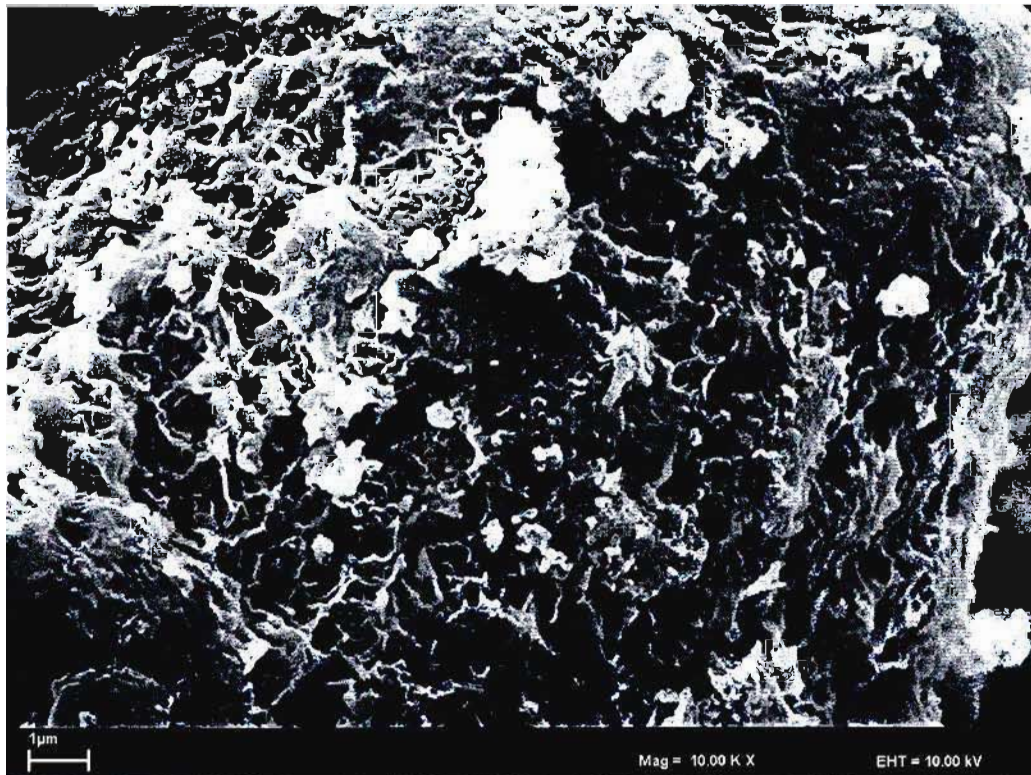


Figure 3BE: SEM image of 49VMgO

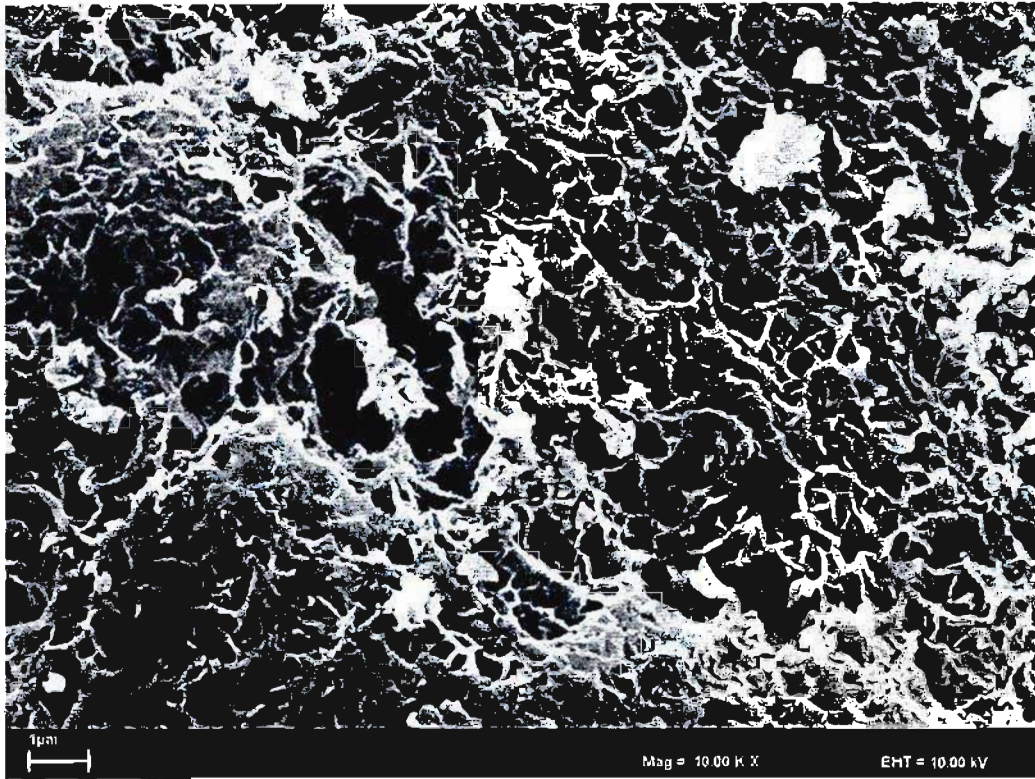


Figure 3BF: SEM image of 60VMgO

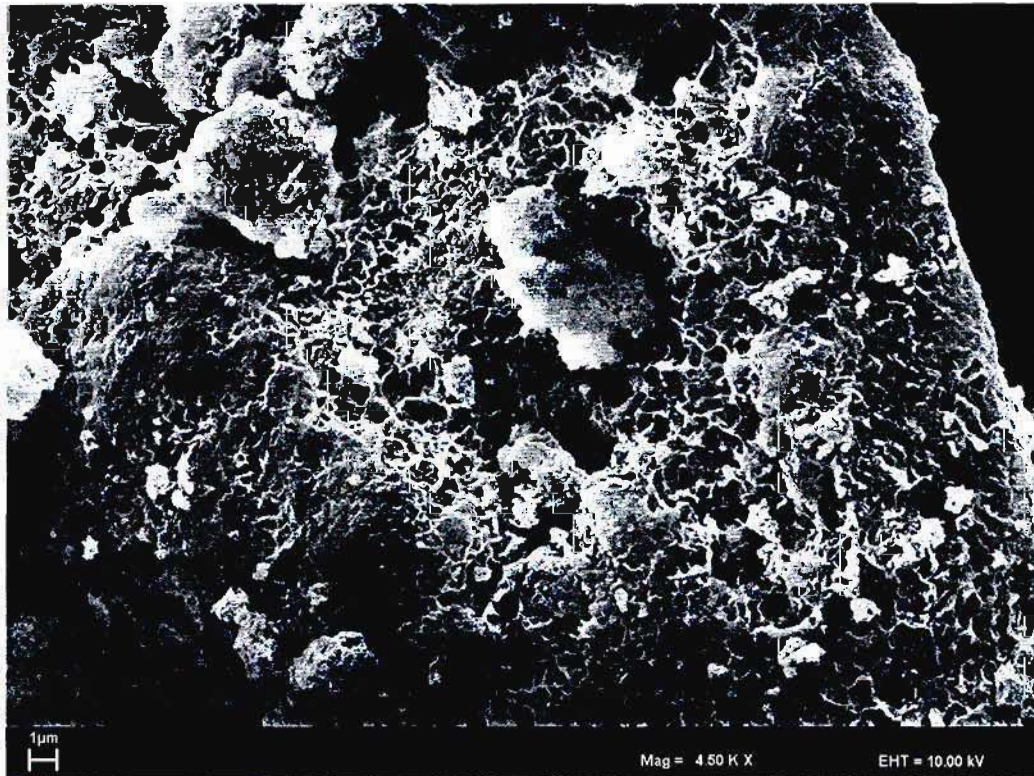


Figure 3BG: SEM image of 60VMgO

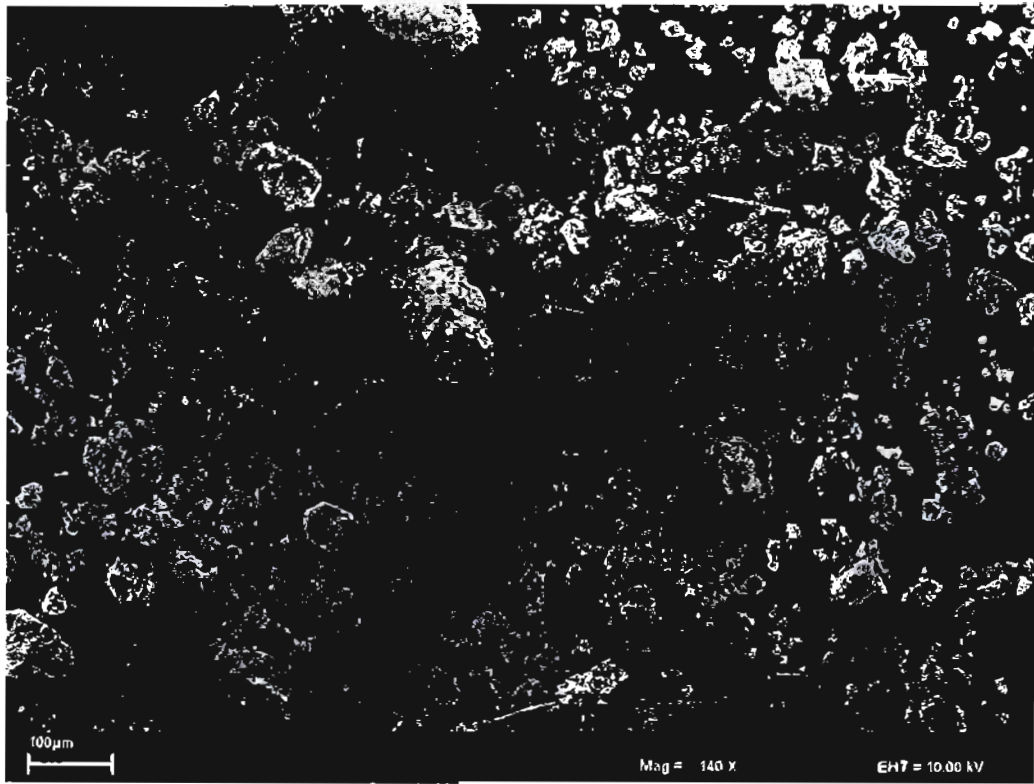


Figure 3BH: SEM image of aged 19VMgO

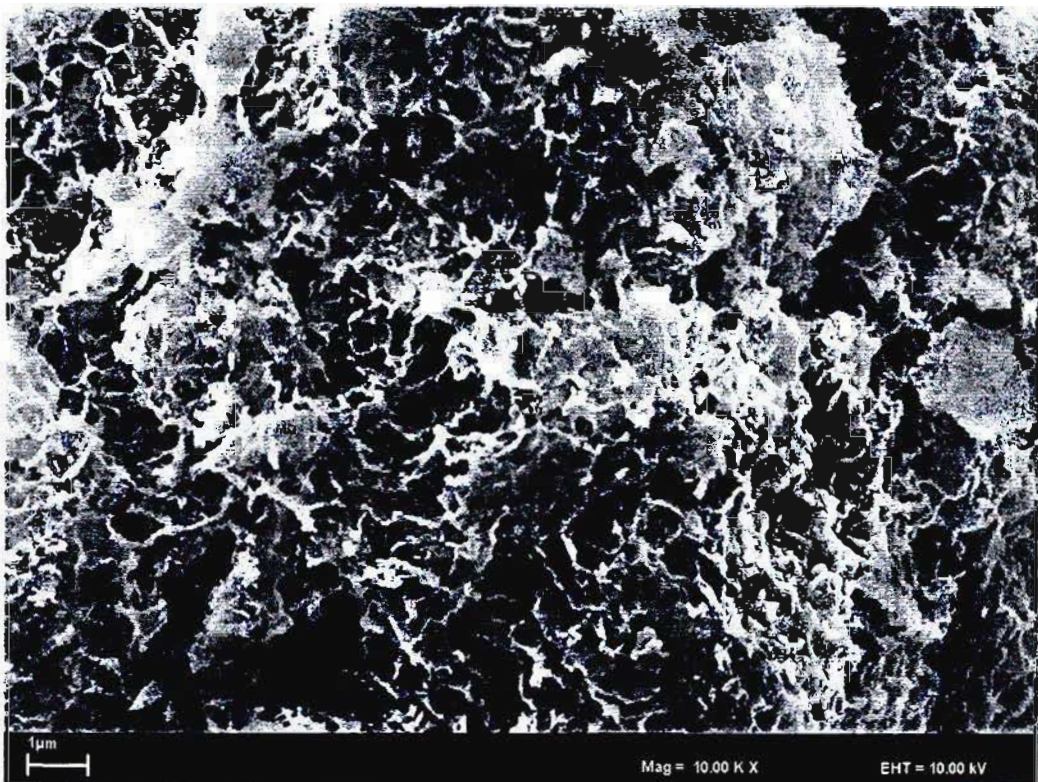


Figure 3BI: SEM image of aged 19VMgO

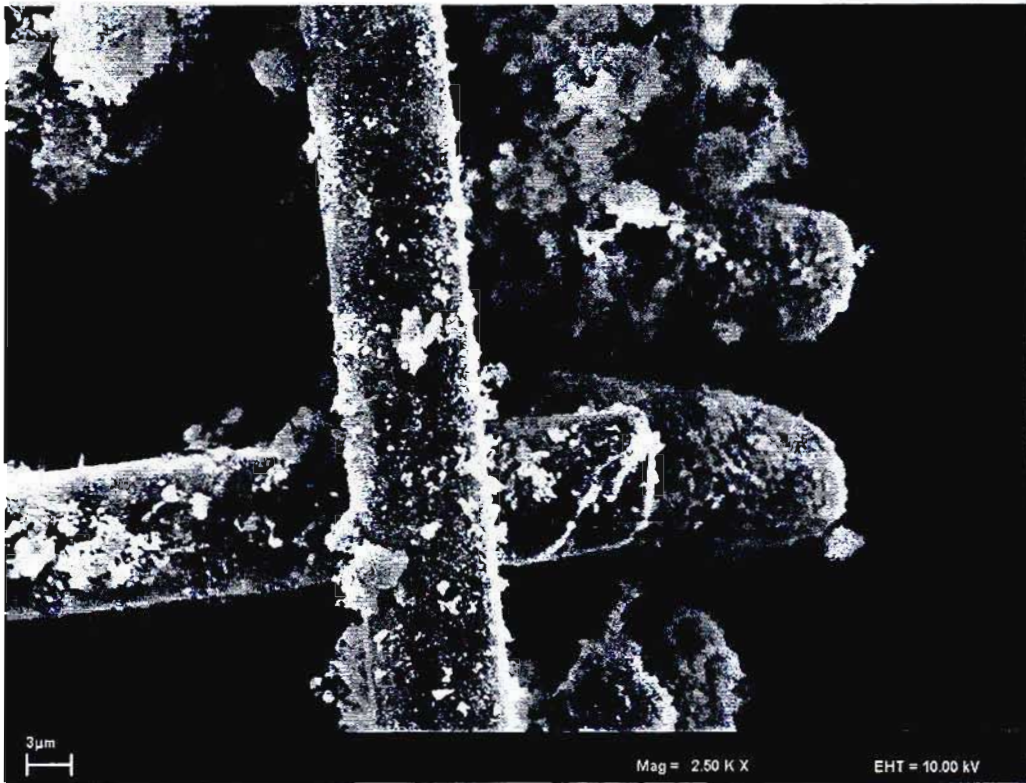


Figure 3BJ: SEM image of aged 19VMgO

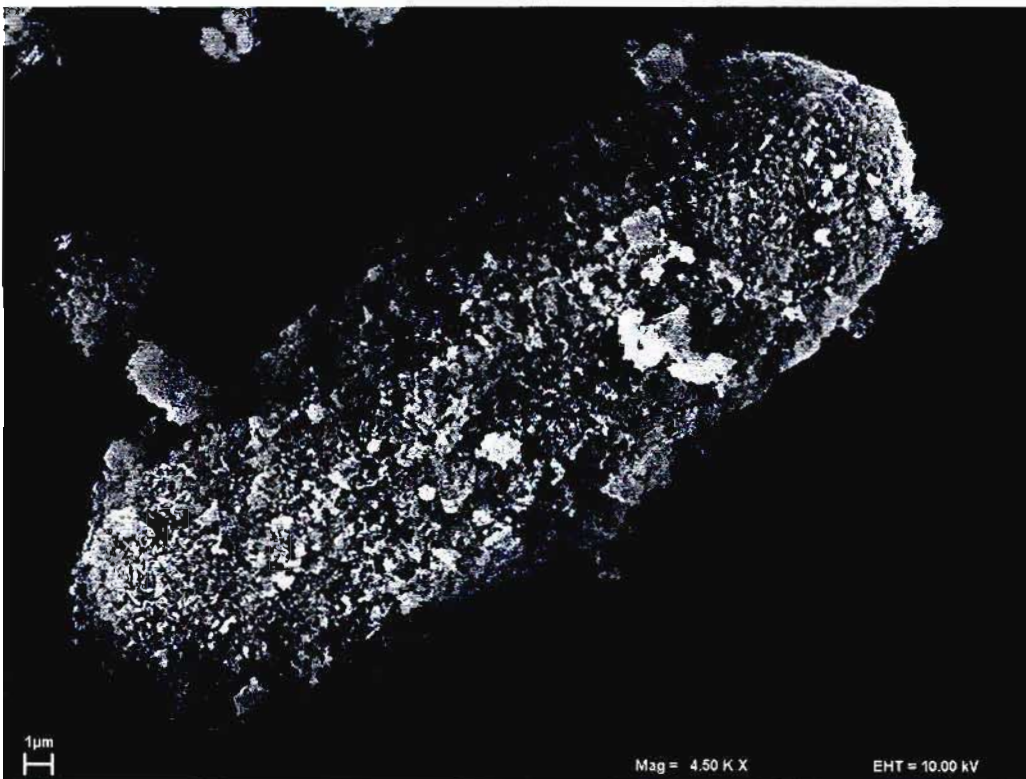


Figure 3BK: SEM image of aged 19VMgO

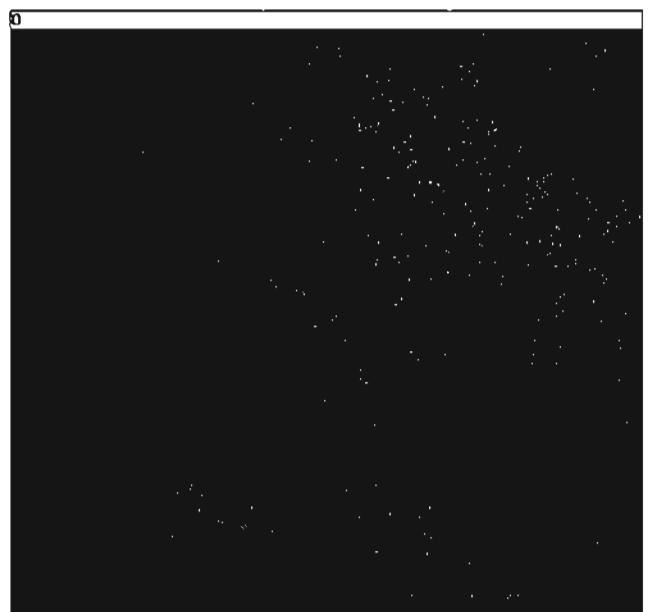
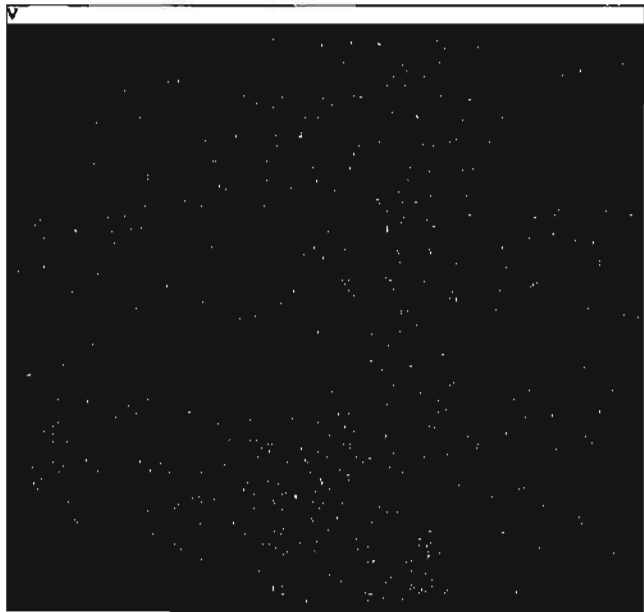
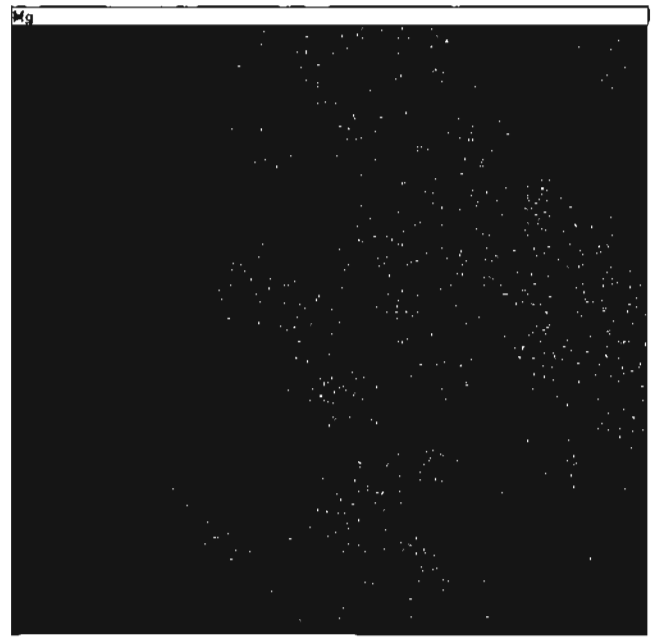
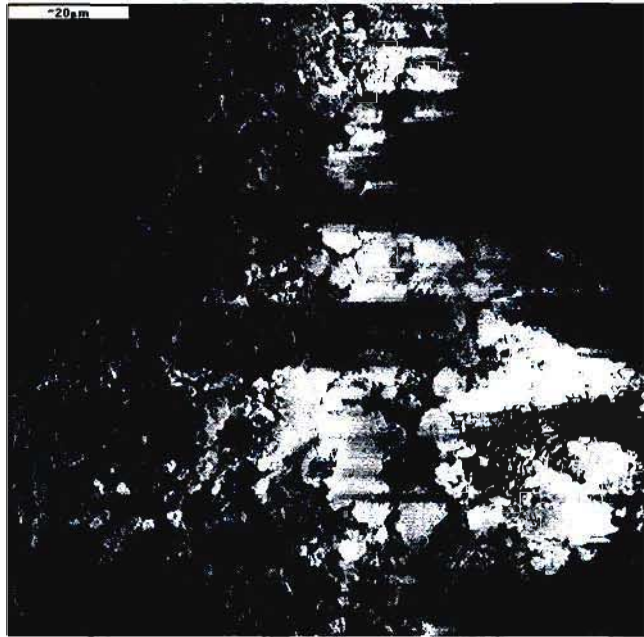


Figure 3BL: SEM image of 19VMgO and the corresponding elemental maps

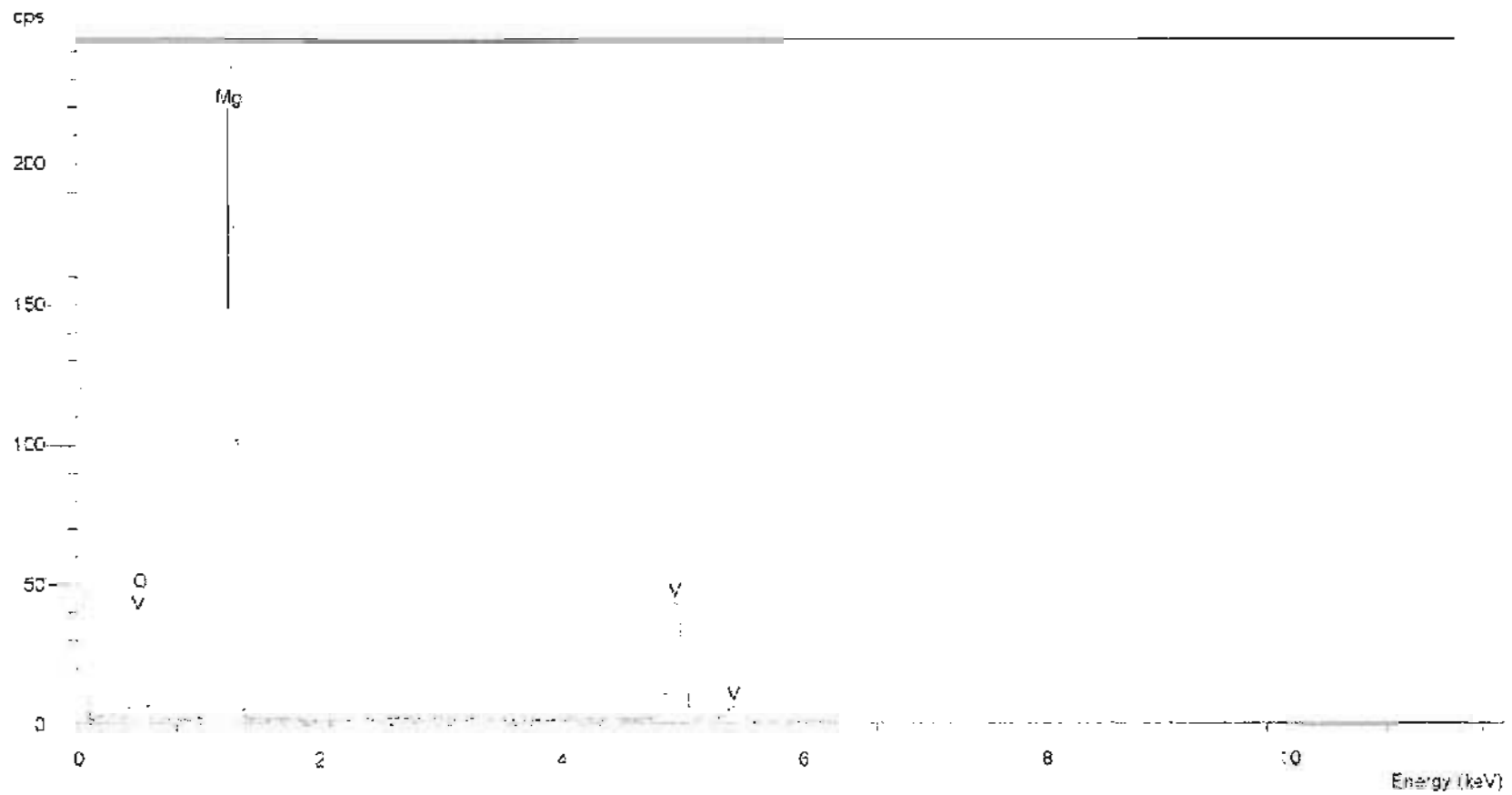


Figure 3BM: EDS spectrum of 19VMgO

APPENDIX 4: PROMOTED VMgO

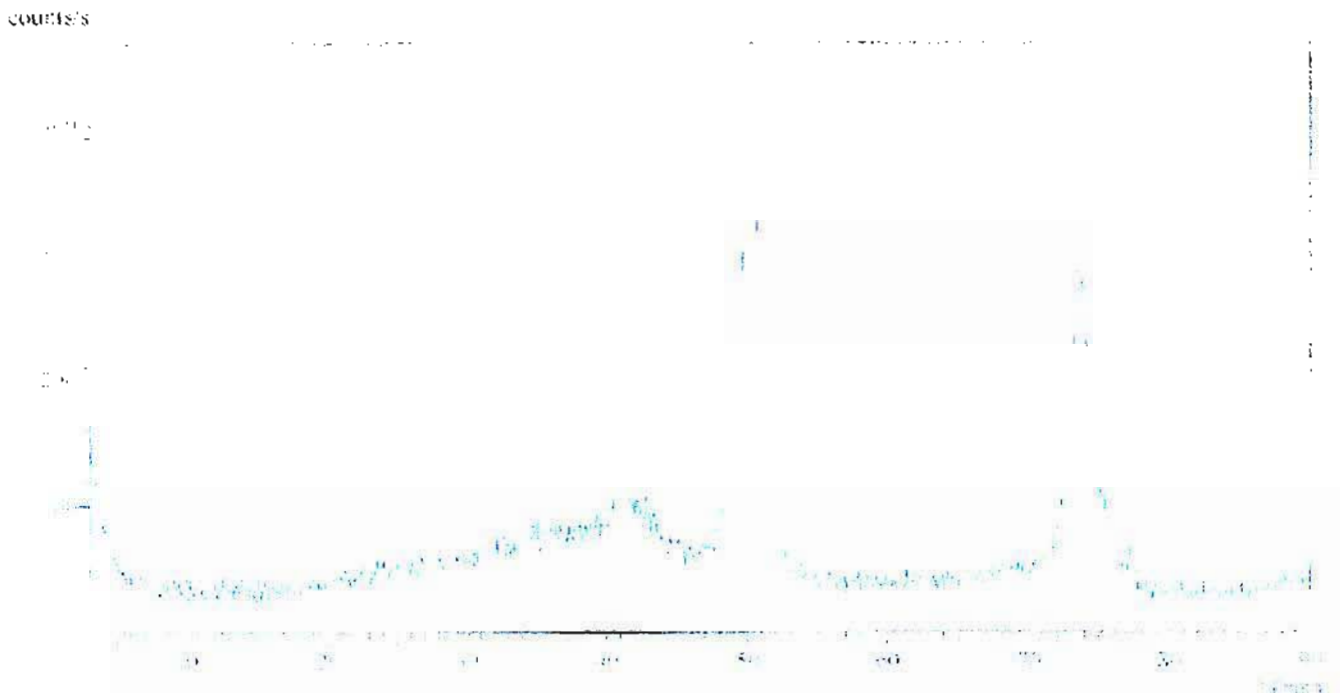


Figure 3BM: Typical XRD spectrum of tellurium promoted VMgO

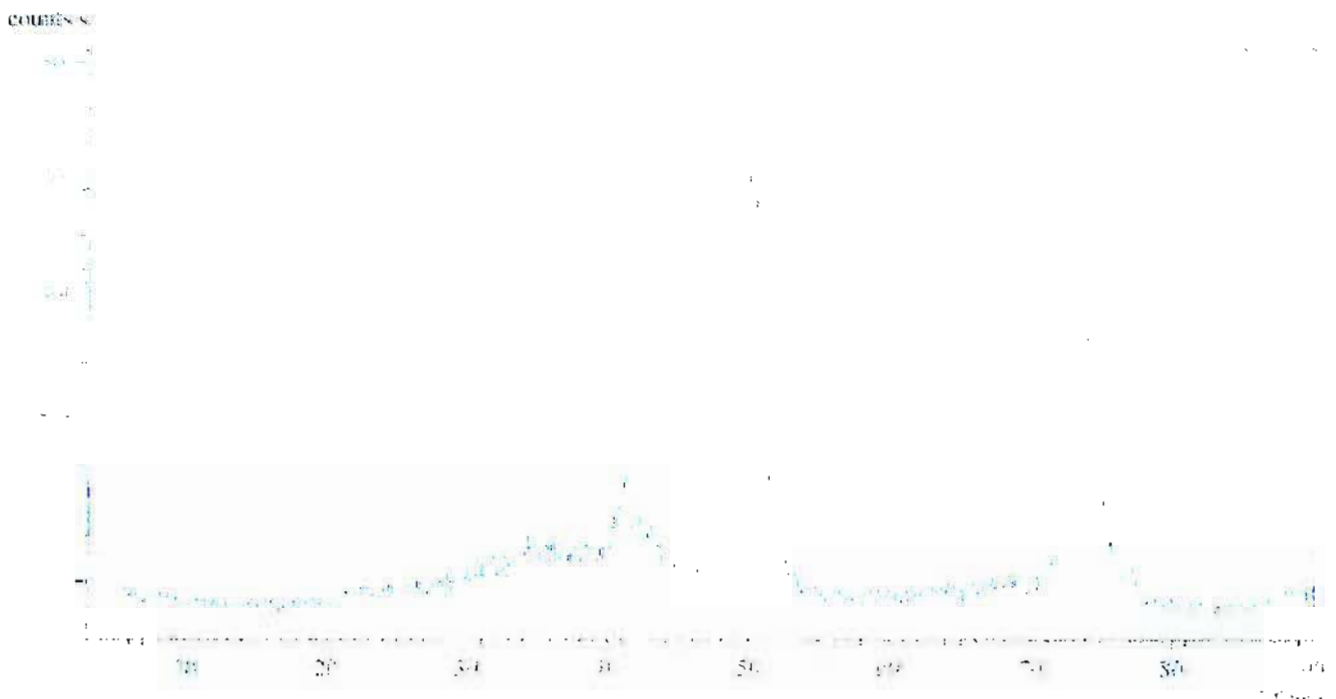


Figure 3BN: Typical XRD spectrum of niobium promoted VMgO

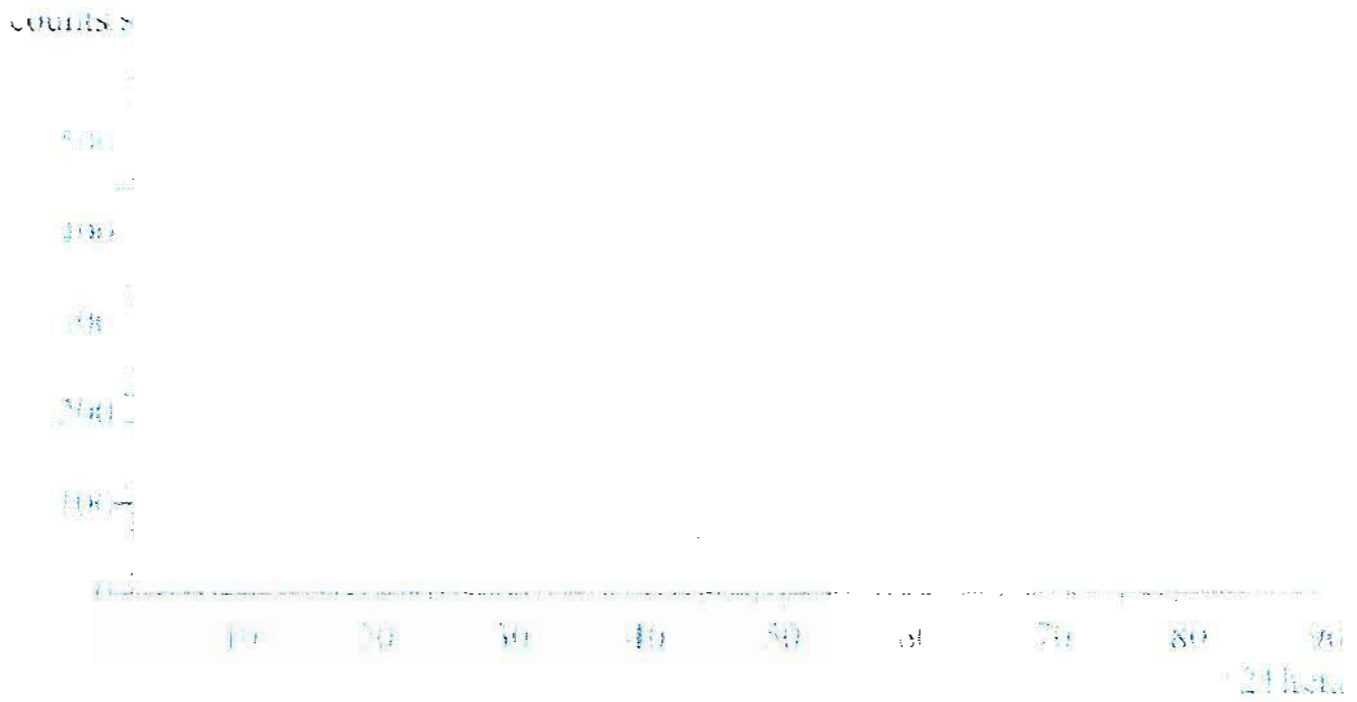


Figure 3BO: Typical XRD spectrum of bismuth promoted VMgO

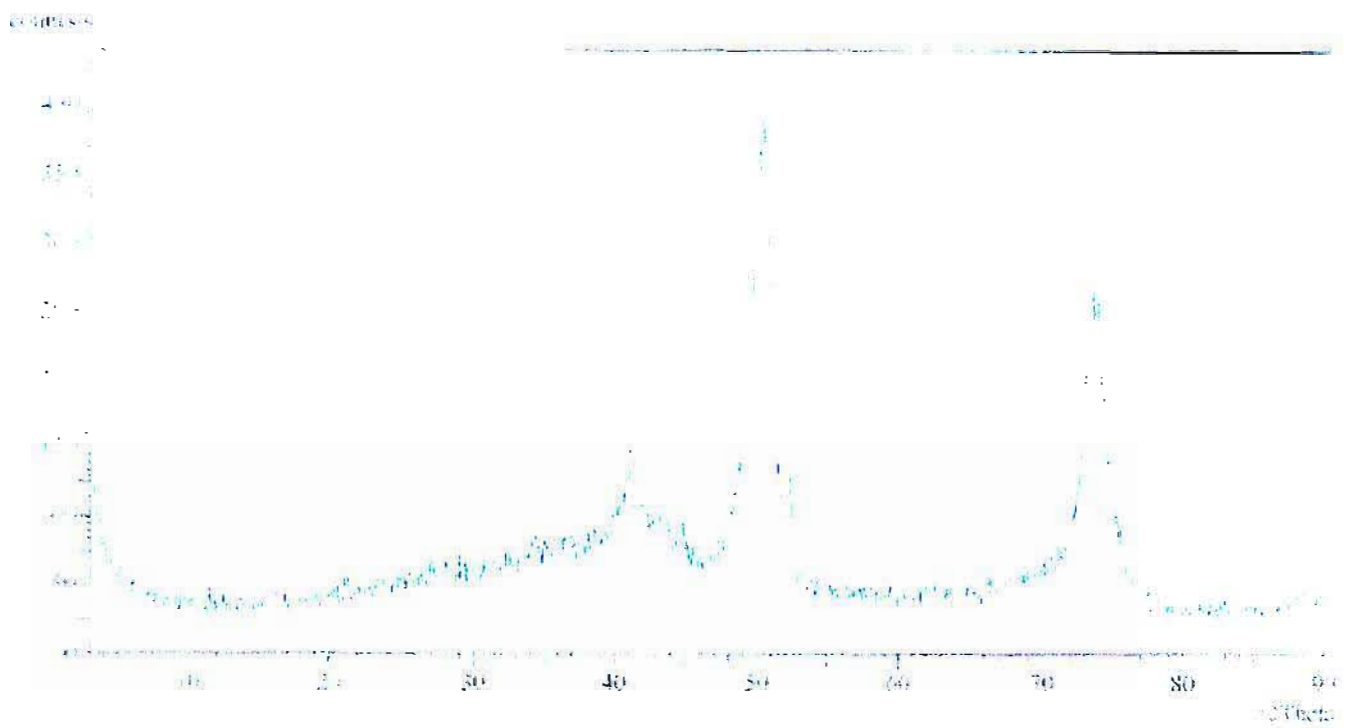


Figure 3BP: Typical XRD spectrum of cesium promoted VMgO



Figure 3BQ: Typical XRD spectrum of antimony promoted VMgO



Figure 3BR: Typical XRD spectrum of molybdenum promoted VMgO



Figure BS: Typical FTIR spectrum for niobium promoted VMgO

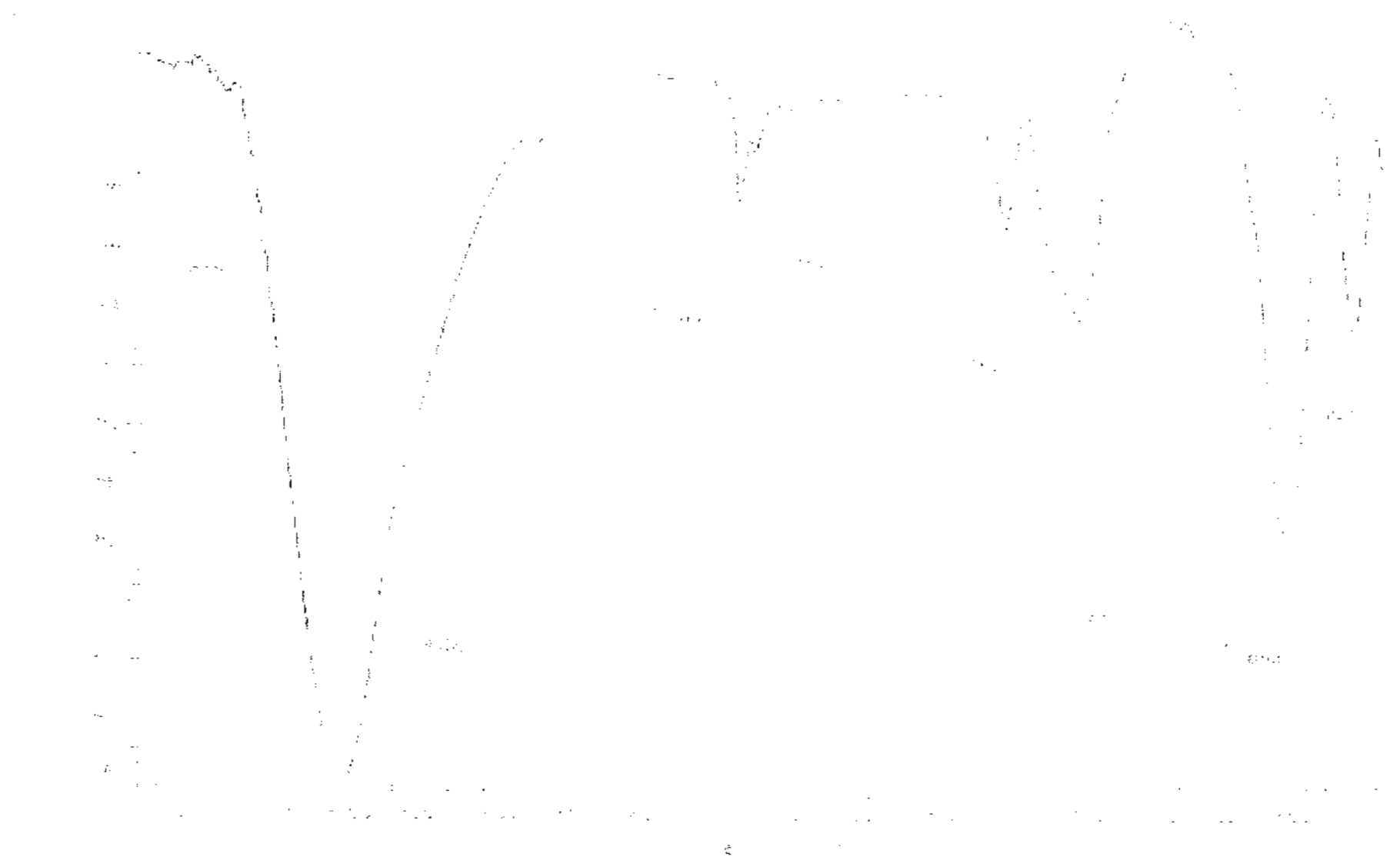


Figure BT: Typical FTIR spectrum for antimony promoted VMgO



Figure BU: Typical FTIR spectrum for molybdenum promoted VMgO



Figure BV: Typical FTIR spectrum for cesium promoted VMgO

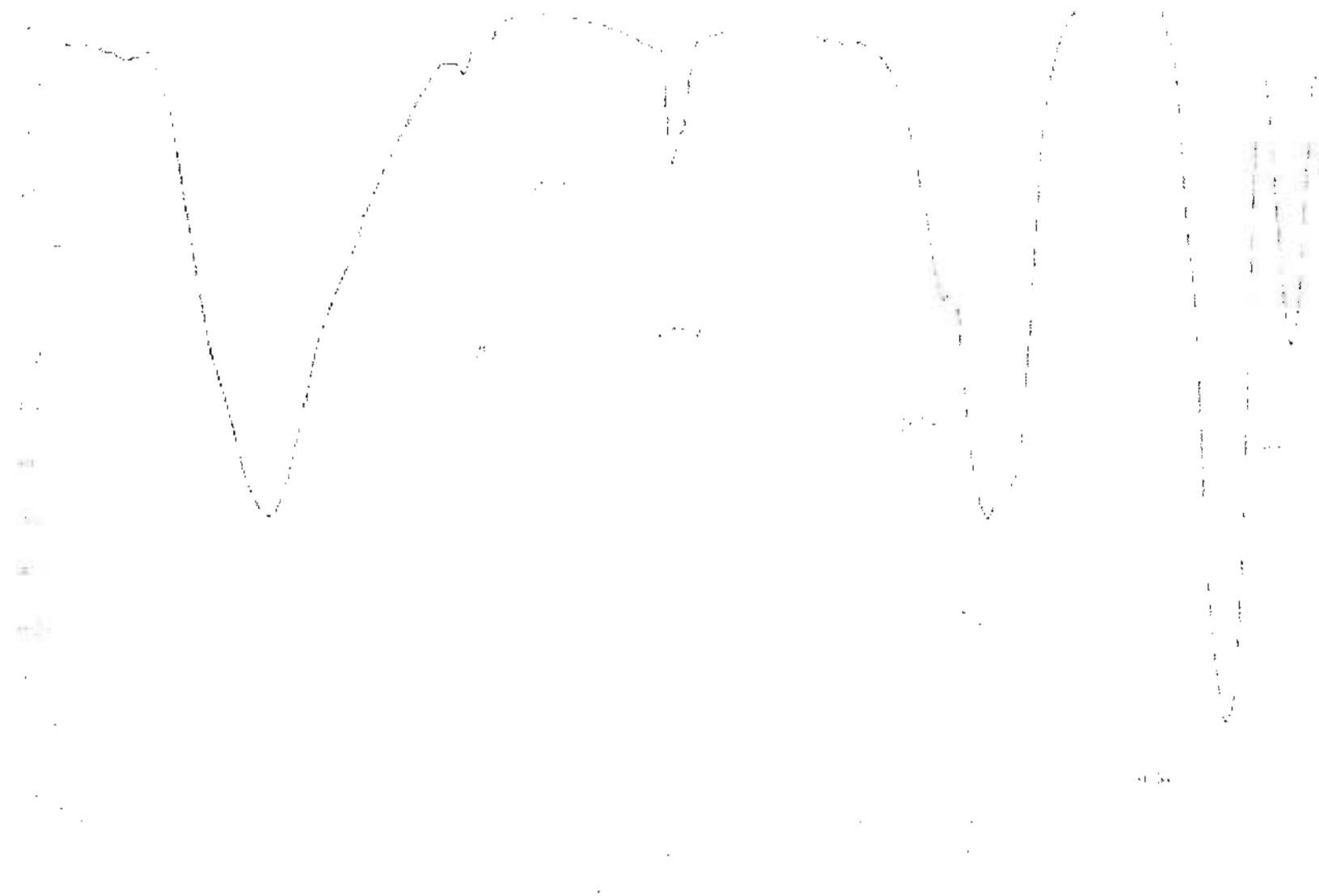


Figure BW: Typical FTIR spectrum for tellurium promoted VMgO

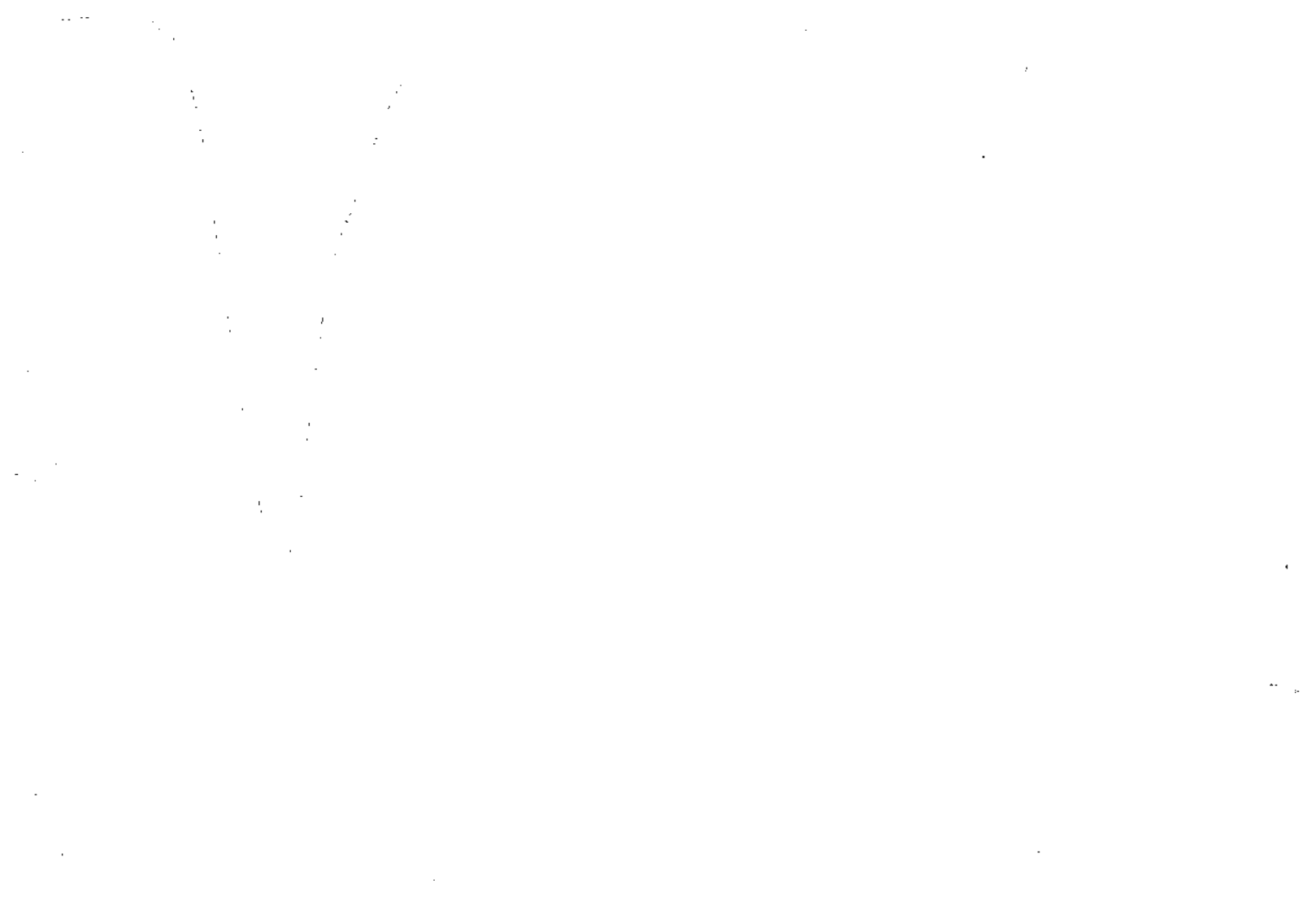


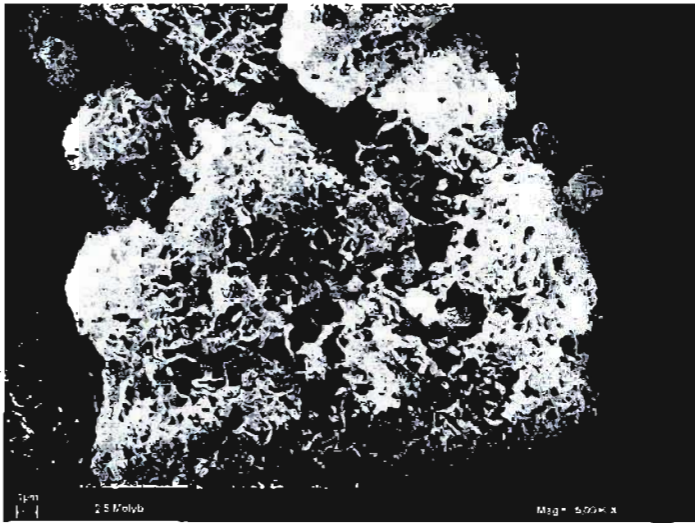
Figure BX: Typical FTIR spectrum for bismuth promoted VMgO



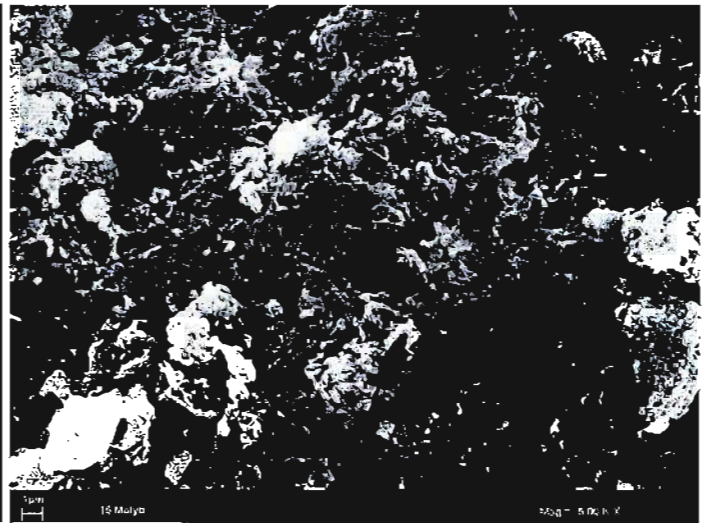
SEM image of 0.5MoVMgO



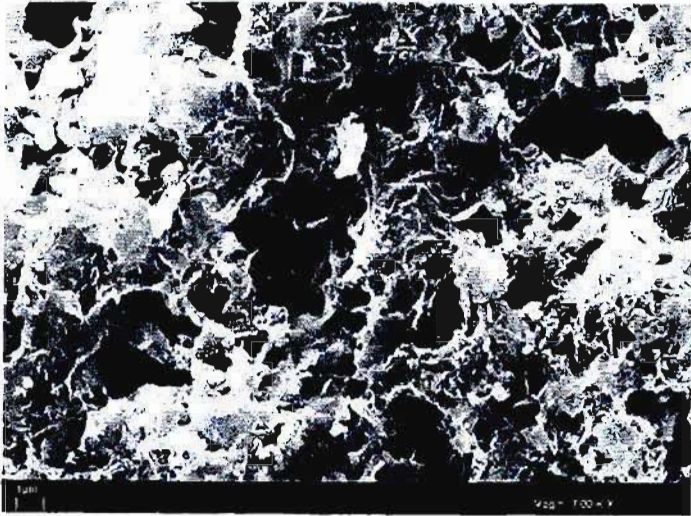
SEM image of 1MoVMgO



SEM image of 2.5MoVMgO



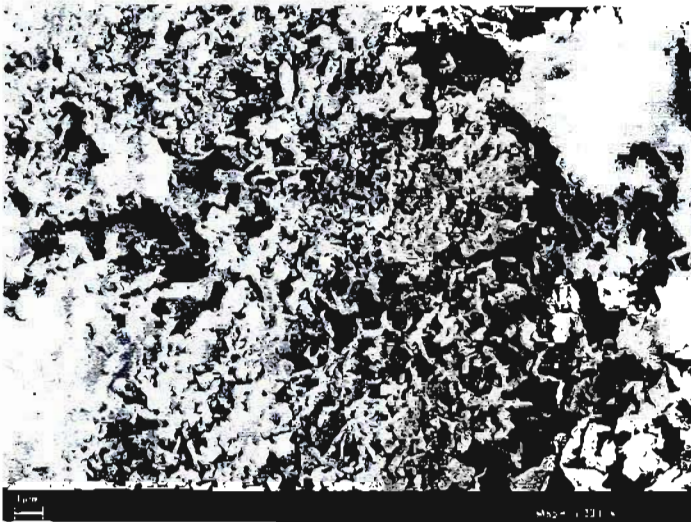
SEM image of 5MoVMgO



SEM image of 0.5TeVMgO



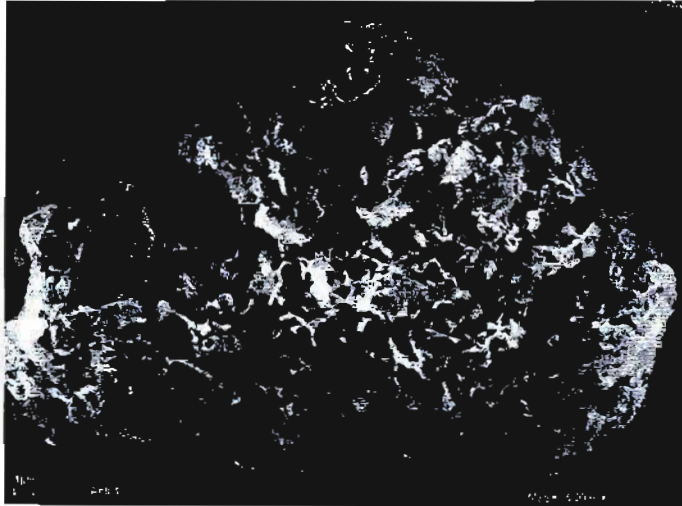
SEM image of 1TeVMgO



SEM image of 2.5TeVMgO



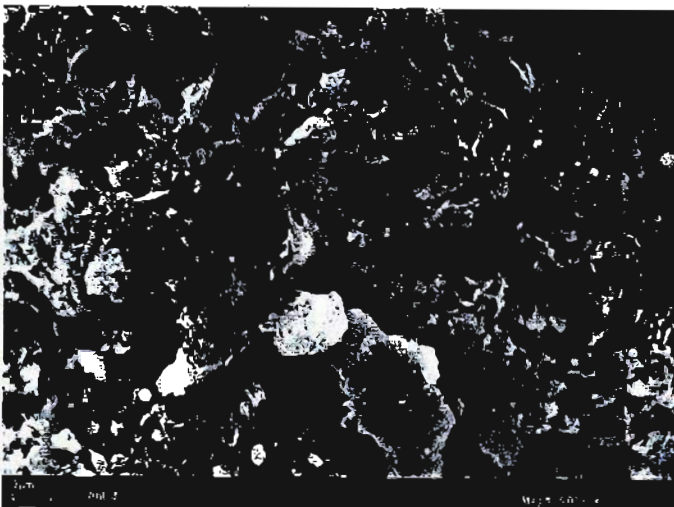
SEM image of 5TeVMgO



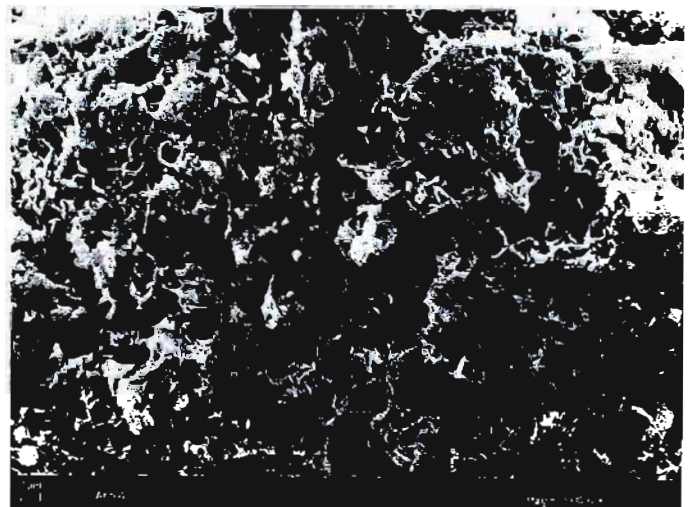
SEM image of 0.5SbVMgO



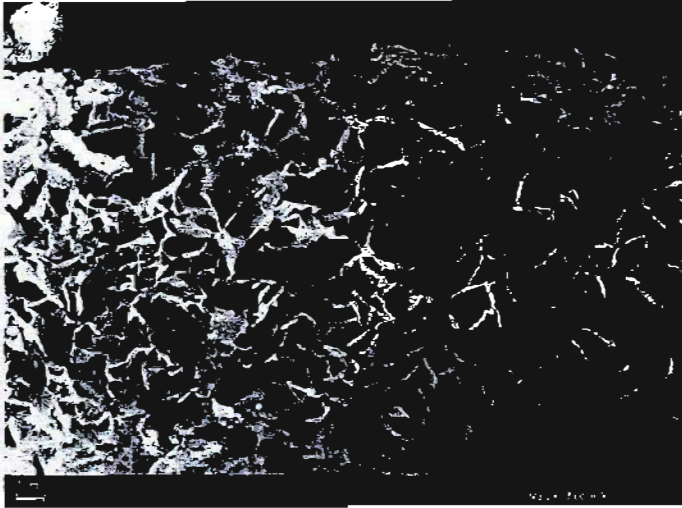
SEM image of 1SbVMgO



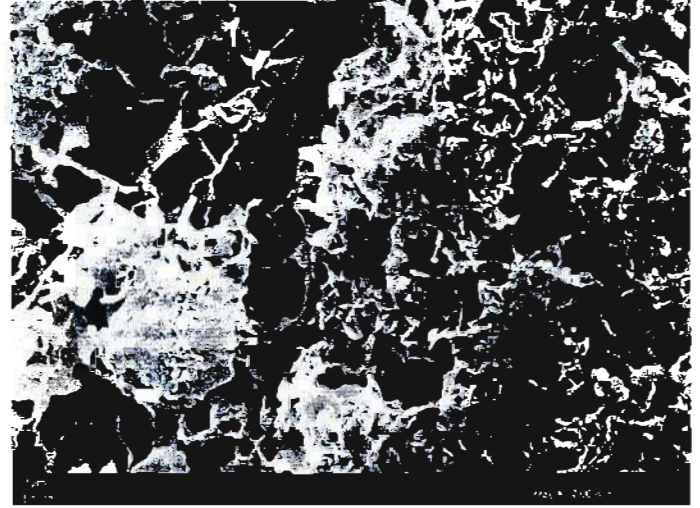
SEM image of 2.5SbVMgO



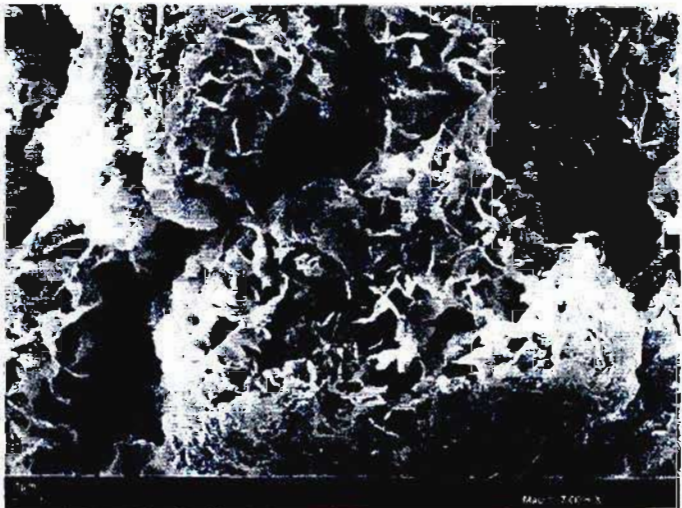
SEM image of 5SbVMgO



SEM image of 0.5NbVMgO



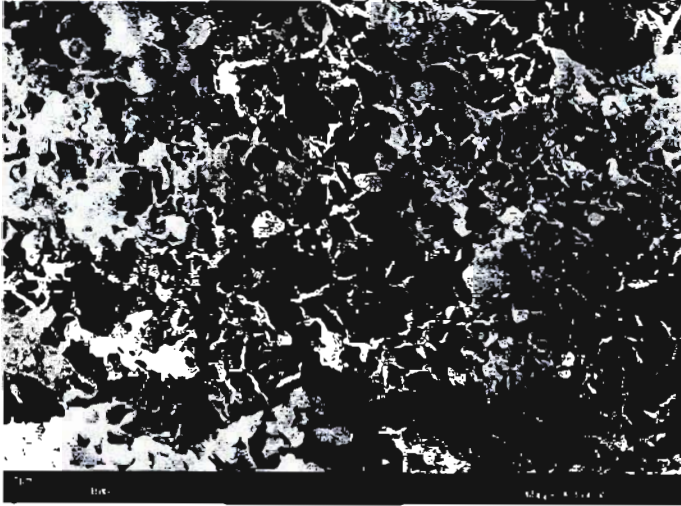
SEM image of 1NbVMgO



SEM image of 2.5NbVMgO



SEM image of 5NbVMgO



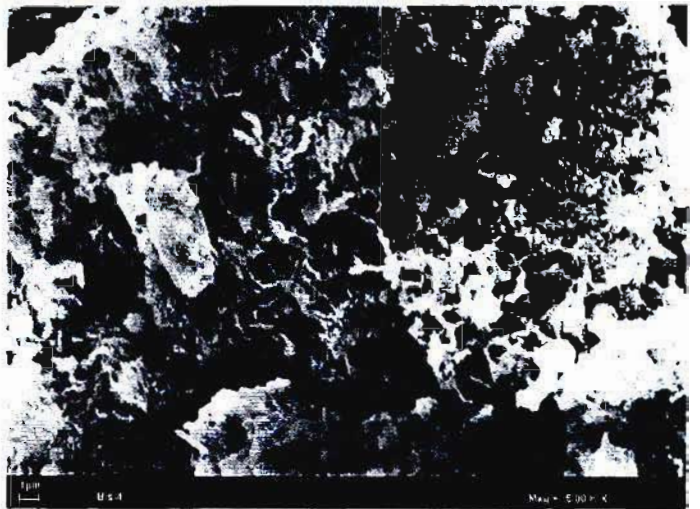
SEM image of 0.5BiVMgO



SEM image of 1BiVMgO



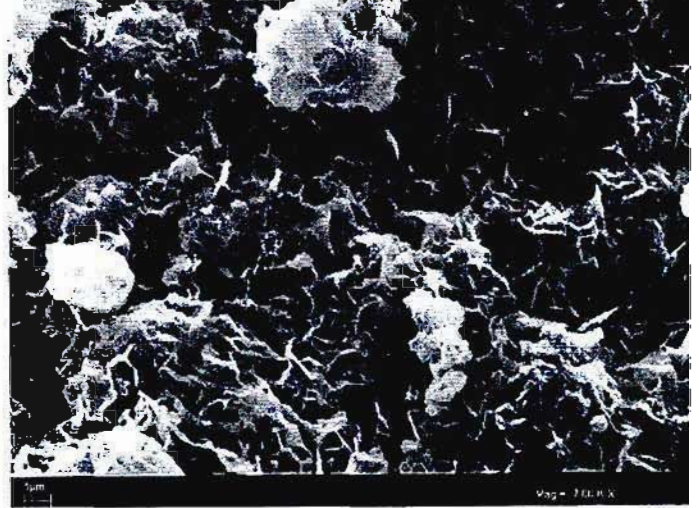
SEM image of 2.5BiVMgO



SEM image of 5BiVMgO



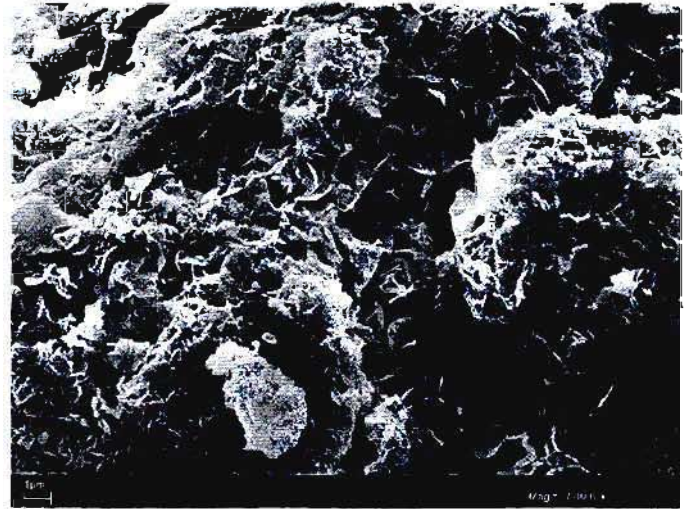
SEM image of 0.5CsVMgO



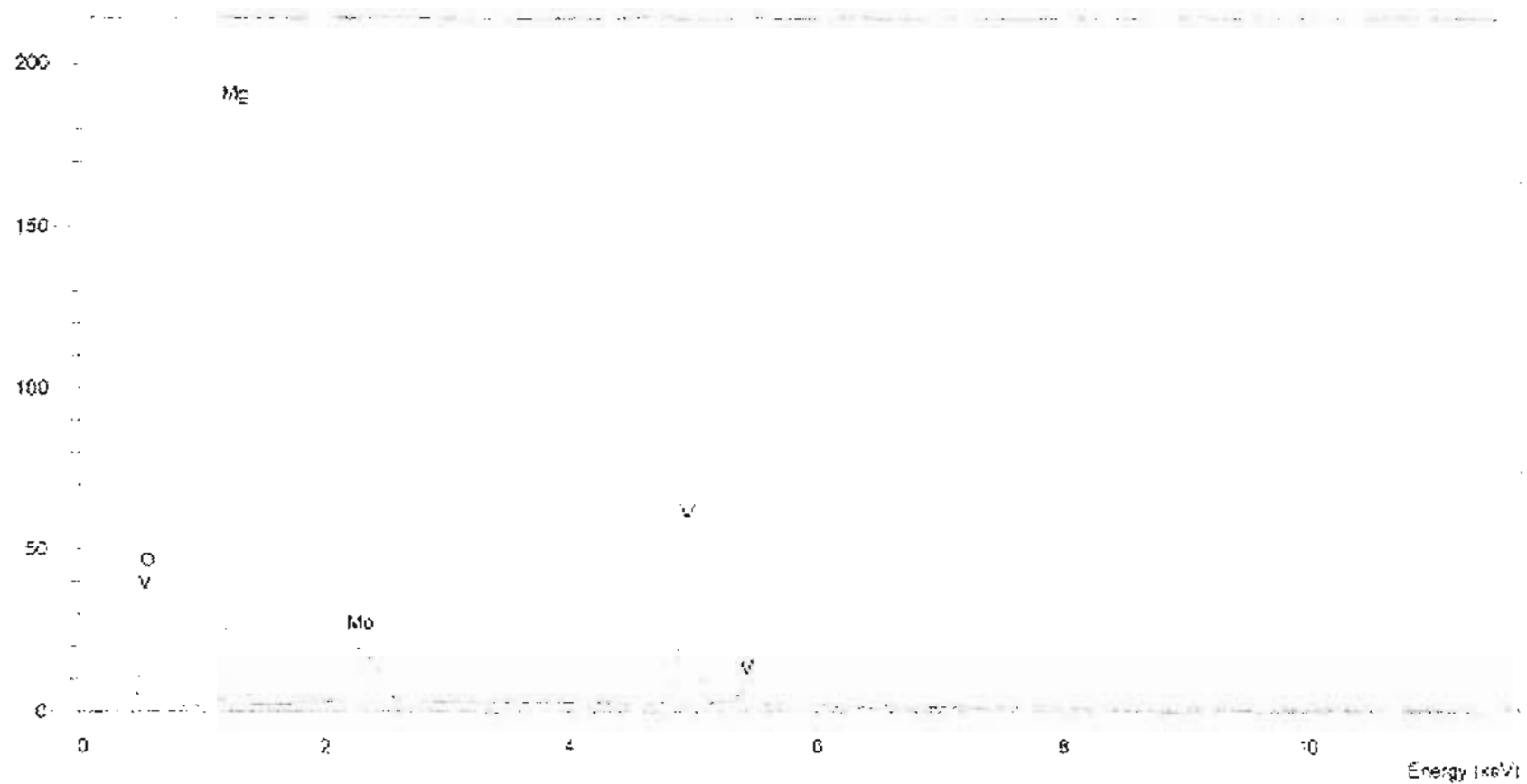
SEM image of 1CsVMgO



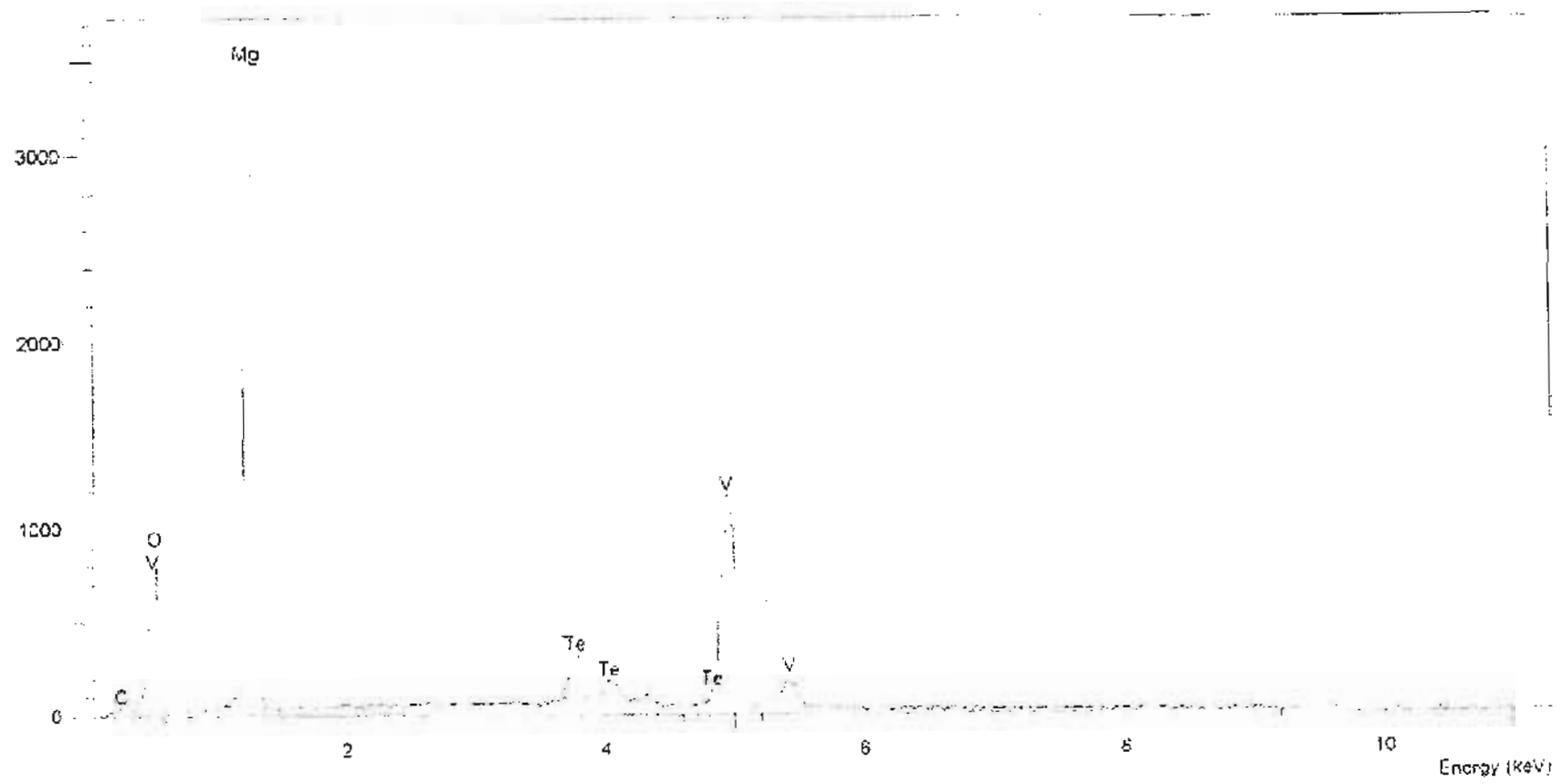
SEM image of 2.5CsVMgO



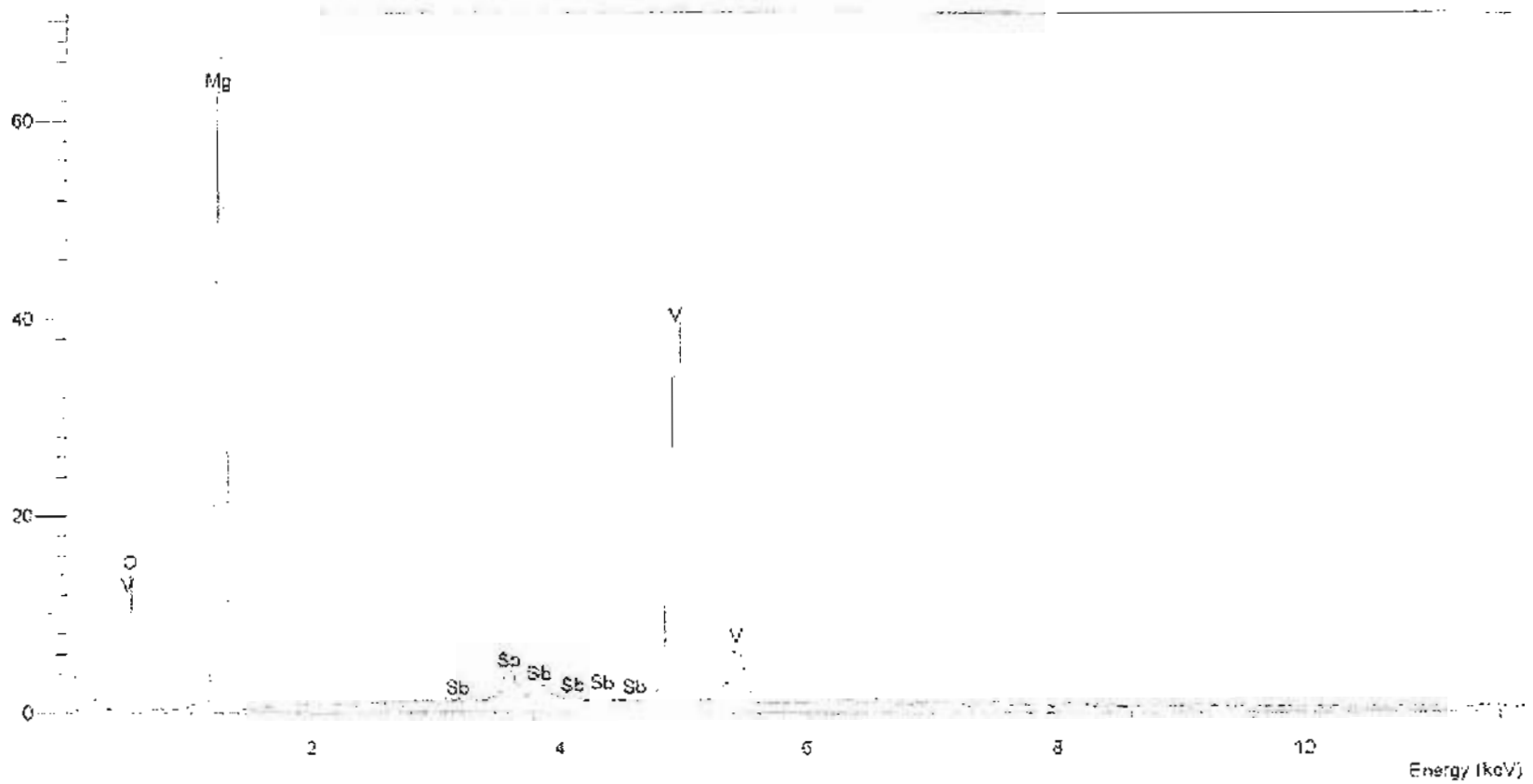
SEM image of 5CsVMgO



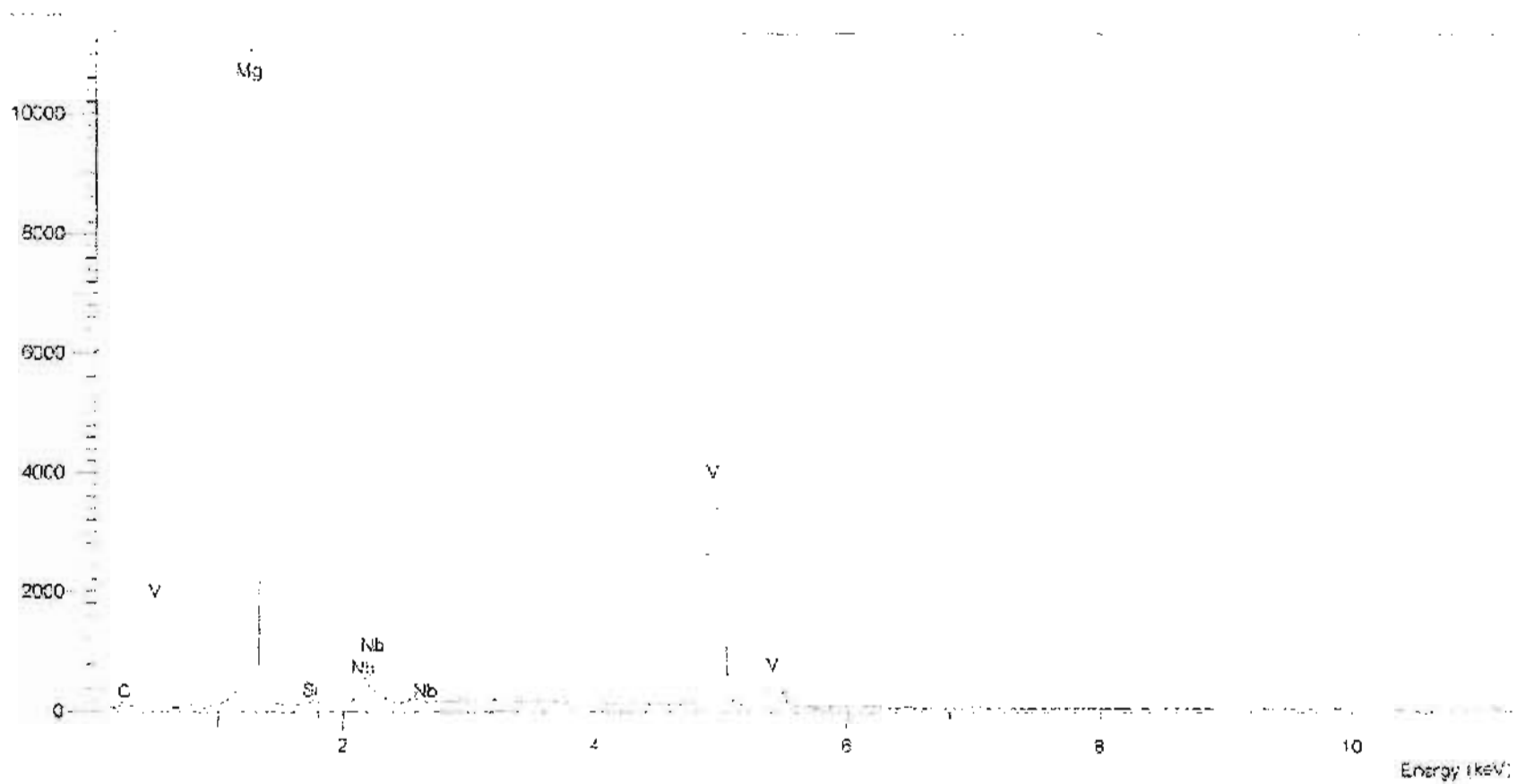
Typical EDS spectrum for molybdenum promoted VMgO



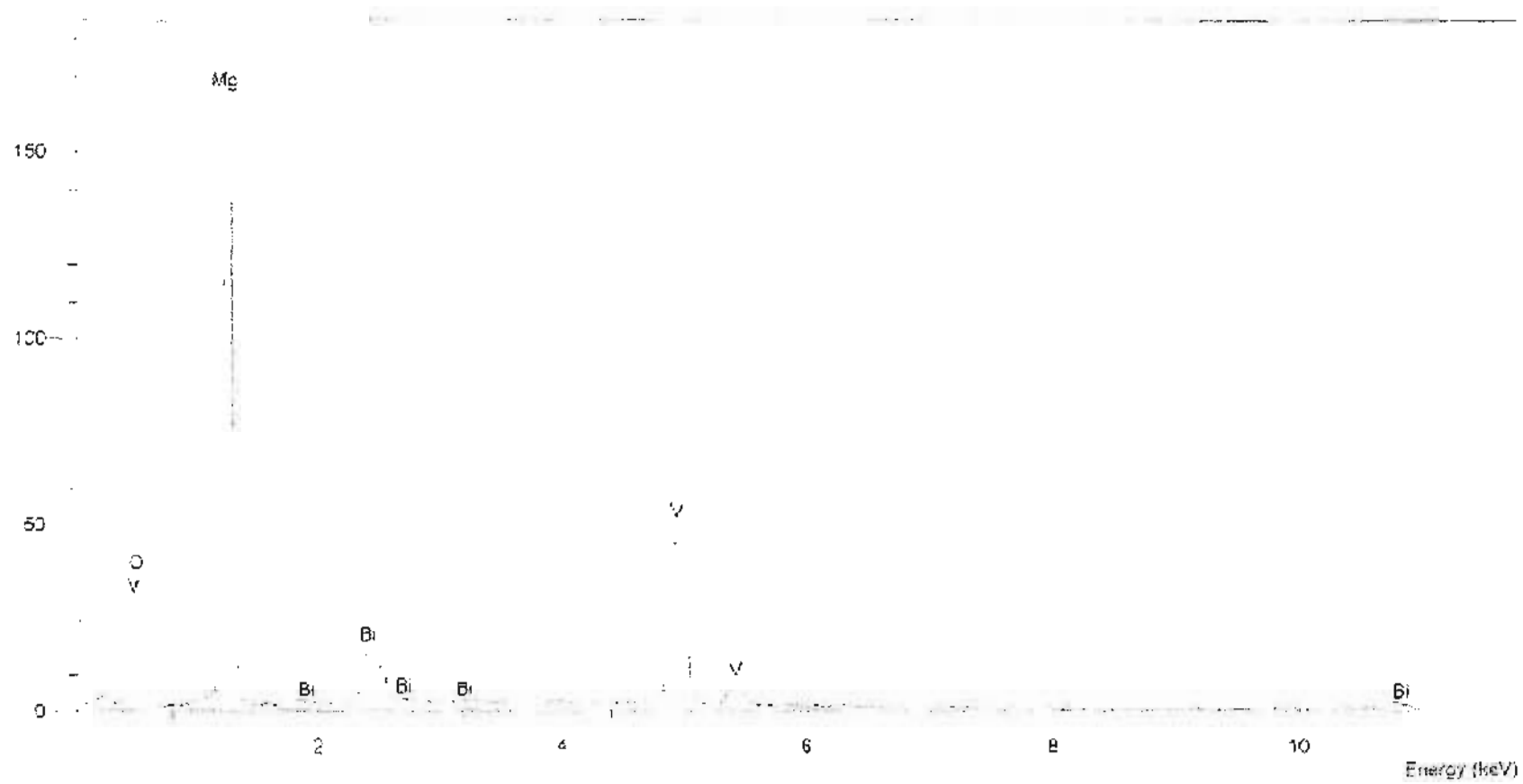
Typical EDS spectrum for tellurium promoted VMgO



Typical EDS spectrum for antimony promoted VMgO



Typical EDS spectrum for niobium promoted VMgO



Typical EDS spectrum for bismuth promoted VMgO



Typical EDS spectrum for cesium promoted VMgO